ELASTODYNAMIC PROBLEMS UNDER MECHANICAL, THERMAL AND ELECTRICAL LOADING

A thesis submitted in fulfilment of the requirements

for the degree of ***Doctor of Philosophy (Science)***

by

SOURAV KUMAR PANJA

DEPARTMENT OF MATHEMATICS

JADAVPUR UNIVERSITY

February 2025

যাদবপুর বিশ্ববিদ্যালয়

FACULTY OF SCIENCE
DEPARTMENT OF MATHEMATICS

JADAVPUR UNIVERSITY
Kolkata - 700 032, India
Telephone : 91 (33) 2457 2269

Certificate

This is to certify that the thesis entitled "ELASTODYNAMIC PROBLEMS UNDER MECHANICAL, THERMAL AND ELECTRICAL LOADING" submitted by "**SOURAV KUMAR PANJA**", who got his name registered (Reg. No. SMATH1101119) on August 8, 2019 with Index No. 11/19/Maths./26 for the award of Ph.D. (Science) Degree of Jadavpur University, is absolutely based upon his own work under the supervision of Prof. Subhas Chandra Mandal, Department of Mathematics, Jadavpur University, Kolkata - 700032 and and that neither this thesis nor any part of it has been submitted for either any degree / diploma or any other academic award anywhere before.

February 2025

03/03/2025

(Subhas Chandra Mandal)

Professor & Head
DEPARTMENT OF MATHEMATICS
Jadavpur University
Kolkata - 700032, West Bengal

Acknowledgements

I would extend my sincerest gratitude and indebtedness to **Dr. Subhas Chandra Mandal**, Professor, Department of Mathematics, Jadavpur University for guiding me throughout the whole tenure of my doctoral programme. Without his continuous support, words of motivation and helping hand in all phases it would not have been possible to complete my work.

I also take this very opportunity to acknowledge the support of the Head of the Department of Mathematics, Jadavpur University and other teachers and staffs for their encouragement. I would also like to thank the Department for providing me all the facilities required to complete my work.

I am grateful to my colleagues Dr. Ujjal Dhabal, Pintu Baidya, Samim Alam and Sandip Mistry at the Department of Mathematics, Jadavpur University for all their kind assistance and co-operation and sharing knowledge that helped me to continue my work.

I feel emotional to express my sincere gratitude to my parents. Without their encouragement, inspiration and ceaseless help, it was not possible for me to accomplish my work.

February 2025

Sourav Kumar Panja

Sourav Kumar Panja 03/03/2025

This thesis is dedicated to my parents,

Jagabandhu Panja

&

Anita panja

for their love, endless support and encouragement.

Contents

Chapter 1

Introduction

1.1 Elasticity

A continuous body can be affected by two types of forces: internal forces and external forces. Internal forces refer to forces that interact between particle constituents of a continuum. A force generated by an external agency is known as an external force. Even when there are no external forces acting on the body, the internal forces still operate. External forces (body and surface forces) are the main cause of continuum deformation. There is a proportionality between the body forces and the volume of its elements, e.g., gravity. Consequently, body forces are also referred to as volume forces since they act on volume elements. Surface forces refer to the forces that are exerted and spread out over a specific area or surface element of an object, in spite of whether that element is part of the object's boundary surface or a random surface within the object. For example, when a body is submerged in a fluid, the hydrostatic pressure exerted on its surface is an example of a surface force. When a continuum solid, such as rocks at normal temperature, is subjected to external loads, it can undergo deformation. However, once the external forces are removed, these solids will return to their original shape and size due to their elastic property. Such a continuum solid that exhibits this elastic behavior is called an elastic body. When an external force is applied to a continuous body, its constituent particles experience a change in their relative positions, causing the body to become strained. This change in position is called deformation. The particles initially resist the change in position, but the external force causes them to shift to some degree. Once the external force is removed, the particles return to their original shape and size. The elastic property of a continuum body is determined by its resistance to this type of

deformation. A body with greater resistance to deformation is said to be more elastic. For example, steel is more elastic than rubber.

A number of remarkable works have been found for the formation and evolution of the theory of elasticity since Galileo's time (1638). Hooke's Law, as defined by Robert Hooke in 1678, expresses the modern expression of the six stress components as a linear function of the strain components. This can be viewed as a generalized form of Hooke's Law. Euler (1766-1783), as a mathematician was interested mainly in the geometric forms of the elastic curves. Navier first obtained the general equilibrium and vibration equations for elastic solid material in 1821. French mathematician Cauchy (1823) assumed distinct conditions to Navier's work and developed the linear theory of elasticity, which is essentially unaltered today.

1.1.1 Stress and Strain

Stresses are forces per unit area that develop within a body to resist deformation, and their accompanying deformation is called **strain**. Therefore, stress and strain appear simultaneously. Dilatation is the strain that results in a change in volume but not in shape. Dilatation comes in two forms: compression, which reduces the volume, and rarefaction, which increases the volume. Shear is another type of elastic deformation that changes the shape but not the volume. For a surface element, ΔA located either inside or on the boundary of a medium, consider a force acting on the surface element be $F\Delta S$. We have

$$\lim_{\Delta A \to 0} \frac{F\Delta A}{\Delta A} = F(x_i, v),$$

where stress vector F describes the amount of force per unit area on a surface element and orientation of the force is determined by the unit normal vector acting at the point. Therefore, the stress force is a tensor quantity that varies with the position and orientation of the surface element. The state of stress at any point in a medium can be fully described by the nine stress tensor components, σ_{ij}. The stress vector F^{ν} acting on a surface with a normal vector ν can be expressed as

$$F^{\nu} = \sigma_{ij}\nu_j. \quad (i,\ j = 1,\ 2,\ 3)$$

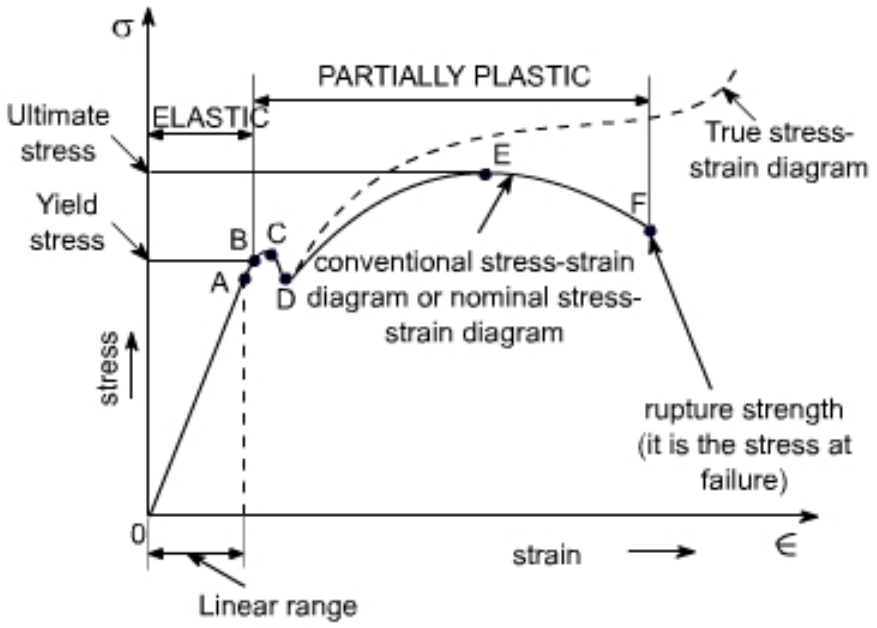

FIGURE 1.1: Stress Strain relationship

The relation of the strain tensor e_{ij} with the components of displacement vector $u = (u_1,\ u_2,\ u_3)$ for a deformable continuum, is written as

$$e_{ij} = \frac{1}{2}\left(\frac{\partial u_i}{\partial x_j} + \frac{\partial u_j}{\partial x_i}\right).$$

Figure 1.1 shows that the variation of stress is linear with strain within the proportional limit (pointed as A in the Figure 1.1). The maximum amount of stress that a material can withstand without undergoing permanent deformation is its elastic limit. Both the elastic and plastic behaviours are found in the body when the applied force exceeds the elastic limit. In numerous materials, the proportional limit and the elastic limit are almost identical to each other.

Once the stress surpasses the elastic limit of a material, it reaches the Yield Point stress, where it deforms plastically and experiences permanent deformation even without a significant increase in load.

As the nominal stress increases, it eventually reaches the ultimate stress point (E). At this point, materials like high-carbon steel fracture instantly. Upon further elongation, the breaking point (F) is reached. At this stage, the material experiences an increase in actual stress but a decrease in actual load in cross-sectional area and nominal stress.

1.1.2 Generalized Hooke's Law

Hooke's law describes the relationship between the stress components, represented by σ_{ij} and the strain components, represented by e_{ij} in an elastic solid. This law states that as long as the strain remains within the elastic limit, the stress is directly proportional to the strain and in mathematically given by

$$\sigma_{ij} = C_{ijkl} e_{kl} \quad (i,\ j,\ k,\ l = 1,\ 2,\ 3) \tag{1.1.1}$$

where C_{ijkl} represents 81 elastic constants. If these elastic constants vary throughout the material, depending on its position, the material is considered to be elastically non-homogeneous or inhomogeneous. Conversely, if the elastic constants are uniform throughout the material, the material is considered to be elastically homogeneous.

Stress symmetry:

The symmetry condition prescribe that the stress components must be identical when the indices are swappe i.e. $\sigma_{ij} = \sigma_{ji}$. As a result, only six stress components are considered to be independent. Hence equation (1.1.1) can be written as

$$\sigma_{ji} = C_{jikl} e_{kl}. \tag{1.1.2}$$

With the aid of equations (1.1.1) and (1.1.2) we have

$$0 = (C_{ijkl} - C_{jikl})\, e_{kl} \implies C_{ijkl} = C_{jikl}. \tag{1.1.3}$$

When considering pairs of indices $i,\ j$ taken together, there are only six unique combinations due to the symmetry conditions. On the other hand, when considering pairs of indices $k,\ l$ taken together, there are nine unique combinations. As a result of this symmetry, the total number of independent elastic constants is reduced from 81 to $6 \times 9 = 54$.

Strain symmetry:

The strain components exhibit symmetry under the symmetry condition, i.e. $e_{ij} = e_{ji}$. So from equation (1.1.1) we write $\sigma_{ij} = C_{ijlk} e_{lk}$. Substituting equation (1.1.3) from equation (1.1.2) we obtain the following equation

$$0 = (C_{ijkl} - C_{ijlk})\, e_{kl} \implies C_{ijkl} = C_{ijlk}. \tag{1.1.4}$$

Equation (1.1.3) indicates that there are six unique combinations of indices $i,\ j$ taken together when $k,\ l$ are fixed. Similarly, equation (1.1.4) suggests that there are six unique combinations of indices $k,\ l$ taken together when $i,\ j$ are fixed. Therefore considering both equations, there are a total of $6 \times 6 = 36$ independent constants for the linear elastic material that exhibits both stress and strain symmetry.

By utilizing the reduced number of stress and strain components and the reduced number of elastic constants, it is possible to express Hooke's law in a simplified form as follows

$$\sigma_i = C_{ij} e_j \quad (i,\ j = 1,\ 2,\ \cdots,\ 6) \tag{1.1.5}$$

where,

$$\sigma_1 = \sigma_{11},\ \sigma_2 = \sigma_{22},\ \sigma_3 = \sigma_{33},\ \sigma_4 = \sigma_{23},\ \sigma_5 = \sigma_{13},\ \sigma_6 = \sigma_{12},$$
$$e_1 = e_{11},\ e_2 = e_{22},\ e_3 = e_{33},\ e_4 = 2e_{23},\ e_5 = 2e_{13},\ e_6 = 2e_{12}.$$

In this context the shear strains can be referred as engineering shear strains.

Due to the existence of strain energy density function, the stiffness coefficients become symmetric i.e. $C_{ij} = C_{ji} \quad (i,\ j = 1,\ 2,\ \cdots,\ 6)$. Thus the stiffness matrix is symmetric with 21 independent elastic constants. The stiffness matrix is given by

$$C_{ij} = \begin{bmatrix} C_{11} & C_{12} & C_{13} & C_{14} & C_{15} & C_{16} \\ & C_{22} & C_{23} & C_{24} & C_{25} & C_{26} \\ & & C_{33} & C_{34} & C_{35} & C_{36} \\ & & & C_{44} & C_{45} & C_{46} \\ & & & & C_{55} & C_{56} \\ & & & & & C_{66} \end{bmatrix}. \tag{1.1.6}$$

A material that possesses 21 independent elastic constants is classified as either "Anisotropic" or "Aleotropic". However, it is possible to further decrease the number of independent elastic constants by exploiting planes of material symmetry, which can be achieved as follows:

Material symmetry:

Symmetry with respect to a plane: If we consider an anisotropic material that exhibits symmetry with respect to a single plane, it is known as a "Monoclinic Material". Such a material is characterized by 13 independent elastic constants, and its stiffness matrix can

be expressed as

$$C_{ij} = \begin{bmatrix} C_{11} & C_{12} & C_{13} & 0 & 0 & C_{16} \\ & C_{22} & C_{23} & 0 & 0 & C_{26} \\ & & C_{33} & 0 & 0 & C_{36} \\ & & & C_{44} & C_{45} & 0 \\ & & & & C_{55} & 0 \\ & & & & & C_{66} \end{bmatrix}. \tag{1.1.7}$$

Symmetry with respect to two orthogonal planes: If a material possesses two perpendicular planes of material symmetry, it is referred to as an "Orthotropic Material". In such a material, the number of independent elastic constants decreases to 9, and the stiffness matrix can be represented as

$$C_{ij} = \begin{bmatrix} C_{11} & C_{12} & C_{13} & 0 & 0 & 0 \\ & C_{22} & C_{23} & 0 & 0 & 0 \\ & & C_{33} & 0 & 0 & 0 \\ & & & C_{44} & 0 & 0 \\ & & & & C_{55} & 0 \\ & & & & & C_{66} \end{bmatrix}. \tag{1.1.8}$$

Transverse Isotropy: This is obtained from an orthotropic material. A transversely isotropic material has only 5 independent elastic constants and the stiffness matrix can be described as

$$C_{ij} = \begin{bmatrix} C_{11} & C_{12} & C_{12} & 0 & 0 & 0 \\ & C_{22} & C_{23} & 0 & 0 & 0 \\ & & C_{23} & 0 & 0 & 0 \\ & & & \frac{C_{22}-C_{23}}{2} & 0 & 0 \\ & & & & C_{66} & 0 \\ & & & & & C_{66} \end{bmatrix}. \tag{1.1.9}$$

Isotropic bodies: There are only 2 independent elastic constants are present for isotropic bodies. The stiffness matrix is written in the following form

$$C_{ij} = \begin{bmatrix} C_{11} & C_{12} & C_{12} & 0 & 0 & 0 \\ & C_{11} & C_{12} & 0 & 0 & 0 \\ & & C_{11} & 0 & 0 & 0 \\ & & & \frac{C_{11}-C_{12}}{2} & 0 & 0 \\ & & & & \frac{C_{11}-C_{12}}{2} & 0 \\ & & & & & \frac{C_{11}-C_{12}}{2} \end{bmatrix}. \tag{1.1.10}$$

Another form of this stiffness matrix is

$$C_{ij} = \begin{bmatrix} \lambda+2\mu & \lambda & \lambda & 0 & 0 & 0 \\ & \lambda+2\mu & \lambda & 0 & 0 & 0 \\ & & \lambda+2\mu & 0 & 0 & 0 \\ & & & \mu & 0 & 0 \\ & & & & \mu & 0 \\ & & & & & \mu \end{bmatrix}, \tag{1.1.11}$$

where $C_{12} = \lambda$ and $C_{11} - C_{12} = 2\mu$.

1.2 Wave Propagation

The occurence of earthquakes can be attributed to the sudden release of energy stored in rocks that have been strained elastically. As a result of this energy release, the ground in the vicinity of the earthquake's epicenter experiences strong shaking, and elastic waves, known as seismic waves, are propagated throughout the planet. While earthquakes pose a significant geological threat for individuals residing in regions susceptible to seismic activity, the seismic waves produced by these events serve as an invaluable tool for investigating the Earth's interior. For over a century, seismology has been a leading field of research focused on the study of earthquakes and the way in which elastic waves move through the Earth. Its finding have been instrumental in enhancing our understanding of the composition and structure of the Earth's subterranean structure of the Earth. When rocks within the Earth break suddenly or an explosion occurs, energy is released in the form of seismic waves that propagate outward in all directions, causing vibrations. These waves travel through the Earth and can be detected and recorded by seismographs. To better understand this phenomenon, one can envision the circular ripples that spread out over the surface of a pond when a stone is tossed into it. **Seismic waves** are diverse in their movement patterns and can be categorized as **body waves** and **surface waves**. Body waves can penetrate through the Earth's interior, while surface waves propagate only along the planet's surface, resembling waves on water. When an earthquake occurs, seismic energy is emitted in the form of both body and surface waves.

The initial two kinds of waves, namely the **P-wave** and **S-wave**, are referred to as Body waves due to their ability to move through the interior of the Earth. **Love** and **Rayleigh** waves are classified as surface waves since they travel across the surface of the Earth. When an earthquake occurs, it emits P and S waves that travel in all directions and as these

waves interact with the Earth's shallow structures, they produce surface waves. The P-wave, characterized by longitudinal motion, causes particles to move in the same direction as the energy is travelling by pulling or pushing them. These waves are the quickest elastic waves and can travel through solid rocks as well as fluids such as water or the liquid layers present in the Earth. The S-wave is distinguished by transverse motion, causing particles to move perpendicular to the direction of wave propagation. S-wave can be polarized into two directions: vertical and horizontal, which are identified as shear vertical(SV) wave and shear horizontal(SH) wave, respectively. The speed at which these body waves travel depends on both the medium's elasticity and its density.

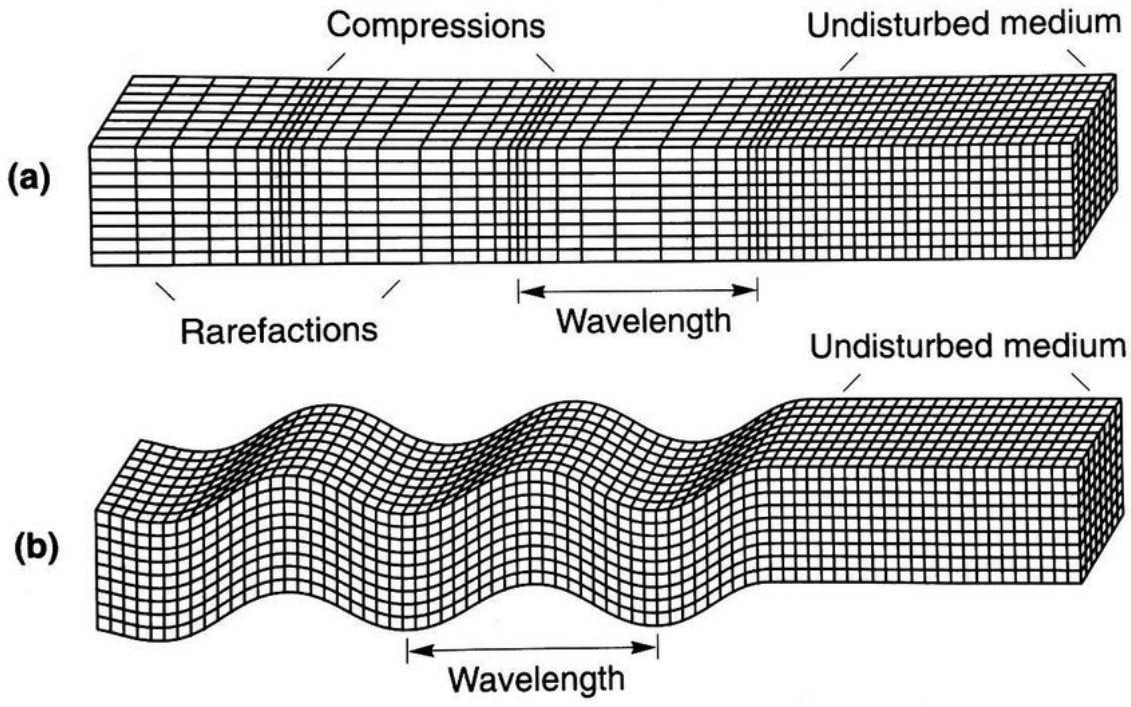

FIGURE 1.2: Body waves: (a) P wave (b) S wave

In 1911, A.E.H. Love, a British mathematician, developed the mathematical model for one type of surface wave, called **Love wave**. This wave is characterized by fast movement and lateral shifting of the ground. It is limited to the earth's surface and causes purely horizontal motion. Lord Rayleigh, a mathematician who predicted the existence of a particular type of surface wave in 1885, gave it the name **Rayleigh wave**. This wave moves along the ground in a rolling motion, similar to the way a wave moves across a body of water. As it rolls, the ground is moved both vertically and horizontally in the same direction as the wave's motion. The majority of earthquake-induced shaking is attributed to the Rayleigh wave, which can be significantly larger than Love wave.

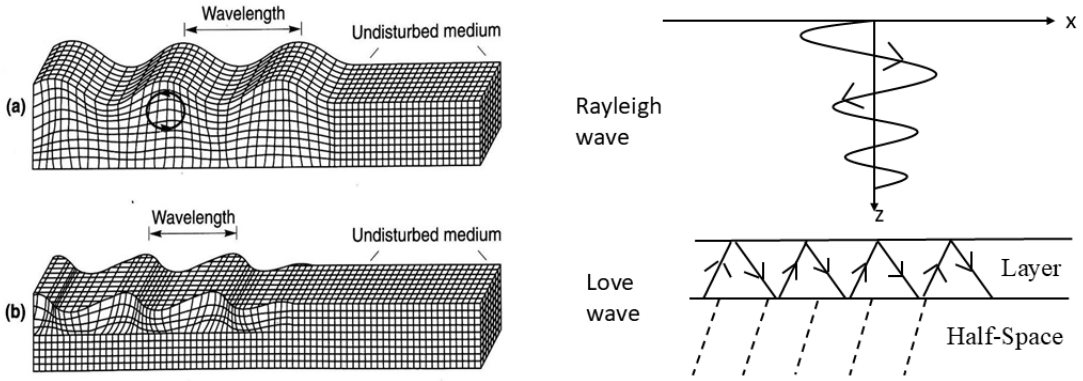

FIGURE 1.3: Surface waves: (a) Rayleigh wave (b) Love wave

Several factors influence the speed at which seismic waves travel, including the rock composition, temperature and pressure. Seismic wave velocity is generally reduced by higher temperatures but is increased by higher pressures. As the weight of the rocks above increases with depth in the Earth, pressure also increases. This explains why pressure tends to increase the speed of seismic waves, while temperature tends to decrease it. In regions where the composition of rock is uniform, the velocity of seismic waves typically increases as depth increases, primarily due to the influence of pressure. Although increasing temperature tends to reduce wave velocity with depth, the impact of pressure is usuallly greater. As a result, the overall effect of increasing depth in uniform rock regions is an increase in seismic wave velocity.

Poisson (1828) studied the transmission of waves in a solid medium and examined the presence of two distinct wave modes: longitudinal and transverse. With the help of normal modes Clebsch (1863) studied the general theory for the free vibration of solid bodies. Saint Venant, a French elasticity theorist, took forward the work of earlier investigators and demonstrated his research results on transverse impact. Rayleigh (1887) studied the propagation of surface waves on a solid. Lamb (1904) was the first to examine the pulse propagation in semi-infinite solids. Love (1927) published his famous book on the mathematical theory of elasticity. Pekeris (1955) solved the Lamb's problem of pulse propagation in a seismic surface.

The study of wave propagation and vibration phenomena was found to be an integral part of seismology, geophysics and for earthquake related research and in the detection of nuclear explosions. The work related to wave propagation in solids can be found in the books written by Kolsky (1963), Hudson (1980), Payton (1983), Bullen et al. (1985), Royer and Dieulesaint (1999), Aki and Richards (2002), Slawinski (2003), Pujol (2003),

Chapman (2004), Miklowitz (2012), Pilant (2012), Achenbach (2012), Graff (2012) and Brekhovskikh (2012).

1.3 Fracture Mechanics

Fracture mechanics is a branch of mechanics that deals with the study of the characteristic of cracks, defects and inclusions in a body under some stress. It is concerned with the failure analysis of a material under external loading, crack initiation, crack growth and propagation of crack. Interaction between cracks and material depends upon types of material, geometry of the crack and loading conditions. Fracture mechanics has extensive applications in various fields like civil engineering, mechanical engineering, aerospace engineering, material science, etc. It is used to predict the materials of a design in engineering structures that can withstand extreme environments and different loading conditions such as aircrafts, bridges and nuclear reactors.

1.3.1 Crack

In structural engineering, the process of crack growth mainly involves the separation and widening of the surfaces comprising the crack. There are three types of fracture (Fig. 1.4) according to external loading conditions:

1. **Mode I fracture:** Mode I fracture also known as opening or tensile fracture, occurs when the applied stress is normal to the crack surface and pull the two sides of the crack to open.

2. **Mode II fracture:** Mode II fracture also referred as sliding mode or the In-Plane shear mode fracture, happens when the applied stress is parallel to the crack surface, perpendicular to the crack front and one side of the crack slide over another.

3. **Mode III fracture:** Mode III fracture also referred to as out-plane mode or tearing mode fracture, arises when the stress applied is parallel to both the crack front and the plane of the crack surface. As a result, the crack surfaces move in parallel with the leading edge of the crack, causing them to tear apart from each other.

Stress intensity factor (SIF) is a physical quantity used in fracture mechanics to measure the local stress concentration at the crack tip and to determine whether a crack will

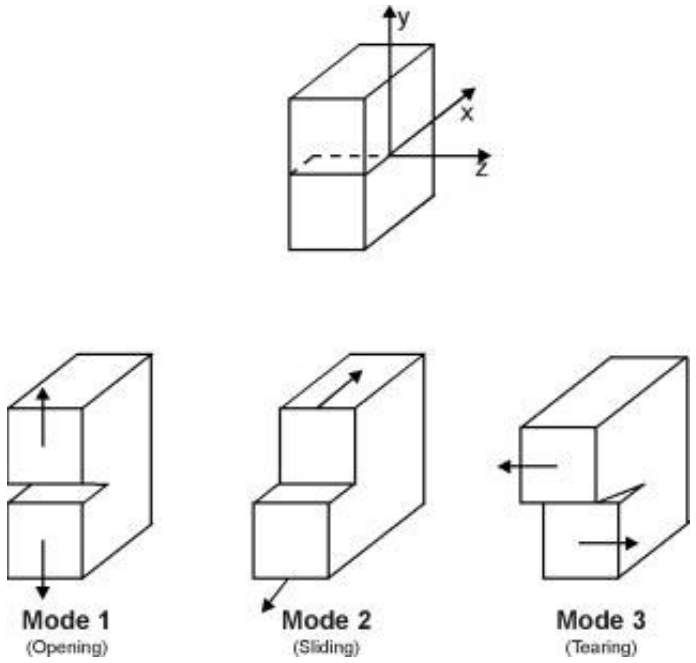

FIGURE 1.4: Modes of crack deformation

propagate and cause failure of the material. **Crack opening displacement (COD)** is another physical quantity in fracture mechanics to measure the amount of deformation or dispalcement between two sides of a crack.

Typically, a traditional analysis involves neglecting the effects of inertia, and the analytical study is regarded as quasi-static. However, some fracture mechanics problems can't be adequately characterized as quasi-static due to factors such as material properties and loading conditions. In such cases, the inertia of the material must be considered in the analysis.

In the early 20th century, Kolosov (1909) and Inglis (1913) solved the basic crack problems. English aeronautical engineer, Griffith (1921) developed the right ideas for the growth of a crack. Weibull (1939a,b) carried forward Griffith's work with thin glass rods and gave a statistical results of fracture. Irwin (1957) invented workable fracture toughness parameters like SIF and energy release rate in LEFM. CTOD parameter is studied by Wells (1961) while Rice (1967) proposed the J-integral concept, a path independent integral, for crack analysis in the nonlinear fracture mechanics. Diffraction of antiplane shear waves by a finite crack was studied by Loeber and Sih (1968). Two coplanar Griffith cracks in an infinite elastic medium was studied by Lowengrub and Srivastava (1968). Interaction of elastic waves with Griffith crack and penny shaped crack is analyzed by Mal (1970a,b, 1972). The diffraction problem of two symmetrical coplanar Griffith cracks situated in an

infinite, isotropic, and homogeneous elastic medium, subject to normally incident longitudinal and antiplane shear waves, was solved by Jain and Kanwal (1972). Itou (1978) investigated the dynamic problem of an infinitely elastic medium that was disrupted by two Griffith cracks lying on the same plane. He examined how a self-balancing pressure system within the medium changed over time in response to harmonic variations. Chen (1978) investigated a dynamic response problem of a finite crack situated in a finite strip. Diffraction of antiplane shear by two coplanar Griffith cracks and two coplanar Griffith cracks under impact load was studied by Itou (1980a,b). Srivastava et al. (1980) examined the interaction of Griffith crack with antiplane shear waves in two bonded dissimilar elastic half-spaces. Stress analysis of a crack under normal and shear impact was presented by Sih and Chen (1980). Interaction of anti-plane shear waves with a Griffith crack in an infinite elastic strip has been studied by Srivastava et al. (1981, 1983). Impact response of a finite crack in an orthotropic medium and an infinite orthotropic strip were studied by Kassir and Bandyopadhyay (1983) and Shindo et al. (1986) respectively. Edge crack problem in orthotropic medium solved by De and Patra (1989). Verma and Jain (1990) addressed a problem related to the diffraction of longitudinal waves that are obliquely incident on an infinite, isotropic and homogeneous elastic medium. The medium is disrupted by two Griffith cracks that are identical, parallel and located on the same plane. Interaction of P waves with four coplanar Griffith cracks in an infinite orthotropic medium was deliberated by Mandal and Ghosh (1994). Elastodynamic response of an orthotropic medium consisting of two and three coplanar Griffith cracks has been studied by Sarkar et al. (1994, 1995). Narita and Shindo (1999b) investigated the piezoelectric effect of anti-plane shear waves by a crack. Zhou et al. (2001) explored the dynamic behavior of two cracks in a piezoelectric material due to anti-plane shear waves. The transient thermal response in a cracked piezoelectric strip was solved by Wang and Mai (2002), while Baksi et al. (2003) examined the impact response in a cracked orthotropic material. Kwon (2004) studied the crack problem in a functionally graded piezoelectric strip under anti-plane shear waves, and Guo et al. (2005) discussed the edge crack scenario in a functionally graded orthotropic strip. Various loading conditions on a penny-shaped crack were discussed by Niraula and Wang (2006), and Wang et al. (2011). Wang and Pan (2008) analytically discussed some crack problems in 1D-hexagonal and 2D-octagonal quasicrystals. Wang and Han (2012a), and Othman and Atwa (2013) analyzed the stress intensity factor of a mode-I crack under the hyperbolic heat conduction law. Yang and Li (2014) examined the impact of magneto-electro-elastic loading on the scattering of SH waves by a crack in a piezoelectric material, while Yang and Li (2015) also solved the scattering of SH waves by a crack in a functionally graded piezoelectric substrate attached to a piezoelectric strip. Mandal and

Mandal (2017) focused on the interface crack in an orthotropic medium, Naskar and Mandal (2018) studied the transient response of P-wave diffraction in an orthotropic medium. Hu et al. (2019), Ma et al. (2023), and Yang et al. (2023a) investigated crack behaviors in 1D hexagonal quasicrystals for surface waves in the presence of the piezoelectric effect. The effect of rotation in a fiber-reinforced thermoelastic medium for a mode-I crack was studied by Lotfy and El-Bary (2024).

1.4 Electromagnetic field in elastic medium

Several decades ago, a new field of study called magnetoelasticity emerged, focusing on the relationship between strain and electromagnetic fields. This field explores the mechanical deformations of solid structures subjected to externally applied magnetic fields. Both magnetic and elastic fields influence the total deformation of the solid body and modify the governing laws. Maxwell's equations (Maxwell, 1873), along with modified Ohm's laws, describe the behavior of the electromagnetic field, while the characteristics of the elastic field are determined by the modified Hooke's law. Additionally, the superposition of the electromagnetic field on the elastic field alters the elastic-stress relationship and field equations through the addition of a new body force known as the Lorentz force.

The famous Maxwell's equations governing the electromagnetic field are

$$\text{div}\ \vec{B} = 0,\ \text{curl}\ \vec{E} = -\frac{\partial \vec{B}}{\partial t},\ \text{curl}\ \vec{H} = \vec{J},\ \vec{B} = \mu_e \vec{H} \text{ and } \vec{J} = \sigma\left(\vec{E} + \frac{\partial \vec{u}}{\partial t} \times \vec{B}\right), \quad (1.4.1)$$

where $\vec{E}$ represents the electric field, $\vec{J}$ denotes the electric current and $\vec{H}$ encompasses both the primary and induced magnetic fields. μ_e is the magnetic permeability and σ is the electrical conductivity.

The Navier's equation in the presence of electromagnetic force for a solid body is given by

$$\text{div}\ \vec{\sum} + \vec{F} + (\vec{J} \times \vec{B}) = \rho \frac{\partial^2 \vec{u}}{\partial t^2}, \quad (1.4.2)$$

where $\vec{\sum}$ is the stress tensor, $\vec{F}$ is the external force per unit volume, $\vec{J} \times \vec{B}$ is the Lorentz force, ρ is the density of the medium and $\vec{u}$ is the displacement vector.

Magnetoelastic materials are now used in high-tech sectors such as microwaves, lasers, and optics due to their ability to convert one form of energy into another, such as mechanical to electrical energy. The impact of electromagnetic fields on cracked surfaces has become

significant due to advancements in applied physical sciences, including MHD devices and fusion power reactors. Over time, magnetoelastic waves have become a focal point of research for many scholars in solid mechanics and fracture mechanics. Knopoff (1955) developed the theory of electromagnetic field, which was subsequently expanded by Kaliski and Petykiewicz (1959). The plane waves propagation problem in an electro magnetic elastic solid is studied by Dunkin and Eringen (1963). Verma (1986) and Verma et al. (1988) discussed the magnetoelastic shear and transverse surface waves in self-reinforced bodis. The work related to wave propagation in elastic solids under electromagnetic field is found in the articles written by Chattopadhyay and Choudhury (1990, 1995), Abd-Alla and Abo-Dahab (2008), Abo-Dahab and Singh (2009), Chattopadhyay et al. (2010, 2011), Chattopadhyay and Singh (2012, 2014), Kumar et al. (2015), Majhi et al. (2017), Ala et al. (2020).

1.5 Thermoelasticity

In the latter half of the 20th century, the study of non-isothermal problems in elasticity gained significance because of its relevance to mechanical, geological, and engineering materials. Thermoelasticity, which integrates the principles of heat conduction and elasticity, is pivotal in various fields such as nuclear reactors, aeronautics, high-energy particle accelerators, earthquake engineering, and soil dynamics. This theory examines the influence of heat on the deformation of elastic media and the reverse effects. Variations in thermal boundary conditions or heat sources over time generate thermal stress, necessitating the use of various coupled thermoelasticity equations to address these challenges.

In 1822, Joseph Fourier formulated the Fourier's law of heat conduction, a fundamental principle that states the behavior of heat transfer in a material. The law states that the rate of heat conduction through a material is proportional to the negative gradient of the temperature and the area through which the heat flows i.e.

$$\vec{q} = -k \text{ grad } T \tag{1.5.1}$$

where $\vec{q}$ represents the heat flux vector, k is the material's thermal conductivity and grad T denotes the temperature gradient vector. The classical theory of thermoelasticity is a foundational framework that combines the principles of heat conduction and elasticity to study the interactions between thermal and mechanical fields in solid materials. This

theory is instrumental in understanding how temperature changes influence the deformation and stress in elastic bodies and vice versa. The heat conduction equation in the classical theory of thermoelasticity is

$$k\nabla^2 T + Q = \rho c\dot{T} \tag{1.5.2}$$

where ∇^2 is the Laplacian operator, Q is the internal heat source per unit volume, ρ is the density and c is the specific heat capacity. The classical theory of thermoelasticity, also known as the uncoupled theory, is parabolic in nature. This traditional theory assumes an infinite velocity for heat wave propagation, which is not physically realistic. To address this paradox of infinite speed, non-classical theories have been introduced and developed. Coupled thermoelasticity theories provide a more accurate and comprehensive understanding of the interactions between thermal and mechanical fields in materials. By incorporating the mutual influences of temperature and deformation, these theories address the limitations of classical thermoelasticity and offer valuable insights for various engineering applications. The coupled thermoelasticity (CTE) theory is introduced by Biot (1956) in which Fourier's law of heat conduction transforms into the diffusion equation. Lord and Shulman (1967) extended the CTE by introducing the one relaxation time parameter that ensured finite speed for thermal signals. The heat conduction under Lord-Shulman (L-S) theory is

$$\alpha\nabla^2 T + \frac{\alpha}{k}Q - \beta\dot{\epsilon}_{kk} = \tau_0\ddot{T} + \dot{T} \tag{1.5.3}$$

where α is the thermal diffusivity, β is a coupling constant, ϵ_{kk} is the volumetric strain and τ_0 is the thermal relaxation time. Green and Lindsay (1972) further extends the L-S theory by introducing two thermal relaxation time in CTE, called temperature rate-dependent theory. In this theory the heat conduction equation is given by

$$\alpha\nabla^2 T + \frac{\alpha}{k}Q - \tau_2\dot{\epsilon}_{kk} = \tau_1\ddot{T} + \dot{T} \tag{1.5.4}$$

where τ_1 and τ_2 are thermal relaxation times.

Green and Naghdi (1992, 1993) investigated the thermoelasticity theory by incorporating more realistic assumptions about heat conduction and material response in 3 models known as G-N theory of type I, II and III. Type I model is the classical theory of thermoelasticity, where heat conduction is described by Fourier's law. Type II model assumes that the rate of temperature change is directly related to the mechanical deformation without any heat flux. Type III model incorporates both the effects of the mechanical deformation and

a non-Fourier heat conduction law, allowing for the presence of thermal waves or finite speed of heat propagation. Simple-phase-lag(SPL) model has been studied by Ozisik and Tzou (1994) via single-phase-lag and Tzou (1995a,b) through dual-phase-lag (1^{st} phase-lag: temperature gradient and 2^{nd} phase-lag: heat flux). Choudhuri (2007) proposed three-phase-lag(TPL) model by incorporating a 3^{rd} phase-lag of the thermal displacement gradient. Effect of rotation, gravity and initial stress on generalized thermoelastic solids under different theories is studied by Othman and Lotfy (2011, 2015) Othman and Atwa (2013); Othman et al. (2014a, 2015); Othman and Abed-Elaziz (2017). Refined multi-phase-lag theory for thermomechanical response of microbeams is examined by Zenkour (2018). Abouelregal (2019, 2020a,b) studied many papers on thermoelasticity model with higher order time derivatives and phase-lags. Recently Lotfy and El-Bary (2024) studied a mode I crack problem with rotational effet in fiber-reinfored thermoelastic medium under L-S theory.

1.6 Quasicrystal

The discovery of quasicrystals in 1982 was a significant milestone in the history of physics. This finding sparked considerable interest among researchers due to the unique properties of these new solid structures. The thermodynamic stability of most quasicrystals produced so far has established them as novel materials, attracting widespread scientific attention.

1.6.1 Discovery of quasicrystal(QC)

The first observation of QCs occurred in April 1982, when D. Shechtman, a guest scholar at the Bureau of Standards in the USA, noticed that a rapidly cooled Al-Mn alloy exhibited five-fold orientational symmetry through electron microscopy. This was evident from the diffraction patterns with bright diffraction spots and sharp Bragg reflections. The five-fold symmetry contradicted the fundamental symmetry laws of crystals, leaving the discovery puzzling and not understood for nearly two years. I. Blech, a colleague of Shechtman's in Israel, provided strong support, suggesting that it might be an icosahedral glass. Following a consultation with D. Gratias, a mathematical crystallographer at the Centre National de la Recherche Scientifique in France, the group submitted a brief article to Physical Review Letters (PRL) in October 1984. The article by Shechtman et al. (1984) was published several weeks later. Four weeks later, Levine and Steinhardt (1984) published their work in Physical Review Letters (PRL), introducing an ordered structure with quasiperiodicity and

formally naming the novel alloy a "quasicrystal". Their theoretical (computed) diffraction pattern matched the experimental observations exceptionally well. Shortly thereafter, other research groups, including Ye et al. (1985) and Zhang et al. (1985), discovered similar structures with five-fold symmetry and icosahedral QCs in Ni-V and Ni-Ti alloys.

Icosahedral QCs are a type of 3D quasicrystal with quasiperiodic atomic arrangements in all three directions. Another example of a 3D QC is the cubic QC, later observed by Feng et al. (1989). Subsequently, 2D QCs were discovered, featuring atomic arrangements that are quasiperiodic in two directions and periodic in the third direction. These correspond to the 5-, 8-, 10-, and 12-fold symmetrical axes of two-dimensional QCs identified so far. This results in four types of 2D QCs, each exhibiting 5-fold (pentagonal), 8-fold (octagonal), 10-fold (decagonal), and 12-fold (dodecagonal) rotational symmetries, as documented by Fung et al. (1986); Urban et al. (1986); Wang et al. (1987). Additionally, there is a class of 1D QCs where the atomic arrangement is quasiperiodic along one axis and periodic in the plane perpendicular to that axis, as reported by Bendersky (1985); Chattopadhyay et al. (1987); Terauchi et al. (1988); Kunji et al. (1987); Yang (1996).

1.6.2 One-dimensional quasicrystals in elasticity

In 1D QCs, the atomic arrangement exhibits a quasiperiodic pattern along one direction, say the $z-$direction, while maintaining a periodic structure in the plane perpendicular to the direction ($xy-$plane). Despite being termed "one-dimensional," the overall structure is three-dimensional, encompassing a three-dimensional body. This type of quasicrystal can be understood as a projection of a periodic crystal from four-dimensional space onto the three-dimensional physical space. Consequently, there are four non-zero displacement components: u_1, u_2, u_3 and w_3 with $w_1 = w_2 = 0$. Therefore, the elasticity of one-dimensional quasicrystals inherently involves a four-dimensional framework.

In Table 1.1, we discuss the crystal systems and Laue classes of one-dimensional quasicrystals, focusing on the concept of point groups, and we do not concern with that.

A theoretical description of the deformed state of quasicrystals (QCs) necessitates the combined analysis of interconnected phonon and phason fields. The presence of phason fields makes the elasticity of QCs more intricate than that of conventional crystals. In QCs, alongside the phonon displacement field $u = (u_1, u_2, u_3)$, there is also a phason displacement field w_3. These fields interact with each other.

TABLE 1.1: Systems, Laue classes and point groups of one-dimensional quasicrystals

Systems	Laue classes	Point groups
Triclinic	1	$1\ \bar{1}$
Monoclinic	2	$2\ \ m_h\ \ 2/m_h$
	3	$2_h\ \ m\ \ 2_h/m$
Orthorhombic	4	$2_h2_h2\ \ mm2\ \ 2_hmm_h\ \ mmm_h$
Tetragonal	5	$4\ \ \bar{4}\ \ 4/m_h$
	6	$42_h2_h\ \ 4mm\ \ \bar{4}2_hm\ \ 4/m_hmm$
Rhombohedral or Trigonal	7	$3\ \ \bar{3}$
	8	$32_h\ \ 3m\ \ \bar{3}m$
Hexagonal	9	$6\ \ \bar{6}\ \ 6/m_h$
	10	$62_h2_h\ \ 6mm\ \ \bar{6}m2_h\ \ 6/m_hmm$

Let us consider the phonon strains ϵ_{ij}, phason strains w_{3j}, the phonon stress τ_{ij} and phason stress H_{3j}. Then the generalized Hooke's laws of the elasticity problem of one-dimensional quasicrystals are

$$\tau_{ij} = C_{ijkl}\epsilon_{kl} + R_{ij3l}w_{3l}, \quad (i,\ j,\ k,\ l = 1,\ 2,\ 3) \tag{1.6.1}$$

$$H_{3j} = R_{kl3j}\epsilon_{kl} + K_{3j3l}w_{3l} \tag{1.6.2}$$

and the equations of equilibrium in the absence of body forces are

$$\begin{aligned} &\partial_1\tau_{11} + \partial_2\tau_{12} + \partial_3\tau_{13} = 0, \\ &\partial_1\tau_{12} + \partial_2\tau_{22} + \partial_3\tau_{23} = 0, \\ &\partial_1\tau_{13} + \partial_2\tau_{23} + \partial_3\tau_{33} = 0, \\ &\partial_1 H_{31} + \partial_2 H_{32} + \partial_3 H_{33} = 0. \end{aligned} \tag{1.6.3}$$

Additionally, geometry equations are expressed as

$$\epsilon_{ij} = \frac{1}{2}\left(\partial_i u_j + \partial_j u_i\right), \quad w_{3j} = \partial_j w_3, \quad i,j = 1,\ 2,\ 3 \tag{1.6.4}$$

with $\partial_j = \frac{\partial}{\partial x_j}$.

Triclinic system:

In the triclinic one-dimensional quasicrystal system, the point group may be 1 or $\bar{1}$, and the stress-strain relationship becomes(Wang et al., 1997)

$$[\tau\ H] = [C\ K\ R][\epsilon\ w] \tag{1.6.5}$$

where

$$[\tau\ H] = [\tau_{11}\ \tau_{22}\ \tau_{33}\ \tau_{23}\ \tau_{31}\ \tau_{12}\ H_{33}\ H_{31}\ H_{32}]^T, \tag{1.6.6}$$

$$[C\ K\ R] = \begin{bmatrix} C & R \\ R^T & K \end{bmatrix}, \tag{1.6.7}$$

$$[\epsilon\ w] = [\epsilon_{11}\ \epsilon_{22}\ \epsilon_{33}\ 2\epsilon_{23}\ 2\epsilon_{31}\ 2\epsilon_{12}\ w_{33}\ w_{31}\ w_{32}]^T. \tag{1.6.8}$$

In equation (1.6.7) the notations C, K and R are defined as follows:

$$C = \begin{bmatrix} C_{1111} & C_{1122} & C_{1133} & C_{1123} & C_{1131} & C_{1112} \\ & C_{2222} & C_{2233} & C_{2223} & C_{2231} & C_{2212} \\ & & C_{3333} & C_{3323} & C_{3331} & C_{3312} \\ & & & C_{2323} & C_{2331} & C_{2312} \\ & & & & C_{3131} & C_{3112} \\ & & & & & C_{1212} \end{bmatrix}, \tag{1.6.9}$$

$$K = \begin{bmatrix} K_{3333} & K_{3331} & K_{3332} \\ & K_{3131} & K_{3132} \\ & & K_{3232} \end{bmatrix} \tag{1.6.10}$$

and

$$R = \begin{bmatrix} R_{1133} & R_{1131} & R_{1132} \\ R_{2233} & R_{2231} & R_{2232} \\ R_{3333} & R_{3331} & R_{3332} \\ R_{2333} & R_{2331} & R_{2332} \\ R_{3133} & R_{3131} & R_{3132} \\ R_{1233} & R_{1231} & R_{1232} \end{bmatrix}. \tag{1.6.11}$$

So, the total independent elastic constants are $n_C + n_K + n_R = 21 + 6 + 18 = 45$.

Monoclinic system:

In the monoclinic 1D QC system, there exist two Laue classes: $2/m_h(2,\ m_h,\ 2/m_h)$ and $2_h/m(2_h,\ m,\ 2_h/m)$. The unique axis for the point groups $(2,\ m_h,\ 2/m_h)$ is the z axis. In this context, the non-zero phonon, phason, and phonon-phason coupling constants will be as follows: $C_{11},\ C_{22},\ C_{33},\ C_{12},\ C_{13},\ C_{16},\ C_{23},\ C_{26},\ C_{36},\ C_{44},\ C_{45},\ C_{55},\ C_{66},\ K_1,\ K_2,\ K_3,\ K_4,\ R_1,\ R_2,\ R_3,\ R_4,\ R_5,\ R_6,\ R_7,\ R_8$. The short notation is used for the phonon elastic constants, such that the index $11 \to 1,\ 22 \to 2,\ 33 \to 3,\ 23 \to 4,\ 31 \to 5,\ 12 \to 6$ andC_{ijkl} is denoted by C_{pq}; for the phason elastic constants, $K_{3131} = K_1,\ K_{3232} = K_2,\ K_{3333} = K_3,\ K_{3132} = K_4$ and for the phonon-phason coupling elastic

constants, $R_{1133} = R_1$, $R_{2233} = R_2$, $R_{3333} = R_3$, $R_{2331} = R_4$, $R_{2332} = R_5$, $R_{3131} = R_6$, $R_{3132} = R_7$ and $R_{1233} = R_8$. Therefore, the total independent elastic constants are $n_C + n_K + n_R = 13 + 4 + 8 = 25$.

The unique axis for the point groups (2_h, m, $2_h/m$) lies in the horizontal plane, e.g. along the y axis. In this context, the corresonding non-zero elastic constants are C_{11}, C_{22}, C_{33}, C_{12}, C_{13}, C_{15}, C_{23}, C_{25}, C_{35}, C_{44}, C_{66}, C_{55}, C_{46}, K_3, K_1, K_5, K_2, R_1, R_2, R_3, R_{12}, R_9, R_{10}, R_{11}, R_6, R_5, R_{13}. The short notation is used for $K_{3331} = K_5$, $R_{3133} = R_{12}$, $R_{1131} = R_9$, $R_{2231} = R_{10}$, $R_{3331} = R_{11}$, $R_{1232} = R_{13}$ and the total number of independent elastic constants are $n_C + n_K + n_R = 13 + 4 + 10 = 27$.

Orthorhombic system:

In this system the point groups (2_h2_h2, $mm2$, 2_hmm_h, mmm_h) belong to the same class and the non-zero elastic constants are C_{11}, C_{22}, C_{33}, C_{12}, C_{13}, C_{23}, C_{44}, C_{55}, C_{66}, K_1, K_2, K_3, R_1, R_2, R_3, R_5, R_6. So, the total independent elastic constants are $n_C + n_K + n_R = 9 + 3 + 5 = 17$.

Tetragonal system:

Two Laue classes, i.e. $4/m_h(4,\ \bar{4},\ 4/m_h)$ and $4/m_hmm(42_h2_h,\ 4mm,\ \bar{4}2_hm,\ 4/m_hmm)$, belong to this system. For the Laue class $4/m_h$, the non-zero elastic constants are $C_{11} = C_{22}$, C_{33}, $C_{44} = C_{55}$, C_{66}, C_{12}, $C_{13} = C_{23}$, $C_{16} = -C_{26}$, K_3, $K_1 = K_2$, $R_1 = R_2$, R_3, $R_5 = R_6$, $R_4 = -R_7$. Hence, the total independent elastic constants are 13.

For the Laue class $4/m_hmm$, the nonzero elatic constants are $C_{11} = C_{22}$, C_{33}, $C_{13} = C_{23}$, C_{66}, C_{12}, $C_{44} = C_{55}$, K_3, $K_1 = K_2$, $R_1 = R_2$, R_3, $R_5 = R_6$.

Trigonal system:

In this system there are two Laue classes $\bar{3}(3$ and $\bar{3})$ and $\bar{3}m(3m,\ 32_h,\ \bar{3}m)$. For the first Laue class i.e. $\bar{3}$, the non-zero elastic constants are $C_{11} = C_{22}$, C_{33}, $C_{44} = C_{55}$, C_{12}, $C_{13} = C_{23}$, $2C_{66} = C_{11} - C_{12}$, $C_{14} = -C_{24} = C_{56}$, $C_{25} = C_{46} = -C_{15}$, K_3, $K_1 = K_2$, $R_1 = R_2$, R_3, $R_5 = R_6$, $R_4 = -R_7$, $R_9 = -R_{10} = -R_{13}$, $R_{1132} = -R_{2232} = R_{1231}$. For the other three point groups ($3m$, 32_h, $\bar{3}m$), we have $C_{15} = 0$, $R_9 = 0$ and $R_4 = 0$ in the elastic constants present in the Laue class $\bar{3}$.

Hexagonal system:

Two Laue classes: $6/m_h(6,\ \bar{6},\ 6/m_h)$ and $6/m_hmm(62_h2_h,\ 6mm,\ \bar{6}m2_h,\ 6/m_hmm)$ belong to this system. The non-zero elastic constants are $C_{11} = C_{22}$, C_{33}, $C_{44} = C_{55}$, C_{12},

$C_{13} = C_{23}$, $2C_{66} = C_{11} - C_{12}$, K_3, and $K_1 = K_2$, and $R_1 = R_2$, R_3, $R_5 = R_6$, $R_4 = R_7$. Therefore, the total number of independent elastic constants are $n_C + n_K + n_R = 5+2+4 = 11$.

For the other Laue class i.e. $6/m_h mm$ the elastic constants are same as the Laue class $6/m_h$ with $R_4 = 0$.

Based on literature review, I represent my thesis into distinct chapters. My research focuses on addressing elastodynamic problems concerning crack geometry. Chapter 2 will provide a concise overview of the methodology utilized in my research work.

In chapter 3, section 3.1 shows how a finite crack interacts with shear waves in an infinite magnetoelastic medium. The boundary value problem of a homogeneous, isotropic elastic material is converted into a Fredholm integral equation of the second kind. This integral equation is then solved using the perturbation method. The research discusses the effects of magnetic field interactions on the crack and calculates the stress intensity factor at the crack tip, presenting these findings for low frequencies. Additionally, the work evaluates and graphically presents the shear stress outside the crack, the crack opening displacement, and the crack energy.

The section 3.2 examines the diffraction of a Griffith crack located in an infinite strip of finite thickness due to the propagation of magnetoelastic shear waves. The study focuses on how a magnetic field affects the interaction with the Griffith crack. The mixed boundary value problem (MBVP) is reduced to dual integral equations. These equations are then transformed into a Fredholm integral equation of the second kind using Abel's transform. The Fox and Goodwin method is employed to numerically solve this integral equation. The analytical expression of stress intensity factor illustrates graphically, comparing scenarios with and without the influence of a magnetic field.

In section 3.3, I addressed the impact load problem on a finite crack within an infinite isotropic medium, considering the presence of a magnetic field on the crack surface. The study employs Laplace and Abel's transforms to convert the boundary value problem into a Fredholm integral equation of the second kind. This equation is solved using the asymptotic series expansion method for low frequencies. Expressions for the stress intensity factor (SIF) and crack opening displacement (COD) are derived in the Laplace transform domain and then converted to the time domain using Zakian's algorithm. The effect of the magnetic field on SIF and COD is analyzed and illustrated with graphs. The findings indicate that ferromagnetic materials like Iron, Cobalt, and Nickel are more effective in

preventing crack growth due to normal impact. However, the magnetic field does not inhibit crack growth in the case of sliding mode.

In chapter 4, section 4.1 presents a refined one-temperature thermoelastic model incorporating higher-order time derivatives and phase-lags to study a Mode-I crack in a rotating fiber-reinforced solid. The crack is stimulated to a specified temperature and normal stress. Using normal mode analysis, exact expressions for displacement, temperature, and stress components are derived. The model includes various generalized thermoelasticity theories as special cases. The convergence of this refined model is tabulated and compared with other theories. Graphical representations illustrate the variations in temperature, displacements, and stresses with respect to crack length, highlighting the effects of phase-lags and thermal relaxation time. The analysis considers several theories, including Refined-phase-lag (RPL), simple-phase-lag (SPL), Green-Naghdi (G-N), Lord-Shulman (L-S), and Coupled thermoelasticity (CTE), both with and without rotation.

Section 4.2 examines the problem of two collinear cracks in an infinite thermoelastic transversely isotropic medium under a non-Fourier heat conduction law. The cracks are thermally insulated, preventing any thermal flow disturbances across them. The mode II thermal stress intensity factor and crack opening displacement are derived for a stress-free boundary condition and plotted to demonstrate the impact of crack length. Additionally, the study explores the behavior of the thermal stress intensity factor under Fourier (parabolic) heat conduction law and for a single crack scenario.

In the section 5.1 of chapter 5 the propagation of Love waves in a multilayered viscoelastic orthotropic medium with initial stress is investigated using a finite difference scheme. A complex dispersion relation is derived for $n-1$ layers over a half-space. For a single layer over a half-space, the real and imaginary parts of the dispersion relation correspond to the dispersion and attenuation curves are found respectively. The dispersion equation is validated against the classical Love wave equation for both single and double layers configurations over a half-space. The stability criterion for the finite difference method is established, along with expressions for phase and group velocities. The study examines how the viscoelastic parameter and initial stress affect the phase velocity and attenuation coefficient of Love waves. Additionally, the changes in phase and group velocity for different Courant numbers are illustrated with graphs.

Section 5.2 investigates the scattering behavior of Love waves induced by an interface crack between an orthotropic elastic layer and an isotropic elastic half-space where the

orthotropic layer serves as a wave guide medium. The Dispersion relation and phase velocity have been obtained by using convenient boundary conditions for the Love wave propagation. Using the method of Fourier transform and integral equation, the study derives the conditions governing wave propagation and scattering phenomena in the interfaced medium. The expression of the most important fracture quantities, such as dynamic stress intensity factor (DSIF) and crack opening displacement (COD) have been obtained and demonstrated graphically. Results demonstrate the dependence of scattering characteristics on the material properties, crack dimensions, layer height and wave frequencies. The findings contribute to a deeper understanding of Love wave propagation in composite materials, with implications for non-destructive testing and evaluation of structural integrity in engineering applications.

Chapter 6 explores the interaction of anti-plane shear waves with two collinear cracks in 1D hexagonal piezoelectric QCs. The MBVP is converted into three pairs of dual integral equations, which are analytically solved via the Hilbert transform. The explicit expressions are derived for the dynamic stress intensity factors (DSIFs) of the phonon and phason fields, COD, and electric displacement (ED). The DSIFs of the phonon and phason fields, COD, and ED are depicted to illustrate the effects of crack length and electric boundary conditions. Additionally, the DSIFs of the phonon field and COD are graphically shown for a single crack.

Chapter 2

Methodology

The research work that we propose mainly concerns Elastodynamic problems, specifically crack problems in elastic, magnetoelastic, thermoelastic, thermoelectric, piezoelectric, etc. composite medium and wave propagation phenomena in layered structure in the presence of viscoelasticity, heterogeneity through varying substances. The discussion is mainly theoretical with an intention to explain the experimental facts of different kind of surface waves and body waves by obtaining the dispersion relation. In case of crack problems our motive is to find the SIF, CTOD, stress components, temperature components, crack energy, etc. to characterize the crack toughness in different composition and to prevent the crack growth. The following methods are useful to solve boundary value problems in elasticity and also for numerical calculation.

1. Dual Integral Equation Method
2. The Solution of Integral Equation by Hilbert Transform Technique
3. The Numerical Solution of Non-singular Linear Integral Equations by Fox and Goodwin Method
4. Numerical Inversion of Laplace Transform
5. Modified Thomson-Haskell's Matrix Method
6. Finite Difference Method

2.1 Dual Integral Equation Method

When a MBVP is prescribed, this approach can be applied adequately. At first the MBVP is reduced to a system of DIEs by the use of Fourier transform or other suitable transform. Then this method is utlized to reduce the set of DIEs to a single Fredholm type integral equation of an unknown function. Once the FIE is solved, the required function can be acquired with the help of simple integrations.

Let us suppose that a MBVP is transformed by suitable integral transform, it can be described by a set of dual integral equations and have the following form

$$\int_0^\infty \xi^{-1}\Big[1+L(\xi)\Big]T(\xi)J_\nu(r\xi)\ d\xi = g(r), \quad 0 \le r < l \tag{2.1.1}$$

$$\int_0^\infty T(\xi)J_\nu(r\xi)\ d\xi = h(r), \qquad r > l \tag{2.1.2}$$

where the functions $L(\xi)$, $g(r)$, and $h(r)$ are known. According to Noble (1963), when $\nu > -\frac{1}{2}$,

$$T(\xi) = \sqrt{\frac{2\xi}{\pi}}\left(\int_0^l x^{1/2}\phi(x)J_{\nu-\frac{1}{2}}(\xi x)\ dx + \int_l^\infty x^{\nu+\frac{1}{2}}\psi(x)J_{\nu-\frac{1}{2}}(\xi x)\ dx\right),$$

where $\phi(x)$ satisfies the FIE

$$\phi(x) + \frac{1}{\pi}\int_0^l \mathcal{M}(y,x)\phi(y)\ dy = x^{-\nu}\mathcal{F}(x) - \mathcal{H}(x), \qquad 0 \le x < l \tag{2.1.3}$$

in which

$$\mathcal{M}(y,x) = \pi\sqrt{yx}\int_0^\infty \xi L(\xi)J_{\nu-\frac{1}{2}}(y\xi)J_{\nu-\frac{1}{2}}(x\xi)\ d\xi,$$

$$\mathcal{F}(x) = \frac{d}{dx}\int_0^x g(r)r^{\nu+1}(x^2-r^2)^{-1/2}\ dr,$$

$$\mathcal{H}(x) = x^{1/2}\int_0^\infty \xi L(\xi)J_{\nu-\frac{1}{2}}(\xi x)d\xi\int_l^\infty t^{\nu+\frac{1}{2}}\psi(t)J_{\nu-\frac{1}{2}}(\xi t)\ dt$$

and

$$\psi(t) = \int_t^\infty h(r)r^{-\nu+1}(r^2-t^2)^{-1/2}\ dr.$$

The integral equation (2.1.3) can be solved for $\phi(x)$ and consequently $T(\xi)$ can be obtained.

2.2 The Solution of Integral Equation by Hilbert Transform Technique

The solution of integral equation (Srivastava and Lowengrub, 1970)

$$\frac{2}{\pi}\int_a^b \frac{xf(x^2)}{x^2-t^2}\,dx = \mathcal{Q}(t), \qquad a<t<b \tag{2.2.1}$$

can be obtained using Hilbert transform technique in the form

$$f(x^2) = -\frac{2}{\pi}\frac{\sqrt{x^2-a^2}}{\sqrt{b^2-x^2}}\int_a^b \frac{\sqrt{b^2-t^2}}{\sqrt{t^2-a^2}}\frac{t\mathcal{Q}(t)}{t^2-x^2}\,dt + \frac{D}{\sqrt{(x^2-a^2)(b^2-x^2)}} \tag{2.2.2}$$

with the condition that $\mathcal{Q}$ must be an even function of t so that integral converges and D is an arbitrary constant.

2.3 The Numerical Solution of Non-singular Linear Integral Equations by Fox and Goodwin Method

An integral equation that has fixed limits is referred to as the Fredholm type, while an integral equation with variable limits is known as the Volterra type. The FIEs of the first and second kind are respectively defined as

$$\int_a^b L(x,y)g(y)\,dy = h(x) \tag{2.3.1}$$

$$\int_a^b L(x,y)g(y)\,dy = h(x)+g(x) \tag{2.3.2}$$

Another type of frequently used equation is given by

$$\lambda\int_a^b L(x,y)g(y)\,dy = h(x) \tag{2.3.3}$$

In equations (2.3.1) and (2.3.2), g is the unknown function, the kernel $L(x,y)$ and the function $h(x)$ are known either analytically, graphically or numerically. On the other hand, equation (2.3.3) requires calculating both the eigen function g and the eigenvalue λ. To solve these equations, we can represent the integral as a finite sum of terms in the form $a_r L(x_s,y_r)g(y_r)$, where the values of L and h are known at discrete points x_s and y_r. This requires a numerical integration procedure.

Numerical Integration

In most cases, it is more advantageous to use formulas based on differences rather than Lagrangian polynomials. With difference formulas, we can stop adding terms once their contributions become insignificant, while with Lagrangian polynomials, we cannot determine the appropriate degree of the polynomial without examining the differences. We can express the finite-difference integration formulas that are widely used in the following manner

$$\frac{1}{l}\int_a^{a+nl} g(x)dx = \frac{1}{2}g_0 + g_1 + ... + g_{n-1} + \frac{1}{2}g_n + \Delta, \tag{2.3.4}$$

where $g_0 = g(a)$, $g_r = g(a + rl)$ and Δ, the difference correction, is a function of the differences of g. The type of difference correction that we employ in integration formulas depends, as it does in differentiation formulas, on whether we want to use central differences or forward and backward differences.

If we use central differences, we can obtain a formula for the simplest case when n=1 and the integral is taken between adjacent pivotal points. The formula is as follows:

$$\frac{1}{l}\int_a^{a+l} g(x)dx = \frac{1}{2}(g_0 + g_1) - \frac{1}{12}\mu\delta^2 g_{\frac{1}{2}} + \frac{11}{720}\mu\delta^4 g_{\frac{1}{2}} + \cdots \tag{2.3.5}$$

and in the general case,

$$\frac{1}{l}\int_a^{a+nl} g(x)dx = \frac{1}{2}g_0 + g_1 + \cdots + g_{n-1} + \frac{1}{2}g_n + \Delta, \tag{2.3.6}$$

$$\Delta = (-\frac{1}{12}\Delta^1 + \frac{1}{24}\Delta^2 - \frac{19}{720}\Delta^3 \cdots)(g_n - g_0). \tag{2.3.7}$$

All the integration formulas mentioned earlier make use of differences that are computed using pivotal points outside the integration range. However, we can obtain a formula that only uses pivotal points within the range of integration by modifying equation (2.3.7) and representing the difference correction in the following way:

$$\Delta = -(\frac{1}{12}\nabla^1 + \frac{1}{24}\nabla^2 + \frac{19}{720}\nabla^3 ...)g_n + (\frac{1}{12}\Delta^1 - \frac{1}{24}\Delta^2 + \frac{19}{720}\Delta^3 ...)g_0. \tag{2.3.8}$$

The above formula is Gregory's integration formula, which is used to solve FIEs.

We only need to compute their solutions at pivotal points within the specified integration range since the kernel may not even be defined outside that range, making the use of formulas such as (2.3.6) impossible. The correction involved in Gregory's formula requires fewer terms, and the smaller coefficients in the formula result in slightly better accuracy.

Solution of Fredholm's equation of the second kind

We consider FIE of the second kind, given by equation (2.3.2).

We can express equation (2.3.2) in the following manner using equation (2.3.4) to represent the integral:

$$l\left[\frac{1}{2}L(x,0)g_0 + L(x,1)g_1 + ... + L(x,n-1)g_{n-1} + \frac{1}{2}L(x,n)g_n + \Delta(x)\right] = h(x) + g(x),$$

where $L(x,j)$ represents the value of $L(x,y)$ at the point (x,sl). We are free to choose any value for x as long as L is defined for that value, but regardless of the choice of x, the same $n+1$ values of g will appear at the equidistant pivotal points of the interval (a,b). To simplify the equation and make it easier to solve, it is preferable to choose the x values to be pivotal points of (a,b) since $g(x)$ is also present on the right side of the equation. By considering all pivotal points, we can transform the integral equation into a system of $(n+1)$ linear simultaneous equations

$$h\left[\frac{1}{2}L(r,0)g_0 + L(r,1)g_1 + ... + L(r,n-1)g_{n-1} + \frac{1}{2}L(r,n)g_n + \Delta_r\right] = h_r + g_r,$$

where $L(i,j)$ is the value of $L(x,y)$ at (rl,sl) and r takes the values $0,1,....,n$. Combining the g_r, we can express the equations as follows

$$\begin{aligned}
&\left(1 - \frac{1}{2}lL(0,0)\right)g_0 - lL(0,1)g_1 \cdots - lL(0,n-1)g_{n-1} - \frac{1}{2}lL(0,n)g_n = -h_0 + l\Delta_0,\\
&-\frac{1}{2}lL(1,0)g_0 + \{1 - lL(1,1)\}g_1 \cdots - lL(1,n-1)g_{n-1} - \frac{1}{2}lL(1,n)g_n = -h_1 + l\Delta_1,\\
&\qquad\qquad\qquad\qquad \cdots\cdots\cdots\cdots\cdots\cdots \qquad\qquad (2.3.9)\\
&-\frac{1}{2}lL(n-1,0)g_0 - lL(n-1,1)g_1 ... + \{1 - lL(n-1,n-1)\}g_{n-1} - \frac{1}{2}lL(n-1,n)g_n =\\
&\qquad\qquad\qquad\qquad\qquad\qquad\qquad\qquad -h_{n-1} + l\Delta_{n-1},\\
&-\frac{1}{2}lL(n,0)g_0 - lL(n,1)g_1 ... - lL(n,n-1)g_{n-1} + \left(1 - \frac{1}{2}lL(n,n)\right)g_n = -h_n + l\Delta_n.
\end{aligned}$$

Let's take a brief look at some of the potential solutions to these equations.

One possible approach for solving these equations is to use the Gregory formula, which expresses the Δ_r as linear functions of the g_r. If we also knew the order of the last significant difference in (2.3.8), we would have a known set of linear functions. We could then move the Δ_r terms from (2.3.9) to the left-hand side and form a set of equations

for the g_r, with different coefficients and only the h_r terms on the right. This method is similar to using a Lagrangian formula to represent the integral. It can be particularly useful for solving Volterra's equation, in which pivotal values of g are obtained successively and it is comparatively easy to find the adequate Lagrangian polynomial. However, for Fredholm's equation, most of the work involved in approximating the entire solution must be done before this information becomes available.

Another possible approach is to select a very small interval h with the aim of minimizing the impact of the Δ_r terms. However, this method may require solving a large number of linear equations, which can be time-consuming and prone to errors due to numerical instability. Alternatively, we could solve the equation while taking into account up to fourth differences in Δ, or even up to sixth differences and then compare the results to see how much these higher-order differences affect the solution.

An iterative approach appears to be more appealing for solving the problem at hand. This method involves first obtaining an initial estimate of the solution by disregarding the Δ_r term in equations (2.3.9) and using the simplest possible quadrature formula. Next, for each value of x we compute the differences between $L(x,0)g_0,\ L(x,1)g_1,$ and so on, using the approximate values of g_r that were just calculated. These differences can then be used to compute all the Δ_r, which are added as corrections to the right-hand side of equations (2.3.9). The corrections to g are then obtained trivially, and the process is repeated until there is no further change.

This technique can be represented using symbolic notation as follows: Let $\mathcal{A}$ represent the square matrix containing the coefficients of g_r, h denote the vector with coefficients h_r and Δ represent the vector with components Δ_r. By solving a series of equations in a sequential manner

$$\begin{aligned}
\mathcal{A}g^{(0)} &= -h, \\
\mathcal{A}g^{(1)} &= l\Delta(g^{(0)}), \\
\mathcal{A}g^{(2)} &= l\Delta(g^{(1)}), \\
&\cdots\cdots
\end{aligned}$$

and the final solution is given by

$$g = g^{(0)} + g^{(1)} + g^{(2)} + \cdots$$

The method described is the same as the one presented in the work of Fox and Goodwin (1953) when dealing with boundary-value problems that involve differential equations.

The selection of the interval l is somewhat arbitrary but requires consideration. We aim to minimize the number of linear equations while ensuring that the finite-difference equations remain meaningful. The method takes into account the examination of differences, thereby safeguarding against erroneous results arising from this aspect. Additionally, it ensures that an appropriate balance is maintained in retaining an adequate number of differences in the quadrature formulas. It should be noted that the truncation point may not necessarily be the same for all values of x.

2.4 Numerical solution of singular integral equation

Let us consider the singular integral equation in the following form

$$\frac{1}{\pi}\int_{-1}^{1}\frac{\psi(t)}{t-x}dt+\int_{-1}^{1}K(x,t)\psi(t)dt=f(x),\quad -1<x<1 \tag{2.4.1}$$

where $\psi(t)$ is unknown, f and K are known functions that are $H-$continuous on the interval $[-1,1]$. The second term in equation (2.4.1) is a bounded function of x as $\psi(t)$ and $K(x,t)$ are $H-$continuous. Therefore, to understand the singular behavior of ψ, it is sufficient to analyze the first part i.e. the dominant part of equation (2.4.1) only.

The unknown function ψ is either bounded or has integrable singularity at end points -1 and 1. In many physical scenarios, ψ represents either a 'potential-type' quantity (like displacement, temperature, electrostatic potential, velocity potential) or a 'flux-type' quantity (such as stress, heat flux, dislocation density, charge density, velocity). However, there are cases where the solution may demand a more pronounced zero condition at the end points (as seen in stress functions or lateral plate displacement) or a stronger singularity (as observed in transverse shear). Taking into account the physical characteristics of the singularity of the function ψ at the end points -1 and 1, we take

$$\psi(t)=w(t)g(t),\quad -1<x<1 \tag{2.4.2}$$

where $g(t)$ is a bounded continuous function in the closed interval $[-1,1]$ and the weight function $w(t)=(1-t)^{\alpha}(1+t)^{\beta}$, $-1<(\alpha,\beta)<1$, $-1<t<1$. We also take $k=-(\alpha+\beta)$.

With the help of equation (2.4.2), the integral equation (2.4.1) becomes

$$\frac{1}{\pi}\int_{-1}^{1}\frac{g(t)}{t-x}w(t)dt+\int_{-1}^{1}K(x,t)g(t)w(t)dt=f(x),\quad -1<x<1. \tag{2.4.3}$$

I. Gauss-Jacobi integration formula for $k=0$

In this case $\psi(t)$ is bounded at one end and exhibits an integrable singularity at the other, one has $\alpha=-\frac{1}{2},\ \beta=\frac{1}{2}$ or $\alpha=\frac{1}{2},\ \beta=-\frac{1}{2}$.

For $\alpha=-\frac{1}{2},\ \beta=\frac{1}{2}$ i.e. $w(t)=\sqrt{\frac{1+t}{1-t}}$, the integral equation (2.4.3) may be reduced to the following system of linear algebraic equations in $g(t_i)$ by Gauss-Jacobi integration formula

$$\sum_{i=1}^{n}\frac{2(1+t_i)}{2n+1}g(t_i)\left[\frac{1}{t_i-x_j}+\pi K(x_j,t_i)\right]=f(x_j),\quad (j=1,2,...,n) \tag{2.4.4}$$

where $t_i=\cos\left(\frac{2i-1}{2n+1}\pi\right),\quad (i=1,2,...,n)$ and $x_j=\frac{2j\pi}{2n+1},\quad (j=1,2,...,n)$. In the second case of $k=0$, i.e., for $\alpha=\frac{1}{2},\ \beta=-\frac{1}{2}$ the weight function is given by $w(t)=\sqrt{\frac{1-t}{1+t}}$. In this context, The integral equation (2.4.3) becomes

$$\sum_{i=1}^{n}\frac{2(1-t_i)}{2n+1}g(t_i)\left[\frac{1}{t_i-x_j}+\pi K(x_j,t_i)\right]=f(x_j),\quad j=1,2,...,n \tag{2.4.5}$$

with $t_i=\cos\left(\frac{2i\pi}{2n+1}\right),\quad (i=1,2,...,n)$ and $x_j=\cos\left(\frac{2j-1}{2n+1}\pi\right),\quad (j=1,2,...,n)$.

II. Gauss-Chebyshev integration formula for $k=1$

If the function $\psi(t)$ has integrable singularities at the end points i.e. $\alpha=-\frac{1}{2}=\beta$ and the weight function $w(t)$ is $\frac{1}{\sqrt{1-t^2}}$. For this problem, following a procedure presented by Erdogan and Gupta (1972); Erdogan et al. (1973), the integral equation (2.4.3) with an additional condition may be expressed as n linear algebraic equations and is given by

$$\sum_{i=1}^{n}\frac{1}{n}g(t_i)\left[\frac{1}{t_i-x_j}+\pi K(x_j,t_i)\right]=f(x_j), \tag{2.4.6}$$

$$\sum_{i=1}^{n}\frac{\pi}{n}g(t_i)=A, \tag{2.4.7}$$

where $t_i=\cos\left(\frac{2i-1}{2n}\pi\right),\quad (i=1,2,...,n)$ and $x_j=\cos\left(\frac{j\pi}{n}\right),\quad (j=1,2,...,n-1)$.

III. Gauss-Chebyshev integration formula for $k=-1$

If the function $\psi(t)$ is bounded at both ends i.e. $\alpha = \frac{1}{2} = \beta$ and the weight function $w(t) = \sqrt{1-t^2}$. Using Gauss-Chebyshev integration formula and following the similar procedure presented by Erdogan and Gupta (1972); Erdogan et al. (1973), the integral equation (2.4.3) can be written as

$$\sum_{i=1}^{n} \frac{1-t_i^2}{n+1} g(t_i) \left[\frac{1}{t_i - x_j} + \pi K(x_j, t_i) \right] = f(x_j), \tag{2.4.8}$$

where $t_i = \cos\left(\frac{i\pi}{n+1}\right), \quad (i = 1, 2, ..., n)$ and $x_j = \cos\left(\frac{\pi}{2}\frac{2j-1}{n+1}\right), \quad (j = 1, 2, ..., n+1)$.

Equation (2.4.8) is satisfied for $n+1$ values of x_j. Since, there are only n unknowns, $g(t_i)$, in (2.4.8), an equation corresponding to one of the x_j's must be ignored. In practice, it is often best to omit the point closest to $x = 0$. Generally n is selected to be an even number and the equation corresponding to $x_{1+\frac{n}{2}} = 0$ is ignored.

2.5 Numerical Inversion of Laplace Transform

Suppose the Laplace transform of the function $f(t)$ is denoted as $\mathcal{F}(s)$ and is defined as follows

$$\mathcal{F}(s) = \int_0^\infty e^{-st} f(t)\, dt, \quad s \geq 0 \ \ (s = \text{transform parameter})$$

Zakian's Algorithm

The algorithm Zakian (1970) is computed $f(t)$ as a sum of weighted nodes of $\mathcal{F}(s)$ and is presented as follows

$$f(t) = \sum_{i=1}^{N} K_i \mathcal{F}(s_i),$$

where the values of K_i, s_i and N are prescribed by a specific method. The algorithm developed by Zakian is presented by Rice and Do (2012). It expresses a time function as a finite series of exponential functions as

$$\sum_{i=1}^{N} K_i e^{\alpha_i t}.$$

The importance of this specification lies in the fact that Zakian's Algorithm exhibits high accuracy when applied to overdamped and mildly underdamped systems. However, it may not provide accurate results for systems characterized by prolonged oscillations.

By utilizing Zakian's Algorithm, we can determine the numerical value of $f(t)$ by employing the following equation when provided with $\mathcal{F}(s)$ and a specific time value t.

$$f(t) = \frac{2}{t} \sum_{i=1}^{5} \Re \left(K_i \mathcal{F} \left(\frac{\alpha_i}{t} \right) \right)$$

Table 2.1 gives the set of five complex constants for α_i and K_i.

TABLE 2.1: Set of five constants for α_i and K_i for the Zakian's Method

i	α_i	K_i
1	12.83767675 + ι 1.666063445	-36902.08210 + ι 196990.4257
2	12.22613209 + ι 5.012718792	61277.02524 - ι 95408.62551
3	10.93430308 + ι 8.409673116	-28916.56288 + ι 18169.18531
4	8.776434715 + ι 11.92185389	4655.361138 - ι 1.901528642
5	5.225453361 + ι 15.72952905	-118.7414011 - ι 141.3036911

Zakian's Algorithm is a fast and straightforward method to compute, but it has a limitation: it cannot calculate the initial value, $f(t)$ at $t = 0$. Additionally, if the system being analyzed has oscillations, the accuracy of $f(t)$ decreases after roughly the second cycle.

Stehfest Algorithm

The method of Stehfest (1970) is adopted for Laplace inversion and given by

$$f(t) = \frac{\ln 2}{t} \sum_{i=1}^{2N} c_i \mathcal{F} \left(\frac{i \ln 2}{t} \right),$$

where $\mathcal{F}(s)$ is the Laplace transform of the function $f(t)$ and

$$c_i = (-1)^{i+N} \sum_{j=\lfloor \frac{i+1}{2} \rfloor}^{\min(i,N)} \frac{j^N (2j)!}{(N-j)!j!(j-1)!(i-j)!(2j-i)!}.$$

This method is sufficiently accurate for a wide range of Laplace transforms (Davies and Martin, 1979).

2.6 Modified Thomson-Haskell's Matrix Method

In accordance with Novotnỳ and Vaněk (1973), we examine a medium that consists of n parallel layers which are homogeneous and isotropic. The n^{th} layer is treated as semi-infinite. As described in Haskell (1953), ω represents the angular frequency, c denotes the phase velocity, $k = \frac{\omega}{c}$ represents the wave number, v corresponds to the transverse displacement, and Y_z signifies the transverse shear stress. Within the m^{th} layer, let's denote the velocity of transverse waves as β_m and the torsion modulus as μ_m. The thickness of the layer can be represented by d_m. We define $r_{\beta_m} = \sqrt{\left(\frac{c^2}{\beta_m^2} - 1\right)}$ for $c \geq \beta_m$ and $r_{\beta_m} = -\iota\sqrt{\left(1 - \frac{c^2}{\beta_m^2}\right)}$ for $c < \beta_m$ and $Q_m = kr_{\beta_m}d_m$. We will assign the upper interface of the m^{th} layer is $(m-1)$ and the lower interface m. According to Haskell (1953), the expression for dimensionless velocity $\frac{\dot{v}}{c}$ and Y_z demonstrate a relationship between the lower and upper interfaces of the m^{th} layer, which can be described as follows:

$$\begin{aligned}\left(\frac{\dot{v}}{c}\right)_m &= \left(\frac{\dot{v}}{c}\right)_{m-1}\cos Q_m + (Y_z)_{m-1}\,\iota\mu_m^{-1}r_{\beta_m}^{-1}\sin Q_m,\\ (Y_z)_m &= \left(\frac{\dot{v}}{c}\right)_{m-1}\iota\mu_m r_{\beta_m}\sin Q_m + (Y_z)_{m-1}\cos Q_m.\end{aligned} \tag{2.6.1}$$

Equation (2.6.1) can be expressed in matrix form:

$$\begin{pmatrix}\frac{\dot{v}}{c}\\ Y_z\end{pmatrix}_m = \mathbf{a_m}\begin{pmatrix}\frac{\dot{v}}{c}\\ Y_z\end{pmatrix}_{\mathbf{m-1}},\ \mathbf{a_m} = \begin{pmatrix}\cos Q_m & \iota\mu_m^{-1}r_{\beta_m}^{-1}\sin Q_m\\ \iota\mu_m r_{\beta_m}\sin Q_m & \cos Q_m\end{pmatrix}. \tag{2.6.2}$$

Put $A = \mathbf{a_{n-1}a_{n-2}}\ldots\mathbf{a_1}$. The dispersion equation becomes

$$A_{21} + \mu_n r_{\beta_n} A_{11} = 0. \tag{2.6.3}$$

Haskell favored the dimensionless quantity $\frac{\dot{v}}{c}$ over the displacement v. It is worth noting that the stress Y_z is not considered a dimensionless quantity. However, Haskell's approach gained widespread adoption in subsequent research papers, particularly in the context of surface wave dispersion.

2.7 Finite Difference Method

Let's examine the wave equation $u_{tt} = c^2 u_{xx}$, where both the temporal and spatial derivatives are of second order. To approximate these derivatives, we use central difference

approximation. By considering a mesh with a size of Δt for the time variable t and a mesh of size Δx for the spatial x, we can denote the grid points as $(x_i,\ t_j) = (i\Delta x,\ j\Delta t)$,

$$u_{tt}\left(i\Delta x,\ j\Delta t\right) = \frac{u_i^{j+1} - 2u_i^j + u_i^{j-1}}{\left(\Delta t\right)^2} + O\left(\Delta t\right)^2,$$
$$u_{xx}\left(i\Delta x,\ j\Delta t\right) = \frac{u_{i+1}^j - 2u_i^j + u_{i-1}^j}{\left(\Delta x\right)^2} + O\left(\Delta x\right)^2,$$

where $u_i^j = u\left(i\Delta x, j\Delta t\right)$, for $i = 0, 1, \cdots, M$, $j = 0, 1, \cdots, N$. By introducing an error of order $O\left((\Delta x)^2 + (\Delta t)^2\right)$, the wave equation at the lattice points can be approximated by the following difference equation

$$\frac{u_i^{j+1} - 2u_i^j + u_i^{j-1}}{\left(\Delta t\right)^2} = c^2 \frac{u_{i+1}^j - 2u_i^j + u_{i-1}^j}{\left(\Delta x\right)^2}. \tag{2.7.1}$$

Denoting

$$s = c^2 \frac{\left(\Delta t\right)^2}{\left(\Delta x\right)^2},$$

and solving for u_i^{j+1}, we can write (2.7.1) as

$$u_i^{j+1} = s\left(u_{i+1}^j + u_{i-1}^j\right) + 2\left(1 - s\right)u_i^j - u_i^{j-1}. \tag{2.7.2}$$

The scheme Mitchell and Mitchell (1969) discussed an explicit method used to compute the numerical solution u_i^j. It is important to note that in order to calculate u_i^{j+1} using the scheme (2.7.2), values from two preceding time steps are utilized.

Now, let's examine the stability of the scheme (2.7.2) by substituting the separated solution $u_i^j = \xi^j e^{\iota k i \Delta x}$. The scheme will be considered stable only if $|\xi| \leq 1$, as any value greater than 1 would cause the scheme to produce exponentially growing solutions.

$$\xi^{j+1} e^{\iota k i \Delta x} = s\left(\xi^j e^{\iota k (i+1)\Delta x} + \xi^j e^{\iota k (i-1)\Delta x}\right) + 2(1-s)\xi^j e^{\iota k i \Delta x} - \xi^{j-1} e^{\iota k i \Delta x}.$$

By dividing both sides of the above equation by u_i^j and rearranging the terms, we can express it as follows:

$$\xi + \frac{1}{\xi} = s\left(e^{\iota k \Delta x} + e^{-\iota k \Delta x}\right) + 2(1-s) = 2 + 2s\left(\cos(k\Delta x) - 1\right).$$

Indicating $d = 2 + 2s\left(\cos(k\Delta x) - 1\right)$, we note that $d \leq 2$, as $\cos(k\Delta x) - 1 \leq 0$.

Then above equation becomes

$$\xi + \frac{1}{\xi} = d, \quad \text{or} \quad \xi^2 - d\xi + 1 = 0,$$

and the roots are

$$\xi_{\pm} = \frac{d \pm \sqrt{d^2 - 4}}{2}.$$

Now, if $d^2 - 4 > 0$, which means that $d < -2$, as d can't be greater than 2, the quadratic equation will yield two distinct real roots. However, one of these roots can be described as

$$\xi_{-} = \frac{d - \sqrt{d^2 - 4}}{2} < \frac{d}{2} < \frac{-2}{2} <= -1,$$

which would make an unstable condition.

In contrast, if the discriminant is non positive, i.e. $d^2 - 4 \leq 0$, which indicates $-2 \leq d \leq 2$, then the roots of the quadratic equation are complex,

$$\xi_{\pm} = \frac{d}{2} \pm \iota \frac{\sqrt{4 - d^2}}{2}, \text{ with norm } |\xi_{\pm}| = \sqrt{\frac{d^2}{4} + \frac{4 - d^2}{4}} = \sqrt{1} = 1.$$

This aligns with our intuitive understanding of solutions to the wave equation, as the separated solution's time component will be

$$T_n = \xi^n = (\cos\theta + \iota \sin\theta)^n = \cos(n\theta) + \iota \sin(n\theta).$$

Hence the stability condition is expressed as, $d^2 - 4 \leq 0$, or $-2 \leq d \leq 2$. When we substitute the relation of d in terms of s, we obtain

$$-2 \leq 2 + 2s\,(\cos(k\Delta x) - 1) \leq 2.$$

The inequality on the right side is consistently satisfied, whereas the most unfavorable scenario for the left inequality occurs when $\cos(k\Delta x) \approx -1$. This results in the inequality $-2 \leq 2 - 4s$. Hence, the stability condition can be summarized as

$$s = c^2 \frac{(\Delta t)^2}{(\Delta x)^2} \leq 1. \tag{2.7.3}$$

By defining the speed of the numerical scheme as the ratio $\frac{\Delta x}{\Delta t}$, the stability condition (2.7.3) can be interpreted as speed of the scheme $\geq c$, where c is the speed of exact solution. Consequently, the essential condition for ensuring stability of the numerical scheme is that the speed of the scheme must be at least as large as the speed of the exact equation.

Alterman and Karal Jr (1968) have used finite difference scheme for propagation of elastic waves in layered media.

Chapter 3

Crack under magnetic field

3.1 Mode-III crack in an infinite medium under magnetic field[1]

3.1.1 Introduction

In modern material science, fracture mechanics is an important branch used to refine the performance of mechanical components. Besides, it covers the study of several laws controlling crack growth. The Griffith theory utters that a crack propagates when the diminution of potential energy because of crack growth crosses over the increase of surface energy due to the formation of a new free surface. This theory is significant for elastic materials. Stress intensity factor(SIF) is one of the most fundamental quantities of crack-related problems. The SIF describes the stress state at the tip of the crack and is used to study failure norm due to fracture. Mal (1970b) has discussed interaction of elastic waves with Griffith cracks in homogeneous infinite elastic medium. Srivastava et al. (1978, 1980) have been treated Griffith crack problems basically located at the interface of two bonded dissimilar elastic half-spaces. Mandal and Mandal (2017) have studied the interface crack problem at orthotropic media.

Even though a number of problems regarding the interaction of crack due to shear waves in infinite elastic medium have been solved, the problem of interaction of a finite crack with shear waves in an infinite magnetoelastic medium is still unsolved. Therefore the present paper goals to examine the interaction of finite crack with shear waves in an infinite

[1]Panja, S. K., & Mandal, S. C. (2021). Interaction of a finite crack with shear waves in an infinite magnetoelastic medium. Applied and Computational Mechanics, 15(1), 45-56.

magnetoelastic medium by using perturbation method. The problem has been deduced to the Fredholm integral equation of 2nd kind using Fourier transformation, solution of the integral equation has been derived for low frequency by asymptotic series expansion method. To show the effect of magnetoelasticity SIF has been plotted graphically. Also, variations of other physical parameters like displacement on crack surface, scattered field, and crack energy have been presented by means of graphs.

3.1.2 Problem formulation

Let us assume a Griffith crack of finite width located at $|x_1| \leq l$, $-\infty \leq y_1 \leq \infty$, $z_1 = 0$ in the infinite medium. We Normalize all lengths by l and taking $\frac{x_1}{l} = x$, $\frac{y_1}{l} = y$, $\frac{z_1}{l} = z$, the new location of the crack become $|x| \leq 1$, $-\infty \leq y \leq \infty$, $z = 0$ (Figure 3.1) symbolized in Cartesian co-ordinate frame (x, y, z). We consider a time harmonic incidental shear wave $q_0 e^{-\iota\omega t}$ propagates along the positive z axis. The term $e^{-\iota\omega t}$ having oscillation is common

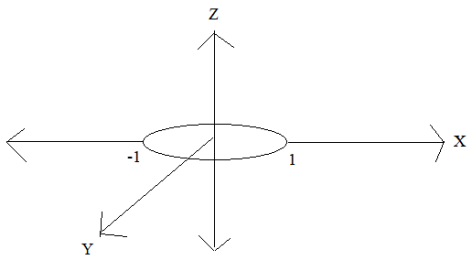

FIGURE 3.1: Configuration of the problem

to all field variables is being suppressed throughout the analysis. The only non dissipating dimensionless displacement component in y direction is considered to be $u_2 = u_2(x, z)$ as shear wave propagating in the z direction here. ∂_x, ∂_y and ∂_z denote the partial derivatives with respect to x, y and z variable respectively. Moreover, partial derivatives with respect to time t is denoted by ∂_t. The governing equations of shear wave propagation in presence of small elastic disturbances for a absolutely conducting isotropic elastic medium are

$$\partial_x \tau_{xy} + \partial_z \tau_{yz} + (\boldsymbol{J} \times \boldsymbol{B})_y + k^2 u_2 = 0, \tag{3.1.1}$$

where $k^2 = \rho\omega^2$ and $(\boldsymbol{J}\times\boldsymbol{B})_y$ is the electromagnetic force ($\boldsymbol{J}$ is the electric current density and $\boldsymbol{B}$ is the magnetic induction vector). The nonzero stress components are

$$\tau_{xy} = \mu\partial_x u_2 \text{ and } \tau_{yz} = \mu\partial_z u_2, \tag{3.1.2}$$

where coefficient μ is the elastic constant for isotropic medium. The popular Maxwell's equations conducting the electromagnetic field are

$$\boldsymbol{\nabla}\cdot\boldsymbol{B} = 0,\ \boldsymbol{\nabla}\times\boldsymbol{E} = -\partial_t\boldsymbol{B},\ \boldsymbol{\nabla}\times\boldsymbol{H} = \boldsymbol{J},\ \boldsymbol{B} = \mu_e\boldsymbol{H} \text{ and } \boldsymbol{J} = \sigma\left(\boldsymbol{E} + \partial_t\boldsymbol{u}\times\boldsymbol{B}\right), \tag{3.1.3}$$

where $\boldsymbol{E}$ is the induced electric field and magnetic field $\boldsymbol{H}$ describes both primary and induced magnetic fields. μ_e and σ are the induced permeability and conduction coefficient respectively. The linear Maxwell's stress tensor $\left(\tau_{ij}^0\right)^{M_x}$ due to the magnetic field is given by $\left(\tau_{ij}^0\right)^{M_x} = \mu_e(H_ib_j + H_jb_i - H_kb_k\delta_{ij})$. Let $\boldsymbol{H} = (H_1, H_2, H_3)$ and $b_i = (b_1, b_2, b_3)$ where b_i is the alter in the magnetic field. We have discarded the displacement current. With the help equation (3.1.3), we write

$$\nabla^2\boldsymbol{H} = \mu_e\sigma\left(\partial_t\boldsymbol{H} - \boldsymbol{\nabla}\times(\partial_t\boldsymbol{u}\times\boldsymbol{H})\right). \tag{3.1.4}$$

Equation (3.1.4) componentwise are

$$\begin{aligned}
\partial_t H_1 &= \frac{1}{\mu_e\sigma}\nabla^2 H_1,\\
\partial_t H_3 &= \frac{1}{\mu_e\sigma}\nabla^2 H_3 \text{ and}\\
\partial_t H_2 &= \frac{1}{\mu_e\sigma}\nabla^2 H_2 + \partial_x\left(H_1\partial_t u_2\right) + \partial_z\left(H_3\partial_t u_2\right).
\end{aligned} \tag{3.1.5}$$

In absolutely conducting medium (i.e. $\sigma\to\infty$), the equations (3.1.5) become

$$\partial_t H_1 = \partial_t H_3 = 0 \tag{3.1.6}$$

and

$$\partial_t H_2 = \partial_x\left(H_1\partial_t u_2\right) + \partial_z\left(H_3\partial_t u_2\right). \tag{3.1.7}$$

It is obvious from equation (3.1.6) that H_1 and H_3 have no perturbation, however equation (3.1.7) shows a small perturbation in H_2, say b. Therefore we have $H_1 = H_1'$, $H_2 = H_2' + b$ and $H_3 = H_3'$, where (H_1', H_2', H_3') are components of the initial magnetic field $\boldsymbol{H'}$. We can write $\boldsymbol{H'} = (H'\cos\theta, 0, H'\sin\theta)$, where $H' = |\boldsymbol{H'}|$ and θ is the angle at which the

wave passes the magnetic field. Thus we have

$$\boldsymbol{H} = (H' \cos\theta, b, H' \sin\theta). \tag{3.1.8}$$

We shall take $b = 0$ as initial value. Substituting equation (3.1.8) in equation (3.1.7), we acquire

$$\partial_t b = \partial_x \left(H' \cos\theta \partial_t u_2\right) + \partial_z \left(H' \sin\theta \partial_t u_2\right). \tag{3.1.9}$$

Integrating with respect to t, we have

$$b = H' \cos\theta \partial_x u_2 + H' \sin\theta \partial_z u_2. \tag{3.1.10}$$

Keeping in mind $\boldsymbol{\nabla}\left(\frac{H^2}{2}\right) = (\boldsymbol{H}\cdot\boldsymbol{\nabla})\,\boldsymbol{H} - (\boldsymbol{\nabla}\times\boldsymbol{H})\times\boldsymbol{H}$ and equation (3.1.3), we get

$$\boldsymbol{J}\times\boldsymbol{B} = \mu_e\left((\boldsymbol{H}\cdot\boldsymbol{\nabla})\,\boldsymbol{H} - \boldsymbol{\nabla}\left(\frac{H^2}{2}\right)\right). \tag{3.1.11}$$

Putting the y component of $\boldsymbol{J}\times\boldsymbol{B}$ in equation (3.1.1), we get the equation of motion in the form

$$P\partial_{xx}u_2 + Q\partial_{zz}u_2 + R\partial_{xz}u_2 + k^2 u_2 = 0, \text{ where } k^2 = \rho\omega^2 \tag{3.1.12}$$

and

$$\begin{aligned} P &= \mu + \mu_e H'^2 \cos^2\theta, \\ Q &= \mu + \mu_e H'^2 \sin^2\theta, \\ R &= \mu_e H'^2 \sin 2\theta. \end{aligned} \tag{3.1.13}$$

The equation (3.1.12) is to be solved subject to the boundary condition

$$\tau_{yz}(x,0) = -q_0, \ |x| \le 1 \tag{3.1.14}$$

and

$$u_2(x,0) = 0, \ |x| > 1 \tag{3.1.15}$$

where q_0 is a known constant. The solution of the equation (3.1.12) can be taken as

$$u_2(x,z) = \int_{-\infty}^{\infty} A(u) e^{-\alpha z} e^{-\beta z} e^{\iota u x} du, \ z > 0 \tag{3.1.16}$$

where $\alpha = \frac{\iota u R}{2Q}$ and $\beta = u\sqrt{\frac{1}{Q}\left(P - \frac{k^2}{u^2}\right) - \left(\frac{R}{2Q}\right)^2}$. The non vanishing stress component is written as

$$\tau_{yz}(x,z) = -\mu \int_{-\infty}^{\infty} (\alpha+\beta)\, A(u) e^{-\alpha z} e^{-\beta z} e^{\iota u x} du, \tag{3.1.17}$$

where $A(u)$ is a unknown function, which is to be determined from the boundary conditions.

3.1.3 Derivation of the integral equation

Boundary conditions (3.1.14) and (3.1.15) leads to following dual integral equation

$$\int_{-\infty}^{\infty} (\alpha+\beta)\, A(u) e^{\iota u x} du = \frac{q_0}{\mu},\ |x| \le 1 \tag{3.1.18}$$

and

$$\int_{-\infty}^{\infty} A(u) e^{\iota u x} du = 0,\ |x| > 1. \tag{3.1.19}$$

Equation (3.1.18) can be written as

$$\int_{-\infty}^{\infty} u\,[1 + H_1(u)]\, A(u) e^{\iota u x} du = \frac{q_0}{\gamma\mu},\ |x| \le 1 \tag{3.1.20}$$

where

$$\begin{aligned} &H_1(u) = \frac{H(u)}{\gamma} - 1,\ H(u) = \frac{\iota R + \sqrt{4Q\left(P - \frac{k^2}{u^2}\right) - R^2}}{2Q}, \\ &\gamma = \frac{\iota R + \sqrt{4QP - R^2}}{2Q} \text{ and } H_1(u) \to 0 \text{ as } u \to \infty. \end{aligned} \tag{3.1.21}$$

Let us assume the trial solution of equations (3.1.19) and (3.1.20) in the form

$$A(u) = \frac{q_0}{\gamma\mu} \int_0^1 r f(r) J_0(ur) dr \tag{3.1.22}$$

so that the equation (3.1.19) is trivially satisfied and equation (3.1.20) converts into

$$\int_0^1 r f(r) \int_0^{\infty} u\,[1 + H_1(u)]\, J_0(ur) \cos(ux) du dr = 1, \tag{3.1.23}$$

where J_0 is a Bessel function of first kind of order zero. Using Abel's transform in equation (3.1.23) and simplifying, we find out the following Fredholm integral equation of 2nd kind

$$f(r) + \int_0^1 sf(s)\kappa(s,r)ds = 1 \tag{3.1.24}$$

where

$$\kappa(s,r) = \int_0^\infty uH_1(u)J_0(us)J_0(ur)du. \tag{3.1.25}$$

It is notable that the kernel $\kappa(s,r)$ depicted by semi infinite integrals has a slow rate of convergence. Following the procedure of simple contour integration Mal (1970b) the infinite integral in (3.1.25) can be reduced into integral with finite limits to make the numerical analysis easier and is given by

$$\kappa(s,r) = -\frac{\iota}{2}\int_0^{\frac{k}{\sqrt{P}}} u\frac{\sqrt{R^2 + \frac{4Qk^2}{u^2} - 4PQ}}{Q\gamma}J_0(us)H_0^{(1)}(ur)du, \quad r > s. \tag{3.1.26}$$

3.1.4 Quantities of physical interest

Stress intensity factor:

Using equations (3.1.17) and (3.1.22) we obtain stress component outside the crack in the following form

$$\tau_{yz}(x,0) = q_0\frac{xf(1)}{\sqrt{x^2-1}} + O(1), \quad |x| > 1. \tag{3.1.27}$$

Defining dimensionless stress intensity factor by

$$K = \lim_{x\to 1^+}\frac{\sqrt{x-1}\,|\tau_{yz}(x,0)|}{q_0},$$

it can be deduced that

$$K = \frac{1}{\sqrt{2}}\,|f(1)|\,. \tag{3.1.28}$$

Crack opening displacemnet:

Another quantity of physical interest is the magnitude of the distance between the two edges of the crack and is calculated as

$$D(x) = |u_2(x,0+) - u_2(x,0-)| = \frac{q_0}{\mu}\left|\int_x^1 \frac{rf(r)}{\sqrt{r^2-x^2}}dr\right|. \tag{3.1.29}$$

In static scenario the crack opening displacement is the distance between two edges of the crack at the centre position of the crack, we write

$$D_0 = \frac{q_0}{\mu}$$

Normalizing $D(x)$ w.r.t the static displacement between two edges of the crack at the centre position of the crack, we get

$$D = \frac{D(x)}{D_0} = \left| \sqrt{1-x^2} f(1) - \int_x^1 \sqrt{r^2-x^2} f'(r) dr \right|, \quad |x| < 1. \tag{3.1.30}$$

Crack energy:

Crack energy can be calculated as

$$\begin{aligned} W^* &= 2q_0 \int_0^1 u_2(x,0) dx \\ &= 2q_0^2 \mu^{-1} \int_0^1 dx \int_x^1 \frac{r}{\sqrt{r^2-x^2}} f(r) dr \\ &= 2q_0^2 \mu^{-1} \int_0^1 r f(r) dr. \end{aligned} \tag{3.1.31}$$

The work done by a constant pressure q_0 to open a Griffith crack is given by

$$W_0 = \frac{q_0^2}{\mu},$$

so that

$$W = \frac{W^*}{W_0} = 2 \int_0^1 r f(r) dr. \tag{3.1.32}$$

Scattered field:

Shear stress $\tau_{yz}(x,z)$ outside crack for $x > 1$ and $z > 1$ is calculated from equations (3.1.17) and (3.1.22) and is written by the expression

$$\tau_{yz}(x,z) = -q_0 \int_0^\infty \int_0^1 (\alpha+\beta) r f(r) J_0(ur) e^{-\alpha z} e^{-\beta z} \cos(ux) du dr. \tag{3.1.33}$$

3.1.5 Solution of the integral equation

The iterative solution of the integral equation has been derived by perturbation method with the help of Srivastava et al. (1980). The iterative solution is valid for small values of k. The Bessel functions $J_0(y)$ and $H_0^{(1)}(y)$ has been expanded in ascending powers of

y as $J_0(y) = \sum_{n=0}^{\infty} a_{2n} y^{2n}$, $H_0^{(1)}(y) = \left(1 + \frac{2\iota}{\pi} log \frac{y}{2}\right) J_0(y) + \iota \sum_{n=0}^{\infty} b_{2n} y^{2n}$ where $a_0 = 1$, the values of a_{2n} and b_{2n} are given by Abramowitz and Stegun (1968). Using the above expression in equation (3.1.26), $\kappa(s,r)$ can be written as

$$\kappa(s,r) = \left(k^2 log\, k\right) \kappa_1(s,r) + \left(k^2\right) \kappa_2(s,r) + \left(k^2 log\, k\right)^2 \kappa_3(s,r) + \left(k^4 log\, k\right) \kappa_4(s,r) + O\left(k^4\right) \tag{3.1.34}$$

where

$$\begin{aligned}
\kappa_1(s,r) &= \frac{M_0}{\pi}, \\
\kappa_2(s,r) &= \frac{N_0}{\pi} + M_0 \left(-\frac{\iota}{2} + \frac{b_0}{2} + \frac{1}{\pi} log \frac{r}{2\sqrt{P}}\right), \\
\kappa_3(s,r) &= 0, \\
\kappa_4(s,r) &= \frac{a_2}{P\pi} \left(s^2 + r^2\right) M_2, \\
M_{2n} &= \int_0^1 \eta_{2n}(u) du, \\
N_{2n} &= \int_0^1 \eta_{2n}(u) log(u) du \\
\text{and } \eta_{2n}(u) &= u^{2n} \frac{\sqrt{R^2u^2 + 4PQ\left(1-u^2\right)}}{PQ\gamma}.
\end{aligned} \tag{3.1.35}$$

Now, $f(s)$ also can be expanded in the form

$$f(s) = f_0(s) + \left(k^2 log\, k\right) f_1(s) + \left(k^2\right) f_2(s) + \left(k^2 log\, k\right)^2 f_3(s) + \left(k^4 log\, k\right) f_4(s) + O\left(k^4\right) \tag{3.1.36}$$

and the following terms are derived

$$\begin{aligned}
f_0(s) &= 1, \\
f_1(s) &= -\frac{M_0}{2\pi}, \\
f_2(s) &= -\frac{N_0}{2\pi} + \frac{M_0}{4} \left(\iota - b_0 + \frac{2}{\pi} log\, 2\sqrt{P}\right) + \frac{M_0}{4\pi} \left(1 - s^2\right), \\
f_3(s) &= \left(\frac{M_0}{2\pi}\right)^2
\end{aligned}$$

and

$$f_4(s) = \frac{M_0}{\pi} \left[\frac{N_0}{2\pi} + \frac{M_0}{4} \left(b_0 - \iota - \frac{2}{\pi} log\, 2\sqrt{P}\right)\right] - \frac{a_2 M_2}{4P\pi} \left(1 + 2s^2\right) - \left(\frac{M_0}{4\pi}\right)^2 \left(3 - 2s^2\right). \tag{3.1.37}$$

Now, we can easily form $f(s)$ with the help of above expression and from equation (3.1.36).

3.1.6 Numerical calculation and discussions

We represent numerical results graphically for various physical quantities of crack due to shear wave propagation in an infinite magnetoelastic isotropic medium. For the case of isotropic elastic medium, we take the following data(Srivastava et al. (1983); Chattopadhyay and Maugin (1985), Gupta and Bhengra (2017) and Maugin (1981)):

$$\rho = 2.7\ gm/cm^3,\ \mu = \frac{E}{2(1+\eta)} \text{ where } \eta = 0.339 \text{ and } E = 7.05 \times 10^{11}\ dyne/cm^2.$$
$$\epsilon = \frac{\mu_e H'^2}{\mu} = 0.0,\ 0.15,\ 0.30;\ \theta = 10^\circ.$$

In figure 3.2 dimensionless SIF K has been plotted against frequency k. The graphs exhibit the effect of stress intensity factor for presence and absence of magnetoelasticity. For $\epsilon = 0.0$ the curve presents SIF without magnetoelasticity and for $\epsilon = 0.15,\ 0.30$ curve shows SIF's nature in magnetoelastic isotropic medium. It is noticeable that the stress intensity factor K decreases after some ascent with increase in frequency k for each instance. In the magnetoelastic medium the decrement rate of stress intensity factor is less than isotropic elastic media.

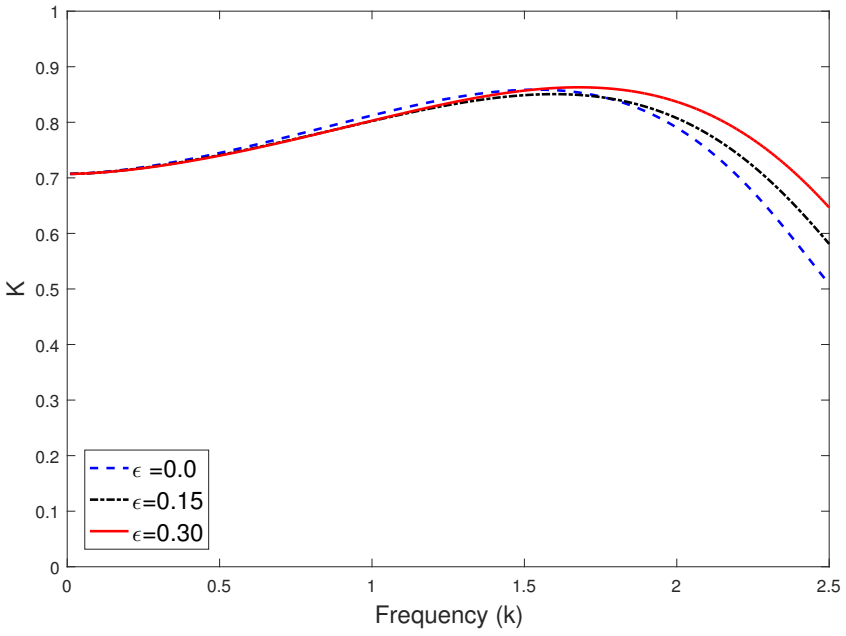

FIGURE 3.2: SIF K against dimensionless frequency (k)

Figure 3.3 is the plot of crack opening displacement (COD) versus crack position x in the absence of magnetoelasticity i.e. $\epsilon = 0$ for different values of frequency. It is visible that COD (D) versus crack position (x) graph is symmetric about $x = 0$, COD grips maximum

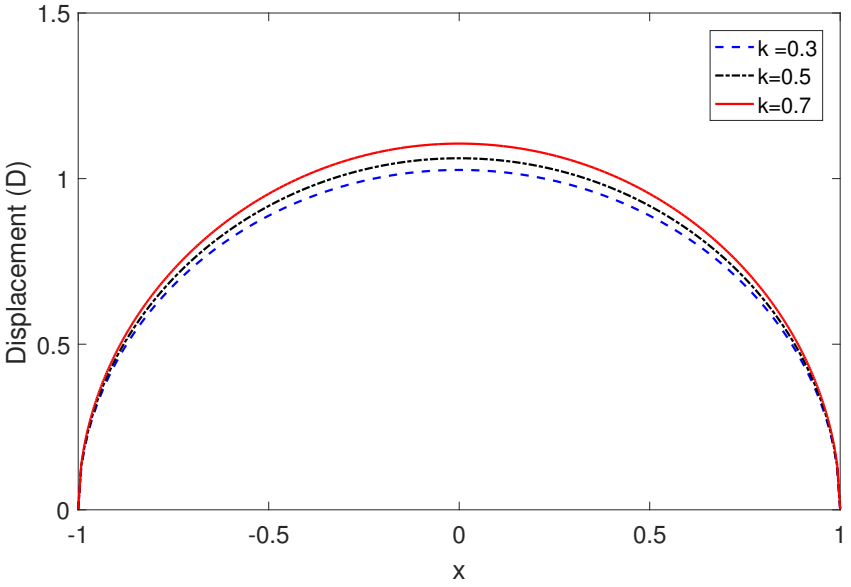

FIGURE 3.3: Displacement D against crack position x

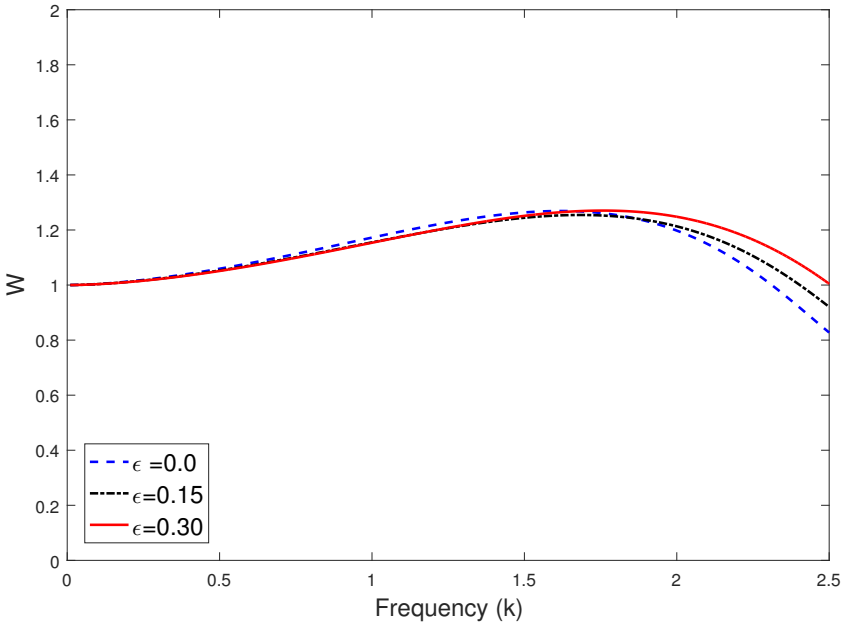

FIGURE 3.4: Crack energy W against dimensionless frequency k

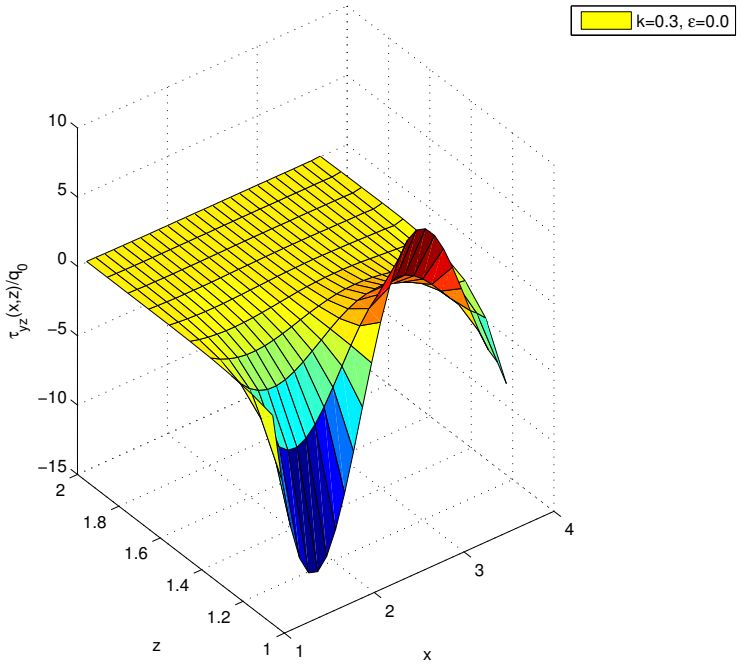

FIGURE 3.5: Scattered field outside the crack

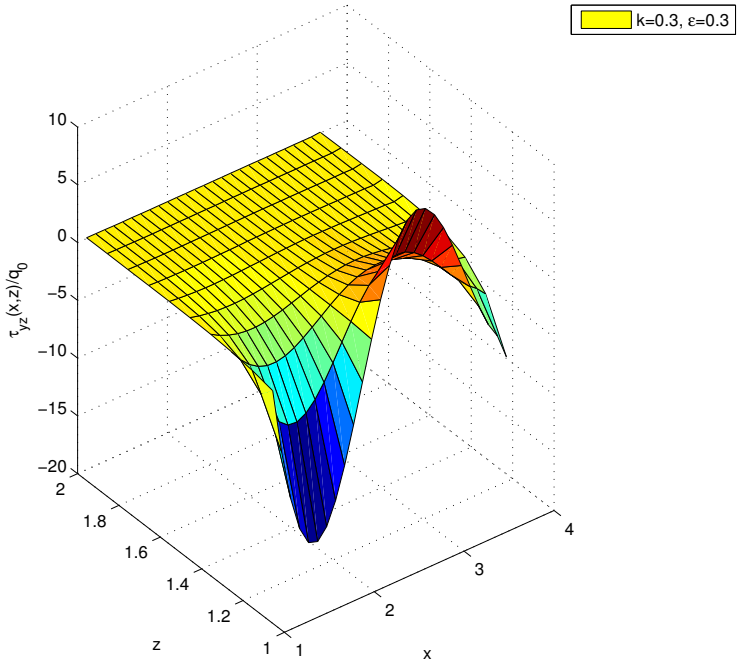

FIGURE 3.6: Scattered field outside the crack

value at $x = 0$ and reaches to zero at the tips of the cracks. COD increases gradually for higher values of frequency k. The change of graphs is insignificant for the magnetoelastic effect.

In figure 3.4 we have plotted the graph of crack energy W versus frequency k. The nature of this graph is quite similar to the graph of stress intensity factor versus frequency. only one thing is noticeable that crack energy W has a low decrement rate rather than stress intensity factor with an increase of frequency.

Figure 3.5 is the surface plot of shear stress just outside the crack for of $k = 0.3$ in the absence of magnetoelasticity. Figure 3.6 show the nature of scattered field in the magnetoelastic medium for $k = 0.3$.

3.1.7 Conclusion

An analytical method for studying the effect of magnetoelasticity on the stress intensity factor of a finite crack in an infinite elastic medium has been made. This analytical method to solve the Fredholm integral equation of 2nd kind is very straightforward and easy to compute while the numerical procedure is very laborious and time- consuming. The following are the outcomes of this study :

- Crack growth is more influential in magnetoelastic medium than without magnetoelastic medium for low frequency. Crack energy carries out the same effect for magnetic field.
- Fracture loses its toughness for higher values of frequency.
- In the neighbourhood of the crack, the dimensionless stress component is very disruptive in nature and loses its divisiveness far away from the crack.

This paper is useful for small cracks and very hard to enlarge this concept for large deformations. Although this research outcome may be very significant to study the fracture toughness, crack tip opening displacement, crack growth controlling development features in the field of fabrication processes in Fracture mechanics.

3.2 Mode-III crack in an infinite strip under magnetic field[2]

3.2.1 Introduction

Cracks or Fractures are present commonly in most of the structural substances, either as natural defects or as a consequence of fabrication process. Crack problems in infinite elastic medium with boundary have more complexity than without boundary since they involve additional geometric parameters describing the dimensions of the solids. Loeber and Sih (1968) have studied diffraction of elastic waves with griffith crack in an infinite medium. Mal (1970b) has studied interaction of elastic waves by griffith crack in isotropic infinite medium. Srivastava et al. (1983) have been solved the problem of interaction of shear waves with a griffith crack in an infinite long elastic strip. Propagation of a crack due to magnetoelastic shear waves in a self-reinforced medium has been examined by Chattopadhyay and Singh (2014). Sarkar et al. (1993) had been studied diffraction of SH waves by a griffith crack, considering a non-homogeneous elastic strip. Chattopadhyay and Maugin (1985) studied the diffraction problem of magnetoelastic shear waves by a rigid strip.

The problem of finding the expression of stress intensity factor of a griffith crack in an infinite elastic strip due to magnetoelastic shear wave propagation has not yet been discussed earlier to the best of author's knowledge. This problem is significant due to the presence of magnetic field with crack in an infinite strip of finite width. A transformation has been applied to simplify the displacement equation due to magnetoelasticity. The problem has been deduced to the Fredholm integral equation of second kind after using Fourier and Abel's transformation. Fox and Goodwin method has been used to solve the integral equation numerically. The SIF at the crack tip has been calculated and depicted by means of graphs for various strip width to show the magnetoelastic effect.

3.2.2 Formulation of the problem

Consider an infinitely long, homogeneous, isotropic elastic strip of width $2h$ occupying $-h \leq x \leq h, \mid y \mid < \infty$. The strip contains a griffith crack of infinite length and finite width located at $\mid x \mid \leq 1, -\infty < y < \infty, z = 0$ (Figure 3.7) referred to Cartesian coordinate system (x, y, z). Equations governing in a perfectly conducting isotropic elastic

[2]Panja, S. K., & Mandal, S. C. (2021). Interaction of magnetoelastic shear waves with a Griffith crack in an infinite strip. Journal of Engineering Mathematics, 126(1), 2.

medium under electromagnetic force $\vec{J} \times \vec{B}$ (the Lorentz force, $\vec{J}$ being the elastic current density and $\vec{B}$ being the magnetic induction vector) are

$$\begin{aligned} \frac{\partial \tau_{xx}}{\partial x} + \frac{\partial \tau_{xy}}{\partial y} + \frac{\partial \tau_{xz}}{\partial z} + \left(\vec{J} \times \vec{B}\right)_x &= \rho \frac{\partial^2 u}{\partial t^2} \\ \frac{\partial \tau_{xy}}{\partial x} + \frac{\partial \tau_{yy}}{\partial y} + \frac{\partial \tau_{yz}}{\partial z} + \left(\vec{J} \times \vec{B}\right)_y &= \rho \frac{\partial^2 v}{\partial t^2} \\ \frac{\partial \tau_{xz}}{\partial x} + \frac{\partial \tau_{yz}}{\partial y} + \frac{\partial \tau_{zz}}{\partial z} + \left(\vec{J} \times \vec{B}\right)_z &= \rho \frac{\partial^2 w}{\partial t^2}. \end{aligned} \tag{3.2.1}$$

The crack is supposed to be excited by a normally incident time harmonic shear wave

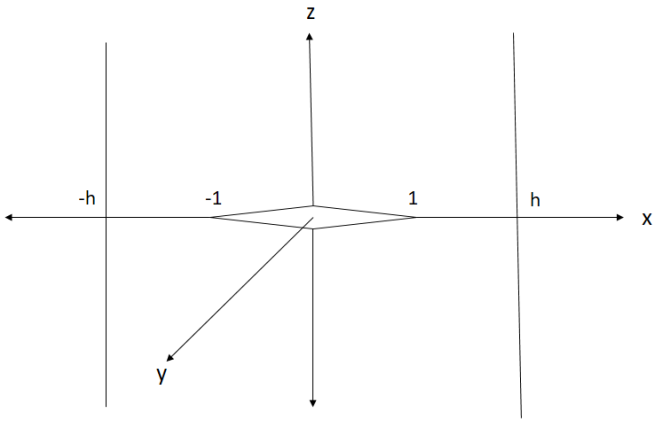

FIGURE 3.7: Geometry of the problem

$q_0 e^{-i\omega t}$ traveling in the positive direction of z axis. We also consider that two edges of the crack do not come in contact in the time of vibration. The non zero displacement component along y axis are assumed to be $v = v(x,\ z,\ t)$ as shear wave propagates along z axis, presumption with $u = w = 0$ and $\frac{\partial}{\partial y} \equiv 0$. Substitution of $v(x,\ z,\ t) = v(x,\ z)e^{-\iota\omega t}$ and above mentioned supposition in equation (3.2.1) reduces to

$$\frac{\partial \tau_{xy}}{\partial x} + \frac{\partial \tau_{yz}}{\partial z} + (\vec{J} \times \vec{B})_y + k^2 v = 0, \tag{3.2.2}$$

in which $\tau_{xy} = \mu \frac{\partial v}{\partial x}$ and $\tau_{yz} = \mu \frac{\partial v}{\partial z}$ are non vanishing stress components and $k^2 = \rho\omega^2$ (ρ is the density and ω is the circular frequency of the incident shear wave). Here μ is the elastic constant for isotropic medium.

The famous Maxwell's equations governing the electromagnetic field are

$$\vec{\nabla}\cdot\vec{B}=0,\ \vec{\nabla}\times\vec{E}=-\frac{\partial\vec{B}}{\partial t},\ \vec{\nabla}\times\vec{H}=\vec{J},\ \vec{B}=\mu_e\vec{H}\text{ and }\vec{J}=\sigma\left(\vec{E}+\frac{\partial\vec{u}}{\partial t}\times\vec{B}\right),\quad(3.2.3)$$

where $\vec{E}$ denotes the induced electric field, $\vec{J}$ denotes the current density vector and magnetic field $\vec{H}$ describes both primary and induced magnetic fields. μ_e and σ are the induced permeability and conduction coefficient respectively. The linearized Maxwell's stress tensor $\left(\tau_{ij}^0\right)^{M_x}$ due to the magnetic field is given by $\left(\tau_{ij}^0\right)^{M_x}=\mu_e(H_ia_j+H_ja_i-H_ka_k\delta_{ij})$. Let $\vec{H}=(H_x,\ H_y,\ H_z)$ and $a_i=(a_1,\ a_2,\ a_3)$ where a_i is the alter in the magnetic field. In writing the above equations, we have ignored the displacement current. From equation (3.2.3), we get

$$\nabla^2\vec{H}=\mu_e\sigma\left(\frac{\partial\vec{H}}{\partial t}-\vec{\nabla}\times\left(\frac{\partial\vec{u}}{\partial t}\times\vec{H}\right)\right).\quad(3.2.4)$$

Equation (3.2.4) can be written in the component form as follows

$$\begin{aligned}\frac{\partial H_x}{\partial t}&=\frac{1}{\mu_e\sigma}\nabla^2H_x,\\ \frac{\partial H_z}{\partial t}&=\frac{1}{\mu_e\sigma}\nabla^2H_z\text{ and}\\ \frac{\partial H_y}{\partial t}&=\frac{1}{\mu_e\sigma}\nabla^2H_y+\frac{\partial\left(H_x\frac{\partial v}{\partial t}\right)}{\partial x}+\frac{\partial\left(H_z\frac{\partial v}{\partial t}\right)}{\partial z}.\end{aligned}\quad(3.2.5)$$

For a perfectly conducting medium (i.e. $\sigma\to\infty$), the equation (3.2.5) becomes

$$\frac{\partial H_x}{\partial t}=\frac{\partial H_z}{\partial t}=0\quad(3.2.6)$$

and

$$\frac{\partial H_y}{\partial t}=\frac{\partial\left(H_x\frac{\partial v}{\partial t}\right)}{\partial x}+\frac{\partial\left(H_z\frac{\partial v}{\partial t}\right)}{\partial z}.\quad(3.2.7)$$

Assume that the primary magnetic field is uniform throughout the space. It is evident from equation (3.2.6) that there is no perturbation in the components H_x and H_z, however equation (3.2.7) indicates that there may be a perturbation in H_y. Therefore, taking a small perturbation, say b_2 in H_y, we have $H_x=H_1'$, $H_y=H_2'+b_2$ and $H_z=H_3'$, where $(H_1',\ H_2',\ H_3')$ are components of the initial magnetic field $\vec{H}'$. We can write $\vec{H}'=(H'\cos\alpha,\ 0,\ H'\sin\alpha)$, where $H'=\mid\vec{H}'\mid$ and α is the angle between the direction of the wave and the magnetic field. Thus we have

$$\vec{H}=(H'\cos\alpha,\ b_2,\ H'\sin\alpha).\quad(3.2.8)$$

We take initial value of b_2 as 0. Using equation (3.2.8) in equation (3.2.7), we get

$$\frac{\partial b_2}{\partial t} = \frac{\partial \left(H' \cos\alpha \frac{\partial v}{\partial t}\right)}{\partial x} + \frac{\partial \left(H' \sin\alpha \frac{\partial v}{\partial t}\right)}{\partial z}. \tag{3.2.9}$$

Integrating with respect to t, we obtain

$$b_2 = H' \cos\alpha \frac{\partial v}{\partial x} + H' \sin\alpha \frac{\partial v}{\partial z}. \tag{3.2.10}$$

Keeping in mind $\vec{\nabla}\left(\frac{H^2}{2}\right) = -\left(\vec{\nabla} \times \vec{H}\right) \times \vec{H} + \left(\vec{H} \cdot \vec{\nabla}\right) \vec{H}$ and equation (3.2.3), we get

$$\vec{J} \times \vec{B} = \mu_e \left(-\vec{\nabla}\left(\frac{H^2}{2}\right) + \left(\vec{H} \cdot \vec{\nabla}\right) \vec{H}\right). \tag{3.2.11}$$

Putting the y component of $\vec{J} \times \vec{B}$ in equation (3.2.2), we write the equation of motion in the form

$$A\frac{\partial^2 v}{\partial x^2} + B\frac{\partial^2 v}{\partial z^2} + C\frac{\partial^2 v}{\partial x \partial z} + k^2 v = 0 \tag{3.2.12}$$

with

$$\begin{aligned} A &= \mu + \mu_e H'^2 \cos^2\alpha, \\ B &= \mu + \mu_e H'^2 \sin^2\alpha, \\ C &= \mu_e H'^2 \sin 2\alpha. \end{aligned} \tag{3.2.13}$$

The equation (3.2.12) is to be solved subject to the boundary condition

$$\tau_{yz}(x, 0) = -q_0, \ | \, x \, | < 1 \tag{3.2.14}$$

$$v(x, 0) = 0, \ 1 \leq | \, x \, | \leq h \tag{3.2.15}$$

and

$$\tau_{xy}(h, z) = \tau_{xy}(-h, z) = 0. \tag{3.2.16}$$

Applying a coordinate transformation Zhou and Wang (2005)

$$\hat{x} = x - ez \text{ and } \hat{z} = cz \tag{3.2.17}$$

where $e = \frac{C}{2B}$, $c = \frac{\beta}{B}$ and $\beta = \sqrt{AB - \frac{C^2}{4}}$, the chain rule of differentiation reduces equation (3.2.12) to the common equation

$$\frac{\partial^2 \hat{v}}{\partial \hat{x}^2} + \frac{\partial^2 \hat{v}}{\partial \hat{z}^2} + k_1^2 \hat{v} = 0; \text{ where } k_1^2 = \frac{4B}{4AB - C^2} k^2. \tag{3.2.18}$$

The solution of equation (3.2.18) can be taken as

$$\hat{v}(\hat{x},\hat{z}) = \int_0^\infty A(\xi)e^{-\gamma_1\hat{z}}\cos(\xi\hat{x})d\xi + \int_0^\infty B(\zeta)\cosh(\gamma_2\hat{x})\sin(\zeta\hat{z})d\zeta \tag{3.2.19}$$

where

$$\gamma_1^2 = \xi^2 - k_1^2 \text{ and } \gamma_2^2 = \zeta^2 - k_1^2 \tag{3.2.20}$$

$A(\xi)$ and $B(\zeta)$, unknown functions are to be determined from the boundary conditions. It is easily verified from equation (3.2.17) that the relevant displacement and stress components can be written as

$$v(x,z) = \hat{v}(\hat{x},\hat{z}), \tag{3.2.21}$$

$$\tau_{yz}(x,z) = -\mu e\frac{\partial\hat{v}(\hat{x},\hat{z})}{\partial\hat{x}} + \mu c\frac{\partial\hat{v}(\hat{x},\hat{z})}{\partial\hat{z}} \tag{3.2.22}$$

and

$$\tau_{xy}(x,z) = \mu\frac{\partial\hat{v}(\hat{x},\hat{z})}{\partial\hat{x}}. \tag{3.2.23}$$

Equations (3.2.17), (3.2.19) and (3.2.21) gives

$$v(x,z) = \int_0^\infty A(\xi)e^{-\gamma_1 cz}\cos(\xi x - \xi ez)d\xi + \int_0^\infty B(\zeta)\cosh(\gamma_2 x - \gamma_2 ez)\sin(\zeta cz)d\zeta, \tag{3.2.24}$$

$$\begin{aligned}\tau_{yz}(x,z) = \mu e\int_0^\infty \xi A(\xi)e^{-\gamma_1 cz}\sin(\xi x - \xi ez)d\xi \\ -\mu e\int_0^\infty \gamma_2 B(\zeta)\sinh(\gamma_2 x - \gamma_2 ez)\sin(\zeta cz)d\zeta \\ -\mu c\int_0^\infty \gamma_1 A(\xi)e^{-\gamma_1 cz}\cos(\xi x - \xi ez)d\xi \\ +\mu c\int_0^\infty \zeta B(\zeta)\cosh(\gamma_2 x - \gamma_2 ez)\cos(\zeta cz)d\zeta\end{aligned} \tag{3.2.25}$$

and

$$\begin{aligned}\tau_{xy}(x,z) = -\mu\int_0^\infty \xi A(\xi)e^{-\gamma_1 cz}\sin(\xi x - \xi ez)d\xi \\ +\mu\int_0^\infty \gamma_2 B(\zeta)\sinh(\gamma_2 x - \gamma_2 ez)\sin(\zeta cz)d\zeta.\end{aligned} \tag{3.2.26}$$

3.2.3 Induction of the integral equation

Boundary conditions (3.2.14) and (3.2.15) result in the following dual integral equations

$$\int_0^\infty \gamma_1 A(\xi)\cos(\xi x)d\xi = \frac{q_0}{\mu c} + \int_0^\infty \zeta B(\zeta)\cosh(\gamma_2 x)d\zeta, \quad |\, x\,| < 1 \tag{3.2.27}$$

and

$$\int_0^\infty A(\xi)\cos(\xi x)d\xi = 0, \quad 1 \leq| \, x \,|\leq h. \tag{3.2.28}$$

Applying the condition (3.2.16) on the boundary of the strip, the following relation between $A(\xi)$ and $B(\zeta)$ is obtained

$$\int_0^\infty \gamma_2 B(\zeta)\sinh(\gamma_2 h)\cosh(\gamma_2 ez)\sin(\zeta cz)d\zeta = \int_0^\infty \xi A(\xi)\sin(\xi h)\cos(\xi ez)e^{-\gamma_1 cz}d\xi$$

which, on using the inversion theorem for Fourier sine and cosine transform and using integration, provides

$$\gamma_2 B(\zeta)\sinh(\gamma_2 h) = \frac{2\iota}{\pi}\int_0^\infty \xi A(\xi)\sin(\xi h)\frac{\zeta}{\gamma_1^2+\zeta^2}d\xi. \tag{3.2.29}$$

Putting the value of $B(\zeta)$ from equation (3.2.29) into the equation (3.2.27) we obtain the following dual integral equations

$$\int_0^\infty \xi\left[1+H(\xi)\right]A(\xi)\cos(\xi x)d\xi = Q(x), \quad |\, x\,| < 1 \tag{3.2.30}$$

and

$$\int_0^\infty A(\xi)\cos(\xi x)d\xi = 0, \quad 1 \leq| \, x \,|\leq h \tag{3.2.31}$$

where

$$Q(x) = \frac{q_0}{\mu c} + \frac{2\iota}{\pi}\int_0^\infty \frac{\cosh(\gamma_2 x)}{\sinh(\gamma_2 h)}\int_0^\infty \frac{\zeta^2\xi}{\gamma_2\left(\gamma_1^2+\zeta^2\right)}A(\xi)\sin(\xi h)d\xi\, d\zeta \tag{3.2.32}$$

and

$$H(\xi) = \frac{\gamma_1}{\xi} - 1. \tag{3.2.33}$$

Simply it can be found that $H(\xi) \to 0$ as $\xi \to \infty$. Let us consider the trial solution of the above dual integral equations in the form

$$A(\xi) = \frac{q_0}{\mu c}\int_0^1 tg(t)J_0(\xi t)dt \tag{3.2.34}$$

such that the equation (3.2.31) is trivially satisfied and equation (3.2.30) reduces to the following Fredholm integral equation of second kind

$$g(t) + \int_0^1 ug(u)L_1(u.t)du = \frac{2\mu c}{\pi q_0}\int_0^t \frac{Q(x)}{\sqrt{t^2-x^2}}dx \tag{3.2.35}$$

with

$$L_1(u,t) = \int_0^\infty \xi H(\xi)J_0(\xi u)J_0(\xi t)d\xi. \tag{3.2.36}$$

Substituting the value of $A(\xi)$ from equation (3.2.34) into equation (3.2.32) we obtain

$$\frac{2\mu c}{\pi q_0}\int_0^t \frac{Q(x)}{\sqrt{t^2-x^2}}dx = 1 - \int_0^1 ug(u)L_2(u,t)du \tag{3.2.37}$$

where

$$L_2(u,t) = -\frac{2\iota}{\pi}\int_0^\infty \frac{\zeta^2}{\gamma_2}\frac{I_0(\gamma_2 t)}{\sinh(\gamma_2 h)}d\zeta \int_0^\infty \frac{\xi\sin(\xi h)}{\gamma_1^2+\zeta^2}J_0(\xi u)d\xi \tag{3.2.38}$$

$L_2(u,t)$ can be rewritten as

$$L_2(u,t) = -\frac{2\iota}{\pi}\int_0^\infty \frac{\zeta^2}{\gamma_2}\frac{I_0(\gamma_2 t)}{\sinh(\gamma_2 h)}K(\zeta,u)d\zeta \tag{3.2.39}$$

where

$$\begin{aligned} K(\zeta,u) &= \int_0^\infty \frac{\xi}{\gamma_1^2+\zeta^2}\sin(\xi h)J_0(\xi u)d\xi; \\ &= \int_0^\infty \frac{\xi}{\xi^2+\gamma_2^2}\sin(\xi h)J_0(\xi u)d\xi; \\ &= \begin{cases} \frac{\pi}{2}e^{-\gamma_2 h}I_0(\gamma_2 u), & \zeta > k_1 \\ \frac{\pi}{2}e^{-\iota\gamma_2' h}I_0(\iota\gamma_2' u), & \zeta < k_1 \end{cases} \end{aligned} \tag{3.2.40}$$

$\gamma_2'^2 = k_1^2 - \zeta^2$ and γ_2 is given by equation (3.2.20). $J_0()$ is the Bessel function of first kind of order zero and $I_0()$ is the modified Bessel function of first kind of order zero. Using equations (3.2.37) and (3.2.35), finally we obtain the following Fredholm integral equation of the second kind

$$g(t) + \int_0^1 ug(u)L(u,t)du = 1, \tag{3.2.41}$$

where the kernel $L(u,t) = L_1(u,t) + L_2(u,t)$.

The integrand present in $L_1(u,t)$ has no poles but it has branch point at the point $\xi = k_1$. The kernel $L_1(u,t)$ has a slow rate of convergence. Following the procedure of simple contour integration Mal (1970b) the infinite integral in (3.2.36) can be reduced into integral

with finite limits to make the numerical calculation easier and is given by

$$L_1(u,t) = -\iota k_1^2 \int_0^1 \sqrt{1-\xi^2} J_0(k_1\xi u) H_0^{(1)}(k_1\xi t) d\xi, \quad t > u. \tag{3.2.42}$$

The integrand in equation (3.2.39) can be written as

$$L_2(u,t) = -\frac{2\iota}{\pi}\left[\int_0^{k_1} + \int_{k_1}^{\infty}\right] \frac{\zeta^2}{\gamma_2} \frac{I_0(\gamma_2 t)}{\sinh(\gamma_2 h)} K(\zeta,u) d\zeta.$$

On making use of the relation (3.2.40) and substituting $\zeta^2 = k_1^2(1-y^2)$ and $\zeta^2 = k_1^2(1+y^2)$ in the integrals $\int_0^{k_1}$ and $\int_{k_1}^{\infty}$ respectively, we get

$$\begin{aligned} L_2(u,t) = \iota k_1^2 \int_0^1 \sqrt{1-y^2} J_0(k_1 y t) J_0(k_1 y u) \csc(k_1 y h) e^{-k_1 y h} dy - \\ \iota k_1^2 \int_0^{\infty} \sqrt{1+y^2} I_0(k_1 y t) I_0(k_1 y u) \frac{e^{-k_1 y h}}{\sinh(k_1 y h)} dy. \end{aligned} \tag{3.2.43}$$

3.2.4 Stress Intensity Factor (SIF)

The stress component $\tau_{yz}(x,\ 0)$ in the neighbourhood of the crack from equations (3.2.25), (3.2.29) and (3.2.34) is given by

$$\tau_{yz}(x,0) = q_0 \frac{x g(1)}{\sqrt{x^2-1}} + O(1), \quad |x| > 1. \tag{3.2.44}$$

Stress Intensity Factor (SIF) describes the stress state at the tip of the crack. Defining dimensionless stress intensity factor K by

$$K = \lim_{x \to 1^+} \left| \frac{\sqrt{x-1}\tau_{yz}(x,0)}{q_0} \right|,$$

we get

$$K = \frac{1}{\sqrt{2}} |g(1)|. \tag{3.2.45}$$

3.2.5 Numerical calculations and graphs

The Fredholm integral equation (3.2.41) of 2nd kind has been solved numerically for a wide range of frequency k_1 by the method of Fox and Goodwin (1953) as it is not solvable analytically.

Once the integral equation (3.2.41) is solved, the SIF is calculated numerically and mapped graphically against frequency k_1 for different values of strip width h and magnetoelastic parameter ϵ. For the case of isotropic magnetoelastic strip, we take the following data (Chattopadhyay et al., 2010; Srivastava et al., 1983; Chattopadhyay and Singh, 2014; Maugin, 1981):

$$\rho = 2.7\ gm/cm^3,\ \mu = \frac{E}{2(1+\eta)} \text{ where } \eta = 0.339 \text{ and } E = 7.05 \times 10^{11}\ dyne/cm^2.$$
$$\epsilon = \frac{\mu_e H'^2}{\mu} = 0.0,\ 0.15,\ 0.30;\ \alpha = 10^\circ, 50^\circ, 90^\circ.$$

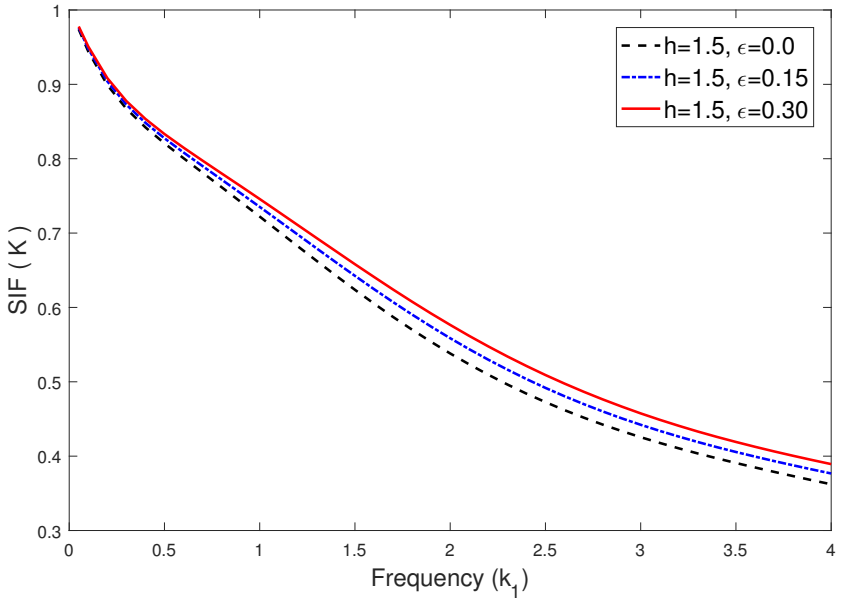

FIGURE 3.8: SIF against frequency

In Figures 3.8-3.10, dimensionless SIF has been plotted graphically against frequency k_1 for various strip width. The graph show the effect of stress intensity factor for presence and absence of magnetoelasticity. For $\epsilon = 0.0$ the curve indicates SIF without magnetoelasticity and for $\epsilon = 0.15,\ 0.30$ curves show SIF in magnetoelastic strip. It is clear that the SIF decreases strictly at first and then SIF decreases slowly with increase in frequency k_1 for each cases. The rate of decrement of SIF is less due to magnetoelasticity. Moreover it is notable that SIF decreases rapidly with increase in strip width h.

Figure 3.11 is the plot of SIF versus frequency for different strip width $h = 1.5,\ 2.0,\ 2.5$ to show the impact of angle α at which the shear wave crosses the magnetic field. We observe that for different angles the variation of SIF in each cases are not significant. The curves for angles $\alpha = 50^\circ$ and 90° are almost coincide for each strip width.

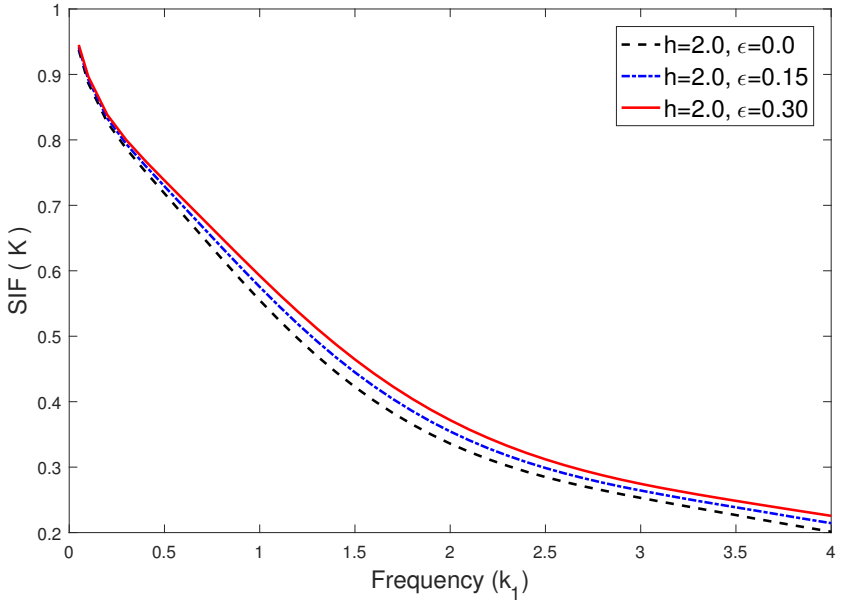

FIGURE 3.9: SIF against frequency

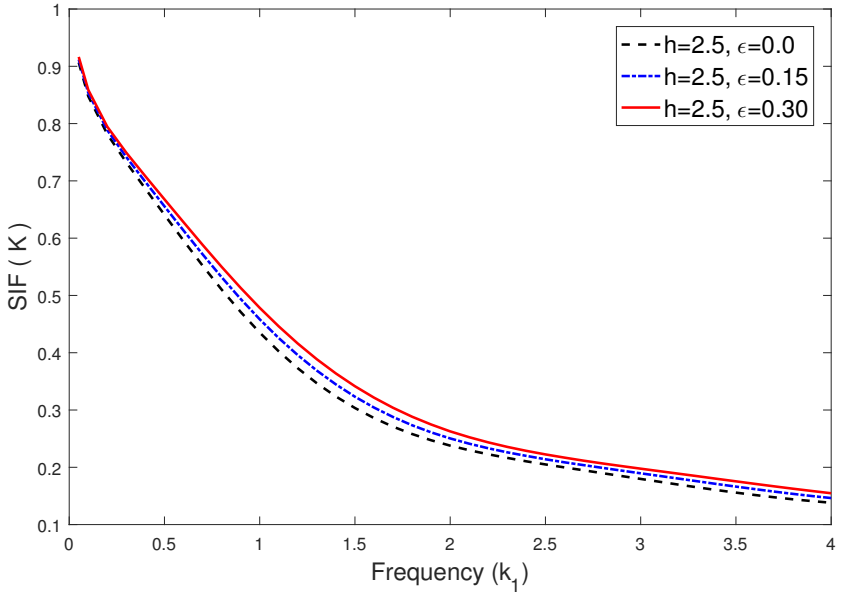

FIGURE 3.10: SIF against frequency

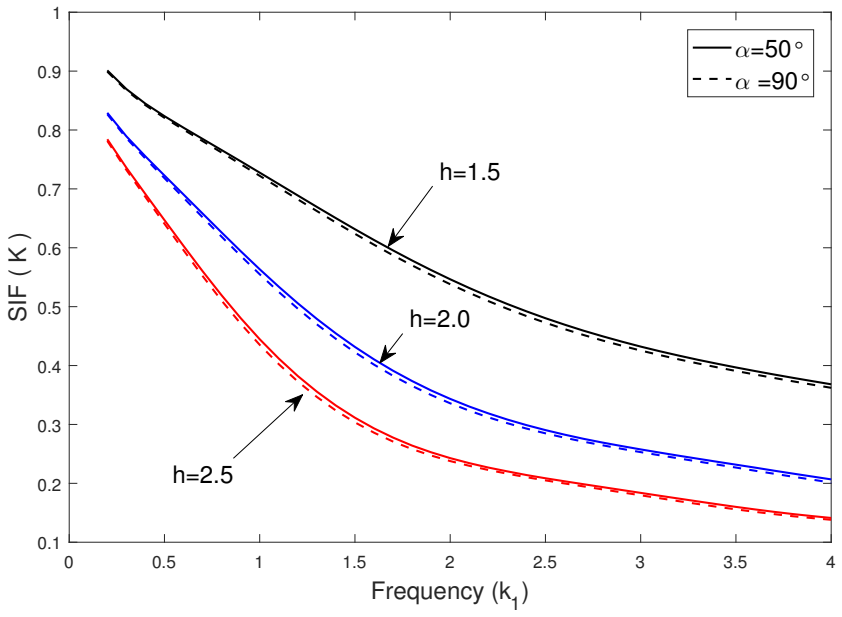

FIGURE 3.11: SIF against frequency

3.2.6 Conclusion

The purpose of the present study is to unfold the behavior of Stress intensity factor of a griffith crack due to magnetoelastic shear waves in an infinite strip. We can conclude following points from this study:

- Initially SIF decreases rapidly but nearly after $k_1 = 2.0$, SIF decrease steadily with increase in k_1. SIF curve tend to zero in absence and presence of magnetoelasticity for large frequency. Therefor SIF can be seized within a certain range of frequency.
- Stress Intensity Factor decreases with increase in strip width.
- SIF is higher in magnetoelastic infinite strip than isotropic infinite strip.

3.3 Impact response of a finite crack in the presence of magnetic field[3]

3.3.1 Introduction

The stress or displacement field in the neighborhood of a crack tip is very functional to characterize a crack. Stress intensity factor is easier for laboratory measurements to determine the material properties. The crack opening displacement is useful for a designer to compare the toughness of materials.

Sih and Chen (1980) has developed an effective procedure for finding SIF by using Laplace and Fourier transforms. Baksi et al. (2003) studied impact response of a cracked orthotropic medium by iteration method. P wave diffraction problem by a crack under normal impact load has been analyzed by Naskar and Mandal (2018). The impact load problem of a cracked in Ferromagnetic medium was discussed by Shindo (1985) with the help of trigonometric series expansion. The impact response of a cracked orthotropic medium has been investigated by Kassir and Bandyopadhyay (1983). The linear magnetoelastic problem with a finite crack for a ferromagnetic solid was investigated by Shindo (1977).

Study of the interaction between the magnetic field and stress and strain in a crack surface is valuable in the nuclear field as magnetic fields generating inside nuclear reactors, influence their design and operations. Whenever a cracked surface is subjected to a sudden load, the crack propagates with an increase in load. A designer intends to prevent crack growth. The effect of magnetic field on the cracked surface has gained a lot of significance due to its rapid development in applied physical sciences like MHD devices, fusion power reactors, etc. We have framed a problem for a finite crack with normal impact load in the presence of a magnetic field. Also, shear impact of a finite crack is discussed in the presence of external magnetic field in present paper.

The stress and displacement components in the vicinity of a crack tip are important for a designer, who improve some features like cutouts, notches, keyways, etc. to resist the crack growth. Stress intensity factor describes the feature of a crack by analyze the stress singularity at crack tip. Fracture toughness in magnetoelastic solid materials can be examined easily by COD.

[3]Panja, S. K., & Mandal, S. C. (2021). Impact response of a finite crack in the presence of magnetic field. Engineering Fracture Mechanics, 253, 107851.

There are many research papers regarding the interaction of a crack due to impact load in an infinite medium, but the effect of a magnetic field of a finite crack due to impact response is still not attempted. This present paper aims to discuss the magnetic effect on SIF and COD of a finite crack in an infinite isotropic elastic medium due to impact load. The boundary value problem has been converted to a Fredholm integral equation of 2nd Kind with the help of Laplace and Abel's transforms. The integral equation with infinite kernel has been solved by Perturbation method (Srivastava et al., 1980) for low frequency. Stress intensity factor and Crack opening displacement have been derived analytically and computed numerically by Laplace inversion in the time domain using the Zakian algorithm. To unfold the effect of magnetic field on a finite crack in an infinite medium SIF and COD have been plotted graphically.

3.3.2 Formulation of the problem

Consider a finite crack occupying $|x| \leq 1,\ -\infty < z < \infty,\ y = 0$ (Figure 3.12) referred to Cartesian co-ordinate system $(x,\ y,\ z)$ in an infinite isotropic elastic medium, is subjected to normal impact load of magnitude τ_0 after time $t = 0$. A magnetic field with uniform intensity $\vec{H} = (0,\ 0,\ H_0)$ is acting in the direction of $z-$ axis on the cracked surface. The

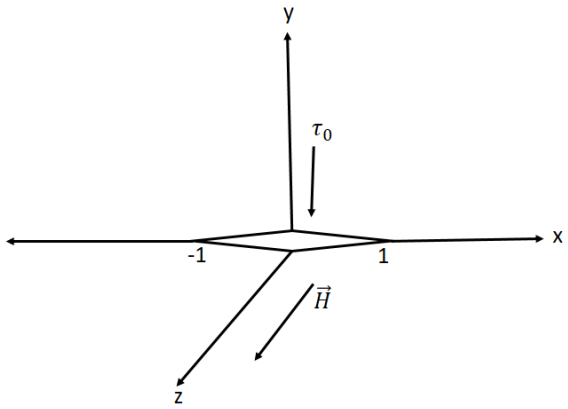

FIGURE 3.12: Geometry of the problem

linear Maxwell's equation governing the electromagnetic field for slowly moving media are:

$$\begin{aligned} &\vec{J} = \vec{\nabla} \times \vec{h} - \epsilon_0 \dot{\vec{E}}, \\ &\vec{\nabla} \times \vec{E} = -\mu_0 \dot{\vec{h}}, \\ &\vec{E} = -\mu_0 \left(\dot{\vec{u}} \times \vec{H} \right) \text{ and} \\ &\vec{\nabla} \cdot \vec{h} = 0, \end{aligned} \tag{3.3.1}$$

where μ_0 is magnetic permeability, ϵ_0 is electric permeability, $\dot{\vec{u}}$ is partial derivative of displacement components with respect to time and $\vec{h} = (0,\ 0,\ h)$ is induced magnetic field, $\vec{E}$ is induced electric field due to initial magnetic field $\vec{H}$.

The displacement equations and the stress-strain relations in an infinite isotropic elastic medium in the presence of electromagnetic force (the Lorentz force) are

$$\rho \ddot{u}_i = \sigma_{ij,j} + \mu_0 \left(\vec{J} \times \vec{H} \right)_i \tag{3.3.2}$$

and

$$\sigma_{ij} = 2\mu e_{ij} + \lambda e \delta_{ij}, \tag{3.3.3}$$

where $\lambda,\ \mu$ are Lame's constants, e is the dilatation, σ_{ij} are the stress components, ρ is the density and δ_{ij} is the Kronecker delta.

P - waves are propagating only in the xy plane, so the non-zero displacement components are $u_1 = u(x,\ y,\ t)$ and $u_2 = v(x,\ y,\ t)$. The strain displacement constitutive relation are

$$\begin{aligned} &e_{xy} = \frac{1}{2} \left(\partial_y u + \partial_x v \right),\ e_{xx} = \partial_x u, \\ &e_{yy} = \partial_y v,\ e_{xz} = e_{yz} = 0 \end{aligned} \tag{3.3.4}$$

and the dilatation e is given by

$$e = \partial_x u + \partial_y v. \tag{3.3.5}$$

Using equations (3.3.1-3.3.5), we obtain the displacement equations in the following form

$$\begin{aligned} \left(\lambda + \mu + \mu_0 H_0^2 \right) \left(\partial_{xx} u + \partial_{xy} v \right) + \mu \left(\partial_{xx} u + \partial_{yy} u \right) = \\ \left(\rho + \mu_0^2 H_0^2 \epsilon_0 \right) \partial_{tt} u \end{aligned} \tag{3.3.6}$$

and

$$\begin{aligned}\left(\lambda+\mu+\mu_0 H_0^2\right)\left(\partial_{xy}u+\partial_{yy}v\right)+\mu\left(\partial_{xx}v+\partial_{yy}v\right)=\\ \left(\rho+\mu_0^2 H_0^2\epsilon_0\right)\partial_{tt}v.\end{aligned} \tag{3.3.7}$$

Introducing the potential functions ϕ and ψ as

$$u=\partial_x\phi-\partial_y\psi,\ v=\partial_y\phi+\partial_x\psi, \tag{3.3.8}$$

equations (3.3.6) and (3.3.7) become

$$\partial_{xx}\phi+\partial_{yy}\phi=k_1^2\partial_{tt}\phi \tag{3.3.9}$$

and

$$\partial_{xx}\psi+\partial_{yy}\psi=k_2^2\partial_{tt}\psi, \tag{3.3.10}$$

where $k_1^2=\frac{\rho+\mu_0^2H_0^2\epsilon_0}{\lambda+2\mu+\mu_0H_0^2}$ and $k_2^2=\frac{\rho+\mu_0^2H_0^2\epsilon_0}{\mu}$.

The problem is symmetric about y axis so, the boundary conditions on the plane $y=0$ can be written as

$$\sigma_{yy}\left(x,\ 0,\ t\right)=-\tau_0H(t),\quad 0\le x\le 1 \tag{3.3.11}$$

$$\sigma_{xy}\left(x,\ 0,\ t\right)=0,\qquad 0\le x<\infty \tag{3.3.12}$$

and

$$v\left(x,\ 0,\ t\right)=0,\qquad x>1 \tag{3.3.13}$$

where $H(t)$ is the Heaviside step function. We utilize Laplace transform to convert the problem from time domain to the domain of Laplace transform parameter (p) with the definition

$$f^*(p)=\int_0^\infty f(t)e^{-pt}dt$$

and

$$f(t)=\frac{1}{2\pi i}\int_{B_r}f^*(p)e^{pt}dp,$$

where B_r denotes the Bromwich path of integration.

The equations (3.3.9) and (3.3.10) reduces with the aid of Laplace transform

$$\partial_{xx}\phi^*+\partial_{yy}\phi^*=\bar{k_1}^2\phi^* \tag{3.3.14}$$

and

$$\partial_{xx}\psi^* + \partial_{yy}\psi^* = \bar{k_2}^2\psi^*, \tag{3.3.15}$$

where $\bar{k_1}^2 = k_1^2 p^2$ and $\bar{k_2}^2 = k_2^2 p^2$.

Now, ϕ^* and ψ^* are the functions of $x,\ y$ and p.

After applying the Laplace transform, the boundary conditions become,

$$\sigma_{yy}^*(x,\ 0,\ p) = -\frac{\tau_0}{p}, \quad 0 \le x \le 1 \tag{3.3.16}$$

$$\sigma_{xy}^*(x,\ 0,\ p) = 0, \qquad 0 \le x < \infty \tag{3.3.17}$$

and

$$v^*(x,\ 0,\ p) = 0, \qquad x > 1. \tag{3.3.18}$$

We consider the solution of equations (3.3.14) and (3.3.15) in the form

$$\phi^*(x,\ y,\ p) = \int_0^\infty A(\xi,\ p)\cos(\xi x)\, e^{-\gamma_1 y} d\xi \tag{3.3.19}$$

and

$$\psi^*(x,\ y,\ p) = \int_0^\infty B(\xi,\ p)\sin(\xi x)\, e^{-\gamma_2 y} d\xi, \tag{3.3.20}$$

where $\gamma_1 = \sqrt{\bar{k_1}^2 + \xi^2}$ and $\gamma_2 = \sqrt{\bar{k_2}^2 + \xi^2}$.

Using equations (3.3.19) and (3.3.20) in equation (3.3.8), u^* and v^* can be written as

$$u^*(x,\ y,\ p) = \int_0^\infty \sin(\xi x)\left[\gamma_2 B(\xi,\ p)\, e^{-\gamma_2 y} - \xi A(\xi,\ p)\, e^{-\gamma_1 y}\right] d\xi \tag{3.3.21}$$

and

$$v^*(x,\ y,\ p) = \int_0^\infty \cos(\xi x)\left[\xi B(\xi,\ p)\, e^{-\gamma_2 y} - \gamma_1 A(\xi,\ p)\, e^{-\gamma_1 y}\right] d\xi. \tag{3.3.22}$$

Applying boundary condition (3.3.17), we obtain

$$A(\xi,\ p) = \alpha B(\xi,\ p) \tag{3.3.23}$$

where $\alpha = \frac{\gamma_2^2+\xi^2}{2\gamma_1\xi}$. Utilizing boundary conditions (3.3.18) and (3.3.16) we get the following dual integral equations

$$\int_0^\infty \cos(\xi x)\, D(\xi,\ p)\, d\xi = 0, \quad x > 1 \tag{3.3.24}$$

and

$$\int_0^\infty \xi \cos(\xi x)\, [H(\xi,\ p) - 1]\, D(\xi,\ p) d\xi = -\frac{\tau_0}{2\mu p}, \quad |x| \leq 1 \tag{3.3.25}$$

where $D(\xi,\ p) = (\xi - \alpha\gamma_1)B(\xi,\ p)$ and
$H(\xi,\ p) = \frac{\alpha\gamma_1^2 - \xi\gamma_2 + \frac{\lambda}{2\mu}\alpha\bar{k_1}^2}{\xi(\xi-\alpha\gamma_1)} + 1 \quad \to\ 0$ as $\xi \to\ \infty$.

3.3.3 Induction of the integral equation

Let the trial solution of the dual integral equations (3.3.24) and (3.3.25) be

$$D(\xi,\ p) = -\frac{\tau_0}{2\mu p}\int_0^1 s g^*(s,\ p) J_0(\xi s) ds. \tag{3.3.26}$$

Solution (3.3.26) automatically satisfies the equation (3.3.24) and with the help of Abel's transform we acquire the Fredholm integral equation of 2nd kind from equation (3.3.25) in the subsequent form

$$\int_0^1 u g^*(u,\ p) L(u,\ s,\ p) du = 1 + g^*(s,\ p) \tag{3.3.27}$$

where

$$L(u,\ s,\ p) = \int_0^\infty \xi H(\xi,\ p) J_0(\xi u) J_0(\xi s) d\xi \tag{3.3.28}$$

The infinite kernel $L(u,\ s,\ p)$ has a slow rate of convergence, so we convert the infinite integral to a finite integral by Contour integration (Mandal and Ghosh, 1994) as

$$\begin{aligned} &L(u,\ s,\ p) = \\ &-\frac{1}{\pi}\int_0^\gamma \bar{k_1}^2 \frac{\frac{\left(2\xi^2-\gamma^2\right)\left[2(1-\xi^2)+\frac{\lambda}{\mu}\right]}{\sqrt{1-\xi^2}} - 4\xi^2\sqrt{\gamma^2-\xi^2}}{\gamma^2} K_0\left(\bar{k_1}\xi s\right) I_0\left(\bar{k_1}\xi u\right) d\xi \\ &-\frac{1}{\pi}\int_\gamma^1 \bar{k_1}^2 \frac{\left(2\xi^2-\gamma^2\right)\left[2(1-\xi^2)+\frac{\lambda}{\mu}\right]}{\gamma^2\sqrt{1-\xi^2}} K_0\left(\bar{k_1}\xi s\right) I_0\left(\bar{k_1}\xi u\right) d\xi, \quad s > u \end{aligned} \tag{3.3.29}$$

where $\gamma = \frac{\bar{k_2}}{\bar{k_1}} < 1$.

3.3.4 Solution of the integral equation

We derived the iterative solution of the integral equation (3.3.27) by perturbtion method. The iterative solution is applicable for small values of $\bar{k_1}$ and $\bar{k_2}$. The modified Bessel function of 1st kind $I_0(z)$ and the modified Bessel function of 2nd kind $K_0(z)$ have been expanded in ascending powers of z as (Abramowitz and Stegun, 1968)

$$I_0(z) = \sum_{n=0}^{\infty} \frac{\left(\frac{z^2}{4}\right)^n}{(n!)^2}$$

and

$$K_0(z) = -\left[\log\left(\frac{z}{2}\right) + c\right] I_0(z) + \frac{\left(\frac{z^2}{4}\right)}{(1!)^2} + \left(1 + \frac{1}{2}\right) \frac{\left(\frac{z^2}{4}\right)^2}{(2!)^2} + \left(1 + \frac{1}{2} + \frac{1}{3}\right) \frac{\left(\frac{z^2}{4}\right)^3}{(3!)^2} + \cdots\cdots,$$

where $c = 0.5772$ (Euler-Mascheroni constant).

Utilizing the above expressions in equation (3.3.29), $L(u,\ s,\ p)$ can be written as

$$\begin{aligned} L(u,\ s,\ p) = &\left(\bar{k_1}^2 \log(\bar{k_1})\right) L_1(u,\ s,\ p) + \left(\bar{k_1}^2\right) L_2(u,\ s,\ p) + \\ &\left(\bar{k_1}^2 \log(\bar{k_1})\right)^2 L_3(u,\ s,\ p) + \left(\bar{k_1}^4 \log(\bar{k_1})\right) L_4(u,\ s,\ p) + \\ &O(\bar{k_1}^4) \end{aligned} \tag{3.3.30}$$

where,

$$
\begin{aligned}
&L_1(u,\ s,\ p) = \frac{M_0 + N_0}{\pi},\\
&L_2(u,\ s,\ p) = \frac{1}{\pi}\left[\left(\bar{M} + \bar{N}\right) + \left(\log s - \log 2 + c\right)\left(M_0 + N_0\right)\right],\\
&L_3(u,\ s,\ p) = 0,\\
&L_4(u,\ s,\ p) = \frac{1}{\pi}\left(\frac{u^2 + s^2}{4}\right)\left(M_2 + N_2\right),\\
&M_{2n} = \int_0^{\gamma} \xi^{2n}\alpha(\xi,\ \gamma)d\xi,\\
&N_{2n} = \int_{\gamma}^{1} \xi^{2n}\beta(\xi,\ \gamma)d\xi,\\
&\bar{M} = \int_0^{\gamma} (\log\xi)\alpha(\xi,\ \gamma)d\xi,\\
&\bar{N} = \int_{\gamma}^{1} (\log\xi)\beta(\xi,\ \gamma)d\xi
\end{aligned}
\tag{3.3.31}
$$

and

$$
\alpha(\xi,\ \gamma) = \frac{\left(2\xi^2 - \gamma^2\right)\left[2\left(1 - \xi^2\right) + \frac{\lambda}{\mu}\right] - 4\xi^2\sqrt{\gamma^2 - \xi^2}\sqrt{1 - \xi^2}}{\gamma^2\sqrt{1 - \xi^2}},
$$

$$
\beta(\xi,\ \gamma) = \frac{\left(2\xi^2 - \gamma^2\right)\left[2\left(1 - \xi^2\right) + \frac{\lambda}{\mu}\right]}{\gamma^2\sqrt{1 - \xi^2}}.
$$

Now, $g^*(s,\ p)$ also be expanded in the form

$$
\begin{aligned}
&g^*(s,\ p) =\\
&g_0^*(s,\ p) + \left(\bar{k_1}^2\log(\bar{k_1})\right)g_1^*(s,\ p) + \left(\bar{k_1}^2\right)g_2^*(s,\ p) +\\
&\left(\bar{k_1}^2\log(\bar{k_1})\right)^2 g_3^*(s,\ p) + \left(\bar{k_1}^4\log(\bar{k_1})\right)g_4^*(s,\ p) + O(\bar{k_1}^4)
\end{aligned}
\tag{3.3.32}
$$

and using equations (3.3.27), (3.3.30) and (3.3.31) the following terms are derived

$$\begin{aligned}
g_0^*(s,\ p) &= -1,\\
g_1^*(s,\ p) &= -\frac{M_0+N_0}{2\pi},\\
g_2^*(s,\ p) &= -\frac{\left(\bar{M}+\bar{N}\right)+\left(\log s-\log 2+c\right)\left(M_0+N_0\right)}{2\pi},\\
g_3^*(s,\ p) &= -\left(\frac{M_0+N_0}{2\pi}\right)^2
\end{aligned} \tag{3.3.33}$$

and

$$\begin{aligned}
g_4^*(s,\ p) = -\frac{1}{\pi}\left(\frac{M_2+N_2}{4}\right)\left(\frac{1}{4}+\frac{s^2}{2}\right)-\left(\frac{M_0+N_0}{4\pi^2}\right)\\
\left[\left(\bar{M}+\bar{N}\right)+\left(\log s-\log 2+c\right)\left(M_0+N_0\right)\right].
\end{aligned}$$

3.3.5 Quantities of physical interest

Stress intensity factor (SIF):

The stress intensity factor is defined as

$$K_I^*(p) = \lim_{x\to 1^+}\sqrt{2(x-1)}|\sigma_{yy}^*(x,\ 0,\ p)|,$$

which can be deduced as

$$K_I^*(p) = \frac{\tau_0}{p}|g^*(1,\ p)|. \tag{3.3.34}$$

Using Laplace inverse transform, stress intensity factor in the time domain is given by

$$K_I(t) = \frac{\tau_0}{2\pi\iota}\int_{B_r}\frac{|g^*(1,p)|}{p}e^{pt}dp, \tag{3.3.35}$$

where B_r is the Bromwich path of integration.

Crack opening displacement (COD):

Another quantity of physical interest is the magnitude of the distance between the two edges of the crack and is calculated as

$$\begin{aligned}
D(x) &= |v(x,\ 0^+,\ p) - v(x,\ 0^-,\ p)|\\
&= \frac{\tau_0}{\mu p}\left|\int_x^1 \frac{sg^*(s,\ p)}{\sqrt{s^2-x^2}}ds\right|.
\end{aligned}$$

Normalizing $D(x)$ w.r.t. the static displacement $\left(\frac{\tau_0}{\mu}\right)$ between two edges of the crack at the mid position of the crack, we obtain

$$\begin{aligned} D &= \left| \int_x^1 \frac{sg^*(s,\ p)}{\sqrt{s^2-x^2}} ds \right| \\ &= \left| \sqrt{1-x^2} g^*(1,\ p) - \int_x^1 \sqrt{s^2-x^2} g^{*'}(s,\ p) ds \right|. \end{aligned} \tag{3.3.36}$$

3.3.6 Shear impact

In this occasion, due to In-plane shear impact, the boundary conditions on $y = 0$ is written as

$$\begin{aligned} &\sigma_{yy}(x,\ 0,\ t) = 0, && 0 \le x < \infty \\ &\sigma_{xy}(x,\ 0,\ t) = -\tau_0 H(t), && 0 \le x \le 1 \\ &u(x,\ 0,\ t) = 0, && x > 1. \end{aligned}$$

In the Laplace transform domain, the above boundary conditions become

$$\sigma^*_{yy}(x,\ 0,\ p) = 0, \qquad 0 \le x < \infty \tag{3.3.37}$$

$$\sigma^*_{xy}(x,\ 0,\ p) = -\frac{\tau_0}{p}, \qquad 0 \le x \le 1 \tag{3.3.38}$$

and

$$u^*(x,\ 0,\ p) = 0, \quad x > 1. \tag{3.3.39}$$

We take the potential functions ϕ^* and ψ^* in the following form

$$u^* = \partial_x \phi^* + \partial_y \psi^* \text{ and } v^* = \partial_y \phi^* - \partial_x \psi^* \tag{3.3.40}$$

with

$$\phi^*(x,\ y,\ p) = \int_0^\infty A_1(\xi,\ p) \sin(\xi x) e^{-\gamma_1 y} d\xi \tag{3.3.41}$$

and

$$\psi^*(x,\ y,\ p) = \int_0^\infty B_1(\xi,\ p) \cos(\xi x) e^{-\gamma_2 y} d\xi. \tag{3.3.42}$$

Applying equations (3.3.41) and (3.3.42) in equation (3.3.40), we get

$$\begin{aligned} &u^*(x,\ y,\ p) = \\ &\int_0^\infty \left[\xi A_1(\xi,\ p) e^{-\gamma_1 y} - \gamma_2 B_1(\xi,\ p) e^{-\gamma_2 y} \right] \cos(\xi x) d\xi \end{aligned}$$

and

$$v^*(x,\ y,\ p) = \int_0^\infty \left[\xi B_1(\xi,\ p)e^{-\gamma_2 y} - \gamma_1 A_1(\xi,\ p)e^{-\gamma_1 y}\right] \sin(\xi x)d\xi.$$

With the aid of boundary condition (3.3.37), we find

$$B_1(\xi,\ p) = \alpha_1 A_1(\xi,\ p) \tag{3.3.43}$$

where $\alpha_1 = \frac{2\mu\gamma_1^2+\lambda\bar{k_1}^2}{2\mu\xi\gamma_2}$. Again, using boundary conditions (3.3.39) and (3.3.38), we obtain the subsequent dual integral equations

$$\int_0^\infty \cos(\xi x)D_1(\xi,\ p)d\xi = 0, \quad |x| > 1 \tag{3.3.44}$$

and

$$\int_0^\infty \xi\cos(\xi x)\left[H_1(\xi,\ p)+1\right]D_1(\xi,\ p)d\xi = \frac{\tau_0}{2\mu p}, \quad |x| \le 1 \tag{3.3.45}$$

where $D_1(\xi,\ p) = (\xi - \gamma_2\alpha_1)\,A_1(\xi,\ p)$ and

$$H_1(\xi,\ p) = \frac{\alpha_1\left(\xi^2+\gamma_2^2\right) - 2\xi\gamma_1}{2\xi\left(\gamma_2\alpha_1 - \xi\right)} - 1 \ \rightarrow\ 0 \ \text{ as } \ \xi \rightarrow\ \infty.$$

Considering the trial solution of the equations (3.3.44) and (3.3.45) as

$$D_1(\xi,\ p) = \frac{\tau_0}{2\mu p}\int_0^1 sh^*(s,\ p)J_0(\xi s)ds.$$

Applying the similar procedure as of normal impact, we derive the following Fredholm integral equation

$$h^*(s,\ p) + \int_0^1 uh^*(u,\ p)T(u,\ s,\ p)du = 1 \tag{3.3.46}$$

where

$$\begin{aligned} T(u,\ s,\ p) = & \frac{2}{\pi\left(2+\frac{\lambda}{\mu}\right)} \\ & \int_0^\gamma \bar{k_1}^2 \frac{\left(1-\xi^2+\frac{\lambda}{2\mu}\right)\left(2\xi^2-\gamma^2\right)}{\sqrt{\gamma^2-\xi^2}} K_0\left(\bar{k_1}\xi s\right) I_0\left(\bar{k_1}\xi u\right) d\xi \\ & - \frac{4}{\pi\left(2+\frac{\lambda}{\mu}\right)}\int_0^1 \bar{k_1}^2\xi^2\sqrt{1-\xi^2}K_0\left(\bar{k_1}\xi s\right) I_0\left(\bar{k_1}\xi u\right) d\xi, \quad s > u. \end{aligned} \tag{3.3.47}$$

Using the same method of solution as given in 'Solution of the integral equation' subsection, we acquired the following terms:

$$T_1(u,\ s,\ p) = \frac{2}{\pi\left(2+\frac{\lambda}{\mu}\right)}\left(-M_0' + 2N_0'\right),$$

$$T_2(u,\ s,\ p) = \frac{2}{\pi\left(2+\frac{\lambda}{\mu}\right)}\times$$

$$\left[\left(-\bar{M}' + 2\bar{N}'\right) + (\log s - \log 2 + c)\left(-M_0' + 2N_0'\right)\right],$$

$$T_3(u,\ s,\ p) = 0,$$

$$T_4(u,\ s,\ p) = \frac{u^2+s^2}{4}\frac{2}{\pi\left(2+\frac{\lambda}{\mu}\right)}\left[-M_2' + 2N_2'\right],$$

$$M_{2n}' = \int_0^\gamma \xi^{2n}\bar{\alpha}(\xi,\ \gamma)d\xi,$$

$$N_{2n}' = \int_0^1 \xi^{2n}\bar{\beta}(\xi),$$

$$\bar{M}' = \int_0^\gamma \log(\xi)\bar{\alpha}(\xi,\ \gamma)d\xi,$$

$$\bar{N}' = \int_0^1 \log(\xi)\bar{\beta}(\xi)d\xi$$

where

$$\bar{\alpha}(\xi,\ \gamma) = \frac{\left(1-\xi^2+\frac{\lambda}{2\mu}\right)\left(2\xi^2-\gamma^2\right)}{\sqrt{\gamma^2-\xi^2}}$$

and

$$\bar{\beta}(\xi) = \xi^2\sqrt{1-\xi^2}$$

with

$$h_0^*(s,\ p) = 1,$$
$$h_1^*(s,\ p) = \frac{M_0' - 2N_0'}{\pi\left(2 + \frac{\lambda}{\mu}\right)},$$
$$h_2^*(s,\ p) =$$
$$\frac{1}{\pi\left(2 + \frac{\lambda}{\mu}\right)}\left[\left(\bar{M}' - 2\bar{N}'\right) + (\log s - \log 2 + c)\left(M_0' - 2N_0'\right)\right],$$
$$h_3^*(s,\ p) = \left[\frac{M_0' - 2N_0'}{\pi\left(2 + \frac{\lambda}{\mu}\right)}\right]^2,$$

and

$$h_4^*(s,\ p) = \frac{M_2' - 2N_2'}{\pi\left(2 + \frac{\lambda}{\mu}\right)}\left(\frac{1}{8} + \frac{s^2}{4}\right) +$$
$$\frac{2\left(M_0' - 2N_0'\right)}{\left[\pi\left(2 + \frac{\lambda}{\mu}\right)\right]^2}\left[\left(\bar{M}' - 2\bar{N}'\right) + (\log s - \log 2 + c)\left(M_0' - 2N_0'\right)\right].$$

The stress intensity factor in the p domain can be defined by

$$K_{II}^*(p) = \lim_{x \to 1^+} \sqrt{2(x-1)}\left|\sigma_{xy}^*(x,\ 0,\ p)\right|,$$

and deduced from above equation as

$$K_{II}^*(p) = \frac{\tau_0}{p}\left|h^*(1,\ p)\right|$$

and in the time domain it becomes

$$K_{II}(t) = \frac{\tau_0}{2\pi\iota}\int_{B_r} \frac{|h^*(1,\ p)|}{p} e^{pt} dp. \tag{3.3.48}$$

3.3.7 Numerical calculation and discussions

We present numerical results by means of graphs for SIF and COD of finite crack due to normal impact and shear impact in the presence and absence of magnetic field for isotropic material Aluminum, we use the following data

$$\rho = 2700\ kg\ m^{-3},\ \ \lambda = 51.08\ GPa,\ \ \mu = 26.32\ GPa$$
$$\mu_0 = 1.7,\ \ \epsilon_0 = 0.3.$$

We have used Zakian Algorithm (Zakian, 1970) for numerical computation of Laplace inversion in equations (3.3.35), (3.3.36) and (3.3.48).

In Fig. 3.13 the value of $\frac{K_I(t)}{\tau_0}$ has been plotted against time t. The graph exhibits the effect of SIF for absence and presence of magnetic field. For $H_0 = 0$ the curve represents SIF without magnetic field and for $H_0 = 5$ and 10 curves depict SIF's nature in magnetic field. It is clear that SIF decreases with increase in time (t). Also, SIF decreases with the increasing values of H_0 that means magnetoelastic materials can prevent the crack propagation. The induced SIF exceeds the fracture toughness periodically. Magnetic field can resist the SIF to exceed the fracture toughness (K_I^c) for a paramagnetic material Aluminum.

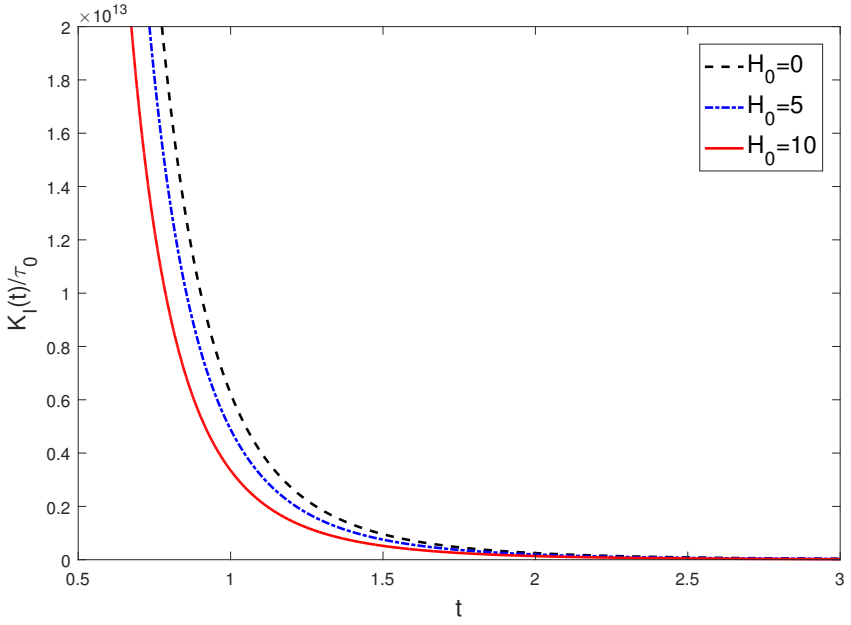

FIGURE 3.13: SIF vs time due to normal impact

Fig. 3.14 is the plot of COD versus crack length (x) in a fixed time $t = 0.5$ for $H_0 = 0,\ 5$ and 10. Notably, COD versus crack length graph is symmetrical about $x = 0$, COD make valleys at the center of the crack and tends to zero at the tips of the crack.

Many researchers have focus to make crack opening displacement elliptical in an infinite medium. In this case the term $\int_x^1 \sqrt{s^2 - x^2} g^{*'}(s,\ p) ds$ in equation (3.3.36) is neglected and the COD becomes $D' = \left|\sqrt{1 - x^2} g^*(1,\ p)\right|$. Fig. 3.16 is the plot D' in time domain versus crack length (x) for $t = 0.5$. It is clear that D' grips highest value at the center of the crack i.e. at $x = 0$. In the presence of magnetic field in elastic medium crack opening

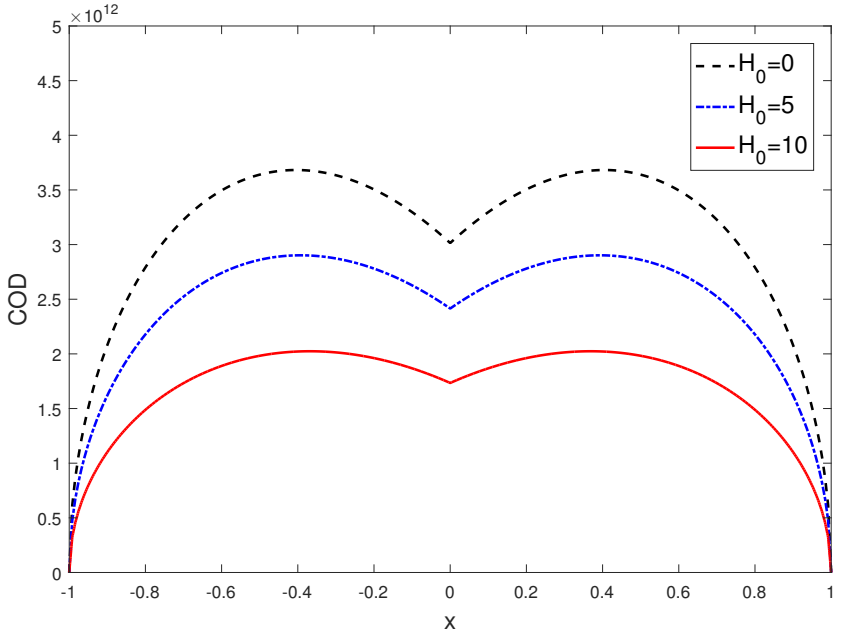

FIGURE 3.14: COD vs crack position

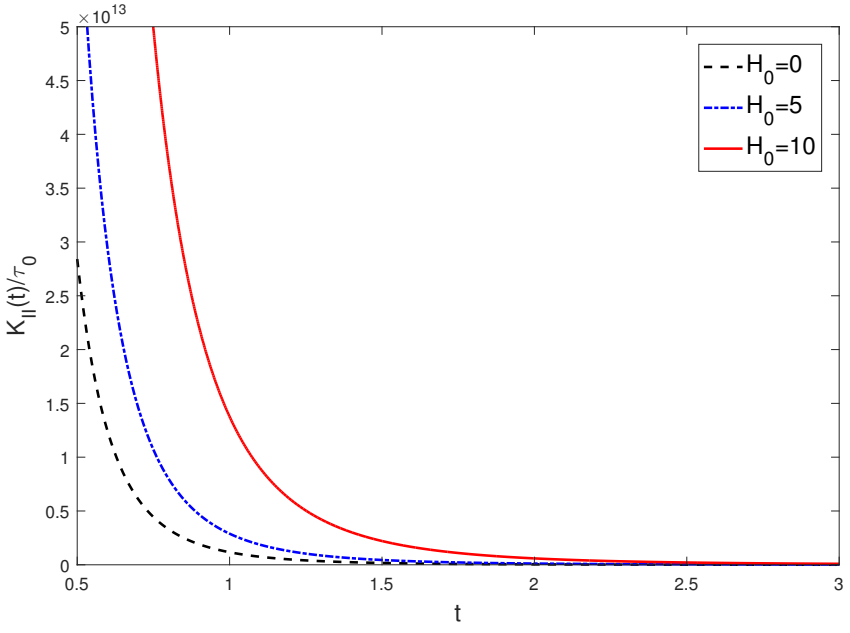

FIGURE 3.15: SIF vs time due to shear impact

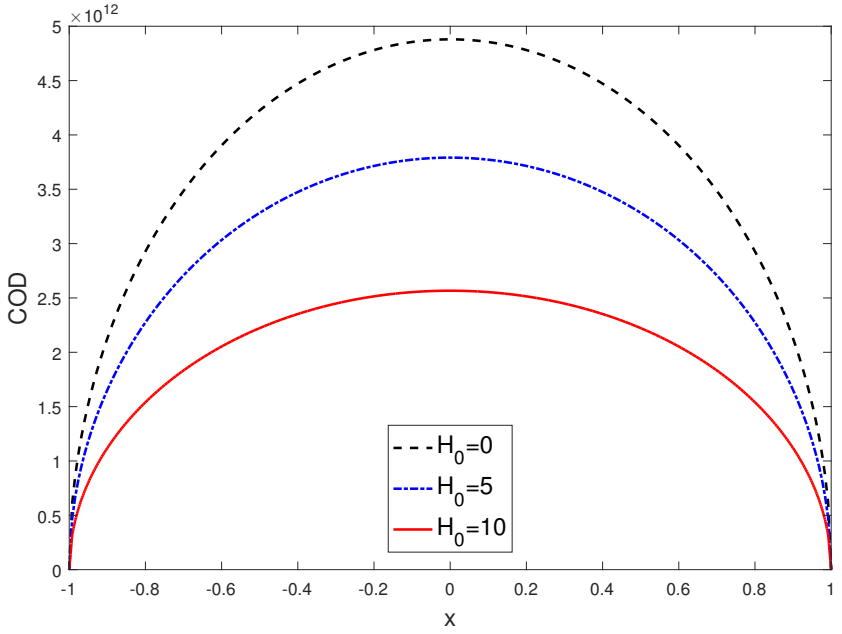

FIGURE 3.16: D' versus Crack position

displacement is smaller than that of without magnetic field. In case of actual COD (D), the term $\int_x^1 \sqrt{s^2 - x^2} g^{*'}(s,\ p) ds$ makes the valley at $x = 0$.

In present problem $\frac{\tau_0}{p} D' = \sqrt{1 - x^2} K_I^*(p)$, which implies crack opening displacement is directly related to the SIF for magnetoelastic materials. So, COD are as viable as SIF to describe the crack features.

In Fig. 3.15 we have plotted SIF $\frac{K_{II}(t)}{\tau_0}$ against t. It is commendable that the impact of stress intensity factor is higher due to magnetic field than that of without magnetic field for in-plane shear loading. SIF decreases gradually with an increase of time t. Stress singularity at the crack tip is emerged due to external magnetic field, so Mode-II (sliding mode) crack propagates faster in the presence of magnetic field.

3.3.8 Conclusion

An analytical approach has been studied to discuss the effect of a magnetic field in the impact response of a finite crack in an infinite isotropic medium. The followings are the outcome of this study:

- SIF and COD are not much effective in the presence of magnetic field due to normal impact. Magnetic field resists the crack opening due to sudden load.

- SIF reaches zero with the increase in time, so crack growth can be arrested after a certain period of time.

In case of a Mode-I (opening mode) crack, the SIF and COD are not so much in the presence of magnetic field as in the absence of magnetic field, so under normal impact magnetic can prevent the crack growth. We have considered a paramagnetic material, in which magnetism disappears on removal of the external magnetic field. Ferromagnetic materials like iron, cobalt, and nickel are more effective at preventing crack growth under normal impact conditions. However, a magnetic field cannot inhibit crack growth in cases of sliding mode.

Chapter 4

Cracks under thermal loading

4.1 A thermoelastic model with higher order time derivatives for a crack in a rotating solid[1]

4.1.1 Introduction

Mode I crack (opening mode) occurs by the stress normal to the plane of the crack and produces the most damage. Many researchers focus on the research on Mode I crack in thermoelastic medium as it is a common theme in various structural designs, which covers the study of different laws to control crack growth. Othman and Atwa (2013) discussed a problem of mode I crack in an infinite thermoelastic medium under G-N theory.

The field of study of thermoelastic wave propagation in a rotating solid has paid attention to many researchers. Since most of the large bodies rotate, it's practical to examine the propagation of thermoelastic waves in a rotating body, taking phase lags into account. The effect of rotation has been discussed on different thermoelastic theories by Othman and Lotfy (2015, 2011); Othman et al. (2014a,b, 2015); Othman and Abed-Elaziz (2017); Said et al. (2022). A mode-I crack problem in a rotating thermoelastic medium under dual-phase-lag model is studied by Abouelregal and Abo-Dahab (2018).

A reinforced concrete material is designed for all conditions of stress and is satisfied all the basic principles of mechanics. The characteristic property of a self-reinforced substance

[1]Panja, S. K., Lahiri, A., & Mandal, S. C. (2023). A thermoelastic model with higher order time derivatives for a crack in a rotating solid. International Journal for Computational Methods in Engineering Science and Mechanics, 24(2), 107-118.

is that the components are bound together within in an elastic condition such that there is no relative displacement within components. A fiber-reinforced composite is useful in the field of Geo-physics and construction sectors due to its low weight and high strength. Belfield et al. (1983) introduce the idea that continuous reinforcement is applicable at every point of an elastic solid. Verma and Rana (1983) used this theme to the rotation of a circular cylindrical tube. The effect of rotation on micropolar thermoelasticity has been studied by Othman and Singh (2007). Sarkar and Atwa (2019) discussed a two-temperature problem of a mode I crack in a fiber-reinforced thermoelastic medium under G-N theory. Recently, Lotfy and El-Bary (2024) studied a mode I crack problem with rotational effect in a fiber-reinforced thermoelastic medium under Lord-Shulman theory.

A fiber-reinforced material is very substantial in microstructure. Usually, manmade and many natural substances such as rocks, concrete, polymers, composites, etc. possess a microstructure. Generalized thermoelasticity theory is very much useful in modern aircraft technology and polymer coating in which extreme thermal stresses produce due to high velocities. The effect of thermal stresses and rotation on a preexisting hairline crack on such kinds of fields is significant. Several attempts related to crack in thermoelastic medium have been done, but a thermoelastic model with refined phase-lags and time derivatives of higher order in presence of a crack for a fiber-reinforced rotating solid has not been studied till now.

In this article, we applied the normal mode analysis to determine the exact expressions of displacement, temperature and stress components of a linearized Mode-I crack under a refined one-temperature thermoelastic theory with time derivatives of higher order and phase-lags. the convergency of the refinement is tabulated and compared with SPL, L-S, G-N and CTE theories. The effect of rotation and phase-lags on different field quantities are analyzed graphically.

4.1.2 Formulation of the problem

Let us consider a linear, infinite homogeneous, fiber-reinforced thermoelastic solid covering the region $R = \{(x,\ y,\ z) :\ -\infty < x < \infty,\ -\infty < y < \infty,\ z = 0\}$, with a finite crack on $|x| < a,\ z = 0$ (Fig. 4.1). The crack is subjected to a prescribed temperature and normal stress distributions.

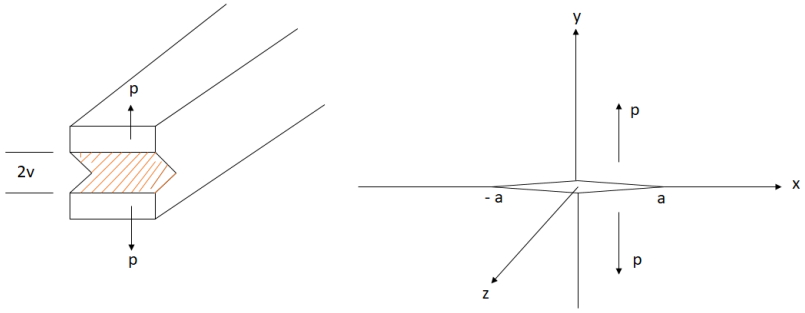

FIGURE 4.1: Geometry of the problem

The constitutive equation for a fiber-reinforced linear thermoelastic solid associated with reinforcement direction $\vec{d}$ (along $x-$ direction) are

$$\begin{aligned}\sigma_{ij} =&\lambda e_{kk}\delta_{ij} + 2\mu_T e_{ij} + \alpha\left(d_k d_m e_{km}\delta_{ij} + d_i d_j e_{kk}\right) + 2\left(\mu_L - \mu_T\right)\left(d_i d_k e_{kj} + d_j d_k e_{ki}\right)\\ &+ \beta d_k d_m e_{km} d_i d_j - \gamma\left(T - T_0\right)\delta_{ij},\quad (i,\ j,\ k,\ m = 1,\ 2,\ 3)\end{aligned} \tag{4.1.1}$$

where σ_{ij} are the stress components, e_{ij} are the strain components; λ, μ_T are elastic constants; α, β, $2\left(\mu_L - \mu_T\right)$ are reinforcement parameters, coupling parameter $\gamma = (3\lambda + 2\mu)\,\alpha_t$, α_t is the coefficient of linear thermal expansion, δ_{ij} is the Kronecker delta and $\vec{d} \equiv (d_1,\ d_2,\ d_3)$ with $d_1^2 + d_2^2 + d_3^2 = 1$. We assume the fiber-reinforcement direction as $(1,\ 0,\ 0)$. The strain components are written in terms of displacement (u_i) as

$$e_{ij} = \frac{1}{2}\left(u_{i,j} + u_{j,i}\right),\quad (i,\ j = 1,\ 2,\ 3). \tag{4.1.2}$$

The plain strain deformation parallel to the $z = 0$ plane and depends on time t is defined as

$$u_1 = u(x,\ y,\ t),\ u_2 = v(x,\ y,\ t),\ u_3 = 0. \tag{4.1.3}$$

With the help of equations (4.1.1)-(4.1.3); the stress components are written as:

$$\sigma_{xx} = P_{11}\partial_x u + P_{12}\partial_y v - \gamma(T - T_0), \tag{4.1.4}$$

$$\sigma_{yy} = P_{22}\partial_y v + P_{12}\partial_x u - \gamma(T - T_0), \tag{4.1.5}$$

$$\sigma_{zz} = P_{12}\partial_x u + \lambda\partial_y v - \gamma(T - T_0), \tag{4.1.6}$$

$$\sigma_{xy} = \mu_L\left(\partial_y u + \partial_x v\right), \quad \sigma_{xz} = \sigma_{yz} = 0, \tag{4.1.7}$$

where

$$\begin{aligned} P_{11} &= \lambda + 2\left(\alpha + \mu_T\right) + 4\left(\mu_L - \mu_T\right) + \beta, \\ P_{12} &= \alpha + \lambda, \quad P_{22} = \lambda + 2\mu_T. \end{aligned} \tag{4.1.8}$$

∂_x, ∂_y and ∂_t denote the partial derivative with respect to x, y and t respectively.

The fiber-reinforced solid is rotating uniformly with an angular velocity $\vec{\Omega} = \Omega\vec{n}$, where $\vec{n}$ is a unit vector describing the direction of the axis of rotation.

The equation of motion in the absence of body force in a rotating frame of reference is given by Lotfy and El-Bary (2024); Othman et al. (2015)

$$\rho\left[\ddot{u}_i + \left\{\vec{\Omega} \times \left(\vec{\Omega} \times \vec{u}\right)\right\}_i + \left(2\vec{\Omega} \times \dot{\vec{u}}\right)_i\right] = \sigma_{ij,j}, \quad (i,j = 1,2,3) \tag{4.1.9}$$

where $\vec{\Omega} \times \left(\vec{\Omega} \times \vec{u}\right)$ is centripetal acceleration due to time varying motion and $\left(2\vec{\Omega} \times \dot{\vec{u}}\right)$ is Corioli's acceleration.

The heat conduction equation in the context of refined phase-lags (RPL) model of generalized thermoelasticity theory is of the form (Zenkour, 2018)

$$K\left(1 + \sum_{n=1}^{N} \frac{\tau_\theta^n}{n!}\frac{\partial^n}{\partial t^n}\right) T_{,ii} = \left(Q + \tau_0\frac{\partial}{\partial t} + \sum_{n=1}^{N} \frac{\tau_q^{n+1}}{(n+1)!}\frac{\partial^{n+1}}{\partial t^{n+1}}\right)\left[\rho C_E\frac{\partial T}{\partial t} + \gamma T_0\frac{\partial}{\partial t}e_{kk}\right] \tag{4.1.10}$$

where K is the thermal conductivity, C_E represents specific heat at constant strain, T denotes the temperature above reference temperature T_0, Q is a parameter responsible for internal heat generation that takes value either 0 or 1 according to the thermoelastic theories and ρ is the density. Moreover, τ_θ is phase-lag (PL) of the temperature gradient, τ_0 is a phase-lag parameter related to the internal energy and τ_q is the phase-lag of the heat flux. The value of N denotes the refinement of the generalized theory of thermoelasticity.

Substituting the values of displacements and stress components from equation (4.1.3)-(4.1.7) into the equation (4.1.9), we obtain the equation of motion in the following form

$$\rho\left(\partial_{tt}u - \Omega^2 u - 2\Omega\partial_t v\right) = P_{11}\partial_{xx}u + Q_2\partial_{xy}v + Q_1\partial_{yy}u - \gamma\partial_x T, \tag{4.1.11}$$

$$\rho\left(\partial_{tt}v - \Omega^2 v + 2\Omega\partial_t u\right) = P_{22}\partial_{yy}v + Q_2\partial_{xy}u + Q_1\partial_{xx}v - \gamma\partial_y T \tag{4.1.12}$$

where $Q_1 = \mu_L$, $Q_2 = P_{12} + \mu_L = \alpha + \lambda + \mu_L$.

We use the following non dimensional variables for further consideration:

$$\begin{aligned} &\bar{x} = c_1\eta x,\ \bar{y} = c_1\eta y,\ \bar{u} = c_1\eta u,\ \bar{v} = c_1\eta v,\ \bar{t} = c_1^2\eta t, \\ &\bar{\tau_0} = c_1^2\eta\tau_0,\ \bar{\tau_\theta} = c_1^2\eta\tau_\theta,\ \bar{\tau_q} = c_1^2\eta\tau_q,\ \bar{\Omega} = \frac{\Omega}{c_1^2\eta} \\ &\theta = \frac{\gamma(T - T_0)}{\lambda + 2\mu_T},\ \bar{\sigma}_{ij} = \frac{\sigma_{ij}}{\mu_T} \end{aligned} \tag{4.1.13}$$

where $\eta = \frac{\rho C_E}{K}$, $c_1^2 = \frac{\lambda+2\mu_T}{\rho}$.

Employing the above non-dimensional expressions in equations (4.1.11), (4.1.12), (4.1.10) and (4.1.4)-(4.1.7), we may recast into dimensionless form (skipping the bar for convenience)

$$\partial_{tt}u - \Omega^2 u - 2\Omega\partial_t v = h_{11}\partial_{xx}u + h_2\partial_{xy}v + h_1\partial_{yy}u - \partial_x\theta, \tag{4.1.14}$$

$$\partial_{tt}v - \Omega^2 v + 2\Omega\partial_t u = h_{22}\partial_{yy}v + h_2\partial_{xy}u + h_1\partial_{xx}v - \partial_y\theta, \tag{4.1.15}$$

$$\begin{aligned} \left(1 + \sum_{n=1}^{N} \frac{\tau_\theta^n}{n!}\frac{\partial^n}{\partial t^n}\right)(\partial_{xx}\theta + \partial_{yy}\theta) = \left(Q + \tau_0\frac{\partial}{\partial t} + \sum_{n=1}^{N}\frac{\tau_q^{n+1}}{(n+1)!}\frac{\partial^{n+1}}{\partial t^{n+1}}\right) \\ \left[\partial_t\theta + \epsilon\frac{\partial}{\partial t}(\partial_x u + \partial_y v)\right], \end{aligned} \tag{4.1.16}$$

$$\mu_T\sigma_{xx} = P_{11}\partial_x u + P_{12}\partial_y v - (\lambda + 2\mu_T)\,\theta, \tag{4.1.17}$$

$$\mu_T\sigma_{yy} = P_{22}\partial_y v + P_{12}\partial_x u - (\lambda + 2\mu_T)\,\theta, \tag{4.1.18}$$

$$\mu_T\sigma_{zz} = P_{12}\partial_x u + \lambda\partial_y v - (\lambda + 2\mu_T)\,\theta, \tag{4.1.19}$$

$$\mu_T\sigma_{xy} = \mu_L\,(\partial_y u + \partial_x v)\,,\ \sigma_{xz} = \sigma_{yz} = 0, \tag{4.1.20}$$

where

$$h_{11} = \frac{P_{11}}{\lambda + 2\mu_T},\ \ h_{22} = \frac{P_{22}}{\lambda + 2\mu_T},\ \ h_1 = \frac{Q_1}{\lambda + 2\mu_T},\ \ h_2 = \frac{Q_2}{\lambda + 2\mu_T}$$
$$\text{and } \epsilon = \frac{\gamma^2 T_0}{\rho C_E\,(\lambda + 2\mu_T)}.$$

4.1.3 Normal mode analysis

Considering that all the field variables are sufficiently smooth on the real line so that normal mode analysis is applicable over these quantities. The solution of the considered

physical variables can be decomposed in terms of normal modes and are given by:

$$[u, v, \theta, \sigma_{ij}](x, y, t) = \left[u^*, v^*, \theta^*, \sigma_{ij}^*\right](x) e^{\omega t + \iota b y}, \tag{4.1.21}$$

where $\left[u^*, v^*, \theta^*, \sigma_{ij}^*\right](x)$ are the amplitudes of the field variables, ω is the angular frequency and b is the wave number.

Substituting equation (4.1.21), into equations (4.1.14)-(4.1.20), we get

$$\left(h_{11}D^2 - P_1\right) u^* + \left(h_3 + \iota b h_2 D\right) v^* = D\theta^*, \tag{4.1.22}$$

$$\left(\iota b h_2 D - h_3\right) u^* + \left(h_1 D^2 - P_2\right) v^* = \iota b \theta^*, \tag{4.1.23}$$

$$P_5 \epsilon D u^* + \iota b \epsilon P_5 v^* = \left(D^2 - b^2 - P_5\right) \theta^*, \tag{4.1.24}$$

$$\mu_T \sigma_{xx}^* = P_{11} D u^* + \iota b P_{12} v^* - \left(\lambda + 2\mu_T\right) \theta^*, \tag{4.1.25}$$

$$\mu_T \sigma_{yy}^* = \iota b P_{22} v^* + P_{12} D u^* - \left(\lambda + 2\mu_T\right) \theta^*, \tag{4.1.26}$$

$$\mu_T \sigma_{zz}^* = P_{12} D u^* + \iota b \lambda v^* - \left(\lambda + 2\mu_T\right) \theta^*, \tag{4.1.27}$$

$$\mu_T \sigma_{xy}^* = \mu_L \left(\iota b u^* + D v^*\right), \ \sigma_{xz}^* = \sigma_{yz}^* = 0 \tag{4.1.28}$$

where

$$D \equiv \frac{d}{dx}, \ P_1 = h_1 b^2 - \Omega^2 + \omega^2, \ P_2 = h_{22} b^2 - \Omega^2 + \omega^2, \ P_3 = 1 + \sum_{n=1}^{N} \frac{\tau_\theta^n}{n!} \omega^n,$$
$$P_4 = Q + \tau_0 \omega + \sum_{n=1}^{N} \frac{\tau_q^{n+1}}{(n+1)!} \omega^{n+1}, \ P_5 = \frac{\omega P_4}{P_3} \text{ and } h_3 = 2\Omega\omega.$$

Eliminating $v^*(x)$ and $\theta^*(x)$ from equations (4.1.22)-(4.1.24), we obtain the following sixth order ordinary differential equation for u^*, v^* and θ^*

$$\left(D^6 - AD^4 + BD^2 - C\right) \left[u^*, v^*, \theta^*\right](x) = 0, \tag{4.1.29}$$

where

$$A = \frac{1}{h_1 h_{11}} \left[h_1 \left(b^2 h_{11} + P_5 h_{11} + P_1 + P_5 \epsilon\right) - b^2 h_2^2 + P_2 h_{11}\right], \tag{4.1.30}$$

$$\begin{aligned} B = & \frac{1}{h_1 h_{11}} \left(P_1 P_5 h_1 + h_3^2 + P_2 P_5 \epsilon + P_2 P_5 h_{11} + P_1 P_2\right) + \\ & \frac{b^2}{h_1 h_{11}} \left(P_5 \epsilon h_{11} + P_1 h_1 - 2 P_5 h_2 \epsilon - b^2 h_2^2 - P_5 h_2^2 + P_2 h_{11}\right), \end{aligned} \tag{4.1.31}$$

$$C = \frac{1}{h_1 h_{11}} \left[P_1 P_2 b^2 + h_3^2 b^2 + P_5 \left(P_1 P_2 + P_1 b^2 \epsilon + h_3^2 \right) \right]. \tag{4.1.32}$$

Equation (4.1.29) can be factored as

$$\prod_{r=1}^{3} \left(D^2 - m_r^2 \right) \left[u^*, v^*, \theta^* \right] (x) = 0, \tag{4.1.33}$$

where $m_r^2,\ (r = 1,\ 2,\ 3)$ are the roots of the above characteristic equation.

The solution (bounded for $x \to \infty$) of the equation (4.1.33) can be written as

$$u^*(x) = \sum_{r=1}^{3} M_r(b,\ \omega) e^{-m_r x}, \tag{4.1.34}$$

$$v^*(x) = \sum_{r=1}^{3} M_r'(b,\ \omega) e^{-m_r x}, \tag{4.1.35}$$

$$\theta^*(x) = \sum_{r=1}^{3} M_r''(b,\ \omega) e^{-m_r x}, \tag{4.1.36}$$

where $M_r,\ M_r'$ and $M_r'',\ (r = 1,\ 2,\ 3)$ are some functions of b and ω.

Using equations (4.1.34)-(4.1.36) into the equations (4.1.22)-(4.1.24), the following relations are found

$$M_r'(b,\ \omega) = H_{1r} M_r(b,\ \omega), \quad r = 1,\ 2,\ 3 \tag{4.1.37}$$

and

$$M_r''(b,\ \omega) = H_{2r} M_r(b,\ \omega), \quad r = 1,\ 2,\ 3 \tag{4.1.38}$$

where

$$H_{1r} = \frac{\iota b h_2 m_r^2 + h_3 m_r - \iota b h_{11} m_r^2 + \iota b P_1}{\iota b h_3 + b^2 h_2 m_r + h_1 m_r^3 - P_2 m_r}, \quad r = 1, 2, 3 \tag{4.1.39}$$

and

$$H_{2r} = \frac{\iota b \epsilon P_5 H_{1r} - \epsilon P_5 m_r}{m_r^2 - b^2 - P_5}, \quad r = 1,\ 2,\ 3. \tag{4.1.40}$$

Therefore, $v^*(x)$ and $\theta^*(x)$ become,

$$v^*(x) = \sum_{r=1}^{3} H_{1r} M_r(b,\ \omega) e^{-m_r x}, \tag{4.1.41}$$

$$\theta^*(x) = \sum_{r=1}^{3} H_{2r} M_r(b,\ \omega) e^{-m_r x}. \tag{4.1.42}$$

Using equations (4.1.34), (4.1.41) and (4.1.42) into the equations (4.1.25)-(4.1.28), we have

$$\mu_T \sigma^*_{xx}(x) = \sum_{r=1}^{3} H_{3r} M_r(b,\ \omega) e^{-m_r x}, \tag{4.1.43}$$

$$\mu_T \sigma^*_{yy}(x) = \sum_{r=1}^{3} H_{4r} M_r(b,\ \omega) e^{-m_r x}, \tag{4.1.44}$$

$$\mu_T \sigma^*_{zz}(x) = \sum_{r=1}^{3} H_{5r} M_r(b,\ \omega) e^{-m_r x}, \tag{4.1.45}$$

$$\mu_T \sigma^*_{xy}(x) = \sum_{r=1}^{3} H_{6r} M_r(b,\ \omega) e^{-m_r x}, \tag{4.1.46}$$

where

$$H_{3r} = -P_{11} m_r + \iota b P_{12} H_{1r} - (\lambda + 2\mu_T) H_{2r}, \quad r = 1,\ 2,\ 3 \tag{4.1.47}$$

$$H_{4r} = \iota b P_{22} H_{1r} - P_{12} m_r - (\lambda + 2\mu_T) H_{2r}, \quad r = 1,\ 2,\ 3 \tag{4.1.48}$$

$$H_{5r} = -P_{12} m_r + \iota b \lambda H_{1r} - (\lambda + 2\mu_T) H_{2r}, \quad r = 1,\ 2,\ 3 \tag{4.1.49}$$

and

$$H_{6r} = \mu_L \iota b - \mu_L m_r H_{1r}, \quad r = 1,\ 2,\ 3. \tag{4.1.50}$$

4.1.4 Boundary conditions and solutions

The boundary surface of the plane is isothermal and is subject to a direct normal point force. The mechanical and thermal boundary conditions at the vertical plane $z = 0$ and in the mid point of the crack at $x = 0$ are in the following form

(i) The crack is mechanically stressed with normal force magnitude p^* i.e.

$$\sigma_{yy}(0,\ y,\ t) = -p(y,\ t) = -p^* e^{\omega t + \iota b y}, \quad |x| < a. \tag{4.1.51}$$

(ii) The crack is subjected to a thermal shock, which leads to

$$\theta(0,\ y,\ t) = f(y,\ t) = f^* e^{\omega t + \iota b y}, \quad |x| < a, \tag{4.1.52}$$

where f^* is a constant temperature.

(iii) The surface is tangential stress free i.e.

$$\sigma_{xy}(0,\ y,\ t) = 0, \quad -\infty < x < \infty. \tag{4.1.53}$$

Operating the boundary conditions (4.1.51)-(4.1.53), we have the following relations

$$\sum_{r=1}^{3} H_{4r} M_r(b,\ \omega) = -p^*, \tag{4.1.54}$$

$$\sum_{r=1}^{3} H_{2r} M_r(b,\ \omega) = f^*, \tag{4.1.55}$$

$$\sum_{r=1}^{3} H_{6r} M_r(b,\ \omega) = 0. \tag{4.1.56}$$

Employing the matrix inversion method for the system of equations (4.1.54)-(4.1.56), we get the values of $M_r,\ (r = 1,\ 2,\ 3)$

$$M_1 = \frac{1}{\Delta}\left[p^*\left(H_{23}H_{62} - H_{22}H_{63}\right) + f^*\left(H_{43}H_{62} - H_{42}H_{63}\right)\right],$$

$$M_2 = \frac{1}{\Delta}\left[p^*\left(H_{21}H_{63} - H_{23}H_{61}\right) + f^*\left(H_{41}H_{63} - H_{43}H_{61}\right)\right],$$

$$M_3 = \frac{1}{\Delta}\left[p^*\left(H_{22}H_{61} - H_{21}H_{62}\right) + f^*\left(H_{42}H_{61} - H_{41}H_{62}\right)\right]$$

where

$$\Delta = H_{41}\left(H_{22}H_{63} - H_{23}H_{62}\right) - H_{42}\left(H_{21}H_{63} - H_{23}H_{61}\right) + H_{43}\left(H_{21}H_{62} - H_{22}H_{61}\right).$$

4.1.5 Special cases

We describe five different thermoelasticity theories (Zenkour, 2018) from the equation (4.1.10) in the following way

- The current refined phase-lags (RPL) thermoelasticity theory is proposed by using $\tau_q = \tau_0 = 0.5 > \tau_\theta = 0.2 > 0,\ Q = 1$ and $N = 3$. Zenkour (2018) discussed the RPL theory provides the efficient and accurate result for $N = 3$. We have checked for higher values also and the results are converging strictly for $N \geq 6$ (Table 4.1).
- The simple-phase-lag (SPL) thermoelasticity theory of Tzou is derived when we put $\tau_q = 0,\ \tau_0 = 0.5 > \tau_\theta = 0.2,\ Q = 1$ and $N = 1$.

- The Lord-Shulman (L-S) thermoelasticity theory is acquired by setting $\tau_\theta = \tau_q = 0,\ \tau_0 = 0.5$ and $Q = 1$.
- The linearized Green-Naghdi(G-N) theory of type II is occurred by setting $\tau_\theta = \tau_q = 0,\ \tau_0 = 1,\ Q = 0$.
- The Coupled thermoelasticity theory (CTE) is proposed when we set $\tau_q = \tau_\theta = \tau_0 = 0$ and $Q = 1$.

TABLE 4.1: Roots of equation (4.1.33) for different thermoelasticity theories

m_i	Ω	CTE	G-N	L-S	SPL	RPL				
						N=3	N=4	N=5	N=6	N=7
m_1	0.0	2.9593	3.5288	3.9551	3.6284	3.6476	3.63483	3.6320	3.6316	3.6316
	0.3	2.9595	3.6831	4.0278	3.6289	3.6925	3.6803	3.6776	3.6772	3.6772
m_2	0.0	4.0641	4.5219	4.6093	4.1655	4.3644	4.3618	4.3608	4.3606	4.3605
	0.3	4.4435	4.7505	4.9187	4.5456	4.7012	4.6979	4.6969	4.6967	4.6967
m_3	0.0	15.0551	15.0551	15.0551	15.0551	15.0551	15.0551	15.0551	15.0551	15.0551
	0.3	14.1678	14.1646	14.1653	14.1669	14.1658	14.1658	14.1658	14.1658	14.1658

4.1.6 Numerical results and discussions

We discuss numerical results by means of graphs of the obtained expression of displacement, temperature and stress components in the presence and absence of rotation. The following physical constants are considered for numerical computation (Lotfy and El-Bary, 2024):

$$\lambda = 7.59 \times 10^9 N/m^2,\ \mu_T = 1.89 \times 10^9 N/m^2,\ \mu_L = 2.45 \times 10^9 N/m^2,$$

$$\alpha = -1.28 \times 10^9 N/m^2,\ \beta = 0.32 \times 10^9 N/m^2,\ \rho = 7800 kg/m^3,$$

$$T_0 = 293K,\ \alpha_t = 1.78 \times 10^{-5} N/m^2,\ K = 386,\ C_E = 383.1 J/(kgK),$$

$$b = 1,\ f^* = 1,\ p^* = 2,\ \omega = 2 + \iota,\ \mu = 3.86 \times 10^{10} kg/(ms^2),\ t = 0.1,\ a = 2.$$

The numerical method indicated here is employed for the distribution of the real part of the temperature (θ), the displacements u and v and the distribution of stresses σ_{yy}, σ_{xx}, σ_{zz} and σ_{xy} for the present problem. The considered physical quantities depend not only on spatial position x and time t but also on thermal relaxation time τ_0 and phase lags τ_θ and τ_q. We considered all variables in the non-dimensional forms.

The delay time τ_θ is generated by the microstructural interactions (small-scale effects of heat transport in space) and the delay time τ_q is originated due to the fast-transient

effects of thermal inertia (small-scale effects of heat transport in time). It is known that the phase-lag of heat flux τ_q can dominate the nature of thermal wave propagation, detain the velocity of thermal wave propagation. The phase-lag of temperature gradient τ_θ supports heat energy diffusion and enacts the behaviors of thermal wave decay in phase-lags heat transfer.

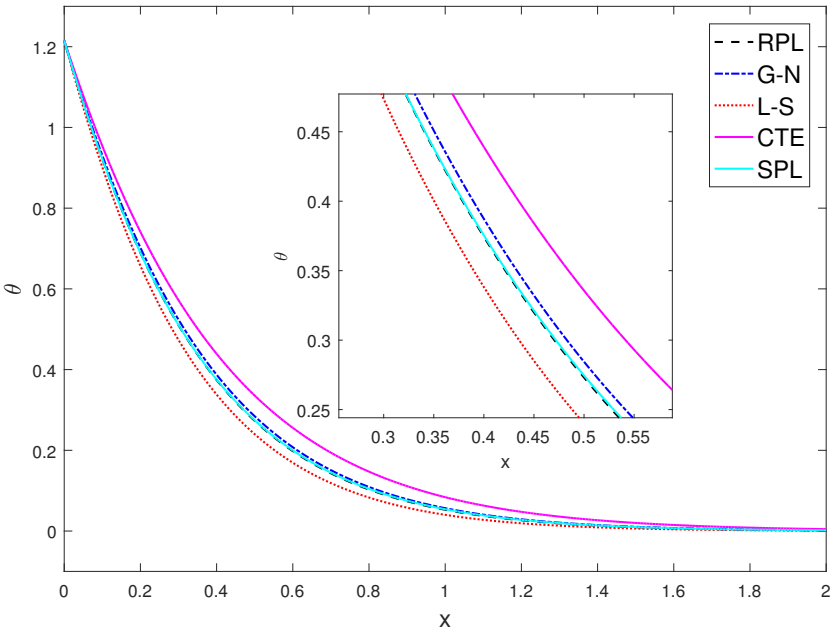

FIGURE 4.2: Temperature θ versus x for $\Omega = 0.0$

Figures 4.2-4.15 are plotted for $0 \leq x \leq 2$ and $y = 0$, represents the crack plane is symmetric with respect to $y-$ plane.

Figures 4.2 and 4.3 are the plots of temperature θ against distance x in the absence ($\Omega = 0.0$) and presence ($\Omega = 0.3$) of rotation. The temperature (θ) reaches peak at the center of the crack and it goes to zero near the edge of the crack for each thermoelasticity theories. The temperature is smallest under L-S theory and greatest for CTE. The nature of temperature curve is agreement with the result found by Abouelregal and Abo-Dahab (2018); Abouelregal (2020a).

In figures 4.4 and 4.5 horizontal displacement (u) has been plotted along the crack (x) for $\Omega = 0.0$ and $\Omega = 0.3$ respectively. Horizontal displacement starts with a negative value and increases with displacement and finally converges to zero for RPL, SPL, L-S and Coupled thermoelasticity theories, while G-N theory shows the reverse effect. Figures 4.6 and 4.7 depict the vertical displacement with x for absence and presence of rotation respectively.

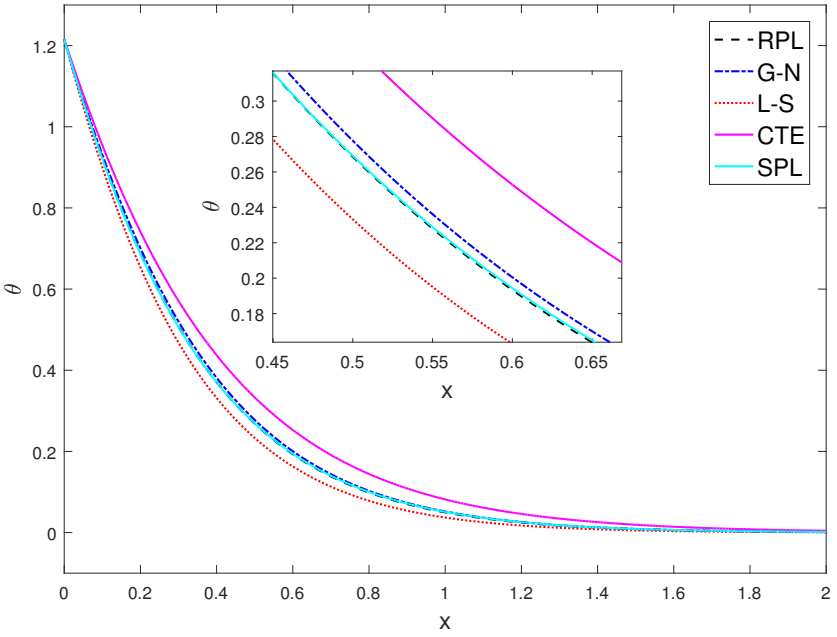

FIGURE 4.3: Temperature θ versus x for $\Omega = 0.3$

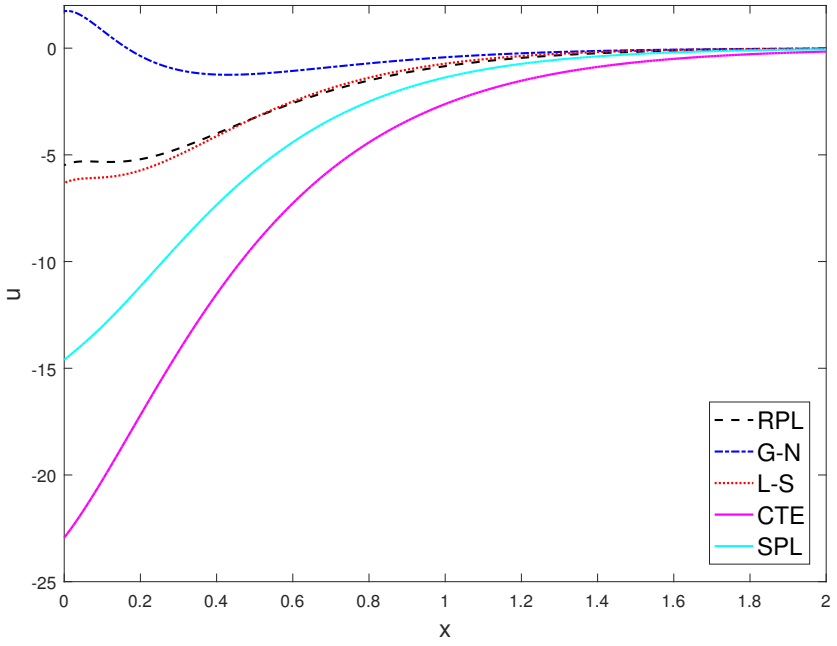

FIGURE 4.4: Displacement u versus x for $\Omega = 0.0$

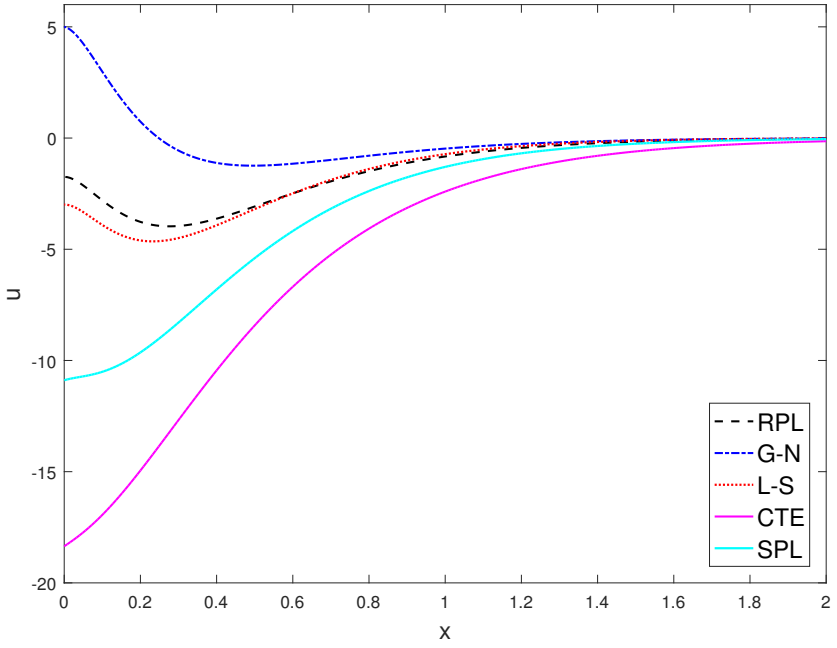

FIGURE 4.5: Displacement u versus x for $\Omega = 0.3$

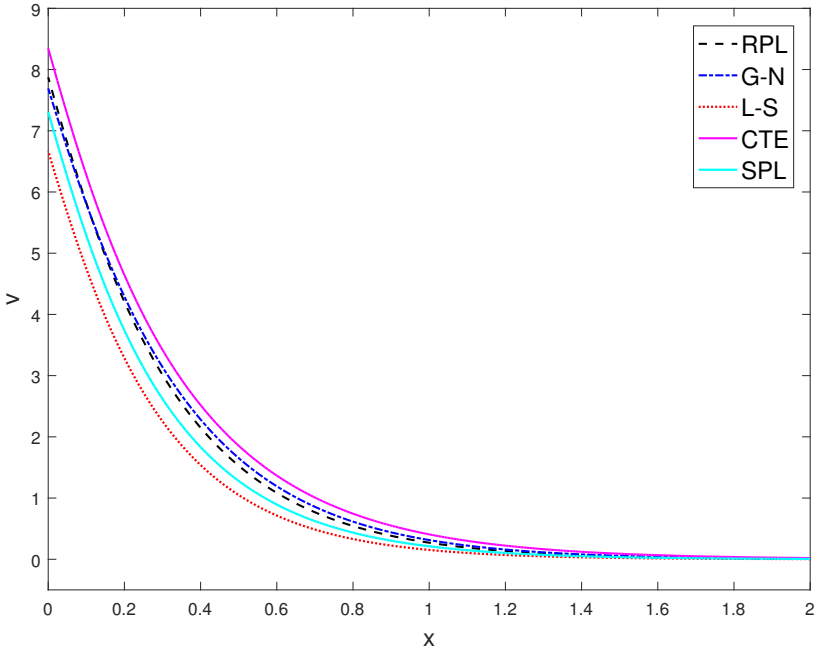

FIGURE 4.6: Displacement v versus x for $\Omega = 0.0$

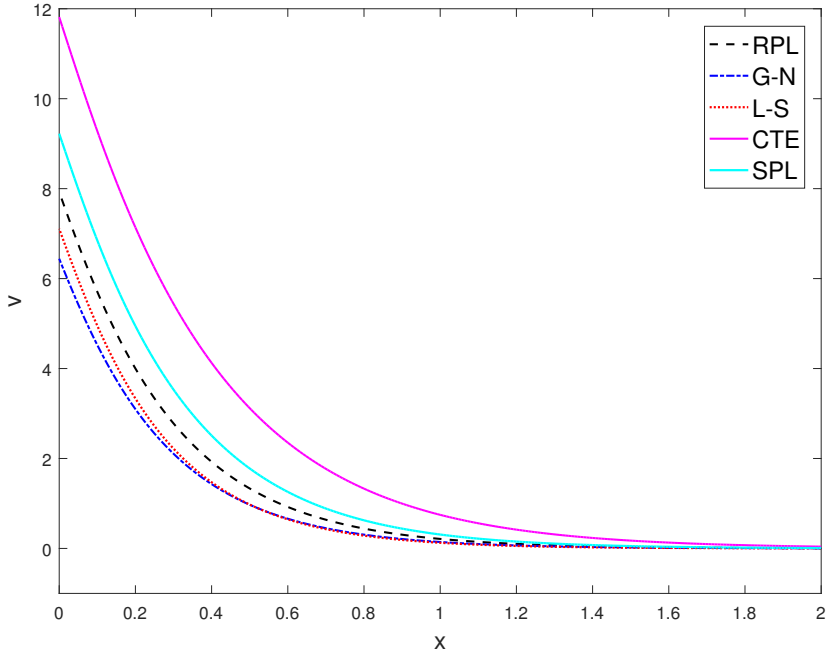

FIGURE 4.7: Displacement v versus x for $\Omega = 0.3$

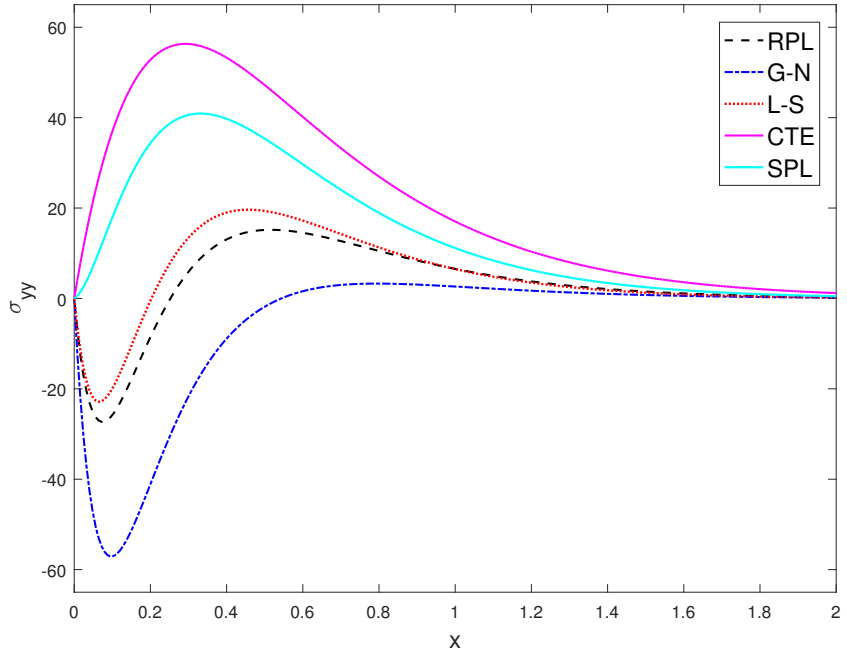

FIGURE 4.8: Stress σ_{yy} versus x for $\Omega = 0.0$

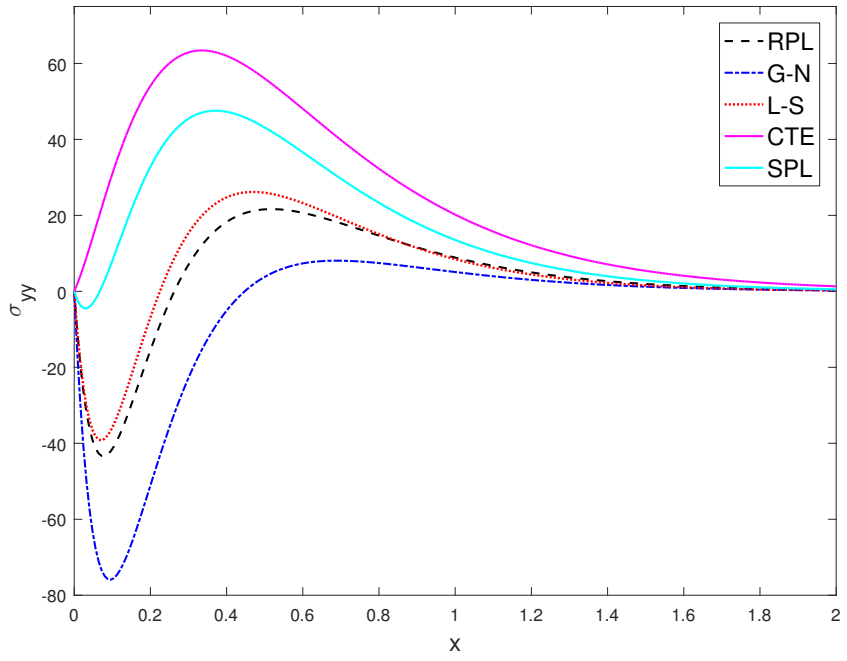

FIGURE 4.9: Stress σ_{yy} versus x for $\Omega = 0.3$

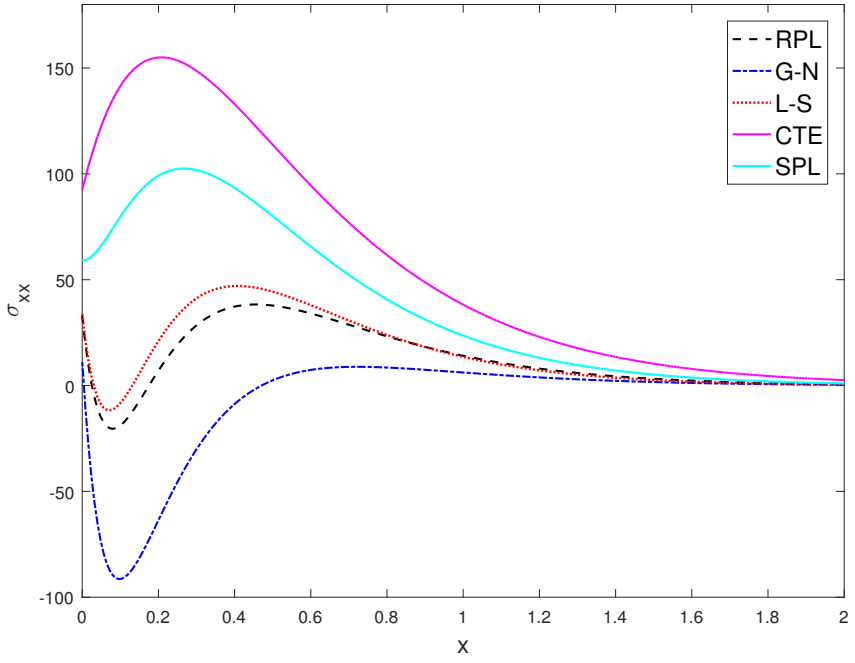

FIGURE 4.10: Stress σ_{xx} versus x for $\Omega = 0.0$

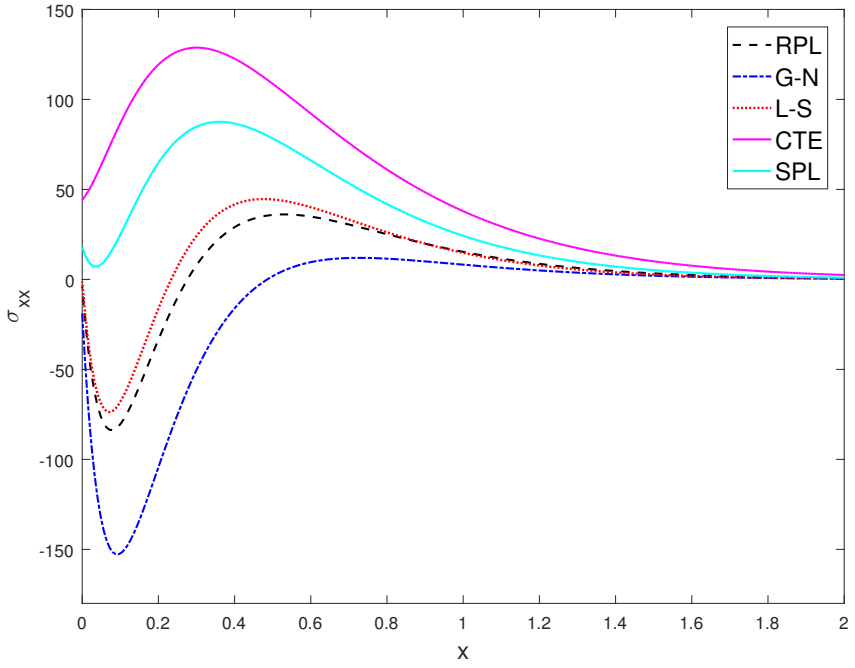

FIGURE 4.11: Stress σ_{xx} versus x for $\Omega = 0.3$

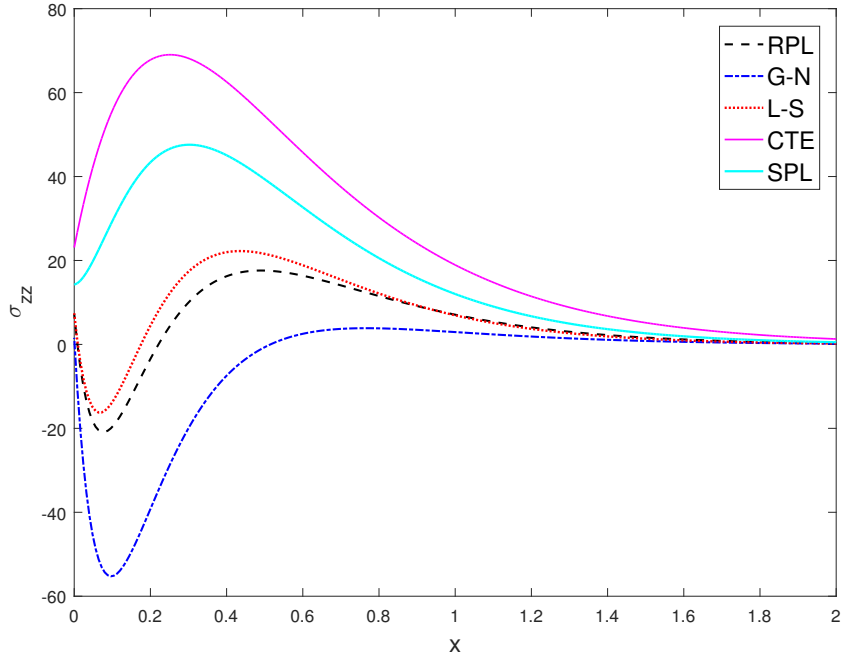

FIGURE 4.12: Stress σ_{zz} versus x for $\Omega = 0.0$

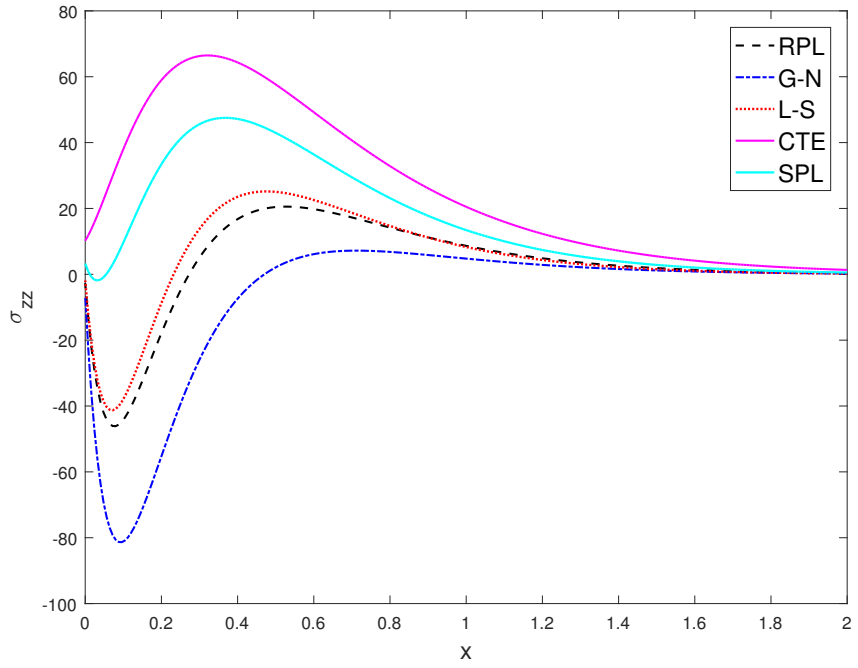

FIGURE 4.13: Stress σ_{zz} versus x for $\Omega = 0.3$

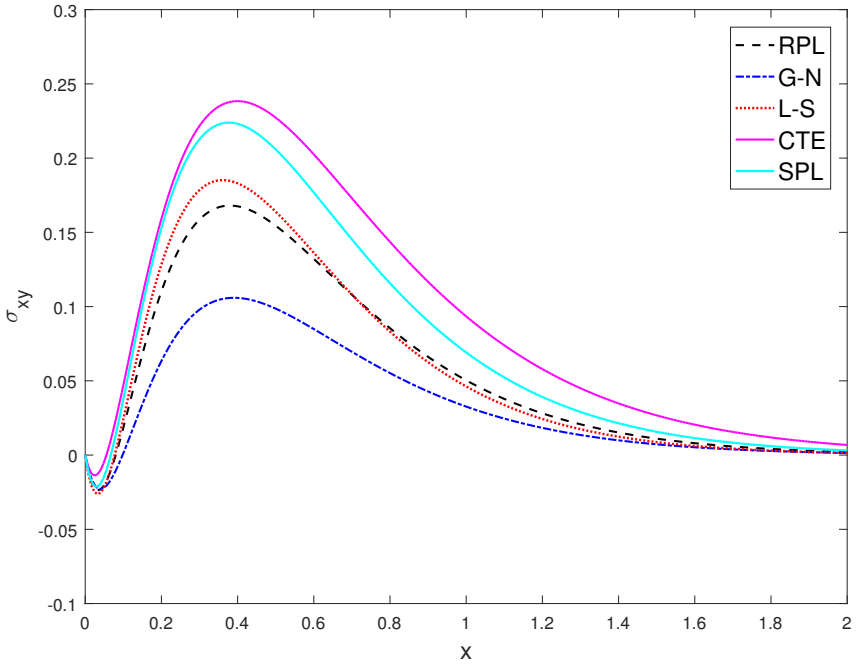

FIGURE 4.14: Stress σ_{xy} versus x for $\Omega = 0.0$

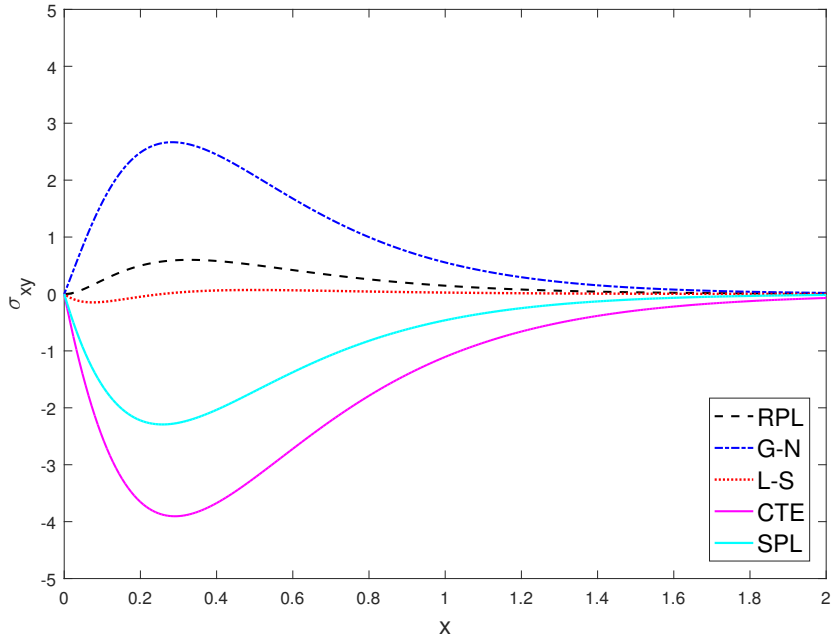

FIGURE 4.15: Stress σ_{xy} versus x for $\Omega = 0.3$

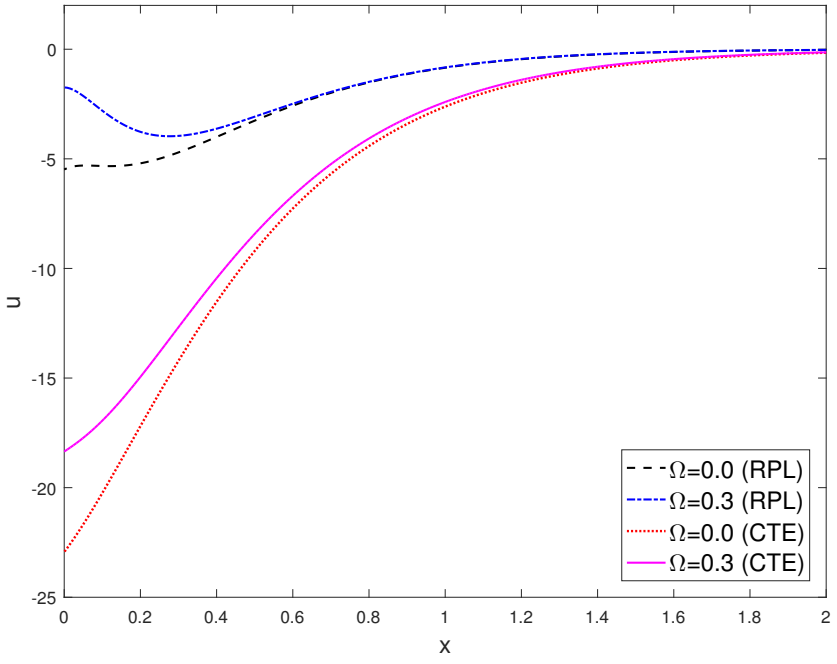

FIGURE 4.16: Displacement u versus x for rotational variation

v has the maximum value at the centre of the crack and decreases with displacement towards zero. Horizontal displacement and vertical displacement show different natures near the centre of the crack. u starts with a highly negative gradient and finishes to zero after a sharp increment, whereas v starts from a positive gradient and converges to zero near the edge of the crack. Alternation of vertical displacement is more convenient in the presence of rotation ($\Omega = 0.3$) than $\Omega = 0.0$. The horizontal displacement (u) and vertical displacement (v) curves are similar in nature with the results obtained by Abouelregal and Abo-Dahab (2018).

Figures 4.8 and 4.9 are the map of vertical stress versus distance x for $\Omega = 0.0$ and $\Omega = 0.3$ respectively. Fig. 10 and Fig. 11 represent the horizontal stress σ_{xx} against x for various thermoelasticity theories in the absence and presence of rotation. It is clear from figures 4.8-4.11 that σ_{yy} and σ_{xx} have decreased initially and then increases with an increase in x for RPL, L-S and G-N theories, whereas in case of SPL and CTE vertical and horizontal stress components increases initially and decreases near the edge of the crack. σ_{yy} and σ_{xx} tend to zero near the end position of the crack. G-N theory and CTE theory show the greatest variation in horizontal and vertical stress distribution whereas Lord-Shulman (L-S) models exhibits the least variation in the distribution of σ_{yy} and σ_{xx}. Horizontal stress (σ_{xx}) and vertical stress (σ_{yy}) curves are similar in nature with the graphs presented by Abouelregal and Abo-Dahab (2018). In figures 4.12 and 4.13 stress σ_{zz} have been mapped along x for $\Omega = 0.0$ and $\Omega = 0.3$. Nature of the curves presented in figures 4.12 and 4.13 are similar with the figures 4.8 and 4.9 respectively.

Figures 4.14 and 4.15 are the plot of shear stress σ_{xy} versus distance x in the absence and presence of rotation. When $\Omega = 0.0$, shear stress σ_{xy} increases in the range $0.05 < x < 0.4$ and decreases in the range $0.4 < x < 2.0$. In the presence of rotation σ_{xy} starts from zero with decreasing nature up to $x < 0.3$ and increases in the range $0.3 < x < 1.2$ for CTE and SPL models. In the case of RPL and G-N theories σ_{xy} increases in the range $0 < x < 0.3$ and after that diminishes towards zero. The shear stress curve is flatter for the L-S theory in the presence of rotation. The shear stress σ_{xy} follows the boundary condition at $x = 0$ and exhibits a different behaviour compared with that of horizontal stress σ_{xx} for LS, G-N and RPL theories. This tendency follows the elastic and thermoelastic characteristics of the solid under consideration. The nature of the shear stress curve is very close to that of Abouelregal and Abo-Dahab (2018) and Othman and Atwa (2013).

The distribution of stresses σ_{yy}, σ_{xx}, σ_{xy} and σ_{zz} in LS theory is close to that in RPL theory, whereas the distribution of stresses in the G-N theory are dissimilar from RPL theory. It is clear from figures 4.4-4.15 that the results for the displacement and stress

distribution with the rotation of the fiber-reinforced medium are uniquely different from those without the rotation i.e. effect of rotation is crucial in thermoelastic theories. 4.16 indicates the rotational effect for horizontal displacement for RPL and CTE model.

It is clear from the temperature distributions that heat passes with finite speeds in the fiber-reinforced medium at a sudden time, which proves that the generalized thermoelasticity theory is very significant for elastic materials. Whereas, the uncoupled classical thermoelasticity theory reports infinite speeds of thermal propagation. So all the field quantities have a very small value for any point in the medium. This suggests that the generalized heat conduction model is not comparable with the classical Fourier's heat conduction law.

4.1.7 Conclusion

An analytic solution for a mode-I crack in the rotating fiber-reinforced solid under the refined phase-lags model is studied. The exact expressions of temperature, displacement and stress components have been derived by normal mode analysis for one temperature theory (1TT). The following bullet points are concluded from this study.

- No significant effect has been observed for rotation in temperature distribution, although the numerical computation for rotational effect is useful in the design and construction of gyroscopes and rotation sensors.
- CTE shows more deviation in the case of horizontal as well as vertical displacement than any other thermoelasticity theories.
- Shear stress alternation is greatest in the case of CTE in the presence and absence of rotation and least in the case of G-N theory in the absence of rotation while in the case of L-S theory in the presence of rotation.
- The thermal stress components have consequential large values in a rotating solid as compared with a non-rotating one.
- Temperature, displacement and stress distribution vanish with displacement for each proposed thermoelasticity theory. These trends follow elastic as well as thermoelastic behaviour of solids under inspection.
- The effect of phase-lags τ_q and τ_θ is notable on the real parts of the physical quantities through different model.

- The CTE theory yields the highest values of all physical quantities while the G-N theory yields the least values. The RPL theory provides the accurate result among these theories due to higher order time derivatives and phase-lags.
- Cracks are in the static condition but external stress is forced to propagate such cracks.
- The highest and the least values of all the field variables except temperature are more prominent in the case of rotating fiber-reinforced solid than without rotation.

The finite crack problem of a solid material under mechanical and thermal loading has extensive applications in civil engineering for design purposes, vehicles industry for designing of load-bearing components, power generation and transmission. This thermoelastic model can be used to understand the process of optical thermal transfer and the interaction between elastic plasma waves and heat. Moreover, this type of problem has various applications in the fabrication process of electronic gadgets, geophysics, earthquake engineering, etc. This current study is based on a widely accepted method and is useful for the investigation of more complicated phenomena in the field of thermoelasticity and engineering fracture mechanics.

4.2 Two collinear cracks in a transversely isotropic medium under the hyperbolic heat conduction law[2]

4.2.1 Introduction

A transversely isotropic material reserves the same properties in one plane and different properties in normal to the plane. In the geophysical concept of rock formations of the crust, the transversely isotropic material played a major role due to its infinite wave length limit property. Transversely isotropic material such as Beryl, Cadmium, Thallium, PZT-4, Barium titanate, etc. are frequently used in crack related problems for their excellent strength capacity and light weight.

The parabolic (classical Fourier) heat conduction law concludes that the heat transmission speed is infinite i.e. a thermal penetration in a material can be propagated instantaneously into any part of the material. The Fourier heat conduction law is rigorously used for many practical engineering composites. However, the Fourier heat conduction law fails at very low temperature, in the presence of large heat flux and for some man made nanomaterials. Non-Fourier (hyperbolic) heat conduction theories have been introduced to describe the solid and fracture upon such type of phenomena where Fourier heat conduction law fails. Cattaneo (1958) and Vernotte (1958) independently modified the Fourier's law by introducing an additional parameter, the thermal relaxation time. The modified law forms a differential equation hyperbolic in nature and also known as hyperbolic heat conduction law. Lewandowska and Malinowski (1998) solved a problem for semi infinite body under hyperbolic heat conduction law. Non-Fourier heat conduction modelling by finite integral transform with a periodic heat flux is studied by Abdel-Hamid (1999). Kar et al. (1992) made comparison between hyperbolic and parabolic heat conduction for different boundary conditions. Hyperbolic heat conduction problem is examined using hybrid Green function method by Chen (2009).

It is very common that temperature variation induces cracks or defects of a material and disrupt the natural thermal flow distribution. The temperature gradient reinforcement may produce thermal stress that causes rapid crack growth. Therefore various analytical and numerical methods have been studied to examine the thermal flow distribution in the substances with fractures. Stress analysis of cracks is a common task to study the fracture criteria in linear elastic theory. Stress singularity around the crack tip i.e. stress intensity

[2]Panja, S. K., & Mandal, S. C. (2023). Two collinear cracks in a transversely isotropic medium under the hyperbolic heat conduction law. Journal of Mechanics of Materials and Structures, 18(3), 375-389.

factor and crack opening displacement are important physical quantities to improve the mechanical performance of materials and components. Jain and Kanwal (1972) obtained a solution for two coplanar Griffith cracks in an elastic medium. Two coplanar Griffith cracks problem is studied in an infinite elastic medium by Lowengrub and Srivastava (1968) using finite Hilbert transform technique. Two coplanar moving cracks in dissimilar elastic media has been discussed by Das and Ghosh (1992). Wu et al. (2017) and Mishra and Das (2018) examined the collinear Griffith crack problems in thermoelastic medium. The problems containing crack in thermoelastic substances under classical Fourier heat conduction law has been examined by Chao and Chang (1993); Chao and Kuo (1993); Dryden and Zok (2001); Gao and Noda (2004). Brock and Hanson (2006) studied a opening mode crack problem with thermal relaxation time in a coupled thermoelastic solid. Wang and Han (2012a); Wang and Li (2013) have researched transient thermal fracture problem under hyperbolic heat conduction law.

This article presents a problem of thermally insulated two collinear cracks under non Fourier heat conduction law with stress free boundary condition. The thermal and mechanical governing equations and boundary conditions are converted to the Laplace transform domain. The heat conduction equation has been reduced to the Fredholm integral equation of 2nd kind and solved by asymptotic series expansion method. A finite Hilbert transform technique is utilized to solve the equilibrium equations in thermoelastic field. The expressions of SIF and COD are obtained in the Laplace transform domain and further this expressions are converted to the time domain with the help of Numerical Laplace inversion (Stehfest, 1970) method. SIF and COD have been mapped against time and distance respectively for various crack lengths under non Fourier and Fourier conduction law.

4.2.2 Formulation of the problem

In the cartesian coordinate system, we consider two collinear finite cracks occupy the position $a < |X| < b$, $-\infty < Z < \infty$, $Y = 0$ in a thermoelastic transversely isotropic medium. The constitutive equations of thermal flux and equilibrium equation for temperature in the absence of internal heat source under non Fourier heat conduction (hyperbolic heat conduction) law are (Tzou, 1995b)

$$q_i(X_i, t') = -k\frac{\partial T(X_i, t')}{\partial X_i} - \tau_q \frac{\partial q_i(X_i, t')}{\partial t'}, \tag{4.2.1}$$

and

$$\rho c\left(\tau_q \frac{\partial^2 T}{\partial t'^2}+\frac{\partial T}{\partial t'}\right)=k\left(\frac{\partial^2 T}{\partial X^2}+\frac{\partial^2 T}{\partial Y^2}+\frac{\partial^2 T}{\partial Z^2}\right), \tag{4.2.2}$$

where q is the heat flux, k is the thermal conductivity coefficient, ρ is the mass density, c is the specific heat and τ_q represents thermal relaxation time associated with the collision frequency of molecules.

The following dimensionless variables are introduced for a more organized study: $t=\frac{t'}{\tau_q}$, $x=\frac{X}{b}$ and $y=\frac{Y}{b}$.

The temperature constitutive equations (4.2.1) and (4.2.2) become:

$$q_y=-\frac{k}{b}\frac{\partial T}{\partial y}-\frac{\partial q_y}{\partial t} \tag{4.2.3}$$

and

$$\frac{\partial^2 T}{\partial t^2}+\frac{\partial T}{\partial t}=\delta^2\left(\frac{\partial^2 T}{\partial x^2}+\frac{\partial^2 T}{\partial y^2}\right) \tag{4.2.4}$$

where $\delta=\frac{l_0}{b}$ with $l_0=\sqrt{\frac{k\tau_q}{\rho c}}$.

The crack location can be written as $h<|x|<1$, $-\infty<z<\infty$, $y=0$, where $h=\frac{a}{b}$.

The problem geometry is symmetric with respect to $x=0$ line, so it is sufficient to analyze the problem in the region $x\geq 0$. Let us consider this problem in the plane $z=0$ so that

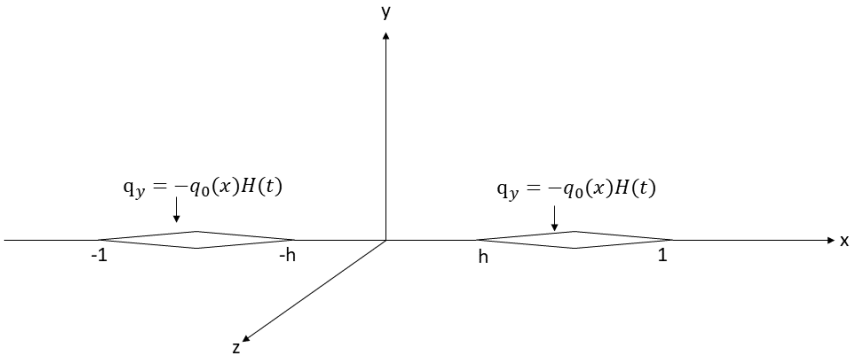

FIGURE 4.17: Geometry of the problem

all the field variables are functions of x, y and t only.

Following Wang and Noda (2004); Niraula and Wang (2006); Wang et al. (2011); Wang and Han (2012b); Wang and Li (2013), we considered two thermally insulated and traction-free cracks, which do not admit any disturbances of thermal flow across the cracks. The crack problem is usually solved by the method of superposition (Rizk and Radwan (1992); Erdogan (1995)) in the field of fracture mechanics. The crack faces are loaded by a sudden thermal flux q_0 along the negative y- direction.

The temperature boundary conditions on the $y = 0$ plane are given by

$$T(x, 0, t) = 0, \quad 0 < x < h, \quad x > 1 \tag{4.2.5}$$

$$q_y(x, 0, t) = -q_0(x)H(t), \quad h < x < 1. \tag{4.2.6}$$

The nonzero thermal stress components are

$$\sigma_{xx} = \frac{C_{11}}{b}\frac{\partial u}{\partial x} + \frac{C_{13}}{b}\frac{\partial v}{\partial y} - \lambda_{11}T, \tag{4.2.7}$$

$$\sigma_{yy} = \frac{C_{13}}{b}\frac{\partial u}{\partial x} + \frac{C_{33}}{b}\frac{\partial v}{\partial y} - \lambda_{22}T, \tag{4.2.8}$$

$$\sigma_{xy} = \frac{C_{44}}{b}\left(\frac{\partial u}{\partial y} + \frac{\partial v}{\partial x}\right), \tag{4.2.9}$$

where $C_{11},\ C_{13},\ C_{33},\ C_{44}$ are elastic constants; u and v are the displacements along x and y axis respectively and $\lambda_{ii}(i = 1,\ 2)$ denotes temperature-stress coefficients.

The balance equations without body forces can be expressed as

$$\frac{\partial}{\partial X}\sigma_{xx} + \frac{\partial}{\partial Y}\sigma_{xy} = 0 \tag{4.2.10}$$

and

$$\frac{\partial}{\partial X}\sigma_{xy} + \frac{\partial}{\partial Y}\sigma_{yy} = 0. \tag{4.2.11}$$

It is well known that in a homogeneous elastic material, a uniform thermal flow does not induce any thermal stress. The effects of heating are noted in the region $y > 0$ as of the presence of the disturbing temperature field. Further the part situated at $y > 0$ exhibits extensions in elastic displacement u and performs on the neighbouring with compressive thermal stresses. The stress free boundary conditions for the elastic field are given by:

$$\sigma_{yy} = 0, \quad 0 \leq x < \infty, \quad y = 0 \tag{4.2.12}$$

$$\sigma_{xy} = 0, \quad h < x < 1, \quad y = 0 \tag{4.2.13}$$

$$u = 0, \quad 0 < x < h, \quad x > 1, \quad y = 0. \tag{4.2.14}$$

We apply Laplace transform to convert the problem from time domain (t) to the Laplace transform domain (p). With the help of Laplace transform the equations (4.2.3)-(4.2.9); (4.2.12)-(4.2.14) transformed as follows:

$$q_y^* = -\frac{k}{b}\frac{\partial T^*}{\partial y} - pq_y^*, \tag{4.2.15}$$

$$T^* = \frac{\delta^2}{p^2 + p}\left(\frac{\partial^2 T^*}{\partial x^2} + \frac{\partial^2 T^*}{\partial y^2}\right), \tag{4.2.16}$$

$$T^*(x, 0, p) = 0, \quad 0 < x < h, \quad x > 1 \tag{4.2.17}$$

$$q_y^*(x, 0, p) = -\frac{q_0(x)}{p}, \quad h < x < 1 \tag{4.2.18}$$

$$\sigma_{xx}^* = \frac{C_{11}}{b}\frac{\partial u^*}{\partial x} + \frac{C_{13}}{b}\frac{\partial v^*}{\partial y} - \lambda_{11}T^*, \tag{4.2.19}$$

$$\sigma_{yy}^* = \frac{C_{13}}{b}\frac{\partial u^*}{\partial x} + \frac{C_{33}}{b}\frac{\partial v^*}{\partial y} - \lambda_{22}T^*, \tag{4.2.20}$$

$$\sigma_{xy}^* = \frac{C_{44}}{b}\left(\frac{\partial u^*}{\partial y} + \frac{\partial v^*}{\partial x}\right), \tag{4.2.21}$$

$$\sigma_{yy}^* = 0, \quad 0 \leq x < \infty, \quad y = 0 \tag{4.2.22}$$

$$\sigma_{xy}^* = 0, \quad h < x < 1, \quad y = 0 \tag{4.2.23}$$

$$u^* = 0, \quad 0 < x < h, \quad x > 1, \quad y = 0. \tag{4.2.24}$$

4.2.3 Solution of the temperature field

The solution of the equation (4.2.16) satisfying the boundary conditions (4.2.17) and (4.2.18) with the help of Fourier transform is given by

$$T^* = \frac{2}{\pi}\int_0^\infty A(s)e^{-s\lambda_0 y}\cos(sx)ds, \tag{4.2.25}$$

where $\lambda_0 = \sqrt{1 + \frac{p^2+p}{\delta^2 s^2}}$.

With the aid of boundary conditions (4.2.17) and (4.2.18), we have the following dual integral equations

$$\int_0^\infty A(s)\cos(sx)ds = 0, \qquad 0 < x < h, \quad x > 1 \tag{4.2.26}$$

and

$$\int_0^\infty s\left[1 + M(\delta s)\right] A(s)\cos(sx)ds = \frac{\pi}{2}p(x), \qquad h < x < 1 \tag{4.2.27}$$

where $M(\delta s) = (\lambda_0 - 1) \to 0$ as $s \to \infty$ and $p(x) = -\frac{b}{k}\frac{1+p}{p}q_0(x)$.

Let us take the solution of the above system of dual integral equations as follows

$$A(s) = \frac{1}{s}\int_h^1 h(t^2)\sin(st)dt \tag{4.2.28}$$

where $h(t^2)$ is an unknown function.

Using the results

$$\int_0^\infty \frac{\sin(st)\cos(sx)}{s}ds = \begin{cases} \frac{\pi}{2}, & t > x \\ 0, & x > t \end{cases}$$

$$\int_0^\infty \frac{\sin(sx)\sin(st)}{s}ds = \frac{1}{2}\ln\left|\frac{x+t}{x-t}\right|,$$

$$\frac{\sin(st)\sin(sx)}{s^2} = \int_0^x\int_0^t \frac{wvJ_0(sw)J_0(sv)}{\sqrt{(x^2-w^2)(t^2-v^2)}}dw\,dv$$

and with the help of equation (4.2.28), equations (4.2.26) and (4.2.27) reduced to the following equations

$$\int_h^1 h(t^2)dt = 0 \tag{4.2.29}$$

and

$$\int_h^1 \frac{th(t^2)}{t^2-x^2}dt + \frac{d}{dx}\int_h^1 h(t^2)dt\int_0^x\int_0^t \frac{wvL(v,w)}{\sqrt{(x^2-w^2)(t^2-v^2)}}dv\,dw = \frac{\pi}{2}p(x), \tag{4.2.30}$$

with

$$L(v,w) = \int_0^\infty sM(\delta s)J_0(sw)J_0(sv)ds. \tag{4.2.31}$$

The infinite integral in equation (4.2.31) has slow rate of convergence. It is converted to the finite integral using contour integration procedure (Mandal and Ghosh, 1994) as

$$L(v,w) = \frac{2}{\pi}\int_0^1 k_s^2\sqrt{1-\eta^2}K_0(k_s\eta w)I_0(k_s\eta v)d\eta \tag{4.2.32}$$

where $k_s = \bar{\delta}\sqrt{p^2+p}$ and $\bar{\delta} = \frac{1}{\delta}$. The modified Bessel function of 1st kind $I_0(z)$ and the modified Bessel function of 2nd kind $K_0(z)$ have been expanded in the form (Abramowitz and Stegun, 1968)

$$I_0(z) = \sum_{n=0}^{\infty} \frac{\left(\frac{z^2}{4}\right)^n}{(n!)^2}$$

and

$$K_0(z) = -\left[\ln\left(\frac{z}{2}\right) + C\right] I_0(z) + \frac{\frac{z^2}{4}}{(1!)^2} + \left(1+\frac{1}{2}\right)\frac{\left(\frac{z^2}{4}\right)^2}{(2!)^2} + \left(1+\frac{1}{2}+\frac{1}{3}\right)\frac{\left(\frac{z^2}{4}\right)^3}{(3!)^2} + \cdots,$$

where $C = 0.5772$ (Euler - Mascheroni constant). $L(v,w)$ can be expressed as

$$L(v,w) = \left(\bar{\delta}^2 \ln \bar{\delta}\right) L_1 + O(\bar{\delta}^2), \tag{4.2.33}$$

with $L_1 = -\frac{1}{2}(p^2+p)$.

Again $h(t^2)$ also be expanded in the form

$$h(t^2) = h_0(t^2) + (\bar{\delta}^2 \ln \bar{\delta}) h_1(t^2) + O(\bar{\delta}^2). \tag{4.2.34}$$

With the aid of equations (4.2.30) and (4.2.34), we acquire the equations

$$\int_h^1 \frac{t}{t^2-x^2} h_0(t^2)dt = \frac{\pi}{2}p(x), \qquad h < x < 1 \tag{4.2.35}$$

and

$$\int_h^1 \frac{t h_1(t^2)}{t^2-x^2}dt = \frac{p^2+p}{2}\int_h^1 t h_0(t^2)dt, \qquad h < x < 1. \tag{4.2.36}$$

The solutions of the system of equations (4.2.35) and (4.2.36) are written as

$$h_0(t^2) = -\frac{b}{k}\frac{1+p}{p} q_0 \frac{t^2 - \frac{E}{F}}{\sqrt{(t^2-h^2)(1-t^2)}} \tag{4.2.37}$$

and

$$h_1(t^2) = -\frac{b}{k}\frac{1+p}{p} q_0 \frac{p^2+p}{4} \frac{\left(1+h^2-2\frac{E}{F}\right)\left(t^2-\frac{E}{F}\right)}{\sqrt{(t^2-h^2)(1-t^2)}}, \tag{4.2.38}$$

where $F = F\left[\frac{\pi}{2}, \sqrt{1-h^2}\right]$ and $E = E\left[\frac{\pi}{2}, \sqrt{1-h^2}\right]$ are the elliptic integrals of first and second kind respectively.

4.2.4 Solution of the thermoelastic field

The thermal stress components in equations (4.2.19)-(4.2.21) and the balance equations (4.2.10) and (4.2.11) yield

$$C_{11}\frac{\partial^2 u^*}{\partial x^2}+(C_{13}+C_{44})\frac{\partial^2 v^*}{\partial x\partial y}+C_{44}\frac{\partial^2 u^*}{\partial y^2}=b\lambda_{11}\frac{\partial T^*}{\partial x} \tag{4.2.39}$$

and

$$(C_{13}+C_{44})\frac{\partial^2 u^*}{\partial x\partial y}+C_{44}\frac{\partial^2 v^*}{\partial x^2}+C_{33}\frac{\partial^2 v^*}{\partial y^2}=b\lambda_{22}\frac{\partial T^*}{\partial y}. \tag{4.2.40}$$

We apply the similar solution procedure studied by Wang and Mai (2002); Wang and Han (2012a); Wang and Li (2013) to solve the equations (4.2.39) and (4.2.40). The homogeneous part of equations (4.2.39) and (4.2.40) are not related with the temperature field and solution of this part can be taken as

$$\begin{Bmatrix} u^*(x,y) \\ v^*(x,y) \end{Bmatrix}=\frac{2}{\pi}\int_0^\infty \sum_{m=1}^{2} F_m(s)\begin{Bmatrix} a_{1m}\sin(sx) \\ a_{2m}\cos(sx) \end{Bmatrix} e^{-s\lambda_m y}ds. \tag{4.2.41}$$

Employing equation (4.2.41) to the homogeneous part of equations (4.2.39) and (4.2.40) yield

$$\begin{bmatrix} C_{11}-C_{44}\lambda_m^2 & -(C_{13}+C_{44})\lambda_m \\ -(C_{13}+C_{44})\lambda_m & C_{33}\lambda_m^2-C_{44} \end{bmatrix}\begin{bmatrix} a_{1m} \\ a_{2m} \end{bmatrix}=\begin{bmatrix} 0 \\ 0 \end{bmatrix}. \tag{4.2.42}$$

Equation (4.2.42) contains four eigen values in the form $\Re(\lambda_1)>0$, $\Re(\lambda_2)>0$,$\Re(\lambda_3=-\lambda_1)<0$ and $\Re(\lambda_4=-\lambda_2)<0$. We consider only positive eigen values to obtain the solution as all the field quantities tends to zero when $y\to\infty$.

The eigen vectors a_{1m} and a_{2m} $(m=1,\ 2)$ can be expressed as

$$a_{1m}=1 \ \text{ and } \ a_{2m}=\frac{C_{11}-C_{44}\lambda_m^2}{(C_{13}+C_{44})\lambda_m}.$$

The particular solution of equations (4.2.39) and (4.2.40) associated with the temperature field, can be written as

$$\begin{Bmatrix} u^*(x,y) \\ v^*(x,y) \end{Bmatrix}=\frac{2}{\pi}b\int_0^\infty \begin{Bmatrix} f_1\sin(sx) \\ f_2\cos(sx) \end{Bmatrix}\frac{1}{s}A(s)e^{-s\lambda_0 y}ds \tag{4.2.43}$$

with the coefficients f_i $(i = 1,\ 2)$, given by

$$\begin{bmatrix} C_{11} - C_{44}\lambda_0^2 & -(C_{13} + C_{44})\lambda_0 \\ -(C_{13} + C_{44})\lambda_0 & C_{33}\lambda_0^2 - C_{44} \end{bmatrix} \begin{bmatrix} f_1 \\ f_2 \end{bmatrix} = \begin{bmatrix} \lambda_{11} \\ -\lambda_0\lambda_{22} \end{bmatrix}. \tag{4.2.44}$$

The final solutions of governing equations (4.2.39) and (4.2.40) are

$$\begin{Bmatrix} u^*(x,y) \\ v^*(x,y) \end{Bmatrix} = \frac{2}{\pi}\int_0^\infty \sum_{m=1}^{2} F_m(s) \begin{Bmatrix} a_{1m}\sin(sx) \\ a_{2m}\cos(sx) \end{Bmatrix} e^{-s\lambda_m y} ds + \frac{2}{\pi} b \int_0^\infty \begin{Bmatrix} f_1 \sin(sx) \\ f_2 \cos(sx) \end{Bmatrix} \frac{1}{s} A(s) e^{-s\lambda_0 y} ds. \tag{4.2.45}$$

Following equations (4.2.20), (4.2.21), (4.2.25) and (4.2.45), we have the expressions as follows

$$\sigma_{yy}^* = \frac{2}{\pi}\sum_{m=1}^{2} \frac{K_{1m}}{b} \int_0^\infty sF_m(s)\cos(sx)e^{-s\lambda_m y} ds + \frac{2}{\pi} D_1 \int_0^\infty A(s)\cos(sx)e^{-s\lambda_0 y} ds, \tag{4.2.46}$$

$$\sigma_{xy}^* = \frac{2}{\pi}\sum_{m=1}^{2} \frac{K_{2m}}{b} \int_0^\infty sF_m(s)\sin(sx)e^{-s\lambda_m y} ds + \frac{2}{\pi} D_2 \int_0^\infty A(s)\sin(sx)e^{-s\lambda_0 y} ds, \tag{4.2.47}$$

where the constants K_{im} $(i = 1,\ 2)$ and D_i $(i = 1,\ 2)$ are as follows

$$\begin{bmatrix} K_{1m} \\ K_{2m} \end{bmatrix} = \begin{bmatrix} C_{13} & -C_{33}\lambda_m \\ -C_{44}\lambda_m & -C_{44} \end{bmatrix} \begin{bmatrix} a_{1m} \\ a_{2m} \end{bmatrix} \tag{4.2.48}$$

and

$$\begin{bmatrix} D_1 \\ D_2 \end{bmatrix} = \begin{bmatrix} C_{13} & -C_{33}\lambda_0 \\ -C_{44}\lambda_0 & -C_{44} \end{bmatrix} \begin{bmatrix} f_1 \\ f_2 \end{bmatrix} + \begin{bmatrix} -\lambda_{22} \\ 0 \end{bmatrix}. \tag{4.2.49}$$

We introduce a new function $F_0(s)$, to determine the unknown real constants $F_m(s)$ $(m = 1,\ 2)$ in the following form

$$\sum_{m=1}^{2} F_m(s)a_{1m} + \frac{A(s)}{s} b f_1 = F_0(s). \tag{4.2.50}$$

Applying the boundary condition (4.2.22), we get

$$\sum_{m=1}^{2} K_{1m}F_m(s) = -\frac{b}{s} D_1 A(s). \tag{4.2.51}$$

Equations (4.2.50) and (4.2.51) forms a linear algebraic system, compactly expressed as

$$F_m(s) = \chi_m^1 F_0(s) - \frac{b}{s}\delta_m A(s) \tag{4.2.52}$$

where, χ_m^1 and δ_m $(m = 1,\ 2)$ are related to

$$\begin{bmatrix} a_{11} & a_{12} \\ K_{11} & K_{12} \end{bmatrix} \begin{bmatrix} \chi_1^1 & \delta_1 \\ \chi_2^1 & \delta_2 \end{bmatrix} = \begin{bmatrix} 1 & f_1 \\ 0 & D_1 \end{bmatrix}. \tag{4.2.53}$$

Using the result $\int_h^1 \frac{\left(t^2-\frac{E}{F}\right)\ln\left|\frac{x+t}{x-t}\right|}{\sqrt{(t^2-h^2)(1-t^2)}}dt = \pi\left(x-\frac{\pi}{2F}\right), \quad h < x < 1$ and from the boundary conditions (4.2.24) and (4.2.23) we obtain a system of dual integral equation as

$$\int_0^\infty F_0(s)\sin(sx)ds = 0, \qquad 0 < x < h, \quad x > 1 \tag{4.2.54}$$

$$\int_0^\infty sF_0(s)\sin(sx)ds = \frac{\pi}{2}P_1(x), \qquad h < x < 1 \tag{4.2.55}$$

where

$$P_1(x) = -\frac{b^2}{\Lambda_{11}k}q_0\left(x-\frac{\pi}{2F}\right)\left(\sum_{m=1}^{2}K_{2m}\delta_m - D_2\right)\left[\frac{1+p}{p} + \bar{\delta}^2\ln\bar{\delta}\frac{(1+p)^2}{4}\left(1+h^2-2\frac{E}{F}\right)\right]$$

with $\Lambda_{11} = \sum_{m=1}^{2} K_{2m}\chi_m^1$.

Following Srivastava and Lowengrub (1970), we consider a solution in the following form

$$F_0(s) = \frac{1}{s}\int_h^1 \frac{g(t^2)}{t}\left(1-\cos(st)\right)dt \tag{4.2.56}$$

provided $\int_h^1 \frac{g(t^2)}{t}dt = 0$.

The solution of the unknown function $g(t^2)$ is given by

$$g(t^2) = \frac{b^2}{k\Lambda_{11}}f(p,h)\left(\frac{E}{F}-\frac{1+h^2}{2}\right)\frac{t^2}{\sqrt{(t^2-h^2)(1-t^2)}} + O(t^2) \tag{4.2.57}$$

where

$$f(p,h) = q_0\left(\sum_{m=1}^{2}K_{2m}\delta_m - D_2\right)\left[\frac{1+p}{p} + \bar{\delta}^2\ln\bar{\delta}\frac{(1+p)^2}{4}\left(1+h^2-2\frac{E}{F}\right)\right].$$

4.2.5 Physical quantities

Stress intensity factor:

The stress intensity factors K_{II}^h and K_{II}^1 at $x = h$ and $x = 1$ respectively are seen to be

$$\begin{aligned} K_{II}^h &= \lim_{x\to h-} \left|\sqrt{2(h-x)}\sigma_{xy}^*\right| \\ &= \frac{b}{k} f(p,h) \left(\frac{E}{F} - \frac{1+h^2}{2}\right) \frac{\sqrt{h}}{\sqrt{1-h^2}} \end{aligned} \tag{4.2.58}$$

and

$$\begin{aligned} K_{II}^1 &= \lim_{x\to 1+} \left|\sqrt{2(x-1)}\sigma_{xy}^*\right| \\ &= \frac{b}{k} f(p,h) \left(\frac{E}{F} - \frac{1+h^2}{2}\right) \frac{1}{\sqrt{1-h^2}}. \end{aligned} \tag{4.2.59}$$

Crack opening displacement:

COD is the magnitude of the distance between the two edges of the crack and is defined as

$$\begin{aligned} D(x) &= |u(x,0+) - u(x,0-)| \\ &= 2\frac{\pi}{4}\int_x^1 \frac{g(t^2)}{t} dt \\ &= -\frac{\pi}{2}\frac{b^2}{k\Lambda_{11}} f(p,h) \left(\frac{E}{F} - \frac{1+h^2}{2}\right) \left[\frac{1}{2\iota}\ln(1-h^2) + \iota \ln\left(\sqrt{1-x^2} + \sqrt{x^2-h^2}\right)\right]. \end{aligned} \tag{4.2.60}$$

We obtained the solution in the Laplace transform domain and now convert it in the time domain by Laplace inversion (Stehfest, 1970).

Special case:

(i) The present problem, transform to a Fourier heat conduction problem if we consider the heat conduction equation as follows

$$q_i\left(X_i, t'\right) = -k\frac{\partial T\left(X_i, t'\right)}{\partial X_i}$$

and

$$\rho c \frac{\partial T}{\partial t'} = k\left(\frac{\partial^2 T}{\partial X^2} + \frac{\partial^2 T}{\partial Y^2} + \frac{\partial^2 T}{\partial Z^2}\right).$$

The SIF and COD are shown graphically in the Numerical calculation and discussions section.

(ii) We converted two collinear cracks to a single crack by taking $h = 0$ and plotted in figure 4.24.

4.2.6 Numerical calculation and discussions

We present numerical results for SIF and COD for two collinear cracks in thermoelastic transversely isotropic medium under non Fourier and Fourier heat conduction law. We use the following data (Wang and Mai, 2002):

$$C_{11} = 7.41 \times 10^{10} Nm^{-2},\ C_{33} = 8.36 \times 10^{10} Nm^{-2},\ C_{12} = 4.52 \times 10^{10} Nm^{-2},$$
$$C_{13} = 3.93 \times 10^{10} Nm^{-2},\ C_{44} = 1.32 \times 10^{10} Nm^{-2},\ \lambda_{11} = 0.621 \times 10^{6} N/m^2K,$$
$$\lambda_{22} = 0.551 \times 10^{6} N/m^2K.$$

The current work is the study of a general mathematical model for the thermal analysis of transversely isotropic solids with two cracks. The solution of the problem is examined in non-dimensional form so that the analysis of the model utlizes to any transversely isotropic materials. For instance, at $25°C$: $\frac{k}{\rho c} = 1.38\ W/m/K$, $\rho c = 1620.6\ kJ/K/m^3$, $\tau_q = 1 \times 10^{-10} s$ and the characteristic length parameter $l_0 = 1.17 \times 10^{-5}\ m$ for quartz glass. Here, $\delta = \frac{l_0}{b}$, i.e. ratio of the characteristic length parameter and position of outer crack tip before making the field variables dimensionless. We fixed $\bar{\delta} = \frac{1}{\delta} = 0.5$ i.e. $\delta = 2$, which implies the characteristic length parameter $l_0 = \sqrt{\frac{k\tau_q}{\rho c}} = 2b$ and we make the dimensionless variables divide by b. So $\bar{\delta} = 0.5$ provides the equivalent information to meet the deficiency of the particulars associated with our considered material data.

Figure 4.18 is the plot of stress intensity factor $\left(\frac{K_{II}^h}{(q_0/k)}\right)$ at the inner crack tip versus time (t) for different values of h and fixed value of $\bar{\delta} = 0.5$ under hyperbolic heat conduction law. Initially SIF increases and reaches its highest value then it decreases with the increasing values of t.

Figure 4.19 is the plot of SIF at $x = h$ against time for $\bar{\delta} = 0.5$ and $h = 0.4,\ 0.5,\ 0.6$ under parabolic heat conduction law. SIF is a smooth function of time (t) for the parabolic heat conduction model. The magnitude of SIF is more in non Fourier model than that of Fourier model.

Figures 4.20 and 4.21 represent SIF $\left(\frac{K_{II}^1}{(q_0/k)}\right)$ at $x = 1$ with time t for $h = 0.4,\ 0.5,\ 0.6$ under non Fourier and Fourier model respectively. SIF is higher at the outer crack tip i.e.

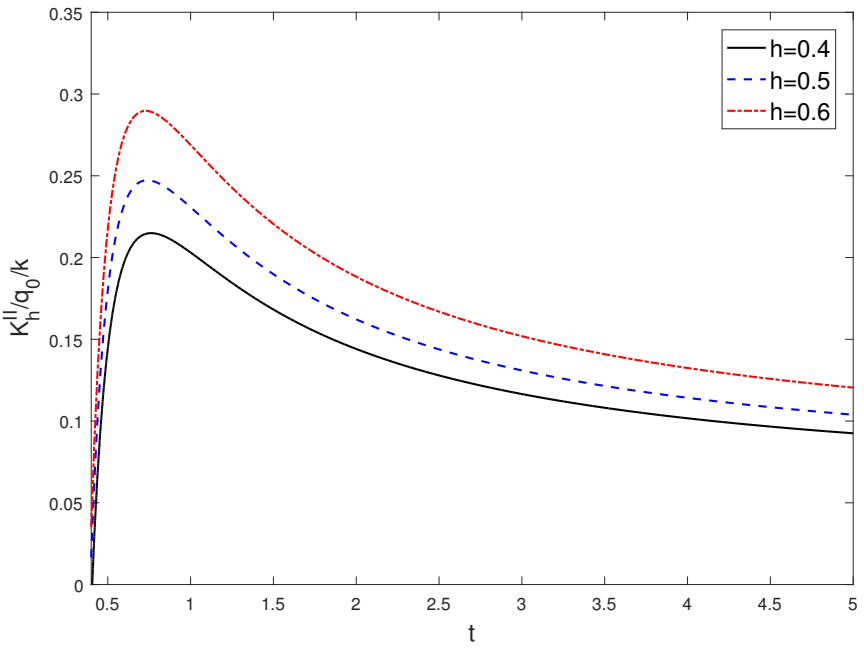

FIGURE 4.18: SIF versus time under non Fouier law

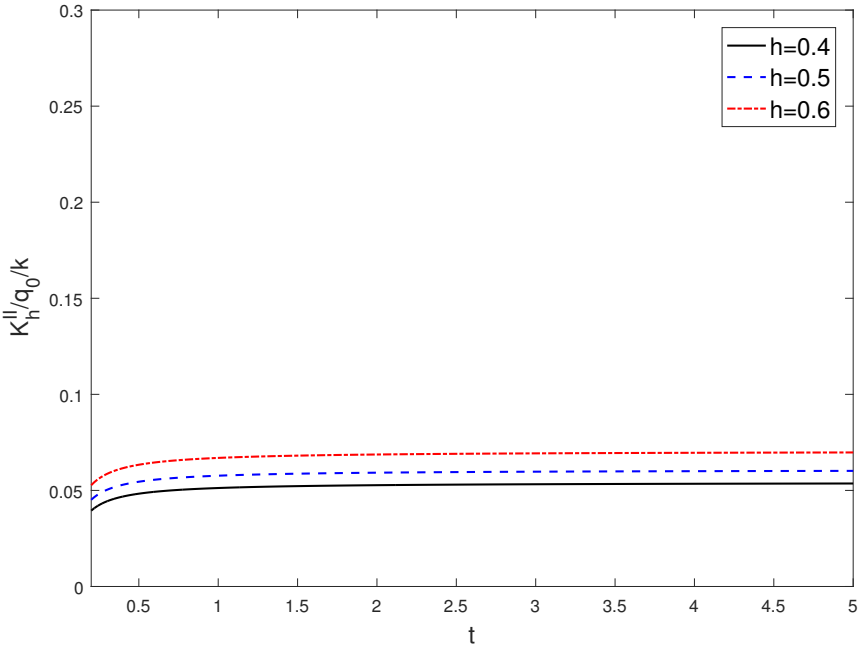

FIGURE 4.19: SIF versus time under Fouier law

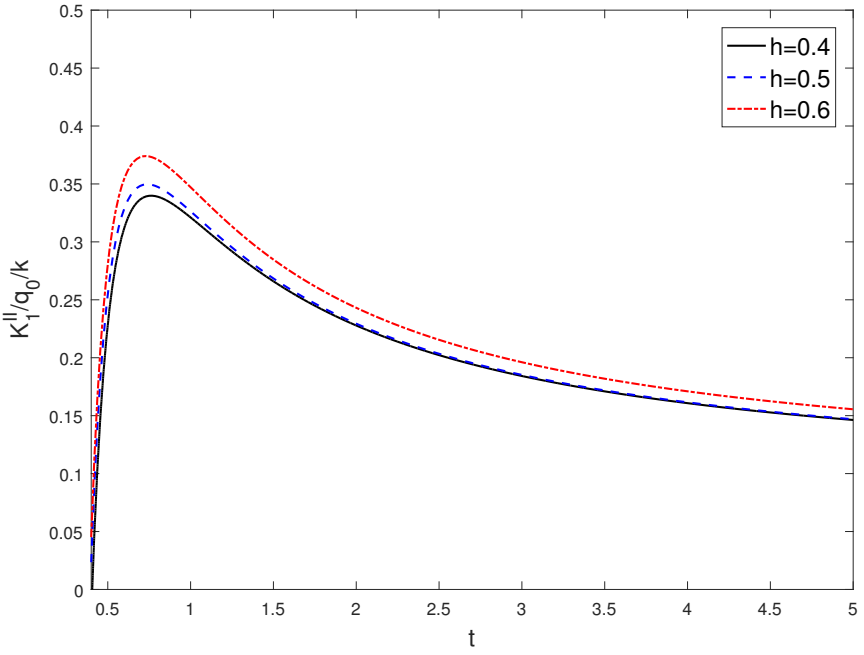

FIGURE 4.20: SIF versus time under non Fouier law

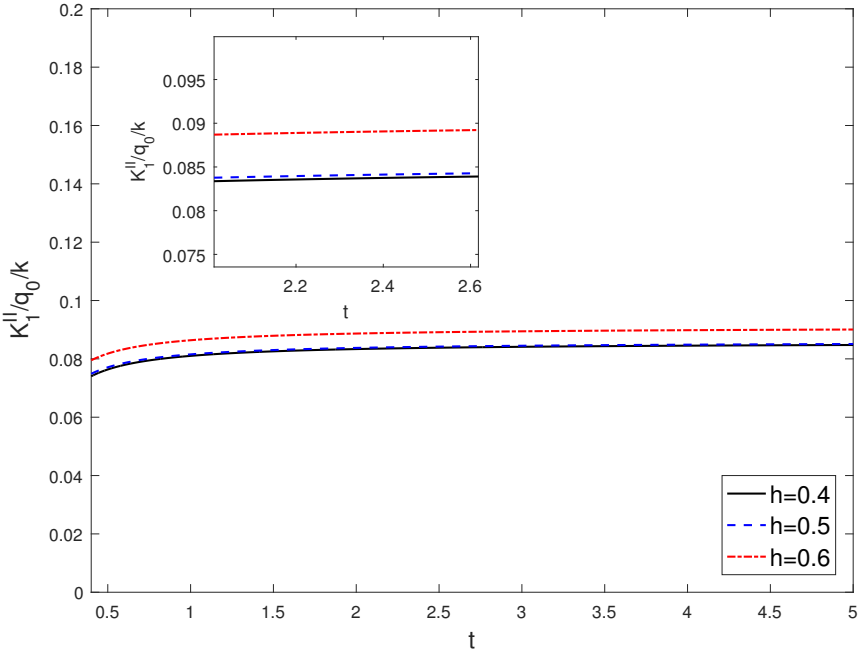

FIGURE 4.21: SIF versus time under Fouier law

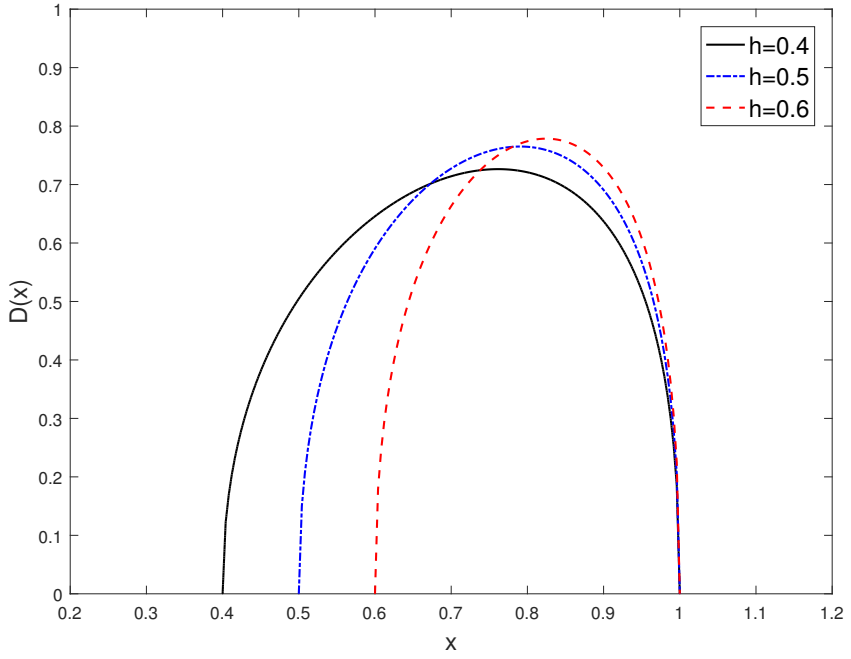

FIGURE 4.22: COD versus crack location under non Fouier law

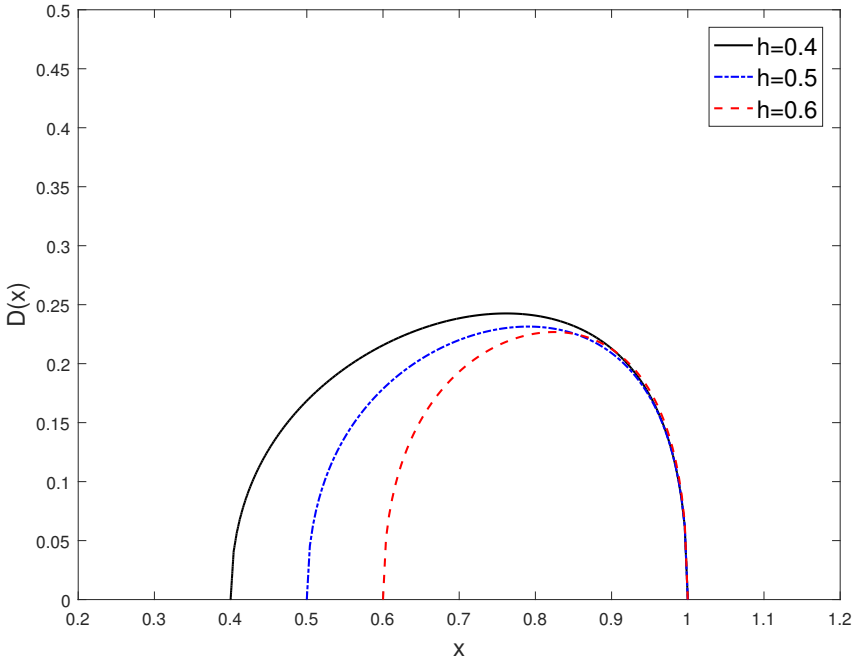

FIGURE 4.23: COD versus crack location under Fouier law

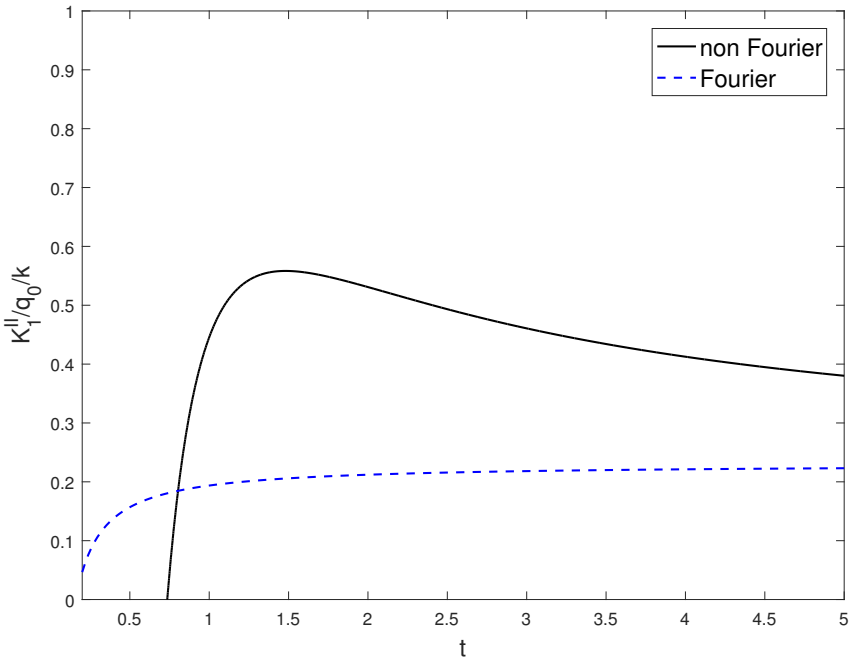

FIGURE 4.24: SIF versus time for single crack

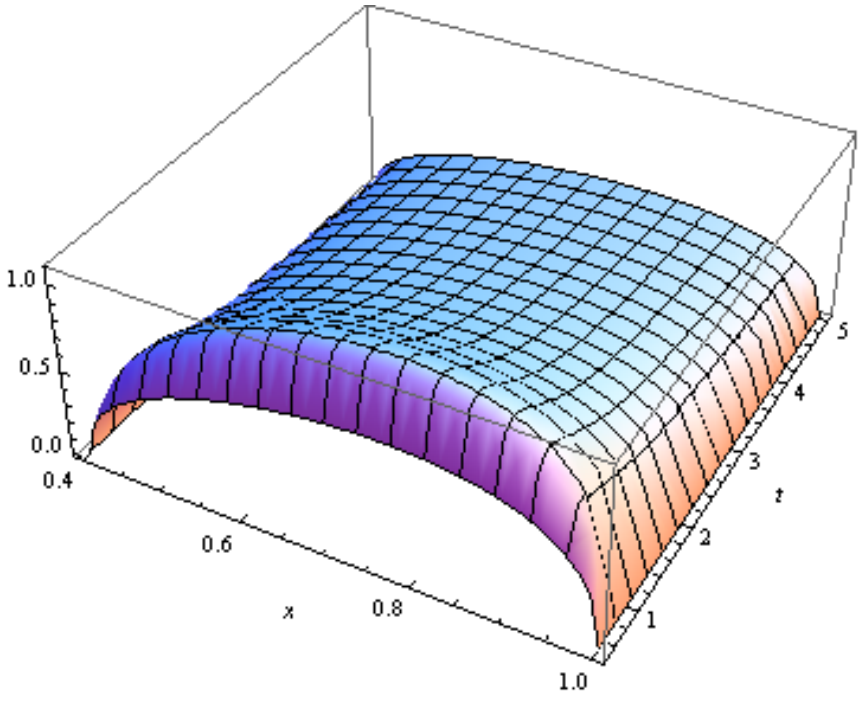

FIGURE 4.25: COD versus crack location and time under non Fouier law

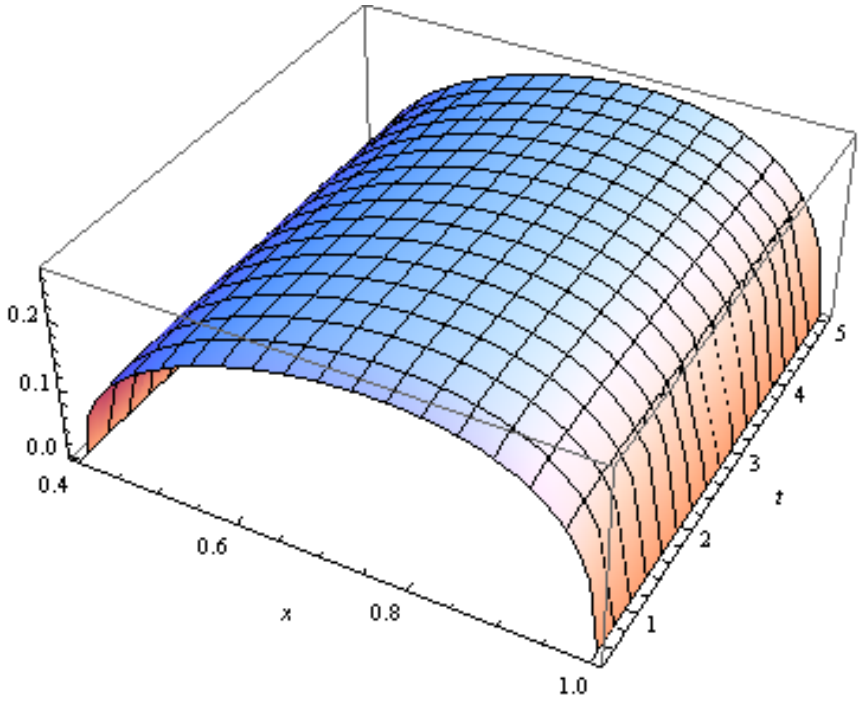

FIGURE 4.26: COD versus crack location and time under Fouier law

$x = 1$ than SIF at the inner crack tip i.e. $x = h$ and SIF sustains similar nature in both crack tip.

In figures 4.18 and 4.20, small oscillation is observed for the stress intensity factor under the non-Fourier model. The thermal relaxation time (τ_q) factor generates a higher thermal stress intensity factor than the classical Fourier's (parabolic) heat conduction law. This indicates that neglecting the non-Fourier effect in thermal conduction will conclude the significant error in attaining the thermal stress intensity factor at the crack tip. When the time increases the oscillation of SIF vanishes and both the hyperbolic and parabolic heat conduction model indicate that SIF curves are similar in nature. The oscillation of thermal SIF is more apparent for $h = 0.6$ than $h = 0.4$, which states that oscillation is more obvious for small crack length than for large crack length.

In figures 4.22 and 4.23, we have mapped crack opening displacement $D(x)$ against distance (x) for various h under non Fourier and Fourier heat conduction respectively. It is evident that COD grips highest value at the center position of the crack and tends to zero at both the crack tip for both model. COD is higher for higher values of h under non Fourier heat conduction but shows reverse effect in case of Fourier heat conduction.

In figure 4.24 SIF $\left(\frac{K_{II}^1}{(q_0/k)}\right)$ has been plotted for single crack ($h = 0$) against time (t) under non Fourier and Fourier heat conduction law. It is clear that the effect of SIF in

the presence of thermal relaxation time parameter is more influential than the absence of thermal relaxation time.

Figures 4.25 and 4.26 present the surface plot of COD versus time and crack location under Non-Fourier and Fourier heat conduction law respectively. The impact of COD decreases with the increasing values of time (t) for non-Fourier heat conduction law but under the Fourier heat conduction law COD remains uniform with an increase of time. Also, It is clear from both figures that COD is non-negative, which is physically persistent for our crack geometry.

4.2.7 Conclusion

Stress intensity factor and crack opening displacement of two collinear thermally insulated crack under non Fourier heat conduction theory have been derived and plotted with respect to time and distance for various length of h. Laplace transform, dual integral equation method, Hilbert transform technique are used to solve this problem. A comparison for SIF and COD is shown between the classical Fourier heat conduction and the non Fourier heat conduction. The following bullet points are noted from this study

- SIF is higher for higher values of h in both cases of non Fourier and Fourier heat conduction law.
- SIF curve is smooth and uniform under Fourier heat conduction law but due to thermal relaxation time parameter SIF increases at first and it decreases for time progresses. There is no difference between Fourier heat conduction and non Fourier heat conduction law at $t \to \infty$.
- In Fourier heat conduction model COD is smaller than that of non Fourier heat conduction model.

Chapter 5

Love wave propagation

5.1 Propagation of Love wave in multilayered viscoelastic orthotropic medium with initial stress[1]

5.1.1 Introduction

In solid mechanics and material science, orthotropic materials have garnered significant recognition due to their importance in engineering applications. The study of wave propagation through orthotropic media is essential in various fields, including optics, biology, seismic engineering, geophysics, acoustics, and electromagnetism. Geophysical research has revealed that the Earth's interior, like its exterior, is layered. This stratification has been inferred indirectly through the travel times of refracted and reflected seismic waves generated by earthquakes. Waves traveling beneath the Earth's surface encounter various layers due to anisotropy. This particular phenomenon are significant to exploration geophysics, geology and seismology also. In the previous years, many works have been done in multilayered media. The propagation of Love waves in an orthotropic granular layer positioned above a semi-infinite granular medium in the presence of initial stress was tested by Ahmed and Abo-Dahab (2010). Nayfeh et al. (1988) studied theoretical wave propagation in multilayered orthotropic media. Recently, Gupta and Bhengra (2017) observed SH-wave propagation in a multilayered magnetoelastic orthotropic composite medium. Kalyani et al. (2008) addressed the monoclinic multilayered problem by Haskell's matrix method and calculated the phase and group velocities through the finite

[1]Panja, S. K., & Mandal, S. C. (2022). Propagation of Love wave in multilayered viscoelastic orthotropic medium with initial stress. Waves in Random and Complex Media, 32(2), 1000-1017.

difference mechanism. Chattopadhyay et al. (2010) investigated shear wave propagation in a magnetoelastic self-reinforced medium using the finite difference method. Finite difference method has also been used in early researches like Alterman and Karal Jr (1968) and Kelly et al. (1976). Thomson et al. (1950) and Haskell (1953) have studied a matrix method to derive the phase velocity dispersion equation for Rayleigh and Love type waves in solid multilayered media.

The viscoelastic property of a material combines two key physical properties: viscosity and elasticity. Important characteristics of viscoelastic materials include their ability to creep, recover, undergo stress relaxation, and absorb energy. These materials can effectively absorb vibrational energies by damping them. In seismological studies the phenomenon "liquefaction" denotes a state in which solid deposits of sand inside the ground are transformed into a state of suspension, so that they behave as a viscous liquid. The asthenosphere, which serves as the transition zone between the less dense crust and the denser mantle, is viscous in nature. This zone is the epicenter of the majority of the dynamic Earth processes that cause earthquakes. So the study of seismic wave propagation in multilayered viscoelastic medium becomes of great importance. Some attempts have been made earlier to study the effect of viscoelasticity in wave propagation. Cooper Jr (1967), and Romeo (2003) have studied the propagation of SH waves in viscoelastic media. Naciri et al. (1989) studied the propagation of harmonic wave in multilayered viscoelastic media.

Variations in the physical and chemical properties of matter are usually linked to its dynamic behavior, making the study of elastic wave propagation on the Earth's interior a crucial field. The stresses present in an elastic body even in the absence of external forces are known as initial stresses, and the body is described as initially stressed. These stresses can significantly affect the elastic waves generated by earthquakes, explorations, or impacts. Biot (1940) demonstrated that initial stresses have a pronounced influence on wave propagation. He demonstrated that the propagation of acoustic waves under initial stress is not same as the stress-free situation and cannot be modeled by incorporating it into the classical theory with stress-dependent elastic coefficients. The development of initial stress in the medium is due to many reasons, for examples, different temperature, process of quenching, gravity variation, creep, differential external forces etc. Torsional wave propagation in a composite layer lying over an anisotropic non-homogeneous half-space under initial stress was observed by Dhua et al. (2015).

Now a days earthquake is a common natural phenomenon. Seismic waves produced by earthquake draws attention for many researchers to study the wave propagation aspects.

Surface waves travel slowly but having larger amplitude can be the most destructive type of seismic wave. Love waves are horizontally polarized shear waves exists in the presence of semi infinite medium. Generally, Earth's interior and the near surface geological structures are majorly constituted of multiple layers of parallel structures of different materials like rocks, crystalline materials and anisotropic material, underground water, oil and gases also. The study of the Earth's interior structure is not possible explicitly. The results collected from the study of wave propagation through different composite medium is one of the valuable informative source to understand the nature of internal structure of the earth. Some materials exhibits viscoelastic properties like wood carbon-epoxy in orthotropic medium. Ground shaking, earthquake loads, stiffness of soil can be visualized through this works. The Earth can be considered an elastic solid layered medium under high initial stress. It is very much crucial to study the impact of initial stress on the propagation of Love waves. We have designed this problem keeping all this things in mind.

Although numerous problems related to seismic wave propagation in multilayered media have been resolved, the problem in a multilayered viscoelastic medium with initial stress remains unexplored. This paper aims to examine the propagation of Love waves in a multilayered viscoelastic orthotropic medium with initial stress using the finite difference technique. The dispersion relation has been derived in a complex form, where the real part provides the dispersion curve and the imaginary part accounts for the attenuation curve. To show the effect of viscoelasticity and initial stress on phase velocity and attenuation, graphs have been plotted separately. Finite difference scheme has been used to determine the stability criterion of steady state solution in terms of stability ratio (Richards and Aki, 1980). The phase and group velocities have been calculated for various stability ratios and are illustrated through graphs.

5.1.2 Formulation of the problem

Let us consider total $(n-1)$ viscoelastic orthotropic layer of width $h_i, i = 1, 2, ..., n-1$ lying over a viscoelastic orthotropic half space under the compressive initial stress T. The x-axis is along the propagation of waves and positive direction of z-axis is vertically downwards as shown in Figure 5.1. The layers are numbered from top to bottom, starting with the uppermost layer as (1) and proceeding downwards to the half-space as (n). Initially stress (T) along the x-axis is considered in the respective layers. The constitutive equation used

in orthotropic model are

$$\begin{aligned}
\tau_{xx} &= C_{11}e_{xx} + C_{12}e_{yy} + C_{13}e_{zz},\\
\tau_{yy} &= C_{12}e_{xx} + C_{22}e_{yy} + C_{23}e_{zz},\\
\tau_{zz} &= C_{13}e_{xx} + C_{23}e_{yy} + C_{33}e_{zz},\\
\tau_{yz} &= 2C_{44}e_{yz},\\
\tau_{xz} &= 2C_{55}e_{xz},\\
\tau_{xy} &= 2C_{66}e_{xy}.
\end{aligned} \tag{5.1.1}$$

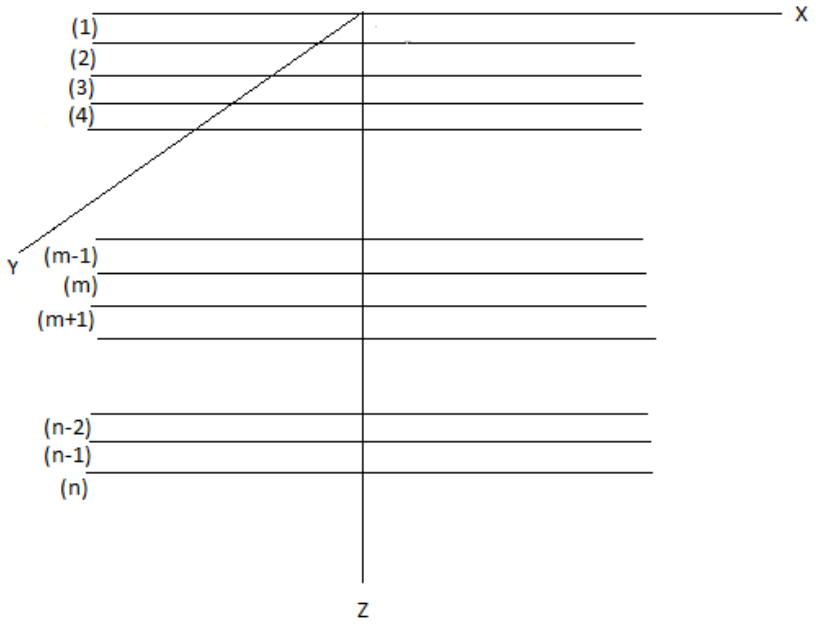

FIGURE 5.1: Geometry of the problem

where $\tau_{xx}, \tau_{yy}, \tau_{zz}, \tau_{yz}, \tau_{xz}, \tau_{xy}$ are the stress components, $C_{ij}, (i, j = 1, 2, ...6)$ are the elastic constants and $e_{xx}, e_{yy}, e_{zz}, e_{yz}, e_{xz}, e_{xy}$ are the strain components. Let (u, v, w) be the displacements along x, y, z axis respectively. Love wave propagation in the x direction causes displacement in the y direction only. So $u = w = 0$, $v = v(x, z, t)$ and $\frac{\partial}{\partial y} \equiv 0$. The

equations of motion in the absence of body forces and in the presence of initial stress are

$$\begin{aligned}
&\frac{\partial}{\partial x}(\tau_{xx}) + \frac{\partial}{\partial y}(\tau_{xy}) + \frac{\partial}{\partial z}(\tau_{xz}) - T(\frac{\partial \Omega_z}{\partial y} - \frac{\partial \Omega_y}{\partial z}) = \rho \frac{\partial^2 u}{\partial t^2} \\
&\frac{\partial}{\partial x}(\tau_{yx}) + \frac{\partial}{\partial y}(\tau_{yy}) + \frac{\partial}{\partial z}(\tau_{yz}) - T(\frac{\partial \Omega_z}{\partial x}) = \rho \frac{\partial^2 v}{\partial t^2} \\
&\frac{\partial}{\partial x}(\tau_{zx}) + \frac{\partial}{\partial y}(\tau_{zy}) + \frac{\partial}{\partial z}(\tau_{zz}) - T(\frac{\partial \Omega_y}{\partial z}) = \rho \frac{\partial^2 w}{\partial t^2}
\end{aligned} \tag{5.1.2}$$

where Ω_x, Ω_y, Ω_z are being used to denote the rotational components along x, y, z respectively; and are defined by

$$\Omega_x = \frac{1}{2}(\frac{\partial w}{\partial y} - \frac{\partial v}{\partial z}),\ \Omega_y = \frac{1}{2}(\frac{\partial u}{\partial z} - \frac{\partial w}{\partial x}),\ \Omega_z = \frac{1}{2}(\frac{\partial v}{\partial x} - \frac{\partial u}{\partial y}). \tag{5.1.3}$$

In this case,

$$\tau_{xx} = \tau_{yy} = \tau_{zz} = 0,\ \tau_{zy} = \tau_{yz} = C_{44}\frac{\partial v}{\partial z},\ \tau_{zx} = \tau_{xz} = 0,\ \tau_{xy} = \tau_{yx} = C_{66}\frac{\partial v}{\partial x},$$

and using above values in equation (5.1.2) we get

$$\frac{\partial}{\partial x}(C_{66}\frac{\partial v}{\partial x}) + \frac{\partial}{\partial z}(C_{44}\frac{\partial v}{\partial z}) - T\frac{\partial}{\partial x}(\frac{1}{2}\frac{\partial v}{\partial x}) = \rho\frac{\partial^2 v}{\partial t^2}.$$

Equation of transversal horizontal displacement in the m^{th} viscoelastic layer in the presence of initial stress is given by

$$\left(\overline{C}_{66}^{(m)} - \frac{T^{(m)}}{2}\right)\frac{\partial^2 v^{(m)}}{\partial x^2} + \overline{C}_{44}^{(m)}\frac{\partial^2 v^{(m)}}{\partial z^2} = \rho_{(m)}\frac{\partial^2 v^{(m)}}{\partial t^2}, \tag{5.1.4}$$

where

$$\overline{C}_{44}^{(m)} = C_{44}^{R(m)} + C_{44}^{I(m)}\frac{\partial}{\partial t} \text{ and } \overline{C}_{66}^{(m)} = C_{66}^{R(m)} + C_{66}^{I(m)}\frac{\partial}{\partial t}.$$

Substituting above relations in equation (5.1.4) we get

$$\begin{aligned}
\left(C_{66}^{R(m)} - \frac{T^{(m)}}{2}\right)\frac{\partial^2 v^{(m)}}{\partial x^2} + C_{44}^{R(m)}\frac{\partial^2 v^{(m)}}{\partial z^2} + C_{66}^{I(m)}\frac{\partial}{\partial t}\left(\frac{\partial^2 v^{(m)}}{\partial x^2}\right) + \\
C_{44}^{I(m)}\frac{\partial}{\partial t}\left(\frac{\partial^2 v^{(m)}}{\partial z^2}\right) = \rho_{(m)}\frac{\partial^2 v^{(m)}}{\partial t^2}
\end{aligned} \tag{5.1.5}$$

5.1.3 Solution

We assume the solution of equation (5.1.4) in the form $v^{(m)} = v_1(z)e^{i(kx-\omega t)}$ which gives,

$$v^{(m)} = \left(A^{(m)}e^{i\alpha_{(m)}z} + B^{(m)}e^{-i\alpha_{(m)}z}\right)e^{i(kx-\omega t)} \tag{5.1.6}$$

where

$$\left(\alpha_{(m)}\right)^2 = \left(\frac{k^2}{\overline{C}_{44}^{(m)}}\right)\left(\rho_{(m)}c^2 - \left(\overline{C}_{66}^{(m)} - \frac{T^{(m)}}{2}\right)\right),\ \omega^2 = k^2c^2 \tag{5.1.7}$$

and $A^{(m)}$, $B^{(m)}$ are arbitrary constants. The shear stress at the boundary of the m^{th} layer is given by:

$$S^{(m-1)} = i\overline{C}_{44}^{(m)}\alpha_{(m)}\left(A^{(m)}e^{i\alpha_{(m)}z} - B^{(m)}e^{-i\alpha_{(m)}z}\right)e^{i(kx-\omega t)}. \tag{5.1.8}$$

Now, shifting the coordinate system from the free surface layer to the $(m-1)^{th}$ interface along z axis, we obtain

$$\left(\frac{\dot{v}}{c}\right)^{(m-1)} = -ik\left(A^{(m)} + B^{(m)}\right)e^{i(kx-\omega t)}. \tag{5.1.9}$$

Equation (5.1.9) represents the dimensionless velocity at the $(m-1)^{th}$ interface. Using equation (5.1.8) shear stress at $(m-1)^{th}$ interface, i.e. at $z = 0$ is

$$S^{(m-1)} = i\overline{C}_{44}^{(m)}\alpha_{(m)}\left(A^{(m)} - B^{(m)}\right)e^{i(kx-\omega t)}. \tag{5.1.10}$$

Similarly at the m^{th} interface i.e. at $z = h_m$; the dimensionless velocity and the shear stress can be expressed as

$$\left(\frac{\dot{v}}{c}\right)^{(m)} = ke^{i(kx-\omega t)}\left[-i\left(A^{(m)} + B^{(m)}\right)\cos\left(\alpha_{(m)}h_m\right) + \left(A^{(m)} - B^{(m)}\right)\sin\left(\alpha_{(m)}h_m\right)\right] \tag{5.1.11}$$

and

$$S^{(m)} = i\overline{C}_{44}^{(m)}\alpha_{(m)}\left[\left(A^{(m)} - B^{(m)}\right)\cos\left(\alpha_{(m)}h_m\right) + i\left(A^{(m)} + B^{(m)}\right)\sin\left(\alpha_{(m)}h_m\right)\right]e^{i(kx-\omega t)}. \tag{5.1.12}$$

Eliminating $A^{(m)}$ and $B^{(m)}$ from equation (5.1.9) to (5.1.12), we get the final expression for dimensionless velocity and shear stress in the matrix form

$$\begin{bmatrix}\left(\frac{\dot{v}}{c}\right)^{(m)} \\ S^{(m)}\end{bmatrix} = a_m\begin{bmatrix}\left(\frac{\dot{v}}{c}\right)^{(m-1)} \\ S^{(m-1)}\end{bmatrix} \tag{5.1.13}$$

where

$$a_m = \begin{bmatrix} \cos\left(\alpha_{(m)} h_m\right) & -ik\left(\overline{C}_{44}^{(m)} \alpha_{(m)}\right)^{-1} \sin\left(\alpha_{(m)} h_m\right) \\ -ik^{-1} \overline{C}_{44}^{(m)} \alpha_{(m)} \sin\left(\alpha_{(m)} h_m\right) & \cos\left(\alpha_{(m)} h_m\right) \end{bmatrix}. \tag{5.1.14}$$

Similarly for the $(m-1)^{th}$ layer we have,

$$\begin{bmatrix} \left(\frac{\dot{v}}{c}\right)^{(m-1)} \\ S^{(m-1)} \end{bmatrix} = a_{m-1} \begin{bmatrix} \left(\frac{\dot{v}}{c}\right)^{(m-2)} \\ S^{(m-2)} \end{bmatrix}, \tag{5.1.15}$$

which is obtained just by replacing m by $(m-1)$ in equation (5.1.14) and (5.1.15). From equations (5.1.13) and (5.1.15) we get

$$\begin{bmatrix} \left(\frac{\dot{v}}{c}\right)^{(m)} \\ S^{(m)} \end{bmatrix} = a_m a_{m-1} \begin{bmatrix} \left(\frac{\dot{v}}{c}\right)^{(m-2)} \\ S^{(m-2)} \end{bmatrix}. \tag{5.1.16}$$

Applying the same procedure to the problem leads to the following relationship:

$$\begin{bmatrix} \left(\frac{\dot{v}}{c}\right)^{(n-1)} \\ S^{(n-1)} \end{bmatrix} = A \begin{bmatrix} \left(\frac{\dot{v}}{c}\right)^{(0)} \\ S^{(0)} \end{bmatrix}, \tag{5.1.17}$$

where $A = a_{(n-1)} a_{(n-2)} \ldots\ldots a_2 a_1$ is (2×2) matrix. Considering A in the form

$$A = \begin{bmatrix} A_{11} & A_{12} \\ A_{21} & A_{22} \end{bmatrix} \tag{5.1.18}$$

which reduces equation (5.1.17) to

$$\begin{aligned} \left(\frac{\dot{v}}{c}\right)^{(n-1)} &= A_{11} \left(\frac{\dot{v}}{c}\right)^{(0)} + A_{12} S^{(0)}, \\ S^{(n-1)} &= A_{21} \left(\frac{\dot{v}}{c}\right)^{(0)} + A_{22} S^{(0)}. \end{aligned} \tag{5.1.19}$$

Replacing m by n in equations (5.1.9) and (5.1.10), we get

$$\begin{aligned} \left(\frac{\dot{v}}{c}\right)^{(n-1)} &= -ik\left(A^{(n)} + B^{(n)}\right) e^{i(kx-\omega t)}, \\ S^{(n-1)} &= i\overline{C}_{44}^{(n)} \alpha_{(n)} \left(A^{(n)} - B^{(n)}\right) e^{i(kx-\omega t)}. \end{aligned} \tag{5.1.20}$$

Using the conditions $S^{(0)} = 0$ and $B^{(n)} = 0$ in equations (5.1.19) and (5.1.20), we get

$$A_{21} = -k^{-1}\overline{C}_{44}^{(n)}\alpha_{(n)}A_{11}. \tag{5.1.21}$$

When $n = 2$, the above equation becomes

$$\tan\left(\alpha_{(1)}h_1\right) = \frac{\overline{C}_{44}^{(2)}\alpha_{(2)}}{\overline{C}_{44}^{(1)}\alpha_{(1)}}, \tag{5.1.22}$$

where

$$\left(\alpha_{(1)}\right)^2 = \frac{k^2}{\overline{C}_{44}^{(1)}}\left[\rho_{(1)}c^2 - \left(\overline{C}_{66}^{(1)} - \frac{T^{(1)}}{2}\right)\right],\ \left(\alpha_{(2)}\right)^2 = \frac{k^2}{\overline{C}_{44}^{(2)}}\left[\left(\overline{C}_{66}^{(2)} - \frac{T^{(2)}}{2}\right) - \rho_{(2)}c^2\right].$$

Using the relations $\overline{C}_{44}^{(i)} = C_{44}^{R(i)} - ikcC_{44}^{I(i)}$, $\overline{C}_{66}^{(i)} = C_{66}^{R(i)} - ikcC_{66}^{I(i)}$ for $(i = 1, 2)$ we can write $\left(\alpha_{(1)}\right)^2 = A + iB$, where

$$A = \frac{2\left(\frac{c}{\beta_{(1)}}\right)^2 - 2\frac{C_{66}^{R(1)}}{C_{44}^{R(1)}} + S_1 - 2\xi_1\xi_2}{1 + \left(\xi_1\right)^2}\frac{k^2}{2},\ B = \frac{\xi_1\left[2\left(\frac{c}{\beta_{(1)}}\right)^2 - 2\frac{C_{66}^{R(1)}}{C_{44}^{R(1)}} + S_1\right] + 2\xi_2}{1 + \left(\xi_1\right)^2}\frac{k^2}{2}$$

and

$$\beta_{(1)} = \sqrt{\frac{C_{44}^{R(1)}}{\rho_{(1)}}},\ S_1 = \frac{T^{(1)}}{C_{44}^{R(1)}},\ \xi_1 = \frac{\omega C_{44}^{I(1)}}{C_{44}^{R(1)}},\ \xi_2 = \frac{\omega C_{66}^{I(1)}}{C_{44}^{R(1)}}.$$

Similarly, we can write $\left(\alpha_{(2)}\right)^2 = A' + iB'$, where

$$A' = \frac{-\left[2\left(\frac{c}{\beta_{(2)}}\right)^2 - 2\frac{C_{66}^{R(2)}}{C_{44}^{R(2)}} + S_2\right] + 2\xi_3\xi_4}{1 + \left(\xi_3\right)^2}\frac{k^2}{2}, B' = -\frac{\xi_3\left[2\left(\frac{c}{\beta_{(2)}}\right)^2 - 2\frac{C_{66}^{R(2)}}{C_{44}^{R(2)}} + S_2\right] + 2\xi_4}{1 + \left(\xi_3\right)^2}\frac{k^2}{2}$$

and

$$\beta_{(2)} = \sqrt{\frac{C_{44}^{R(2)}}{\rho_{(2)}}},\ S_2 = \frac{T^{(2)}}{C_{44}^{R(2)}},\ \xi_3 = \frac{\omega C_{44}^{I(2)}}{C_{44}^{R(2)}},\ \xi_4 = \frac{\omega C_{66}^{I(2)}}{C_{44}^{R(2)}}.$$

In fact, wave number k is complex and it can be written as $k = Re(k) + iIm(k)$ with $\delta = \frac{Im(k)}{Re(k)}$ as an attenuation coefficient. From equation (5.1.22) we get the dispersion and

damping equation respectively as,

$$\frac{\tan(E)-\tan(E)[\tanh(F)]^2}{1+[\tan(E)\tanh(F)]^2}=\frac{(C_{44}^{R(2)}C'+\omega C_{44}^{I(2)}D')(C_{44}^{R(1)}C+\omega C_{44}^{I(1)}D)}{(C_{44}^{R(1)}C+\omega C_{44}^{I(1)}D)^2+(C_{44}^{R(1)}D-\omega C_{44}^{I(1)}C)^2}+\frac{(C_{44}^{R(2)}D'-\omega C_{44}^{I(2)}C')(C_{44}^{R(1)}D-\omega C_{44}^{I(1)}C)}{(C_{44}^{R(1)}C+\omega C_{44}^{I(1)}D)^2+(C_{44}^{R(1)}D-\omega C_{44}^{I(1)}C)^2} \tag{5.1.23}$$

and

$$\frac{\tanh(F)+\tanh(F)[\tan(E)]^2}{1+[\tan(E)\tanh(F)]^2}=\frac{(C_{44}^{R(2)}D'-\omega C_{44}^{I(2)}C')(C_{44}^{R(1)}C+\omega C_{44}^{I(1)}D)}{(C_{44}^{R(1)}C+\omega C_{44}^{I(1)}D)^2+(C_{44}^{R(1)}D-\omega C_{44}^{I(1)}C)^2}-\frac{(C_{44}^{R(2)}C'+\omega C_{44}^{I(2)}D')(C_{44}^{R(1)}D-\omega C_{44}^{I(1)}C)}{(C_{44}^{R(1)}C+\omega C_{44}^{I(1)}D)^2+(C_{44}^{R(1)}D-\omega C_{44}^{I(1)}C)^2}, \tag{5.1.24}$$

where $C+iD=\alpha_{(1)}$, $C'+iD'=\alpha_{(2)}$ and $E=Ch_1$, $F=Dh_1$.

5.1.4 Special cases

When $C_{44}^{I(1)}=C_{44}^{I(2)}=C_{66}^{I(1)}=C_{66}^{I(2)}=0$, equation (5.1.23) becomes

$$\tan\left[kh_1\sqrt{\frac{\rho_{(1)}c^2-C_{66}^{R(1)}+\frac{T^{(1)}}{2}}{C_{44}^{R(1)}}}\right]=\frac{C_{44}^{R(2)}}{C_{44}^{R(1)}}\frac{\sqrt{\frac{C_{66}^{R(2)}-\rho_{(2)}c^2-\frac{T^{(2)}}{2}}{C_{44}^{R(2)}}}}{\sqrt{\frac{\rho_{(1)}c^2-C_{66}^{R(1)}+\frac{T^{(1)}}{2}}{C_{44}^{R(1)}}}}. \tag{5.1.25}$$

When $T^{(1)}=T^{(2)}=0$, i.e. initial stress is absent, and $C_{66}^{R(i)}$, $C_{44}^{R(i)}\to\mu_{(i)}$; $(i=1,2)$ then we have,

$$\tan\left(kh_1\sqrt{\frac{c^2}{(\beta'_{(1)})^2}-1}\right)=\frac{\mu_{(2)}}{\mu_{(1)}}\frac{\sqrt{1-\frac{c^2}{(\beta'_{(2)})^2}}}{\sqrt{\frac{c^2}{(\beta'_{(1)})^2}-1}}, \tag{5.1.26}$$

where $(\beta'_{(i)})^2=\frac{\mu_{(i)}}{\rho_{(i)}}$, $(i=1,2)$. The above equation represents a classical Love wave equation when an isotropic layer of finite thickness lying over an isotropic half space and the damping part is absent. The classical Love equation is agreed with Love (2013).

For $n = 3$ equation (5.1.21) takes the form

$$\tan(\alpha_{(2)}h_2) = \frac{\overline{C}_{44}^{(3)}\alpha_{(3)} - \overline{C}_{44}^{(1)}\alpha_{(1)}\tan(\alpha_{(1)}h_1)}{\overline{C}_{44}^{(2)}\alpha_{(2)} - \left(\overline{C}_{44}^{(2)}\alpha_{(2)}\right)^{-1}\overline{C}_{44}^{(1)}\alpha_{(1)}\overline{C}_{44}^{(3)}\alpha_{(3)}\tan(\alpha_{(1)}h_1)}, \tag{5.1.27}$$

where

$$\left(\alpha_{(i)}\right)^2 = \frac{k^2}{\overline{C}_{44}^{(i)}}\left[\rho_{(i)}c^2 - \left(\overline{C}_{66}^{(i)} - \frac{T^{(i)}}{2}\right)\right],\ (i = 1, 2)$$

and

$$\left(\alpha_{(3)}\right)^2 = \frac{k^2}{\overline{C}_{44}^{(3)}}\left[\left(\overline{C}_{66}^{(3)} - \frac{T^{(3)}}{2}\right) - \rho_{(3)}c^2\right].$$

For isotropic medium and without initial stress i.e. $T^{(i)} = 0, C_{66}^{I(i)} = C_{44}^{I(i)} = 0; C_{66}^{R(i)}, C_{44}^{R(i)} \to \mu_{(i)};\ (i = 1, 2, 3)$ the equation (5.1.27) becomes

$$\tan\left(kh_2\sqrt{\frac{c^2}{(\beta'_{(2)})^2} - 1}\right) = \frac{\mu_{(3)}\sqrt{1 - \frac{c^2}{(\beta'_{(3)})^2}} - \mu_{(1)}\sqrt{\frac{c^2}{(\beta'_{(1)})^2} - 1}\tan\left(kh_1\sqrt{\frac{c^2}{(\beta'_{(1)})^2} - 1}\right)}{\mu_{(2)}\sqrt{\frac{c^2}{(\beta'_{(2)})^2} - 1} - \left(\mu_{(2)}\sqrt{\frac{c^2}{(\beta'_{(2)})^2} - 1}\right)^{-1}\mu_{(3)}\sqrt{1 - \frac{c^2}{(\beta'_{(3)})^2}}\mu_{(1)}\sqrt{\frac{c^2}{(\beta'_{(1)})^2} - 1}\tan\left(kh_1\sqrt{\frac{c^2}{(\beta'_{(1)})^2} - 1}\right)}, \tag{5.1.28}$$

where $(\beta'_{(i)})^2 = \frac{\mu_{(i)}}{\rho_{(i)}}$, $(i = 1, 2, 3)$. The above equation is standard Love wave equation when two layers of finite width h_1, h_2 respectively, overlying a half space. Using function $H(n - a)$ defined as

$$H(n - a) = \begin{cases} 0, & \text{n} < a \\ 1, & \text{n} \geq a \end{cases}$$

The generalized dispersion equation, $(n - 1)$ layers of finite width overlie a half space may be written as

$$\zeta_n = \overline{C}_{44}^{(n)}\alpha_{(n)}\gamma_n, \tag{5.1.29}$$

where

$$\zeta_n = \overline{C}_{44}^{(1)}\alpha_{(1)}\tan(\alpha_{(1)}h_1) + \overline{C}_{44}^{(2)}\alpha_{(2)}\tan(\alpha_{(2)}h_2)H(n-3) + EH(n-4),$$

$$\gamma_n = 1 - \overline{C}_{44}^{(1)}\alpha_{(1)}\left(\overline{C}_{44}^{(2)}\alpha_{(2)}\right)^{-1}\tan(\alpha_{(1)}h_1)\tan(\alpha_{(2)}h_2)H(n-3) - FH(n-4),\ n = 2,3,4....,$$

$$E = \overline{C}_{44}^{(3)}\alpha_{(3)}\tan(\alpha_{(3)}h_3)\gamma_3 + \overline{C}_{44}^{(4)}\alpha_{(4)}\tan(\alpha_{(4)}h_4)\gamma_4 + \cdots\cdots + \overline{C}_{44}^{(n-1)}\alpha_{(n-1)}\tan(\alpha_{(n-1)}h_{n-1})\gamma_{n-1},$$

$$F = \left(\overline{C}_{44}^{(3)}\alpha_{(3)}\right)^{-1}\tan(\alpha_{(3)}h_3)\zeta_3 + \left(\overline{C}_{44}^{(4)}\alpha_{(4)}\right)^{-1}\tan(\alpha_{(4)}h_4)\zeta_4 + \cdots\cdots + \left(\overline{C}_{44}^{(n-1)}\alpha_{(n-1)}\right)^{-1}\tan(\alpha_{(n-1)}h_{n-1})\zeta_{n-1}$$

and

$$\left(\alpha_{(n)}\right)^2 = \frac{k^2}{\overline{C}_{44}^{(n)}}\left[\left(\overline{C}_{66}^{(n)} - \frac{T^{(n)}}{2}\right) - \rho_{(n)}c^2\right].$$

5.1.5 Stability crietrion, phase velocity and group velocity

To implement finite difference scheme, we divide a finite rectangular section of the medium. The xz-plane is discretized into a grid with equal increments of Δx and Δz along the x and z axes, respectively. The time axis is discretized by the step size Δt. The space time grids are defined as follows

$$x_l = l\Delta x,\ l = 0,1,2,....L,\ z_m = m\Delta z,\ m = 0,1,2,....M,\ t_w = w\Delta t,\ w = 0,1,2,....W.$$

Let us denote $v^{(m)}(x_l, z_m, t_w)$ by $v_{l,m}^w$. The Taylor's expansion of $v_{l+1,m}^w$ and $v_{l-1,m}^w$ can be written as

$$v_{l+1,m}^w = v_{l,m}^w + \Delta x\frac{\partial v}{\partial x} + \frac{\Delta x^2}{2!}\frac{\partial^2 v}{\partial x^2} + \frac{\Delta x^3}{3!}\frac{\partial^3 v}{\partial x^3} + \cdots\cdots \tag{5.1.30}$$

and

$$v_{l-1,m}^w = v_{l,m}^w - \Delta x\frac{\partial v}{\partial x} + \frac{\Delta x^2}{2!}\frac{\partial^2 v}{\partial x^2} - \frac{\Delta x^3}{3!}\frac{\partial^3 v}{\partial x^3} + \cdots\cdots. \tag{5.1.31}$$

From equations (5.1.30) and (5.1.31) we get,

$$\frac{\partial v}{\partial x} = \frac{v_{l+1,m}^w - v_{l-1,m}^w}{2\Delta x}, \tag{5.1.32}$$

$$\frac{\partial^2 v}{\partial x^2} = \frac{v_{l+1,m}^w - 2v_{l,m}^w + v_{l-1,m}^w}{(\Delta x)^2} \tag{5.1.33}$$

which are central difference approximation to $\frac{\partial v}{\partial x}$ and $\frac{\partial^2 v}{\partial x^2}$ respectively with error of order $O(\Delta x^2)$. Similarly, the central difference approximation to $\frac{\partial v}{\partial z}$, $\frac{\partial^2 v}{\partial z^2}$ and $\frac{\partial^2 v}{\partial t^2}$ with error of

second order can be given as

$$\frac{\partial v}{\partial z} = \frac{v^w_{l,m+1} - v^w_{l,m-1}}{2\Delta z}, \tag{5.1.34}$$

$$\frac{\partial^2 v}{\partial z^2} = \frac{v^w_{l,m+1} - 2v^w_{l,m} + v^w_{l,m-1}}{(\Delta z)^2}, \tag{5.1.35}$$

and

$$\frac{\partial^2 v}{\partial t^2} = \frac{v^{w+1}_{l,m} - 2v^w_{l,m} + v^{w-1}_{\boldsymbol{l},m}}{(\Delta t)^2} \tag{5.1.36}$$

respectively. Therefore we can write,

$$\frac{\partial^3 v}{\partial x^2 \partial t} = \frac{v^{w+1}_{l+1,m} - 2v^{w+1}_{l,m} + v^{w+1}_{l-1,m} - v^{w-1}_{l+1,m} + 2v^{w-1}_{l,m} - v^{w-1}_{l-1,m}}{2\Delta t(\Delta x)^2} \tag{5.1.37}$$

and

$$\frac{\partial^3 v}{\partial z^2 \partial t} = \frac{v^{w+1}_{l,m+1} - 2v^{w+1}_{l,m} + v^{w+1}_{l,m-1} - v^{w-1}_{l,m+1} + 2v^{w-1}_{l,m} - v^{w-1}_{l,m-1}}{2\Delta t(\Delta z)^2}. \tag{5.1.38}$$

Now, using the obtained finite difference approximations in equation (5.1.5), we get

$$\begin{aligned}\left(C^{R(m)}_{66} - \frac{T^{(m)}}{2}\right)\frac{v^w_{l+1,m} - 2v^w_{l,m} + v^w_{l-1,m}}{(\Delta x)^2} + C^{R(m)}_{44}\frac{v^w_{l,m+1} - 2v^w_{l,m} + v^w_{l,m-1}}{(\Delta z)^2} + \\ C^{I(m)}_{66}\frac{v^{w+1}_{l+1,m} - 2v^{w+1}_{l,m} + v^{w+1}_{l-1,m} - v^{w-1}_{l+1,m} + 2v^{w-1}_{l,m} - v^{w-1}_{l-1,m}}{2\Delta t(\Delta x)^2} + \\ C^{I(m)}_{44}\frac{v^{w+1}_{l,m+1} - 2v^{w+1}_{l,m} + v^{w+1}_{l,m-1} - v^{w-1}_{l,m+1} + 2v^{w-1}_{l,m} - v^{w-1}_{l,m-1}}{2\Delta t(\Delta z)^2} = \rho_{(m)}\frac{v^{w+1}_{l,m} - 2v^w_{l,m} + v^{w-1}_{\boldsymbol{l},m}}{(\Delta t)^2}.\end{aligned} \tag{5.1.39}$$

To analyze the stability of the aforementioned scheme, we take initial errors in v at $t = 0$. Assuming a disturbance at (l, m, w) of the form:

$$E(v^w_{l,m}) = A\, exp[-i\omega(w\Delta t) + ik(l\Delta x) + ik(m\Delta z)], \tag{5.1.40}$$

where k is fixed and we aim to derive the dispersion relation $\omega(k)$. The relation describes the time dependence of the error. The error satisfies the same equation as the solution. We substitute equation (5.1.40) in equation (5.1.39) and get

$$\begin{aligned}\frac{\rho_{(m)}}{(\Delta t)^2}\sin^2\left(\frac{\omega\Delta t}{2}\right) = \frac{\sin^2\left(\frac{k\Delta x}{2}\right)}{(\Delta x)^2}\left(C^{R(m)}_{66} - \frac{T^{(m)}}{2}\right) + C^{R(m)}_{66}\frac{\sin^2\left(\frac{k\Delta z}{2}\right)}{(\Delta z)^2} - \\ iC^{I(m)}_{66}\sin(\omega\Delta t)\frac{\sin^2\left(\frac{k\Delta x}{2}\right)}{\Delta t(\Delta x)^2} - iC^{I(m)}_{44}\sin(\omega\Delta t)\frac{\sin^2\left(\frac{k\Delta z}{2}\right)}{\Delta t(\Delta z)^2}.\end{aligned} \tag{5.1.41}$$

For $\Delta x = \Delta z$, equation (5.1.41) becomes

$$\frac{\rho_{(m)}}{(\Delta t)^2}\sin^2\left(\frac{\omega\Delta t}{2}\right) = \frac{\sin^2\left(\frac{k\Delta x}{2}\right)}{(\Delta x)^2}\left[C_{66}^{R(m)} - \frac{T^{(m)}}{2} + C_{44}^{R(m)}\right] - i\sin(\omega\Delta t)\frac{\sin^2\left(\frac{k\Delta x}{2}\right)}{\Delta t(\Delta x)^2}\left[C_{66}^{I(m)} + C_{44}^{I(m)}\right]. \tag{5.1.42}$$

The stability condition for the problem comes from $\sin\left(\frac{\omega\Delta t}{2}\right) \leq 1$. Which implies

$$\frac{\Delta t}{\Delta x}\frac{1}{\sqrt{\rho_{(m)}}}\left[C_{66}^{R(m)} - \frac{T^{(m)}}{2} + C_{44}^{R(m)} - \frac{1}{\Delta t}\left(C_{66}^{I(m)} + C_{44}^{I(m)}\right)\right]^{\frac{1}{2}} \leq 1. \tag{5.1.43}$$

Consequently ω will be real, and the error will not increase with time, which provides a steady-state solution. We can approximate $\sin\delta = \delta$ and $\cos\delta = 1$ for small δ. The approximation can be utilized in equation (5.1.42) when step length Δx, Δz, Δt are very small and we get

$$\frac{\omega}{k} = \frac{1}{\sqrt{\rho_{(m)}}}\left[C_{66}^{R(m)} - \frac{T^{(m)}}{2} + C_{44}^{R(m)} - \frac{1}{\Delta t}\left(C_{66}^{I(m)} + C_{44}^{I(m)}\right)\right]^{\frac{1}{2}} = c_0, \tag{5.1.44}$$

the local wave velocity. In view of equation (5.1.44) the stability condition (5.1.43) gives $p \leq 1$, where $p = c_0\frac{\Delta t}{\Delta x}$ is stability ratio (Courant number) upholds the result Richards and Aki (1980). Using relations $\lambda = \frac{2\pi}{k}$ and $\omega = kc$ in equation (5.1.42), we get the non-dimensional expression of phase velocity as

$$\frac{c}{c_0} = \frac{\lambda}{\Delta x}\frac{1}{p\pi}\sin^{-1}\left[p\sin\left(\frac{\pi\Delta x}{\lambda}\right)\right], \tag{5.1.45}$$

where $\frac{\Delta x}{\lambda}$ is known as dispersion parameter. From equation (5.1.45) we derive the non-dimensional expression for corresponding group velocity in terms of stability ratio as

$$\frac{\left(\frac{\partial\omega}{\partial k}\right)}{c_0} = \frac{\cos\left(\frac{\pi\Delta x}{\lambda}\right)}{\sqrt{1 - p^2\sin^2\left(\frac{\pi\Delta x}{\lambda}\right)}}.$$

5.1.6 Numerical calculation and discussion

We represent numerical results by means of graphs of the acquired complex dispersion relation for single layer lying over a half-space to study the effect of viscoelastic and initial stress parameters on phase velocity and attenuation coefficient of Love wave. For

the purpose of numerical computation, the following data has been considered (Kalyani, 1990):

$$\text{Orthotropic layer: } C_{44}^{R(1)} = 4.35\ GPa,\ C_{66}^{R(1)} = 5.0\ GPa,\ \rho_{(1)} = 9890\ Kg/m^3,$$
$$\text{Orthotropic half-space: } C_{44}^{R(2)} = 5.3\ GPa,\ C_{66}^{R(2)} = 6.47\ GPa,\ \rho_{(2)} = 3400\ Kg/m^3.$$

In Figure 5.2 dimensionless phase velocity ($\frac{c}{\beta_{(1)}}$) has been plotted against dimensionless wave number $Re(kH)$ for fixed values of $\xi_1 = \xi_2 = 0.1$. Figure 5.2 exhibits the effect of different viscoelastic parameter on the phase velocity through dispersion curve. Curve 1 represents the phase velocity when viscoelasticity is absent in the half-space and curve 2 represents phase velocity in viscoelastic medium. The phase velocity decreases steadily with the increase of wave number. In the orthotropic medium dispersion curve coincides with curve 1 and in the absence of viscoelastic layer dispersion curve coincides with curve 2, so have not been plotted here.

In Figure 5.3 we have mapped the graph for attenuation coefficient (δ) against dimensionless wave number $Re(kH)$. Figure 5.3 establishes the effect of various viscoelastic parameter on the attenuation coefficient through attenuation curve. In Figure 5.3 the values of both ξ_3 and ξ_4 have been taken as 0.0 and 0.1 with the fixed value of 0.1 for both ξ_1 and ξ_2. When $\xi_3 = \xi_4 = 0$ then we acquire attenuation coefficient in the absence of viscoelasticity in half-space. Attenuation coefficient in viscoelastic medium is represented by curve 2. Attenuation coefficient rises very quickly with the increase of dimensionless wave number. Moreover attenuation coefficient is higher in the presence of viscoelastic half-space than without viscoelasticity in the half-space. In the absence of viscoelastic layer damping vanishes.

In Figure 5.4, phase velocity ($\frac{c}{\beta_{(1)}}$) has been plotted against wave number $Re(kH)$ through dispersion curve, for presence and absence of dimensionless initial stress parameters. Curve 1 describes the phase velocity in viscoelastic medium without any initial stress and curve 2 shows the effect of initial stress associated with phase velocity in viscoelastic medium. It has also been observed that the phase velocity decreases with increase of dimensionless wave number.

In Figure 5.5, attenuation coefficient (δ) has been plotted against wave number $Re(kH)$ through attenuation curve for dimensionless $S_{(i)} = 0.0$ and $0.1 (i = 1, 2)$. The first curve presents attenuation coefficient without initial stress and second curve depicts attenuation coefficient in the initially stressed medium. As the dimensionless wave number increases

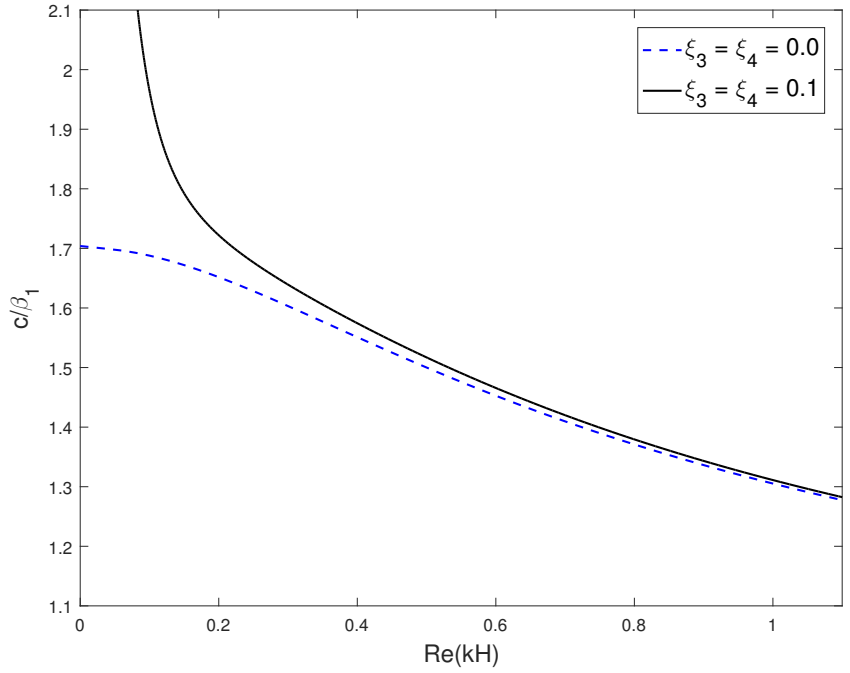

FIGURE 5.2: Phase velocity versus wave number for viscoelastic parameters

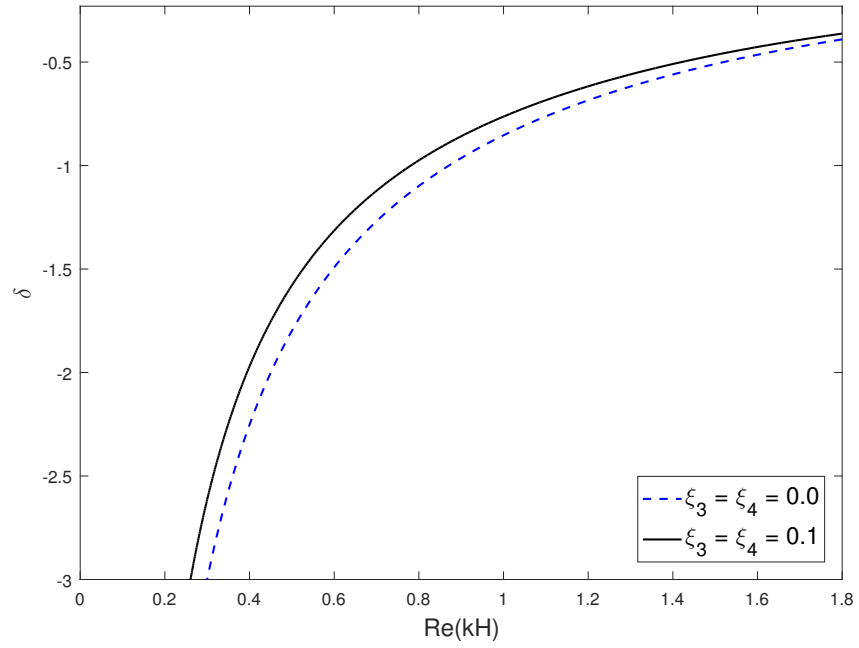

FIGURE 5.3: Attenuation coefficient versus wave number for viscoelastic parameters

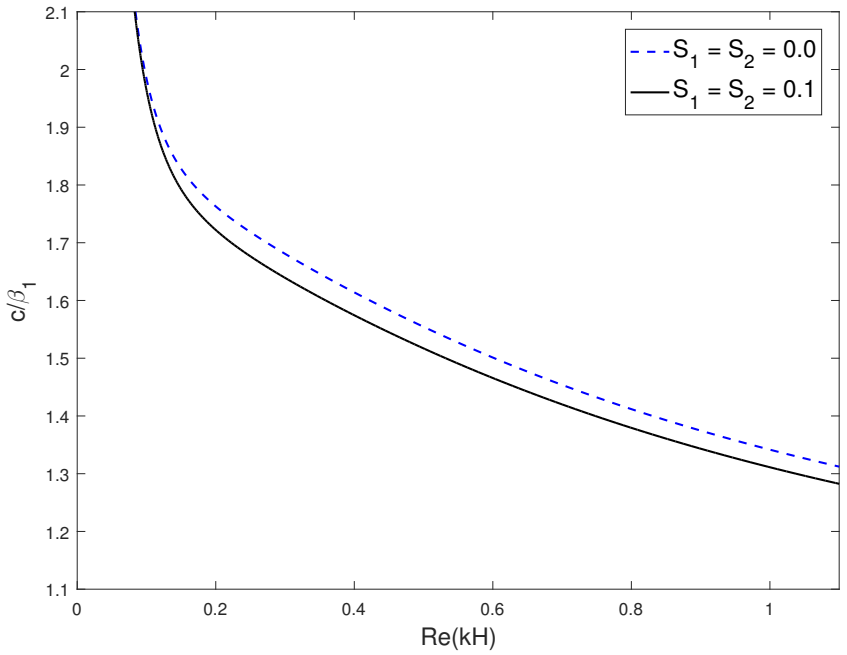

FIGURE 5.4: Phase velocity versus wave number for different values of dimensionless initial stress parameter

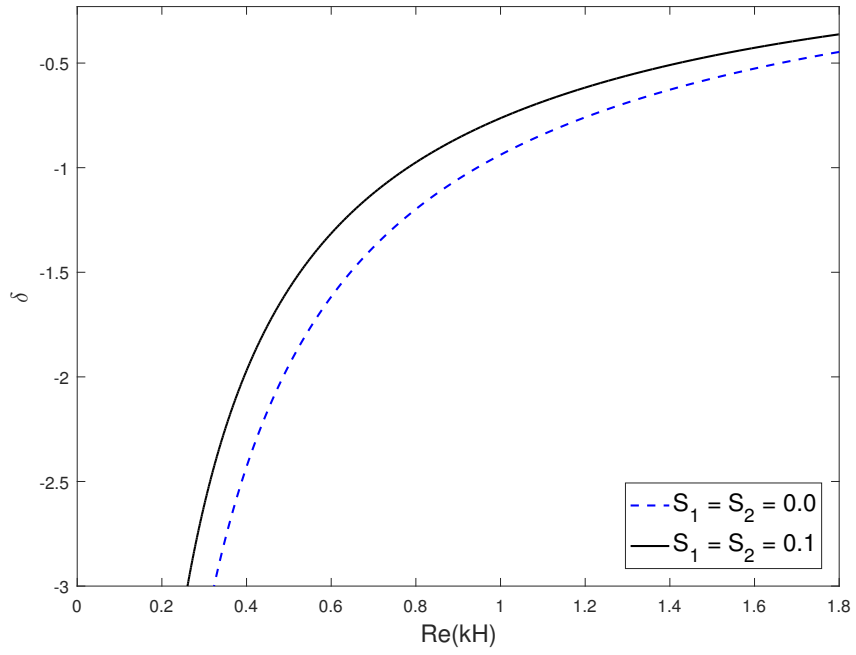

FIGURE 5.5: Attenuation coefficient versus wave number for different values of dimensionless initial stress parameter

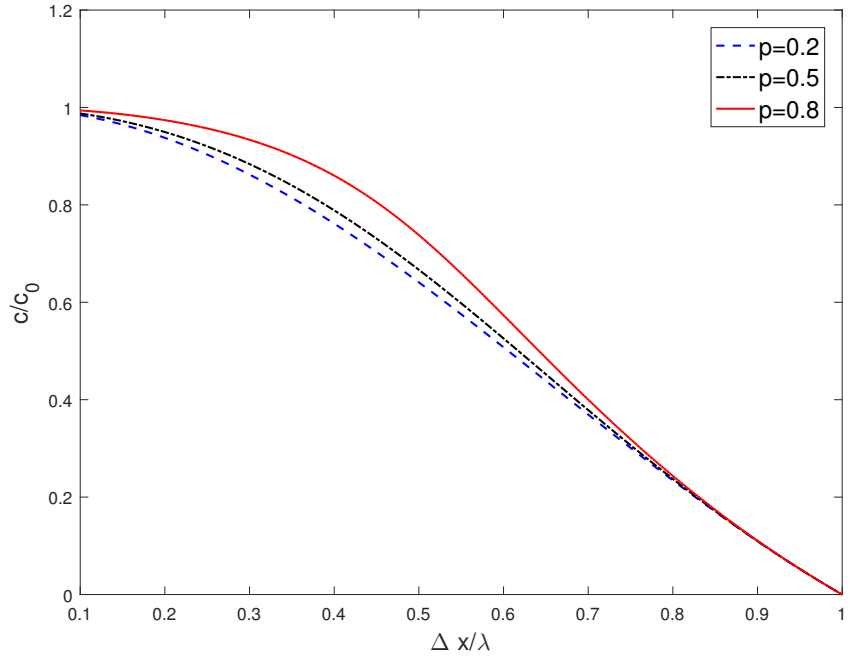

FIGURE 5.6: Dimensionless phase velocity against dispersion parameter for different values of stability ratio(Courant number) p

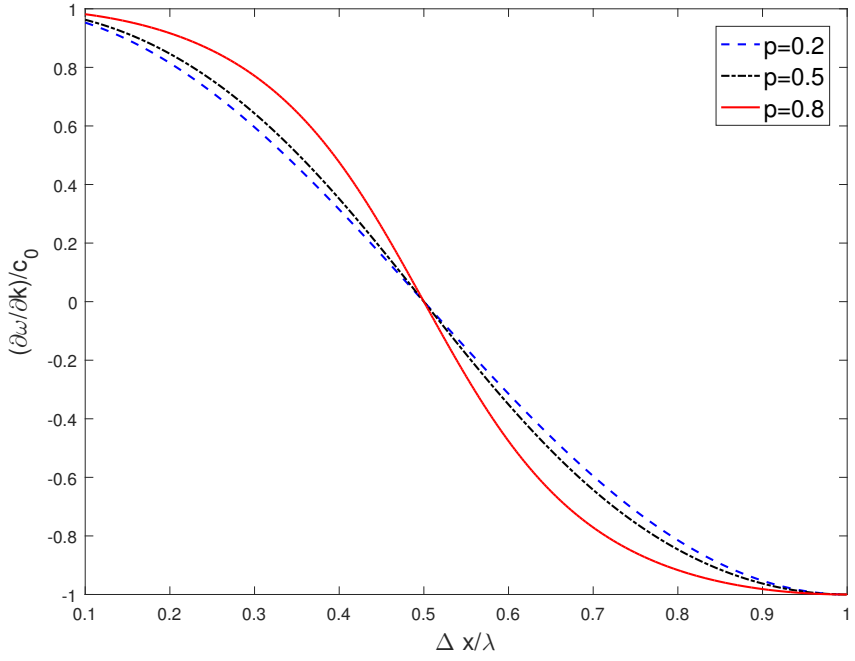

FIGURE 5.7: Dimensionless group velocity against dispersion parameter for different values of stability ratio(Courant number) p

the attenuation coefficient increases monotonically and tends to zero level. The nature of damping curve is very close to that of Singh et al. (2017) and Kumari et al. (2019).

Figure 5.6 depicts dimensionless phase velocity versus dispersion parameter graph, for different values of p. Dimensionless phase velocity decreases rapidly with increase in dispersion parameter. Phase velocity increases with the increasing stability ratio, supporting the fact that the finite difference scheme approaches to its accuracy with increment in the stability ratio.

In Figure 5.7, the plot illustrates the variation of dimensionless group velocity with the dispersion parameter for different values of p. The figure clearly shows that the group velocity decreases steadily as the dispersion parameter increases. Moreover, as the stability ratio increases, the group velocity also increases. Notably, at a specific point where $(\frac{\Delta x}{\lambda}) = 0.5$, the curves exhibit a reversal in their behavior, known as a critical point. This result is agreement with the result found by Chattopadhyay et al. (2010).

5.1.7 Conclusion

The purpose of the present study is to unfold the behavior of viscoelasticity and initial stress parameter on the phase velocity and attenuation coefficient of Love wave propagating in a multilayered orthotropic medium. Traditional analytical methods have not been able to provide accurate and effective solutions due to complexity of multiple layers. The FDM is very useful tool to produce steady state solution as this problem is related to time domain. The closed form of complex dispersion relation has been deduced by matrix method. Some special cases has been derived and we obtained the standard Love wave equation. The effect of Courant number on phase and group velocity are also established in this study. The important points from this study are highlighted as follows:

- Love wave propagates more fluently in viscoelastic medium than viscoelastic elastic layer lying over orthotropic half-space. There is no significant effect of viscoelstic parameter associated with phase velocity for high frequency.
- In the absence of initial stress, phase velocity decreases not so much as in the pre-stressed medium.
- Effect of initial stress associated with attenuation coefficient is more influential than effect of viscoelastic parameter. Attenuation coefficient increases rapidly in the pre-stressed medium.

- The attenuation coefficient is tending to zero with increase in real part of wave number.
- At specific values of the dispersion parameter, both dimensionless phase velocity and group velocity decrease to the extent that Love wave propagation is inhibited.

The study dealing with multiple layers has established some facts on phase velocity and attenuation coefficient due to viscoelasticity and initial stress factor which may provide valuable information for assortment of some particular structural material that endures in construction fields. Moreover this paper furnish some consequences about wave propagation in composite media which is concerned with the fields of Geophysics, Geology and Solid Mechanics.

5.2 Interaction of Love wave with an interface crack

5.2.1 Introduction

Love waves, a type of surface wave, play a critical role in various fields, including geophysics, seismology, and nondestructive testing. These waves, characterized by their horizontal shear motion, are highly sensitive to the properties and geometries of the media through which they propagate. The study of Love waves in composite materials, especially those involving interfaces between different types of media, has garnered significant attention due to its practical applications in evaluating the integrity of layered structures.

In many engineering and geological scenarios, materials are not homogeneous but rather composite, consisting of different layers with varying mechanical properties. One common configuration is an orthotropic layer, which has direction-dependent properties, bonded to an isotropic half-space, which has uniform properties in all directions. Understanding the interaction of Love waves with such interfaces is crucial for accurate modeling and analysis of wave propagation in these systems.

Initially, Love (1911) examined a layered system with perfect bonding at the interface, comprising an isotropic elastic layer on an isotropic substrate. Then, extensive research has been conducted on love wave propagation in various media. Considering functionally graded and piezoelectric media, Li et al. (2004), Salah et al. (2011), Du et al. (2007), Cao et al. (2009) investigated the propagation of Love waves in layered structures. The influence of anisotropy on Love wave propagation has also been explored. Gupta et al. (2013) explored Love wave propagation in a layered system with an underlying stressed half-space and a non-homogeneous substratum. Chen et al. (2022) explored Love wave propagation in layered piezoelectric structures with a conductive polymer layer on an unbounded piezoelectric substrate. Panja and Mandal (2022) analyzed the behavior of the Love wave in orthotropic multilayers, demonstrating the impact of material properties on the characteristics of the waves.

The scattering of elastic waves by cracks is a well-established field. The diffraction of anti-plane shear waves by a crack in a layered composite was examined by Keer and Luong (1974). Additionally, Love wave propagation is numerically investigated, and stress intensity factors are found for a number of scenarios. Panja and Mandal (2021) treated a crack and contact problem for anti-plane shear wave in the magnetoelastic medium. A particular challenge in this context is the presence of interface cracks, which can significantly alter the wave propagation characteristics. Interface cracks are common defects that may

arise due to manufacturing flaws, thermal stresses, or mechanical loading. They can act as scatterers, reflecting and diffracting incident waves, thus complicating the wave field. This scattering effect needs to be thoroughly understood to assess structural integrity and predict the behavior of the material under dynamic loading conditions. Research by Yang and Bogy (1985) explored the scattering of elastic waves by interface cracks in layered isotropic half-spaces, providing an early understanding of scattering phenomena. Scattering of the surface waves by a sub-surface crack was analyzed by Achenbach and Brind (1981). Stress intensity factors for a horizontal subsurface crack under time harmonic excitation were computed by Keer et al. (1984). The Love wave interactions with a surface-breaking crack normal to the free surface was investigated by Angel (1986). Neerhoff (1979) described the diffraction of Love waves by a stress-free finite-width crack in the interface of a layered composite. Narita and Shindo (1999a) investigated an interface crack in the piezoelectric and orthotropic layer. Narita and Shindo (1998) investigated the scattering of Love waves by cracks within piezoelectric media. Scattering of love waves by an interface crack between a piezoelectric layer and an elastic substrate has been studied by Bin et al. (2002) and Gu et al. (2002a). Then, Gu et al. (2002b) also found the transient response for dissimilar piezoelectric layers, while Kundu (1987) computed the transient response of two co-linear interface cracks in a layered half-space. Farnell and Adler (2012) extensively investigated elastic waves scattering in thin layers.

For the anti-plane scattering of Love waves by a surface-breaking crack normal to the free surface of an ultra-thin layer bonded to a semi-infinite medium, an analytical solution has been presented by Shodja et al. (2017). Ma et al. (2023) studied the Love wave scattering by an interface crack between a half-space elastic substrate and a one-dimensional (1D) hexagonal quasicrystal (QC) coating. The analysis of Love-type waves in functionally graded composite Structure with an imperfect interface have been explored by Sadab and Kundu (2024).

Despite the extensive research on wave propagation in homogeneous and isotropic media, studies addressing the scattering of Love waves by interface cracks in composite systems are relatively few. This research aims to fill this gap by analyzing the scattering of Love waves by an interface crack between an orthotropic layer and an isotropic half-space. Utilizing advanced mathematical techniques such as Fourier transforms and integral equations, this study seeks to elucidate the scattering mechanisms and quantify the impact of various parameters on wave propagation.

The outcomes of this research are expected to enhance the understanding of wave-material interactions in composite structures, providing valuable insights for the development of

more effective non-destructive evaluation methods and improving the design of materials and structures with enhanced durability and performance.

5.2.2 Formulation of the problem

Consider an orthotropic layer of infinite length and finite thickness h, bonded to a half space of isotropic substrate as shown in Figure 5.8. Refer to a Cartesian coordinate system (x, y, z) with origin located in the center of the crack with a positive z-axis that indicates vertically downwards. Assume that a crack of length $2c$ lies on the interface along the x-axis and extending to infinity in y direction to allow a state of anti-plane shear. A Love wave is supposed to propagate along the x-axis.

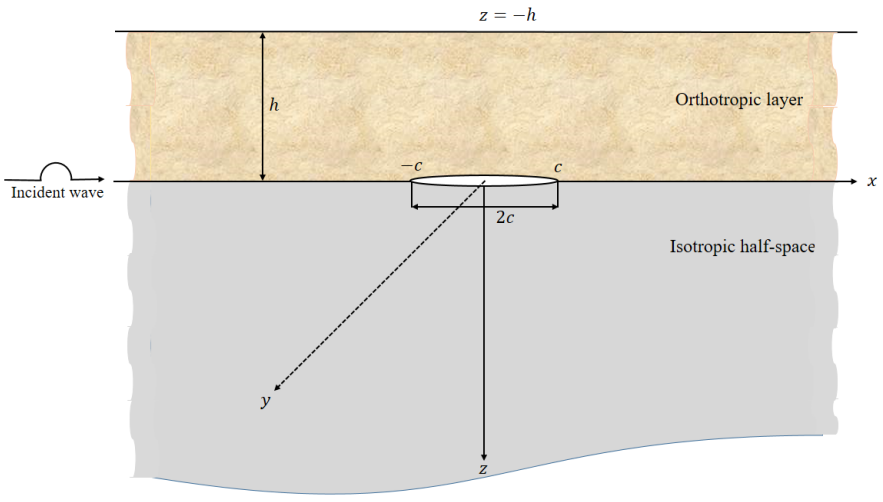

FIGURE 5.8: Geometry of the problem

The anti-plane problem has following assumptions:

$$\hat{u}_x^{(i)} = 0 = \hat{u}_z^{(i)} \quad \text{and} \quad \hat{u}_y^{(i)} = \hat{u}_y^{(i)}(x, z, t) = u_y^{(i)}(x, z)e^{-\iota\omega t}, \quad i = 1, 2 \tag{5.2.1}$$

where the superscript $()^{(1)}$ and $()^{(2)}$ represents the layer and half space respectively, ω is the circular frequency and $u_j^{(i)}$, $j = x, y, z$ represents the displacement components along the three axes.

The constitutive relationship can be expressed as follows:

$$\hat{\tau}_{yz}^{(1)} = C_{44}^{(1)} \frac{\partial \hat{u}_y^{(1)}}{\partial z}, \quad \hat{\tau}_{xy}^{(1)} = C_{66}^{(1)} \frac{\partial \hat{u}_y^{(1)}}{\partial x}, \tag{5.2.2}$$

and

$$\hat{\tau}_{yz}^{(2)} = \mu^{(2)} \frac{\partial \hat{u}_y^{(2)}}{\partial z}, \quad \hat{\tau}_{xy}^{(2)} = \mu^{(2)} \frac{\partial \hat{u}_y^{(2)}}{\partial x} \tag{5.2.3}$$

where $\hat{\tau}_{yz}^{(i)}$, $\hat{\tau}_{xy}^{(i)}$ $(i = 1, 2)$ are stress components; $C_{44}^{(1)}$, $C_{66}^{(1)}$ are elastic constants of orthotropic layer and $\mu^{(2)}$ is the shear modulus of isotropic half space.

The equation of motion for our problem are given by

$$\frac{\partial \hat{\tau}_{xy}^{(i)}}{\partial x} + \frac{\partial \hat{\tau}_{yz}^{(i)}}{\partial z} = \rho^{(i)} \frac{\partial^2 \hat{u}_y^{(i)}}{\partial t^2}, \quad i = 1, 2 \tag{5.2.4}$$

where $\rho^{(i)}$ $(i = 1, 2)$ are the mass densities of orthotropic layer and isotropic half space respectively.

With the help of Equations (5.2.1), (5.2.2) and (5.2.3), the above Equation (5.2.4) become

$$\frac{\partial^2 \hat{u}_y^{(1)}}{\partial x^2} + Q \frac{\partial^2 \hat{u}_y^{(1)}}{\partial z^2} + k_1^2 \hat{u}_y^{(1)} = 0, \tag{5.2.5}$$

and

$$\frac{\partial^2 \hat{u}_y^{(2)}}{\partial x^2} + \frac{\partial^2 \hat{u}_y^{(2)}}{\partial z^2} + k_2^2 \hat{u}_y^{(2)} = 0, \tag{5.2.6}$$

where $Q = \frac{C_{44}^{(1)}}{C_{66}^{(1)}}$, $k_1^2 = \frac{\omega^2}{c_v^2}$, $k_2^2 = \frac{\omega^2}{c_s^2}$, $c_v = \sqrt{\frac{C_{66}^{(1)}}{\rho^{(1)}}}$ and $c_s = \sqrt{\frac{\mu^{(2)}}{\rho^{(2)}}}$.

Here, c_v and c_s are the velocities of the shear waves in the orthotropic layer and the isotropic half-space respectively.

Incident Fields: It is commonly recognized that the current problem can be viewed as the superposition of an incident wave scattering problem in a structure with an identical configuration, with the exception that the far field without an incident wave and the crack is absent. The first problem is considered in this section. The appropriate solutions of the Equations (5.2.5) and (5.2.6) can be expressed as

$$u_y^{(1)inc}(x, z) = \left(A_1^{inc} \, e^{\frac{r_1^{inc} z}{\sqrt{Q}}} + A_2^{inc} \, e^{-\frac{r_1^{inc} z}{\sqrt{Q}}} \right) e^{\iota k x} \tag{5.2.7}$$

$$u_y^{(2)inc}(x, z) = \left(A_3^{inc} \, e^{-r_2^{inc} z} \right) e^{\iota k x} \tag{5.2.8}$$

where k is the wave number and the superscript 'inc' denotes the incident field quantities and A_1^{inc}, A_2^{inc} and A_3^{inc} are the constants to be determined later, the parameter r_1^{inc} and r_2^{inc} are given by $r_1^{inc} = \sqrt{k^2 - k_1^2}$ and $r_2^{inc} = \sqrt{k^2 - k_2^2}$.

With the help of Equations (5.2.1), (5.2.7) and (5.2.8), the stress components $\hat{\tau}_{yz}^{(i)inc}$ $(i = 1, 2)$ become

$$\hat{\tau}_{yz}^{(1)inc}(x,z,t) = \tau_{yz}^{(1)inc}(x,z)e^{-\iota\omega t} = \sqrt{C_{44}^{(1)}C_{66}^{(1)}}\; r_1^{inc}\left(A_1^{inc}\; e^{\frac{r_1^{inc}z}{\sqrt{Q}}} - A_2^{inc}\; e^{-\frac{r_1^{inc}z}{\sqrt{Q}}}\right) e^{\iota kx}e^{-\iota\omega t} \tag{5.2.9}$$

and

$$\hat{\tau}_{yz}^{(2)inc}(x,z,t) = \tau_{yz}^{(2)inc}(x,z)e^{-\iota\omega t} = -\mu^{(2)}r_2^{inc}A_3^{inc}e^{-r_2^{inc}z}e^{\iota kx}e^{-\iota\omega x} \tag{5.2.10}$$

Boundary conditions can be written as (In absence of the crack)

$$u_y^{(1)inc}(x,0) = u_y^{(2)inc}(x,0), \quad -\infty < x < \infty \tag{5.2.11}$$

$$\tau_{yz}^{(1)inc}(x,0) = \tau_{yz}^{(2)inc}(x,0), \quad -\infty < x < \infty \tag{5.2.12}$$

$$\tau_{yz}^{(1)inc}(x,-h) = 0, \quad -\infty < x < \infty \tag{5.2.13}$$

Using the boundary conditions above, we get

$$A_1^{inc} + A_2^{inc} = A_3^{inc} \tag{5.2.14}$$

$$\sqrt{C_{44}^{(1)}C_{66}^{(1)}}\; r_1^{inc}\left(A_1^{inc} - A_2^{inc}\right) = -\mu^{(2)}r_2^{inc}A_3^{inc} \tag{5.2.15}$$

$$A_1^{inc}\; e^{\frac{-r_1^{inc}h}{\sqrt{Q}}} = A_2^{inc}\; e^{\frac{r_1^{inc}h}{\sqrt{Q}}} \tag{5.2.16}$$

From these three Equations (5.2.14), (5.2.15) and (5.2.16), eliminating arbitrary constants, we get the dispersion relation as

$$\tanh\left(\frac{r_1^{inc}h}{\sqrt{Q}}\right) = -\frac{\mu^{(2)}r_2^{inc}}{r_1^{inc}\sqrt{C_{44}^{(1)}C_{66}^{(1)}}} \tag{5.2.17}$$

Using the well known fact that Love wave velocity is greater than the shear wave velocity of layer and less than the shear wave velocity of half space i.e, $c_v < c_L < c_s$ where $c_L = \frac{\omega}{k}$, the above dispersion equation becomes

$$\tanh\left(\frac{k_1h}{\sqrt{Q}}\sqrt{1-\frac{k^2}{k_1^2}}\right) = \frac{\mu^{(2)}\sqrt{(\frac{k}{k_1})^2-\delta^2}}{\sqrt{C_{44}^{(1)}C_{66}^{(1)}}\sqrt{1-(\frac{k}{k_1})^2}} \tag{5.2.18}$$

where $\delta = \frac{k_2}{k_1}(< 1)$.

The shear stress in the crack position by the incident field is expressed as

$$\hat{\tau}(x,t) = \tau(x)e^{-\iota\omega t} = \hat{\tau}_{yz}^{(2)inc}(x,0,t) = \tau_0 e^{\iota(kx-\omega t)},\ -c < x < c \tag{5.2.19}$$

where $\tau_0 = -\mu^{(2)} r_2^{inc} A_3^{inc}$. Since the time factor $e^{-\iota\omega t}$ is common to every field variable in a steady-state environment, it will not be included in the computations that follow.

Scattering Fields: The solution of Equation (5.2.5) and (5.2.6) can be assumed as Gu et al. (2002a)

$$u_y^{(1)sca}(x,z) = \int_{-\infty}^{\infty} \left(A_1(\xi)\ e^{\frac{r_1^{sca} z}{\sqrt{Q}}} + A_2(\xi)\ e^{-\frac{r_1^{sca} z}{\sqrt{Q}}} \right) e^{-\iota\xi x} d\xi \tag{5.2.20}$$

and

$$u_y^{(2)sca}(x,z) = \int_{-\infty}^{\infty} A_3(\xi)\ e^{-r_2^{sca} z}\ e^{-\iota\xi x} d\xi \tag{5.2.21}$$

where superscript '*sca*' stands for quantities of the scattering field, $A_1(\xi)$, $A_2(\xi)$ and $A_3(\xi)$ are unknown to be determined. The parameters r_1^{sca} and r_2^{sca} are given by $r_1^{sca} = \sqrt{\xi^2 - k_1^2}$ and $r_2^{sca} = \sqrt{\xi^2 - k_2^2}$. To determine the scattering fields of the crack, the boundary conditions include:
(i) The crack surface boundary condition:

$$\tau_{yz}^{(1)sca}(x,0) = \tau_{yz}^{(2)sca}(x,0) = -\tau_0 e^{\iota kx},\ -c < x < c \tag{5.2.22}$$

(ii) The continuity conditions at the interface:

$$u_y^{(1)sca}(x,0) = u_y^{(2)sca}(x,0),\ \ |x| > c \tag{5.2.23}$$

$$\tau_{yz}^{(1)sca}(x,0) = \tau_{yz}^{(2)sca}(x,0),\ \ |x| > c \tag{5.2.24}$$

(iii) The free surface condition:

$$\tau_{yz}^{(1)sca}(x,-h) = 0,\ \ -\infty < x < \infty. \tag{5.2.25}$$

With the help of Equations (5.2.2),(5.2.3), (5.2.20) and (5.2.21), the expression of stress components $\tau_{yz}^{(i)sca}$ $(i = 1, 2)$ are written as

$$\tau_{yz}^{(1)sca}(x,z) = \sqrt{C_{44}^{(1)} C_{66}^{(1)}} \int_{-\infty}^{\infty} r_1^{sca} \left(A_1(\xi)\ e^{\frac{r_1^{sca} z}{\sqrt{Q}}} - A_2(\xi)\ e^{-\frac{r_1^{sca} z}{\sqrt{Q}}} \right) e^{-\iota\xi x} d\xi \tag{5.2.26}$$

$$\tau_{yz}^{(2)sca}(x,z) = -\mu^{(2)} \int_{-\infty}^{\infty} r_2^{sca} A_3(\xi)\ e^{-r_2^{sca} z}\ e^{-\iota\xi x} d\xi. \tag{5.2.27}$$

Using the boundary conditions (5.2.22)-(5.2.25), we obtain the following dual integral equations as follows:

$$\int_{-\infty}^{\infty} B(\xi) e^{-\iota\xi x} d\xi = 0, |x| > c \tag{5.2.28}$$

and

$$\int_{-\infty}^{\infty} \frac{\sqrt{C_{44}^{(1)} C_{66}^{(1)}}\, \mu^{(2)} r_1^{sca} r_2^{sca}}{\Delta(\xi)} B(\xi) e^{-\iota\xi x} d\xi = -\tau_0 e^{\iota k x}, -c < x < c \tag{5.2.29}$$

where

$$B(\xi) = \frac{\mu^{(2)} r_2^{sca} (1 + e^{-\frac{2r_1^{sca} h}{\sqrt{Q}}}) + \sqrt{C_{44}^{(1)} C_{66}^{(1)}}\ r_1^{sca}\ (1 - e^{-\frac{2r_1^{sca} h}{\sqrt{Q}}})}{\mu^{(2)} r_2^{sca}} A_1(\xi) \tag{5.2.30}$$

and

$$\Delta(\xi) = \mu^{(2)} r_2^{sca} \coth\left(\frac{r_1^{sca} h}{\sqrt{Q}}\right) + \sqrt{C_{44}^{(1)} C_{66}^{(1)}}\ r_1^{sca} \tag{5.2.31}$$

Consider a trial solution of the dual integral equations (5.2.28) and (5.2.29) by

$$B(\xi) = -\frac{\iota}{2\pi\xi} \int_{-c}^{c} f(t)\ e^{\iota\xi t} dt \tag{5.2.32}$$

Equations (5.2.28) and (5.2.32) give the single value condition

$$\int_{-c}^{c} f(t) dt = 0 \tag{5.2.33}$$

With the help of Equation (5.2.32), the non-homogeneous part of dual integral equation (5.2.29) becomes

$$\frac{A}{\pi} \int_{-c}^{c} \frac{f(t)}{t - x} dt + \frac{1}{\pi} \int_{-c}^{c} f(t) L(t,x) dt = -\tau_0 e^{\iota k x} \tag{5.2.34}$$

where

$$L(t,x) = \int_0^{\infty} \left(\frac{\sqrt{C_{44}^{(1)} C_{66}^{(1)}}\ \mu^{(2)} r_1^{sca} r_2^{sca}}{\xi \Delta(\xi)} - A \right) \sin[\xi(t - x)] d\xi \tag{5.2.35}$$

with

$$A = \lim_{\xi \to \infty} \frac{\sqrt{C_{44}^{(1)} C_{66}^{(1)}}\ \mu^{(2)} r_1^{sca} r_2^{sca}}{\xi \Delta(\xi)} \tag{5.2.36}$$

The singularities in the integrand of $L(t,x)$ are two branch points at k_2 and k_1 and few numbers of poles that occur in the complex $\xi-$plane at the zeros of $\Delta(\xi)$. The method

simply modifies the contour of integration below the real ξ-axis to ensure that no poles lie on the integration path. The contour made up of C_j $(j = 1, 2, 3, ..., M)$ shown in Fig. 5.9

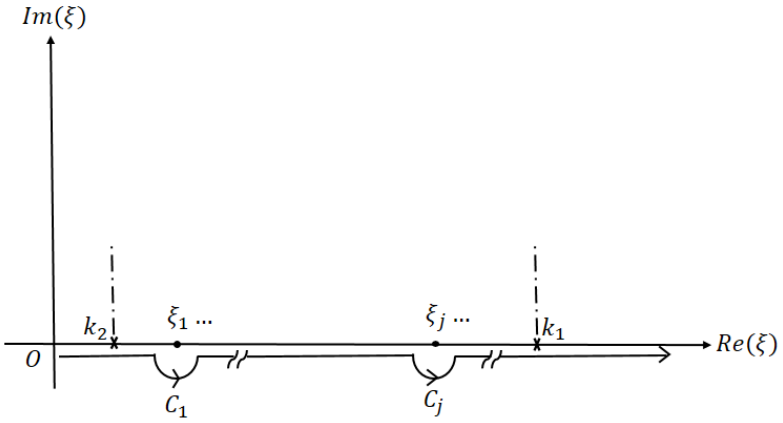

FIGURE 5.9: Geometry of the problem

$L(t, x)$ can be written as

$$L(t,x) = L_0^{\delta}(t,x) + L_{\delta}^{1}(t,x) + L_1^{\infty}(t,x) \tag{5.2.37}$$

where

$$L_0^{\delta}(t,x) = k_1 \int_0^{\delta} \left(\frac{-\sqrt{C_{44}^{(1)} C_{66}^{(1)}} \left(\mu^{(2)}\right)^2 \sqrt{1-\xi^2}(\delta^2-\xi^2) \cot\left(\frac{k_1 h}{\sqrt{Q}}\sqrt{1-\xi^2}\right)}{\xi\left[\left(\mu^{(2)}\right)^2 (\delta^2-\xi^2)\cot^2\left(\frac{k_1 h}{\sqrt{Q}}\sqrt{1-\xi^2}\right) + C_{44}^{(1)} C_{66}^{(1)}(1-\xi^2)\right]} \right.$$
$$\left. + \frac{-\iota C_{44}^{(1)} C_{66}^{(1)} \mu^{(2)} (1-\xi^2)\sqrt{\delta^2-\xi^2}}{\xi\left[\left(\mu^{(2)}\right)^2 (\delta^2-\xi^2)\cot^2\left(\frac{k_1 h}{\sqrt{Q}}\sqrt{1-\xi^2}\right) + C_{44}^{(1)} C_{66}^{(1)}(1-\xi^2)\right]} - A \right) \sin\left[k_1\xi(t-x)\right] d\xi, \tag{5.2.38}$$

$$L_{\delta}^{1}(t,x) = k_1 \int_{\delta}^{1} \left(\frac{-\sqrt{C_{44}^{(1)} C_{66}^{(1)}}\mu^{(2)}\sqrt{1-\xi^2}\sqrt{\xi^2-\delta^2}}{\xi\left[\mu^{(2)}\sqrt{(\xi^2-\delta^2)}\cot\left(\frac{k_1 h}{\sqrt{Q}}\sqrt{1-\xi^2}\right) - \sqrt{C_{44}^{(1)} C_{66}^{(1)}}\sqrt{(1-\xi^2)}\right]} - A \right) \sin\left[k_1\xi(t-x)\right] d\xi$$
$$+ F_M, \tag{5.2.39}$$

$$L_1^{\infty}(t,x) =$$

$$k_1 \int_1^{\infty} \left(\frac{\sqrt{C_{44}^{(1)} C_{66}^{(1)}}\,\mu^{(2)} \sqrt{\xi^2-1}\sqrt{\xi^2-\delta^2}}{\xi\left[\mu^{(2)}\sqrt{(\xi^2-\delta^2)}\coth\left(\frac{k_1 h}{\sqrt{Q}}\sqrt{\xi^2-1}\right) + \sqrt{C_{44}^{(1)} C_{66}^{(1)}}\sqrt{\xi^2-1}\right]} - A \right) \sin\left[k_1\xi(t-x)\right] d\xi \tag{5.2.40}$$

and

$$F_M = -\iota\pi \sum_{j=1}^{M} \frac{\sqrt{C_{44}^{(1)} C_{66}^{(1)}}\,\mu^{(2)} \sqrt{\xi_j^2-k_1^2}\sqrt{\xi_j^2-k_1^2\delta^2}}{\xi_j \Delta'(\xi_j)} \sin\left[\xi_j(t-x)\right], \tag{5.2.41}$$

with $\delta = \frac{k_2}{k_1}(<1)$ and $\Delta^{'}(\xi_j) = \frac{d}{d\xi}[\Delta(\xi)]$ evaluated at $\xi = \xi_j$.

Here, M is the number of roots of the equation $\Delta(\xi) = 0$. The term F_M represents the addition of a free wave solution that will ensure that the scattered wave solution excludes standing wave (Keer and Luong, 1974; Narita and Shindo, 1998).

Farnell and Adler (2012) demonstrated that in the "loading" scenario where the shear wave velocity of the layer is lower than that of the substrate, a single Rayleigh-type pole appears solely on the real ξ-axis. Note that kernel assume only one principal value integral for $\xi_j = k$ with $k_2 < k < k_1$ (Keer and Luong, 1974).

If we put $\lambda = \frac{t}{c}$ and $\mu = \frac{x}{c}$, then the integral equation (5.2.34) becomes

$$\frac{A}{\pi}\int_{-1}^{1} \frac{f(c\lambda)}{\lambda-\mu} d\lambda + \frac{1}{\pi}\int_{-1}^{1} f(c\lambda) c\left[L_0^{\delta}(c\lambda, c\mu) + L_{\delta}^{1}(c\lambda, c\mu) + L_1^{\infty}(c\lambda, c\mu)\right] d\lambda = -\tau_0 e^{\iota kc\mu} \tag{5.2.42}$$

Let, $f(c\lambda) = F_1(\lambda)$ and $c\left[L_0^{\delta}(c\lambda, c\mu) + L_{\delta}^{1}(c\lambda, c\mu) + L_1^{\infty}(c\lambda, c\mu)\right] = K(\lambda,\mu)$, then the equation (5.2.42) becomes

$$\frac{A}{\pi}\int_{-1}^{1} \frac{F_1(\lambda)}{\lambda-\mu} d\lambda + \frac{1}{\pi}\int_{-1}^{1} F_1(\lambda) K(\lambda,\mu) d\lambda = -\tau_0 e^{\iota kc\mu} \tag{5.2.43}$$

with the condition

$$\int_{-1}^{1} F_1(\lambda) d\lambda = 0. \tag{5.2.44}$$

Considering, the singularity at the tip of the crack, we assume

$$F_1(\lambda) = \frac{\tau_0\ F(\lambda)}{\sqrt{1-\lambda^2}}. \tag{5.2.45}$$

Applying Gauss-Chebyshev integral formulae (Erdogan and Gupta, 1972), the above equations can be transformed into a system of algebraic equations:

$$\frac{A}{n}\sum_{l=1}^{n}\frac{F(\lambda_1)}{\lambda_l-\mu_m}+\frac{1}{n}\sum_{l=1}^{n}F(\lambda_l)K(\lambda_l,\mu_m)=e^{\iota kc\mu_m} \tag{5.2.46}$$

and

$$\frac{1}{n}\sum_{l=1}^{n}F(\lambda_l)=0 \tag{5.2.47}$$

where

$$\lambda_l=\cos\left[\frac{\pi(2l-1)}{2n}\right],\quad l=1,2,3,...,n\quad\text{and}\quad \mu_m=\cos\left[\frac{\pi m}{n}\right],\quad m=1,2,3,...,n-1. \tag{5.2.48}$$

5.2.3 Quantities of physical interest

Dynamic Stress intensity factors (DSIFs): DSIF is a crucial parameter in fracture mechanics that characterizes the stress concentration at the crack tip. Higher DSIF values indicate a greater potential for crack propagation. The normalized DSIFs at the left and right crack tips are defined by

$$\frac{K_{III}^{L}}{\tau_0\sqrt{c}}=\lim_{x\to -c^-}\sqrt{2(x+c)}\,\frac{\tau_{yz}^{(2)sca}(x,0)}{\tau_0\sqrt{c}}=AF(-1) \tag{5.2.49}$$

and

$$\frac{K_{III}^{R}}{\tau_0\sqrt{c}}=\lim_{x\to c^+}\sqrt{2(x-c)}\,\frac{\tau_{yz}^{(2)sca}(x,0)}{\tau_0\sqrt{c}}=-AF(+1). \tag{5.2.50}$$

The normalized dynamic stress intensity factors depend on $F(1)$ and $F(-1)$, which may be determined from the extrapolation formula (Krenk, 1975; Achenbach and Brind, 1981).

$$F(1)=\frac{1}{n}\sum_{l=1}^{n}\frac{\sin\left[\frac{2n-1}{4n}(2l-1)\pi\right]F(\lambda_l)}{\sin\left[\frac{(2l-1)\pi}{4n}\right]} \tag{5.2.51}$$

$$F(-1)=\frac{1}{n}\sum_{l=1}^{n}\frac{\sin\left[\frac{2n-1}{4n}(2l-1)\pi\right]F(\lambda_{n+1-l})}{\sin\left[\frac{(2l-1)\pi}{4n}\right]}. \tag{5.2.52}$$

Crack Opening Displacement (COD): The crack opening displacement is calculated as follows:

$$\Delta u_y^{(sca)}(x,0)=\frac{1}{2}\int_x^c f(t)dt,\quad -c\le x\le c \tag{5.2.53}$$

and the normalized COD is given by

$$COD = \frac{\Delta u_y^{(sca)}(x,0)}{\tau_0 c} = \frac{1}{2\tau_0 c}\int_x^c f(t)dt, \quad -c \leq x \leq c. \tag{5.2.54}$$

5.2.4 Numerical results and discussions

In this study, we have considered three linear elastic materials namely Copper(Cu), Aluminium(Al) and Graphite Epoxy composite for the numerical calculation and to demonstrate the graphical results. The elastic constants of these media are given as:

Cu: $\rho^{(1)} = 8960kg/m^3$; $\mu^{(1)} = 4.78 \times 10^{10}N/m^3$

Al: $\rho^{(2)} = 2700kg/m^3$; $\mu^{(2)} = 2.65 \times 10^{10}N/m^3$

Graphite/Epoxy: $\rho^{(1)} = 1600kg/m^3$; $C_{44}^{(1)} = 0.337 \times 10^{10}N/m^3$; $C_{66}^{(1)} = 0.748 \times 10^{10}N/m^3$

Here, we have considered two cases as follows:

Case-I (Orthotropic layer over isotropic half-space): In this case we have taken the half-space as Aluminium(Al) and the layer as Graphite Epoxy composite.

Case-II (Isotropic layer over isotropic half-space): In this case we have taken the half-space as Aluminium(Al) and the layer as Copper(Cu).

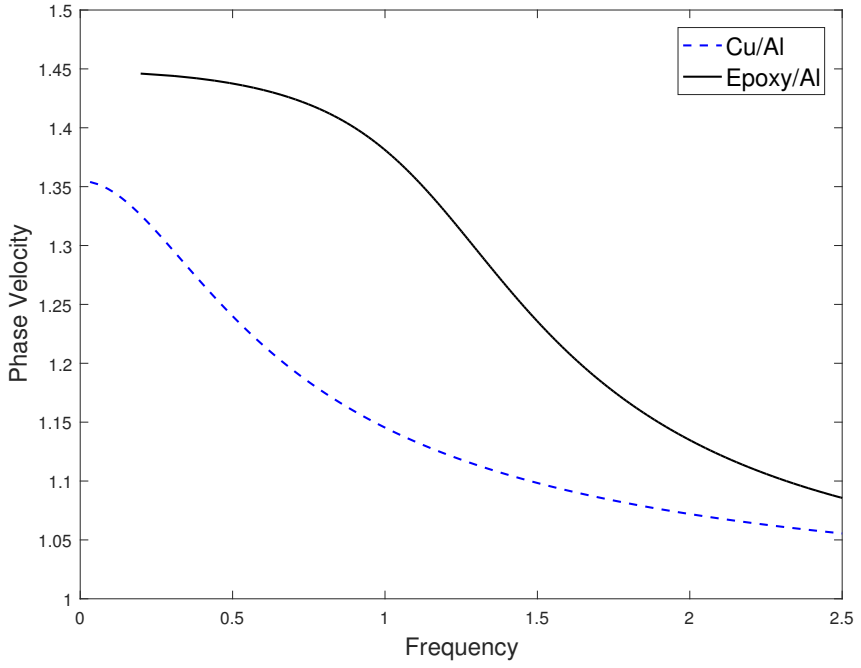

FIGURE 5.10: Phase velocity versus frequency

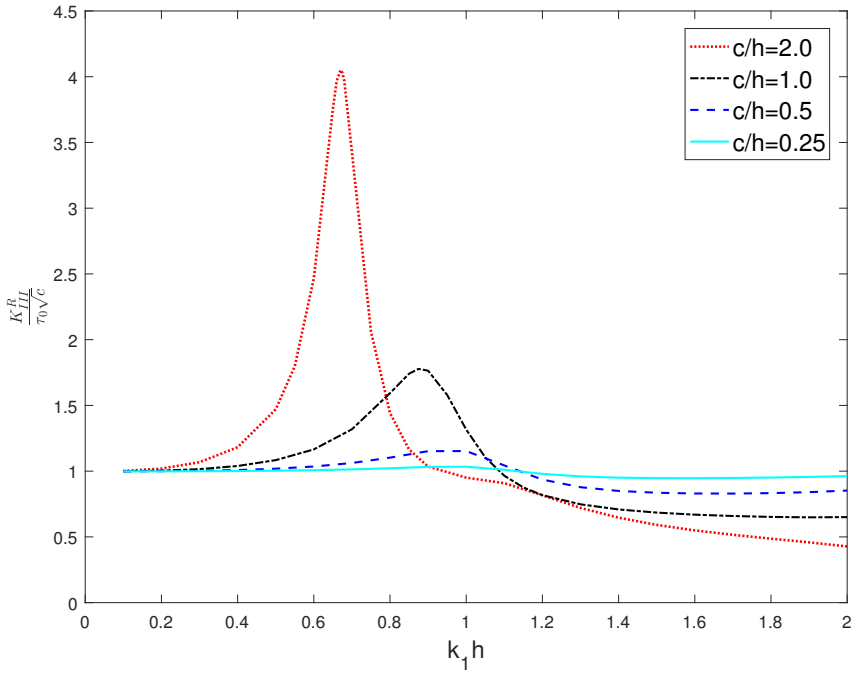

FIGURE 5.11: Stress intensity factor vs wave number at the right tip of the crack for case-I

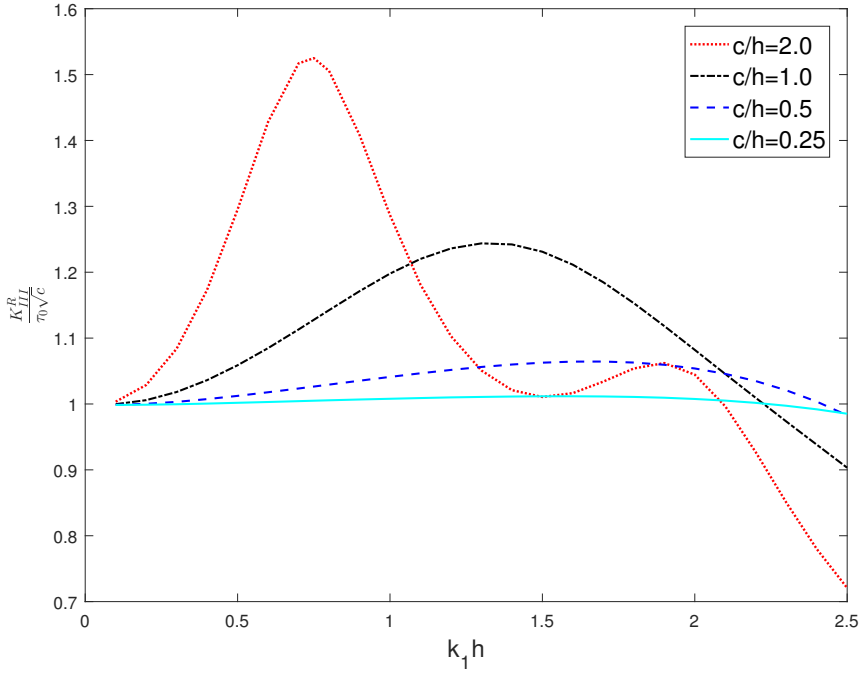

FIGURE 5.12: Stress intensity factor vs wave number at the right tip of the crack for case-II

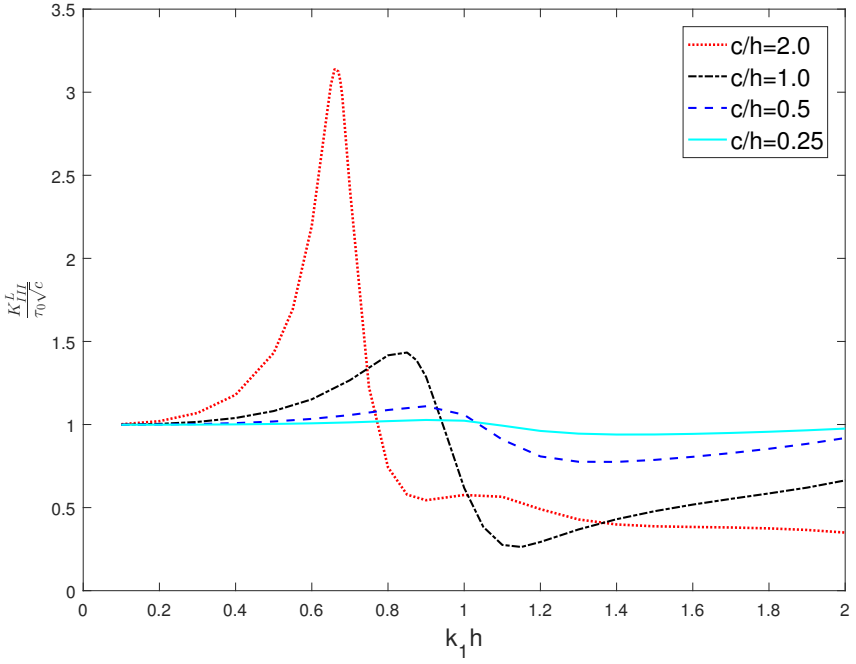

FIGURE 5.13: Stress intensity factor vs wave number at the left tip of the crack for case-I

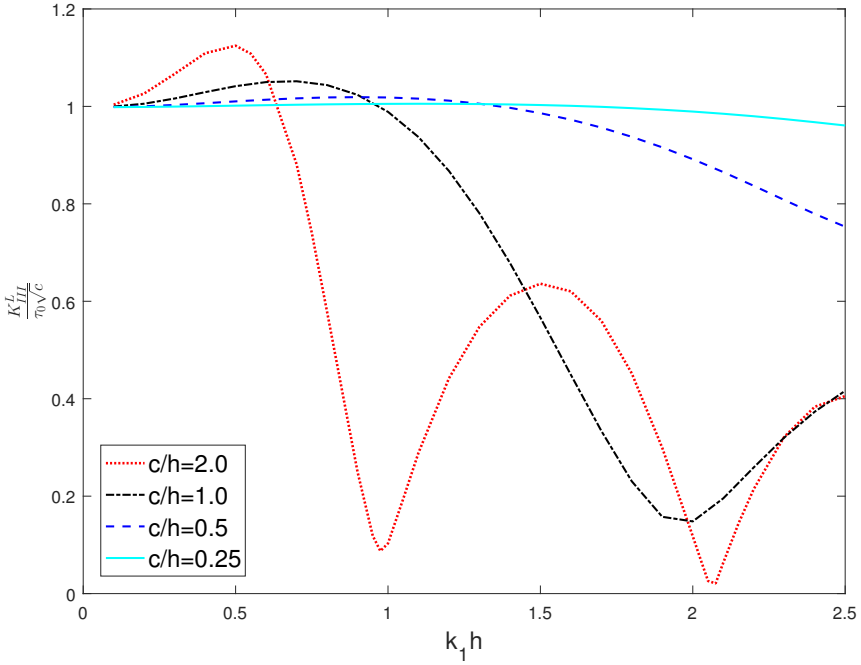

FIGURE 5.14: Stress intensity factor vs wave number at the left tip of the crack for case-II

Fig. 5.10 shows the variations in phase velocity against the frequency of the Love wave for the both cases. It can be seen from the figure that the phase velocity is decreasing in nature with respect to increase of frequency. It can also be seen that when both media are taken isotropic, the phase velocity is lower compared to case II that is, when the composite case (orthotropic over isotropic) is considered.

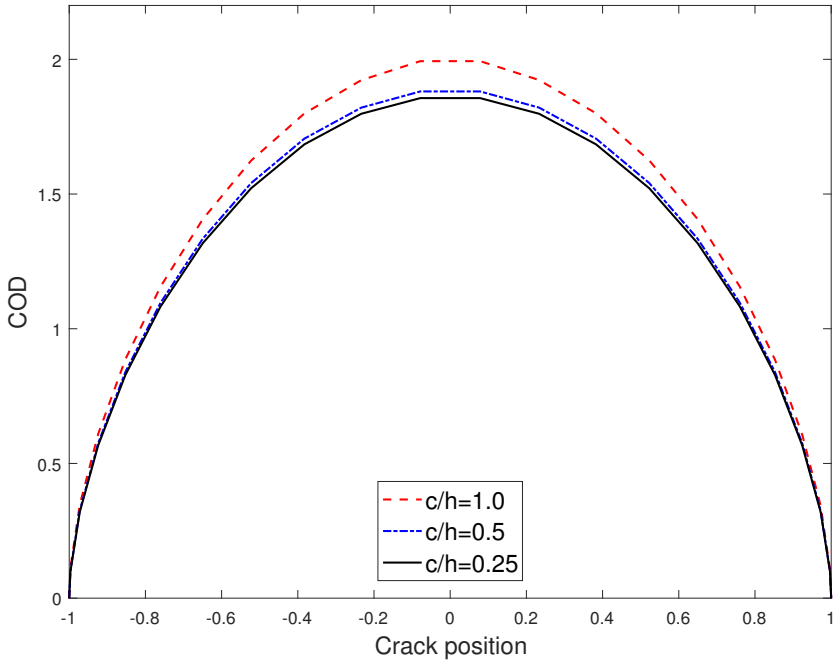

FIGURE 5.15: Crack opening displacement versus crack position for case-I

The figures 5.11 to 5.14 depict the relationship between the frequency of the incident Love wave and the normalized dynamic stress intensity factor (DSIF) at the crack tips for the different values of $c/h = 0.25, 0.50, 1.0, 2.0$. Figures 5.11 and 5.12 show the normalized DSIF vs wave number at the right tip of the crack for case-I and case-II respectively, while figures 5.13 and 5.14 represent the same for the left tip of the crack. These figures are likely to show a non-monotonic behaviour of normalized DSIF with the increase of frequency. In the two material combinations(case-I, case-II), it is observed that the values of c/h increase along with the peak values and vibration magnitude of the normalized DSIF at the left and right crack tips. Normalized DSIF attains its maximum more quickly for higher value of c/h. Comparing figures 5.11, 5.12 with 5.13, 5.14, it is found that the higher value of normalized DSIF exists at the right tip of the crack than the left crack tip. Moreover, it can be seen that the values of normalized DSIF are greater in the system consisting of an orthotropic layer and an isotropic half-space (case-I) than the system consisting of an

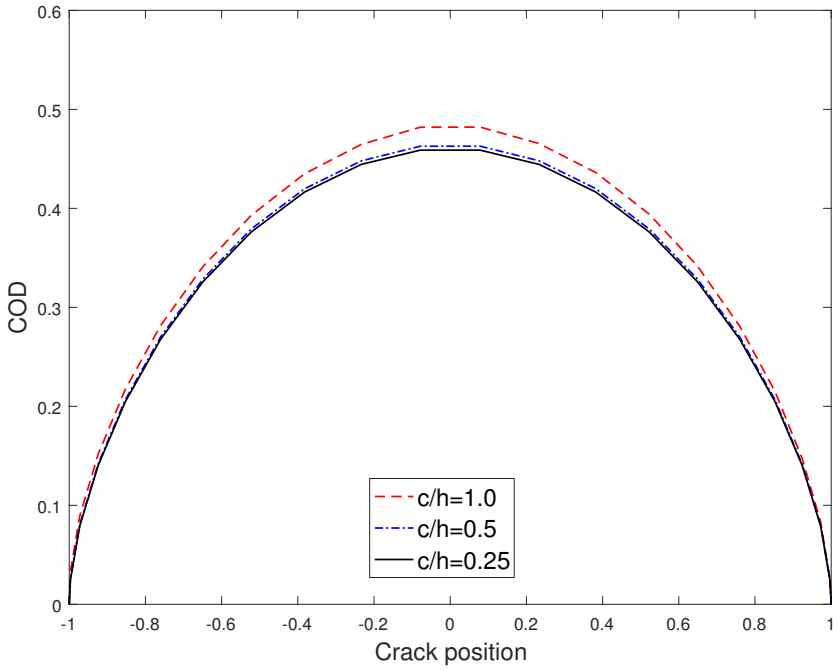

FIGURE 5.16: Crack opening displacement versus crack position for case-II

isotropic layer and an isotropic half-space (case-II) at the both left and right tips of the crack. In all cases, the normalized DSIF are higher whenever the values of the ratio c/h is higher.

Fig. 5.15 and 5.16 show the plot of normalized crack opening displacement (COD) versus crack position for fixed normalized frequency 0.5 and for different values of $c/h = 0.25, 0.50, 1.0$. It is notable that the graph is symmetric about $x = 0$, the normalized COD achieves its highest value at point $x = 0$ and reaches a zero value at the tips of the crack. The value of normalized COD is higher whenever the value of c/h is higher.

5.2.5 Conclusion

This study has comprehensively analyzed the scattering of Love waves by an interface crack in a composite system consisting of an orthotropic layer bonded to an isotropic half-space. Employing Fourier transforms and integral equations, we derived the governing conditions and explored the scattering phenomena in detail. We have also derived the expressions of stress intensity factor (DSIF) and crack opening displacement (COD) and presented them graphically. The results highlight the significant influence of crack's size, layer height, and material properties on the SIF and COD. The key findings of this research include:

1. The size of the interface crack plays crucial role in determining the scattering patterns and have significant impacts on SIF and COD. Larger cracks result in more pronounced scattering effects, altering the wave field significantly, and the values of SIF and COD are also high.

2. The scattering characteristics were found to be dependent on the orthotropic material properties of the layer, crack dimensions, and incident wave frequencies.

3. The scattering effects are frequency-dependent, with higher frequencies exhibiting more complex scattering behavior.

4. The study derived the dispersion relation and analyzed the impact of the interface crack on the phase velocity of Love waves.

The insights gained from this study enhance our understanding of Love wave propagation in composite materials, particularly in the presence of interface cracks. These findings have practical implications for non-destructive testing and structural health monitoring, offering a theoretical foundation for developing more accurate diagnostic tools and methods.

Future research can extend this work by considering more complex crack geometries, the interaction of multiple cracks, and the effects of transient wave forms under different loading conditions.

Chapter 6

Cracks in 1D hexagonal piezoelectric quasicrystals

6.1 Interaction of anti-plane shear waves with two collinear cracks in 1D hexagonal piezoelectric quasicrystals[1]

6.1.1 Introduction

Quasicrystals(QCs) possess long-range order and aperiodic structures with quasi-periodic translational symmetry, are different from traditional crystals and amorphous glassy models. QCs are first observed in melt-spun ribbons of a stiffened Al-Mn alloy by Shechtman et al. (1984). The phonons and phasons excitations are found in QCs. The phonon fields are related to conventional crystals, which can cast the volume and shape of cell. The phason field is a new type of excitation found in QCs and describes the local regroup of atoms in a structure. QCs have significant properties (Fan, 2011) such as high strength, low thermal conductivity, small friction factors, corrosion insusceptiblity and special electric characteristics, that can improve the wear resistance and service life of structural devices. Owing to the unique properties and lattice structures, QCs are used in automotive industry, energy engineering, aerospace surface modification, solar cells, nuclear fuel containers, thermoelectric converters, optical metal making factories and many more high-tech industries. 1D hexagonal quasicrystals are the most simple class of quasicrystals, contains

[1]Panja, S. K., & Mandal, S. C. (2024). Interaction of anti-plane shear waves with two collinear cracks in 1D hexagonal piezoelectric quasicrystals. ZAMM-Journal of Applied Mathematics and Mechanics/Zeitschrift für Angewandte Mathematik und Mechanik, 104(2), e202300393.

a single quasiperiodic axis. Fan et al. (1999) studied the coupling effect of phonon and phason fields in 1D hexagonal quasicrystals induced by running screw dislocation.

Piezoelectricity is a property that emerges from the breaking of inversion symmetry in crystal structures. In materials where the inversion symmetry is broken, mechanical stress leads to the generation of electric charges, resulting in the piezoelectric effect. While certain QCs may indeed exhibit piezoelectricity due to their specific symmetry breaking arrangements. Hu et al. (2000) discovered the non-zero piezoelectric coefficients of some typical QCs. Rama Mohana Rao et al. (2007) derived the maximum number of independent non-zero piezoelectric and piezomagnetic coefficients of QCs.

From the 19^{th} century, many researchers have focused on the study of elastic wave interaction with defects such as cracks, holes and dislocations firmly act the mechanical component of solids and can dilute their strength. Two coplanar Griffith cracks in an orthotropic medium is studied by Sarkar et al. (1994). Narita and Shindo (1999b), Zhou et al. (2001) and Yang and Li (2015) investigated the scattering of antiplane shear waves with cracks in piezoelectric material. A study of crack face boundary conditions viz. impermeable, semi-permeable and permeable in piezoelectric strip for two equal collinear cracks is reported by Bhargava and Verma (2016). Recently Dhabal et al. (2022) studied two collinear cracks stimulated by shear wave in magnetoelastic orthotropic medium.

In the frame of continuum mechanics, the elastic analysis of PQCs with cracks has drawn much interest of researchers in the field of solid mechanics, material science, applied and computational mathematics, physics of condensed matter, fracture mechanics and others. Research works have been done for fracture statics of PQCs by Guo et al. (2016); Yang et al. (2017); Zhou and Li (2018, 2019a); Hu et al. (2019); Zhou et al. (2021); Cheng et al. (2021). Some research works on piezoelectricity have been studied by Fang et al. (2022) and Zhu et al. (2017).

The coupling effect of phonon and phason fields make the QCs elastic equation complicated in case of dynamic formulation and very few works have been reported for dynamic fracture deformation in QCs. Wang (2006) studied the general solution for 3D dynamic problems in one dimensional hexagonal quasicrystals. Tupholme (2017) derived the closed expressions of mechanical and electric field of moving crack in 1D hexagonal PQCs due to dynamic irregular loadings. A Yoffe type running crack in 1D hexagonal PQCs under anti-plane shear load is examined by Zhou and Li (2019b). Yang et al. (2023a,b) studied the dynamic crack problem in a non-homogeneous 1D hexagonal PQCs under SH-wave. Shear wave

interaction with two collinear dynamic cracks in 1D hexagonal PQCs is not studied yet according to the authors knowledge.

In this paper, two collinear cracks in 1D hexagonal PQCs subjected to antiplane shear wave is studied. The electrically semi-permeable crack face boundary condition is assumed and the MBVP is converted to three pairs of dual integral equations by Fourier transform. Further, the system of equations is solved by applying Hilbert transform (Srivastava and Lowengrub, 1970). The explicit expressions of phonon and phason elastic fields and the electric field at crack faces are obtained and DSIFs, COD and ED are derived in closed form. Some special case studies are discussed. To depict the effect of crack length and electric boundary conditions the numerical values of DSIFs and COD have been plotted graphically.

6.1.2 Description and formulation of the problem

We consider a 1D hexagonal PQCs containing two symmetrical collinear cracks located in the region $b \leq |X| \leq c,\ Y = 0,\ |Z| < \infty$. Normalizing all the lengths with respect to c and setting $\frac{X}{c} = x,\ \frac{Y}{c} = y,\ \frac{Z}{c} = z$ and $\frac{b}{c} = d$, the new locations of the cracks become $d \leq |x| \leq 1, y = 0, |z| < \infty$(Fig. 6.1) and quasiperiodic direction is taken along the z axis.

Within the framework of the linear elasticity theory of 1D hexagonal PQCs, the constitutive equations can be written as (Wang and Pan, 2008)

$$
\begin{aligned}
\hat{\tau}_{xx} &= C_{11}\hat{\varepsilon}_{xx} + C_{12}\hat{\varepsilon}_{yy} + C_{13}\hat{\varepsilon}_{zz} + R_1\hat{w}_{zz} - e_{31}\hat{E}_z \\
\hat{\tau}_{yy} &= C_{12}\hat{\varepsilon}_{xx} + C_{11}\hat{\varepsilon}_{yy} + C_{13}\hat{\varepsilon}_{zz} + R_1\hat{w}_{zz} - e_{31}\hat{E}_z \\
\hat{\tau}_{zz} &= C_{13}\hat{\varepsilon}_{xx} + C_{13}\hat{\varepsilon}_{yy} + C_{33}\hat{\varepsilon}_{zz} + R_2\hat{w}_{zz} - e_{33}\hat{E}_z \\
\hat{\tau}_{xy} &= \hat{\tau}_{yx} = 2C_{66}\hat{\varepsilon}_{xy} \\
\hat{\tau}_{xz} &= \hat{\tau}_{zx} = 2C_{44}\hat{\varepsilon}_{zx} + R_3\hat{w}_{zx} - e_{15}\hat{E}_x \\
\hat{\tau}_{yz} &= \hat{\tau}_{zy} = 2C_{44}\hat{\varepsilon}_{zy} + R_3\hat{w}_{zy} - e_{15}\hat{E}_y \\
\hat{\mathcal{H}}_{zx} &= 2R_3\hat{\varepsilon}_{zx} + K_2\hat{w}_{zx} - d_{15}\hat{E}_x \\
\hat{\mathcal{H}}_{zy} &= 2R_3\hat{\varepsilon}_{zy} + K_2\hat{w}_{zy} - d_{15}\hat{E}_y \\
\hat{\mathcal{H}}_{zz} &= R_1\left(\hat{\varepsilon}_{xx} + \hat{\varepsilon}_{yy}\right) + R_2\hat{\varepsilon}_{zz} + K_1\hat{w}_{zz} - d_{33}\hat{E}_z \\
\hat{\mathcal{D}}_x &= 2e_{15}\hat{\varepsilon}_{zx} + d_{15}\hat{w}_{zx} + \epsilon_{11}\hat{E}_x \\
\hat{\mathcal{D}}_y &= 2e_{15}\hat{\varepsilon}_{zy} + d_{15}\hat{w}_{zy} + \epsilon_{11}\hat{E}_y \\
\hat{\mathcal{D}}_z &= e_{31}\left(\hat{\varepsilon}_{xx} + \hat{\varepsilon}_{yy}\right) + e_{33}\hat{\varepsilon}_{zz} + d_{33}\hat{w}_{zz} + \epsilon_{33}\hat{E}_z,
\end{aligned}
\tag{6.1.1}
$$

with $\hat{\varepsilon}_{ij} = \frac{1}{2}\left(\partial_j \hat{u}_i + \partial_i \hat{u}_j\right)$, $\hat{w}_{zj} = \partial_z \hat{w}_j$ and $\hat{E}_j = -\partial_j \hat{\varphi}$, $(i,\ j = x, y, z)$. Here, $\hat{\tau}_{ij}$, $\hat{\mathcal{H}}_{ij}$ $(i,\ j = x, y, z)$ are the phonon and phason stress components; $\hat{\varepsilon}_{ij}$, $\hat{w}_{ij}$ $(i,\ j = x, y, z)$ denote phonon and phason strains; $\hat{E}_j$, $\hat{\mathcal{D}}_j$ $(j = x, y, z)$ refer to electric fields and electric displacements; C_{11}, C_{12}, C_{13}, C_{33}, C_{44}, C_{66} are phonon elastic constants; K_1, K_2 represent phason elastic constants; R_i $(i = 1, 2, 3)$ denote phonon-phason coupling elastic moduli; e_{31}, e_{33}, e_{15}, d_{15}, d_{33} are piezoelectric coefficients; ϵ_{11}, ϵ_{33} are dielectric coefficients; $\hat{u}_i(x, y, t)$, $\hat{w}_j(x, y, t)$ are the displacements of phonon and phason fields and $\hat{\varphi}(x, y, t)$ signifies the electric potential.

The equations of motion for 1D hexagonal PQCs in the absence of body force and electric charge density are as follows:

$$\begin{aligned}
&\partial_x \hat{\tau}_{xx} + \partial_y \hat{\tau}_{xy} + \partial_z \hat{\tau}_{xz} = \rho \partial_{tt} \hat{u}_x \\
&\partial_x \hat{\tau}_{yx} + \partial_y \hat{\tau}_{yy} + \partial_z \hat{\tau}_{yz} = \rho \partial_{tt} \hat{u}_y \\
&\partial_x \hat{\tau}_{zx} + \partial_y \hat{\tau}_{zy} + \partial_z \hat{\tau}_{zz} = \rho \partial_{tt} \hat{u}_z \\
&\partial_x \hat{\mathcal{H}}_{zx} + \partial_y \hat{\mathcal{H}}_{zy} + \partial_z \hat{\mathcal{H}}_{zz} = \rho \partial_{tt} \hat{w}_z \\
&\partial_x \hat{\mathcal{D}}_x + \partial_y \hat{\mathcal{D}}_y + \partial_z \hat{\mathcal{D}}_z = 0,
\end{aligned} \tag{6.1.2}$$

where ρ is the density of the QCs and t denotes time.

We assume that the time harmonic incidental shear wave with amplitude τ_0 propagating at $y \to \infty$. So, the non-zero displacement and electric potential components are $\hat{u}_z(x, y, t)$, $\hat{w}_z(x, y, t)$ and $\hat{\varphi}(x, y, t)$.

The constitutive equations (6.1.1) are simplified as follows Yang et al. (2023a,b):

$$\begin{aligned}
\hat{\tau}_{zy} &= C_{44}\partial_y \hat{u}_z + R_3 \partial_y \hat{w}_z + e_{15}\partial_y \hat{\varphi} \\
\hat{\tau}_{zx} &= C_{44}\partial_x \hat{u}_z + R_3 \partial_x \hat{w}_z + e_{15}\partial_x \hat{\varphi} \\
\hat{\mathcal{H}}_{zy} &= R_3 \partial_y \hat{u}_z + K_2 \partial_y \hat{w}_z + d_{15}\partial_y \hat{\varphi} \\
\hat{\mathcal{H}}_{zx} &= R_3 \partial_x \hat{u}_z + K_2 \partial_x \hat{w}_z + d_{15}\partial_x \hat{\varphi} \\
\hat{\mathcal{D}}_y &= e_{15}\partial_y \hat{u}_z + d_{15}\partial_y \hat{w}_z - \epsilon_{11}\partial_y \hat{\varphi} \\
\hat{\mathcal{D}}_x &= e_{15}\partial_x \hat{u}_z + d_{15}\partial_x \hat{w}_z - \epsilon_{11}\partial_x \hat{\varphi},
\end{aligned} \tag{6.1.3}$$

where $\hat{u}_z(x,\ y,\ t)$ and $\hat{w}_z(x,\ y,\ t)$ denote the displacements of phonon and phason fields.

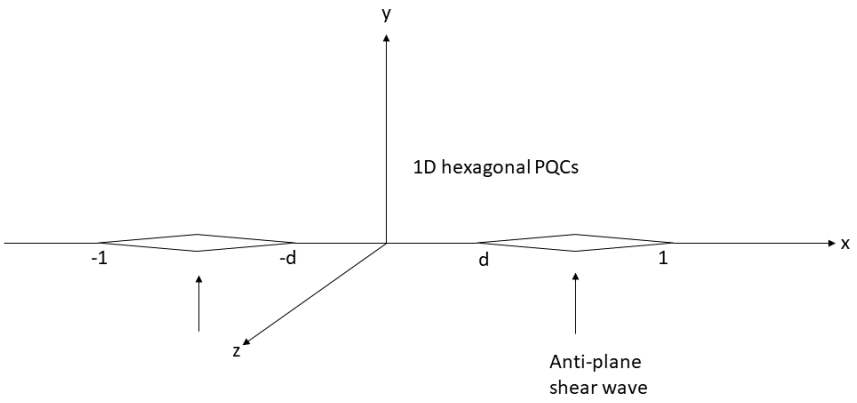

FIGURE 6.1: Geometry of the problem

The equations of motion for 1D hexagonal PQCs subjected to anti-plane shear wave are as follows:

$$\begin{aligned} &\partial_x \hat{\tau}_{zx} + \partial_y \hat{\tau}_{zy} = \rho \partial_{tt} \hat{u}_z \\ &\partial_x \hat{\mathcal{H}}_{zx} + \partial_y \hat{\mathcal{H}}_{zy} = \rho \partial_{tt} \hat{w}_z \\ &\partial_x \hat{\mathcal{D}}_x + \partial_y \hat{\mathcal{D}}_y = 0. \end{aligned} \tag{6.1.4}$$

Inserting equation (6.1.3) in (6.1.4) and using $\hat{u}_z(x,y,t) = u_z(x,y)e^{-\iota\omega t}$, $\hat{w}_z(x,y,t) = w_z(x,y)e^{-\iota\omega t}$, $\hat{\varphi}(x,y,t) = \varphi(x,y)e^{-\iota\omega t}$, $\hat{\tau}_{ij}(x,y,t) = \tau_{ij}(x,y)e^{-\iota\omega t}$, $\hat{\mathcal{H}}_{ij}(x,y,t) = \mathcal{H}_{ij}(x,y)e^{-\iota\omega t}$, $\hat{\mathcal{D}}_x(x,y,t) = \mathcal{D}_x(x,y)e^{-\iota\omega t}$ and $\hat{\mathcal{D}}_y(x,y,t) = \mathcal{D}_y(x,y)e^{-\iota\omega t}$ we obtain,

$$C_{44}\nabla^2 u_z + R_3\nabla^2 w_z + e_{15}\nabla^2\varphi + k_s^2 u_z = 0 \tag{6.1.5a}$$

$$R_3\nabla^2 u_z + K_2\nabla^2 w_z + d_{15}\nabla^2\varphi + k_s^2 w_z = 0 \tag{6.1.5b}$$

$$e_{15}\nabla^2 u_z + d_{15}\nabla^2 w_z - \epsilon_{11}\nabla^2\varphi = 0 \tag{6.1.5c}$$

where $k_s^2 = \rho\omega^2$, where ω is the angular frequency and ∇^2 is the two dimensional Laplace operator.

Substituting $\nabla^2\varphi$ from (6.1.5c) into the equations (6.1.5a) and (6.1.5b) and eliminating φ we acquire

$$\begin{aligned} \mathcal{C}\nabla^2 u_z + \mathcal{R}\nabla^2 w_z + k_s^2 u_z = 0 \\ \mathcal{R}\nabla^2 u_z + \mathcal{K}\nabla^2 w_z + k_s^2 w_z = 0 \end{aligned} \tag{6.1.6}$$

where, $\mathcal{C} = C_{44} + \frac{e_{15}^2}{\epsilon_{11}}$, $\mathcal{R} = R_3 + \frac{e_{15}d_{15}}{\epsilon_{11}}$ and $\mathcal{K} = K_2 + \frac{d_{15}^2}{\epsilon_{11}}$.

In order to decouple the equation (6.1.6), we introduce three unknown displacement functions $\varphi_1(x,y)$, $\varphi_2(x,y)$ and $\varphi_3(x,y)$ are as follows

$$\begin{aligned} u_z(x,y) &= a\varphi_1(x,y) - \mathcal{R}\varphi_2(x,y) \\ w_z(x,y) &= \mathcal{R}\varphi_1(x,y) + a\varphi_2(x,y) \\ \varphi(x,y) &= \varphi_3(x,y) + \frac{e_{15}a + d_{15}\mathcal{R}}{\epsilon_{11}}\varphi_1(x,y) + \frac{d_{15}a - e_{15}\mathcal{R}}{\epsilon_{11}}\varphi_2(x,y), \end{aligned} \tag{6.1.7}$$

where, $a = \frac{1}{2}\left[(\mathcal{C}-\mathcal{K}) + \sqrt{(\mathcal{C}-\mathcal{K})^2 + 4\mathcal{R}^2}\right]$.

With the help of equation (6.1.7); equations (6.1.6) and (6.1.5c) are converted into

$$\begin{aligned} \nabla^2\varphi_1 + \frac{k_s^2}{\mathcal{K}+a}\varphi_1 = 0 \\ \nabla^2\varphi_2 + \frac{k_s^2}{\mathcal{C}-a}\varphi_2 = 0 \\ \nabla^2\varphi_3 = 0. \end{aligned} \tag{6.1.8}$$

With the aid of equation (6.1.7), the stress and electric displacement components are found in the following forms:

$$\begin{aligned} \tau_{zy} &= (\mathcal{R}^2 + a\mathcal{C})\partial_y\varphi_1 + \mathcal{R}(a-\mathcal{C})\partial_y\varphi_2 + e_{15}\partial_y\varphi_3 \\ \tau_{zx} &= (\mathcal{R}^2 + a\mathcal{C})\partial_x\varphi_1 + \mathcal{R}(a-\mathcal{C})\partial_x\varphi_2 + e_{15}\partial_x\varphi_3 \\ \mathcal{H}_{zy} &= \mathcal{R}(a+\mathcal{K})\partial_y\varphi_1 + (a\mathcal{K} - \mathcal{R}^2)\partial_y\varphi_2 + d_{15}\partial_y\varphi_3 \\ \mathcal{H}_{zx} &= \mathcal{R}(a+\mathcal{K})\partial_x\varphi_1 + (a\mathcal{K} - \mathcal{R}^2)\partial_x\varphi_2 + d_{15}\partial_x\varphi_3 \\ \mathcal{D}_x &= -\epsilon_{11}\partial_x\varphi_3 \\ \mathcal{D}_y &= -\epsilon_{11}\partial_y\varphi_3. \end{aligned} \tag{6.1.9}$$

Tian-Hu and Zi-Yuan (1994) defined a limited permeable electric boundary condition, expressed as $D_y^+ = D_y^-$; $D_y^+ = -\varepsilon_a\frac{(\varphi^+ - \varphi^-)}{(u_y^+ - u_y^-)}$, with the y axis assumed to be normal to the crack surface and ε_a is the permittivity of air(as the crack interior is filled with air).

However, based on the work by Sun et al. (2005) it has been determined that this particular limited permeable boundary condition is not appropriate for addressing our mode-III crack problem, as there is no opening displacement $(u_y^+ - u_y^-)$ associated with this specific crack mode. In the case of a mode-III crack, following the approach proposed by Kwon (2004) and Kwon and Lee (2003), we define the electric displacement as

$$\mathcal{D}_y(x,0) = \mathcal{D}_y^c - \mathcal{D}_0, \quad d \le |x| \le 1,$$

where $\mathcal{D}_y^c$ is the normal component of the electric displacement on the crack surfaces and $\mathcal{D}_0$ is electric loading without any crack.

The mechanical and electric boundary conditions are considered as follows:

$$\begin{aligned}
&u_z(x,0) = 0,\ w_z(x,0) = 0,\ \varphi(x,0) = 0, \quad |x| < d,\ |x| > 1 \\
&\tau_{zy}(x,0) = -\tau_0, \quad d \le |x| \le 1 \\
&\mathcal{H}_{yz}(x,0) = 0, \quad d \le |x| \le 1 \\
&\mathcal{D}_y(x,0) = -\mathcal{D}_0(1 - \mathcal{D}_r), \quad d \le |x| \le 1.
\end{aligned} \tag{6.1.10}$$

$\mathcal{D}_r = \frac{\mathcal{D}_y^c}{\mathcal{D}_0}$ is the electric crack condition parameter(ECCP), introduced by Kwon (2003). As per Yang and Li (2015) when $\mathcal{D}_r = 0$, the crack is characterized as impermeable.

6.1.3 Induction of dual integral equations

Using Fourier transform, the general solution of equation (6.1.8) is given by (Yang et al., 2023a,b)

$$\begin{aligned}
\varphi_1(x,y) &= \frac{2}{\pi}\int_0^\infty \mathcal{A}_1(s)e^{-\gamma_1 y}\cos(sx)ds \\
\varphi_2(x,y) &= \frac{2}{\pi}\int_0^\infty \mathcal{A}_2(s)e^{-\gamma_2 y}\cos(sx)ds \\
\varphi_3(x,y) &= \frac{2}{\pi}\int_0^\infty \mathcal{A}_3(s)e^{-sy}\cos(sx)ds
\end{aligned} \tag{6.1.11}$$

where, $\gamma_1 = \sqrt{s^2 - \frac{k_s^2}{\mathcal{K}+a}}$, $\gamma_2 = \sqrt{s^2 - \frac{k_s^2}{\mathcal{C}-a}}$ and $\mathcal{A}_1(s)$, $\mathcal{A}_2(s)$ and $\mathcal{A}_3(s)$ are unknown functions subjected to be determined by the boundary conditions.

The displacements and the electric potential are written from the equations (6.1.7) and (6.1.11) in the form

$$\begin{aligned}
u_z(x,y) =& \frac{2a}{\pi}\int_0^\infty \mathcal{A}_1(s)e^{-\gamma_1 y}\cos(sx)ds - \frac{2\mathcal{R}}{\pi}\int_0^\infty \mathcal{A}_2(s)e^{-\gamma_2 y}\cos(sx)ds \\
w_z(x,y) =& \frac{2\mathcal{R}}{\pi}\int_0^\infty \mathcal{A}_1(s)e^{-\gamma_1 y}\cos(sx)ds + \frac{2a}{\pi}\int_0^\infty \mathcal{A}_2(s)e^{-\gamma_2 y}\cos(sx)ds \\
\varphi(x,y) =& \frac{2}{\pi}\frac{e_{15}a + d_{15}\mathcal{R}}{\epsilon_{11}}\int_0^\infty \mathcal{A}_1(s)e^{-\gamma_1 y}\cos(sx)ds + \frac{2}{\pi}\frac{d_{15}a - e_{15}\mathcal{R}}{\epsilon_{11}}\int_0^\infty \mathcal{A}_2(s)e^{-\gamma_2 y}\cos(sx)ds \\
&+ \frac{2}{\pi}\int_0^\infty \mathcal{A}_3(s)e^{-sy}\cos(sx)ds.
\end{aligned} \tag{6.1.12}$$

With the help of equations (6.1.9) and (6.1.11), the expressions of stress and electric displacement are found as

$$\begin{aligned}
\tau_{zy}(x,y) =& -\frac{2(a\mathcal{C}+\mathcal{R}^2)}{\pi}\int_0^\infty \gamma_1\mathcal{A}_1(s)e^{-\gamma_1 y}\cos(sx)ds - \frac{2(a-\mathcal{C})\mathcal{R}}{\pi}\int_0^\infty \gamma_2\mathcal{A}_2(s)e^{-\gamma_2 y}\cos(sx)ds \\
&- \frac{2e_{15}}{\pi}\int_0^\infty s\mathcal{A}_3(s)e^{-sy}\cos(sx)ds \\
\mathcal{H}_{zy}(x,y) =& -\frac{2(a+\mathcal{K})\mathcal{R}}{\pi}\int_0^\infty \gamma_1\mathcal{A}_1(s)e^{-\gamma_1 y}\cos(sx)ds - \frac{2(a\mathcal{K}-\mathcal{R}^2)}{\pi}\int_0^\infty \gamma_2\mathcal{A}_2(s)e^{-\gamma_2 y}\cos(sx)ds \\
&- \frac{2d_{15}}{\pi}\int_0^\infty s\mathcal{A}_3(s)e^{-sy}\cos(sx)ds \\
\mathcal{D}_y(x,y) =& \frac{2\epsilon_{11}}{\pi}\int_0^\infty s\mathcal{A}_3(s)e^{-sy}\cos(sx)ds.
\end{aligned} \tag{6.1.13}$$

Using equations (6.1.12) and (6.1.13) in the boundary conditions (6.1.10), the three pairs of dual integral equations are obtained

$$\int_0^\infty \mathcal{A}_1(s)\cos(sx)ds = 0, \quad |x| < d, \ |x| > 1 \tag{6.1.14a}$$

$$\int_0^\infty \gamma_1\mathcal{A}_1(s)\cos(sx)ds = \mathcal{Q}, \ d \le |x| \le 1, \tag{6.1.14b}$$

$$\int_0^\infty \mathcal{A}_2(s)\cos(sx)ds = 0, \quad |x| < d, \ |x| > 1 \tag{6.1.15a}$$

$$\int_0^\infty \gamma_2\mathcal{A}_2(s)\cos(sx)ds = \mathcal{T}, \ d \le |x| \le 1, \tag{6.1.15b}$$

$$\int_0^\infty \mathcal{A}_3(s)\cos(sx)ds = 0, \quad |x| < d, \ |x| > 1 \tag{6.1.16a}$$

$$\int_0^\infty s\mathcal{A}_3(s)\cos(sx)ds = \frac{\pi}{2}\mathcal{P}, \ d \le |x| \le 1, \tag{6.1.16b}$$

where, $\mathcal{Q} = -\frac{\pi}{2}\frac{\tau_0(1-\chi_1)}{(\mathcal{N}-\mathcal{M})\mathcal{R}(a+\mathcal{K})}$, $\mathcal{T} = -\frac{\pi}{2}\frac{\tau_0(1-\chi_2)}{(\mathcal{M}-\mathcal{N})(a\mathcal{K}-\mathcal{R}^2)}$, $\mathcal{P} = -\frac{\mathcal{D}_0(1-\mathcal{D}_r)}{\epsilon_{11}}$, $\mathcal{M} = \frac{a\mathcal{C}+\mathcal{R}^2}{\mathcal{R}(a+\mathcal{K})}$, $\mathcal{N} = \frac{(a-\mathcal{C})\mathcal{R}}{(a\mathcal{K}-\mathcal{R}^2)}$, $\chi_1 = \frac{\mathcal{D}_0(1-\mathcal{D}_r)}{\tau_0}\left(\mathcal{N}\frac{d_{15}}{\epsilon_{11}} - \frac{e_{15}}{\epsilon_{11}}\right)$ and $\chi_2 = \frac{\mathcal{D}_0(1-\mathcal{D}_r)}{\tau_0}\left(\mathcal{M}\frac{d_{15}}{\epsilon_{11}} - \frac{e_{15}}{\epsilon_{11}}\right)$.

6.1.4 Solution

Following Srivastava and Lowengrub (1970) and Sarkar et al. (1994), let us assume the solution of dual integral equations (6.1.16) is of the form

$$\mathcal{A}_3(s) = \frac{1}{s}\int_d^1 h(t^2)\sin(st)dt \tag{6.1.17}$$

with

$$\int_d^1 h(t^2)dt = 0, \tag{6.1.18}$$

where $h(t^2)$ is an unknown function.

Using the finite Hilbert transform technique used by Srivastava and Lowengrub (1970), $h(t^2)$ is derived as

$$h(t^2) = \mathcal{P}\sqrt{\frac{t^2-d^2}{1-t^2}} + \frac{C_1}{\sqrt{(t^2-d^2)(1-t^2)}}. \tag{6.1.19}$$

Here, C_1 is calculated from equation (6.1.18) and we get,

$$C_1 = \mathcal{P}\left(d^2 - \frac{E}{F}\right), \tag{6.1.20}$$

where $E = E\left[\frac{\pi}{2}, \sqrt{1-d^2}\right]$ and $F = F\left[\frac{\pi}{2}, \sqrt{1-d^2}\right]$ are the elliptic integrals of 2^{nd} and 1^{st} kind respectively.

So, $h(t^2)$ is written from the equations (6.1.19) and (6.1.20) as

$$h(t^2) = -\frac{\mathcal{D}_0(1-\mathcal{D}_r)}{\epsilon_{11}}\frac{t^2 - \frac{E}{F}}{\sqrt{(1-t^2)(t^2-d^2)}}. \tag{6.1.21}$$

Electric displacement is calculated and is given by

$$\mathcal{D}_y(x,0) = -\mathcal{D}_0(1-\mathcal{D}_r)\left[1 - \frac{x^2 - \frac{E}{F}}{\sqrt{(x^2-1)(x^2-d^2)}}\right], \quad x < -1, \ -d < x < d, \ x > 1. \tag{6.1.22}$$

In order to solve the dual integral equations (6.1.14), we assume

$$\mathcal{A}_1(s) = \frac{1}{s}\int_d^1 f(t^2)\sin(st)dt \tag{6.1.23}$$

where $f(t^2)$ is an unknown function to be computed by the boundary conditions.

Putting the value of $\mathcal{A}_1(s)$ from equation (6.1.23) into equation (6.1.14a) and using the result from Gradshteyn and Ryzhik (2014)

$$\int_0^\infty \frac{\sin(st)\cos(sx)}{s}ds = \begin{cases} \frac{\pi}{2}, & t > x \\ 0, & x > t \end{cases}$$

it is noted that the selection $\mathcal{A}_1(s)$ guides to the equation

$$\int_d^1 f(t^2)dt = 0. \tag{6.1.24}$$

Further using the relations

$$\int_0^\infty \frac{\sin(st)\sin(sx)}{s}ds = \frac{1}{2}\log\left|\frac{t+x}{t-x}\right|$$

and

$$\frac{\sin(sx)\sin(st)}{s^2} = \int_0^x\int_0^t \frac{wvJ_0(sw)J_0(sv)dvdw}{\sqrt{x^2-w^2}\sqrt{t^2-v^2}}$$

and from equations (6.1.14b) and (6.1.23), we get

$$\int_d^1 \frac{tf(t^2)dt}{t^2-x^2} = \mathcal{Q} - \frac{d}{dx}\int_d^1 f(t^2)dt\int_0^x\int_0^t \frac{vwL(v,w)dwdv}{\sqrt{x^2-w^2}\sqrt{t^2-v^2}}, \ d \le |x| \le 1 \tag{6.1.25}$$

where

$$L(v,w) = \int_0^\infty s\left(\frac{\gamma_1}{s} - 1\right)J_0(sw)J_0(sv)ds. \tag{6.1.26}$$

Employing contour integration (Mal, 1970b) the above integral is converted to the following finite integrals

$$L(v,w) = -\iota k_s^2 \int_0^{\frac{1}{\sqrt{\mathcal{K}+a}}} \sqrt{\frac{1}{\mathcal{K}+a} - \eta^2} J_0(k_s\eta v) H_0^{(1)}(k_s\eta w) d\eta, \quad w > v. \tag{6.1.27}$$

Using the asymptotic expansion of Bessel function $J_0()$ and Hankel function $H_0^{(1)}$ for small arguments in equation (6.1.27), we obtain

$$L(v,w) = \frac{2}{\pi} L_0 k_s^2 \log k_s + O(k_s^2) \tag{6.1.28}$$

where

$$L_0 = \int_0^{\frac{1}{\sqrt{\mathcal{K}+a}}} \sqrt{\frac{1}{\mathcal{K}+a} - \eta^2} d\eta. \tag{6.1.29}$$

Now, assume $f(t^2)$ in the following form

$$f(t^2) = f_0(t^2) + (k_s^2 \log k_s) f_1(t^2) + O(k_s^2). \tag{6.1.30}$$

Using the above expression of $f(t^2)$ and the value of $L(v,w)$ given by the equation (6.1.28) into equation (6.1.25) and equating the coefficients of similar power of k_s we get

$$\int_d^1 \frac{t f_0(t^2)}{t^2 - x^2} dt = \mathcal{Q}, \quad d \le |x| \le 1 \tag{6.1.31}$$

and

$$\int_d^1 \frac{t f_1(t^2)}{t^2 - x^2} dt = -\frac{2}{\pi} L_0 \int_d^1 t f_0(t^2) dt, \quad d \le |x| \le 1. \tag{6.1.32}$$

Employing Hilbert transform, from (6.1.31) and (6.1.32) we obtain

$$f_0(t^2) = \frac{2}{\pi} \mathcal{Q} \sqrt{\frac{t^2 - d^2}{1 - t^2}} + \frac{D_1}{\sqrt{(1-t^2)(t^2-d^2)}} \tag{6.1.33}$$

and

$$f_1(t^2) = -\frac{2}{\pi} L_0 \left[\frac{\mathcal{Q}(1-d^2)}{\pi} + D_1 \right] \sqrt{\frac{t^2 - d^2}{1 - t^2}} + \frac{D_2}{\sqrt{(1-t^2)(t^2-d^2)}}, \tag{6.1.34}$$

where D_1 and D_2 are constants to be determined with the aid of the following condition

$$\int_d^1 f_0(t^2) dt = 0$$

and

$$\int_d^1 f_1(t^2)dt = 0.$$

Putting the values of $f_0(t^2)$ and $f_1(t^2)$ in the above two conditions, yields

$$D_1 = \frac{2}{\pi}\mathcal{Q}\left(d^2 - \frac{E}{F}\right) \tag{6.1.35}$$

and

$$D_2 = \frac{2}{\pi^2}L_0\mathcal{Q}\left[1 + d^2 - \frac{2E}{F}\right]\left[\frac{E}{F} - d^2\right]. \tag{6.1.36}$$

We get the expression of $f(t^2)$ from the equations (6.1.30), (6.1.33), (6.1.34), (6.1.35) and (6.1.36) as follows

$$f(t^2) = \frac{\tau_0(1-\chi_1)}{(\mathcal{N}-\mathcal{M})\mathcal{R}(a+\mathcal{K})}\frac{\left(t^2 - \frac{E}{F}\right)}{\sqrt{(1-t^2)(t^2-d^2)}}\left[-1 + (k_s^2\log k_s)\frac{L_0}{\pi}\left(1 + d^2 - \frac{2E}{F}\right)\right] + O(k_s^2). \tag{6.1.37}$$

Again, we assume the solution of dual integral equations (6.1.15) as

$$\mathcal{A}_2(s) = \frac{1}{s}\int_d^1 g(t^2)\sin(st)dt. \tag{6.1.38}$$

Using the same solution procedure for dual integral equations (6.1.14), we obtain

$$g(t^2) = \frac{\tau_0(1-\chi_2)}{(\mathcal{M}-\mathcal{N})(a\mathcal{K}-\mathcal{R}^2)}\frac{\left(t^2 - \frac{E}{F}\right)}{\sqrt{(1-t^2)(t^2-d^2)}}\left[-1 + (k_s^2\log k_s)\frac{M_0}{\pi}\left(1 + d^2 - \frac{2E}{F}\right)\right] + O(k_s^2) \tag{6.1.39}$$

where

$$M_0 = \int_0^{\frac{1}{\sqrt{\mathcal{C}-a}}}\sqrt{\frac{1}{\mathcal{C}-a} - \eta^2}d\eta. \tag{6.1.40}$$

6.1.5 Fracture mechanics quantities

Dynamic Stress intensity factors (DSIFs)

Due to the symmetry between two collinear cracks, the analysis focuses solely on the right crack to determine the DSIFs. The non-vanishing phonon and phason stress outside the

right crack can be expressed respectively as

$$\tau_{zy}(x,0)=\begin{cases}\frac{\tau_0(1-\chi_1)\mathcal{M}}{\mathcal{N}-\mathcal{M}}\left[1+\frac{x^2-\frac{E}{F}}{\sqrt{(1-x^2)(d^2-x^2)}}\right]\left[1-\frac{L_0}{\pi}\left(1+d^2-\frac{2E}{F}\right)k_s^2\log k_s\right]\\ +\frac{\tau_0(1-\chi_2)\mathcal{N}}{\mathcal{M}-\mathcal{N}}\left[1+\frac{x^2-\frac{E}{F}}{\sqrt{(1-x^2)(d^2-x^2)}}\right]\left[1-\frac{M_0}{\pi}\left(1+d^2-\frac{2E}{F}\right)k_s^2\log k_s\right]\\ +\frac{e_{15}}{\epsilon_{11}}\mathcal{D}_0(1-\mathcal{D}_r)\left[1+\frac{x^2-\frac{E}{F}}{\sqrt{(1-x^2)(d^2-x^2)}}\right]+O(k_s^2), & 0<x<d\\ \frac{\tau_0(1-\chi_1)\mathcal{M}}{\mathcal{N}-\mathcal{M}}\left[1-\frac{x^2-\frac{E}{F}}{\sqrt{(x^2-1)(x^2-d^2)}}\right]\left[1-\frac{L_0}{\pi}\left(1+d^2-\frac{2E}{F}\right)k_s^2\log k_s\right]\\ +\frac{\tau_0(1-\chi_2)\mathcal{N}}{\mathcal{M}-\mathcal{N}}\left[1-\frac{x^2-\frac{E}{F}}{\sqrt{(x^2-1)(x^2-d^2)}}\right]\left[1-\frac{M_0}{\pi}\left(1+d^2-\frac{2E}{F}\right)k_s^2\log k_s\right]\\ +\frac{e_{15}}{\epsilon_{11}}\mathcal{D}_0(1-\mathcal{D}_r)\left[1-\frac{x^2-\frac{E}{F}}{\sqrt{(x^2-1)(x^2-d^2)}}\right]+O(k_s^2), & x>1\end{cases} \tag{6.1.41}$$

and

$$\mathcal{H}_{zy}(x,0)=\begin{cases}\frac{\tau_0(1-\chi_1)}{\mathcal{N}-\mathcal{M}}\left[1+\frac{x^2-\frac{E}{F}}{\sqrt{(1-x^2)(d^2-x^2)}}\right]\left[1-\frac{L_0}{\pi}\left(1+d^2-\frac{2E}{F}\right)k_s^2\log k_s\right]\\ +\frac{\tau_0(1-\chi_2)}{\mathcal{M}-\mathcal{N}}\left[1+\frac{x^2-\frac{E}{F}}{\sqrt{(1-x^2)(d^2-x^2)}}\right]\left[1-\frac{M_0}{\pi}\left(1+d^2-\frac{2E}{F}\right)k_s^2\log k_s\right]\\ +\frac{d_{15}}{\epsilon_{11}}\mathcal{D}_0(1-\mathcal{D}_r)\left[1+\frac{x^2-\frac{E}{F}}{\sqrt{(1-x^2)(d^2-x^2)}}\right]+O(k_s^2), & 0<x<d\\ \frac{\tau_0(1-\chi_1)}{\mathcal{N}-\mathcal{M}}\left[1-\frac{x^2-\frac{E}{F}}{\sqrt{(x^2-1)(x^2-d^2)}}\right]\left[1-\frac{L_0}{\pi}\left(1+d^2-\frac{2E}{F}\right)k_s^2\log k_s\right]\\ +\frac{\tau_0(1-\chi_2)}{\mathcal{M}-\mathcal{N}}\left[1-\frac{x^2-\frac{E}{F}}{\sqrt{(x^2-1)(x^2-d^2)}}\right]\left[1-\frac{M_0}{\pi}\left(1+d^2-\frac{2E}{F}\right)k_s^2\log k_s\right]\\ +\frac{d_{15}}{\epsilon_{11}}\mathcal{D}_0(1-\mathcal{D}_r)\left[1-\frac{x^2-\frac{E}{F}}{\sqrt{(x^2-1)(x^2-d^2)}}\right]+O(k_s^2), & x>1\end{cases} \tag{6.1.42}$$

The phonon DSIFs for right crack are defined as

$$K_d^{\tau}=\lim_{x\to d-}\left[\sqrt{(d-x)}\tau_{zy}(x,0)\right],\ \ 0<x<d \tag{6.1.43}$$

and

$$K_1^{\tau}=\lim_{x\to 1+}\left[\sqrt{(x-1)}\tau_{zy}(x,0)\right],\ \ x>1 \tag{6.1.44}$$

The phason DSIFs for right crack are defined as

$$K_d^{\mathcal{H}}=\lim_{x\to d-}\left[\sqrt{(d-x)}\mathcal{H}_{zy}(x,0)\right],\ \ 0<x<d \tag{6.1.45}$$

$$K_1^{\mathcal{H}}=\lim_{x\to 1+}\left[\sqrt{(x-1)}\mathcal{H}_{zy}(x,0)\right],\ \ x>1. \tag{6.1.46}$$

The normalized phonon DSIFs for right crack are computed from equations (6.1.41), (6.1.43) and (6.1.44) as

$$\begin{aligned}\frac{K_d^{\tau}}{\tau_0} =& \frac{(1-\chi_1)\mathcal{M}}{\mathcal{N}-\mathcal{M}}\frac{d^2-\frac{E}{F}}{\sqrt{2d(1-d^2)}}\left[1-\frac{L_0}{\pi}\left(1+d^2-\frac{2E}{F}\right)k_s^2\log k_s\right]\\ &+\frac{(1-\chi_2)\mathcal{N}}{\mathcal{M}-\mathcal{N}}\frac{d^2-\frac{E}{F}}{\sqrt{2d(1-d^2)}}\left[1-\frac{M_0}{\pi}\left(1+d^2-\frac{2E}{F}\right)k_s^2\log k_s\right]\\ &+\frac{e_{15}}{\epsilon_{11}}\frac{\mathcal{D}_0(1-\mathcal{D}_r)}{\tau_0}\frac{d^2-\frac{E}{F}}{\sqrt{2d(1-d^2)}}+O(k_s^2)\end{aligned} \tag{6.1.47}$$

and

$$\begin{aligned}\frac{K_1^{\tau}}{\tau_0} =& -\frac{(1-\chi_1)\mathcal{M}}{\mathcal{N}-\mathcal{M}}\frac{1-\frac{E}{F}}{\sqrt{2(1-d^2)}}\left[1-\frac{L_0}{\pi}\left(1+d^2-\frac{2E}{F}\right)k_s^2\log k_s\right]\\ &-\frac{(1-\chi_2)\mathcal{N}}{\mathcal{M}-\mathcal{N}}\frac{1-\frac{E}{F}}{\sqrt{2(1-d^2)}}\left[1-\frac{M_0}{\pi}\left(1+d^2-\frac{2E}{F}\right)k_s^2\log k_s\right]\\ &-\frac{e_{15}}{\epsilon_{11}}\frac{\mathcal{D}_0(1-\mathcal{D}_r)}{\tau_0}\frac{1-\frac{E}{F}}{\sqrt{2(1-d^2)}}+O(k_s^2).\end{aligned} \tag{6.1.48}$$

Also the normalized phason DSIFs for right crack are computed from equations (6.1.42), (6.1.45) and (6.1.46) as

$$\begin{aligned}\frac{K_d^{\mathcal{H}}}{\tau_0} =& \frac{(1-\chi_1)}{\mathcal{N}-\mathcal{M}}\frac{d^2-\frac{E}{F}}{\sqrt{2d(1-d^2)}}\left[1-\frac{L_0}{\pi}\left(1+d^2-\frac{2E}{F}\right)k_s^2\log k_s\right]\\ &+\frac{(1-\chi_2)}{\mathcal{M}-\mathcal{N}}\frac{d^2-\frac{E}{F}}{\sqrt{2d(1-d^2)}}\left[1-\frac{M_0}{\pi}\left(1+d^2-\frac{2E}{F}\right)k_s^2\log k_s\right]\\ &+\frac{d_{15}}{\epsilon_{11}}\frac{\mathcal{D}_0(1-\mathcal{D}_r)}{\tau_0}\frac{d^2-\frac{E}{F}}{\sqrt{2d(1-d^2)}}+O(k_s^2)\end{aligned} \tag{6.1.49}$$

and

$$\begin{aligned}\frac{K_1^{\mathcal{H}}}{\tau_0} =& -\frac{(1-\chi_1)}{\mathcal{N}-\mathcal{M}}\frac{1-\frac{E}{F}}{\sqrt{2(1-d^2)}}\left[1-\frac{L_0}{\pi}\left(1+d^2-\frac{2E}{F}\right)k_s^2\log k_s\right]\\ &-\frac{(1-\chi_2)}{\mathcal{M}-\mathcal{N}}\frac{1-\frac{E}{F}}{\sqrt{2(1-d^2)}}\left[1-\frac{M_0}{\pi}\left(1+d^2-\frac{2E}{F}\right)k_s^2\log k_s\right]\\ &-\frac{d_{15}}{\epsilon_{11}}\frac{\mathcal{D}_0(1-\mathcal{D}_r)}{\tau_0}\frac{1-\frac{E}{F}}{\sqrt{2(1-d^2)}}+O(k_s^2).\end{aligned} \tag{6.1.50}$$

Crack opening displacement (COD)

The COD can be written as

$$\begin{aligned}\Delta u_z(x,0) &= u_z(x,0+) - u_z(x,0-)\\ &= \frac{2a}{\pi}\int_x^1 f(t^2)dt - \frac{2\mathcal{R}}{\pi}\int_x^1 g(t^2)dt, \quad d \le x \le 1.\end{aligned} \tag{6.1.51}$$

Further, substituting equations (6.1.37) and (6.1.39) into equation (6.1.51), the COD is derived as

$$\begin{aligned}&\Delta u_z(x,0) =\\ &\frac{2a}{\pi}\frac{(1-\chi_1)}{(\mathcal{N}-\mathcal{M})\mathcal{R}(a+\mathcal{K})}\left[1-\frac{L_0}{\pi}\left(1+d^2-\frac{2E}{F}\right)k_s^2\log k_s\right]\left[\frac{E}{F}F(\lambda_1,\lambda_2)-E(\lambda_1,\lambda_2)\right]\\ &-\frac{2\mathcal{R}}{\pi}\frac{(1-\chi_2)}{(\mathcal{M}-\mathcal{N})(a\mathcal{K}-\mathcal{R}^2)}\left[1-\frac{M_0}{\pi}\left(1+d^2-\frac{2E}{F}\right)k_s^2\log k_s\right]\left[\frac{E}{F}F(\lambda_1,\lambda_2)-E(\lambda_1,\lambda_2)\right]\\ &+O(k_s^2), \quad d \le x \le 1\end{aligned} \tag{6.1.52}$$

where, $\lambda_1 = \arcsin\sqrt{\frac{1-x^2}{1-d^2}}$, $\lambda_2 = \sqrt{1-d^2}$.

6.1.6 Special cases

1. If we neglect the piezoelectric effect i.e. the relevant material properties vanish, viz. $e_{15} = 0$, $d_{15} = 0$, $\epsilon_{11} = 0$ and $\mathcal{D}_0 = 0$, the PQCs become a usual QCs. In this case, $\mathcal{C} = C_{44}$, $\mathcal{R} = R_3$, $\mathcal{K} = K_2$, $\chi_1 = 0$, $\chi_2 = 0$ and the normalized DSIFs of the phonon and phason fields are obtained

$$\begin{aligned}\frac{K_d^\tau}{\tau_0} =& \frac{\mathcal{M}}{\mathcal{N}-\mathcal{M}}\frac{d^2-\frac{E}{F}}{\sqrt{2d(1-d^2)}}\left[1-\frac{L_0}{\pi}\left(1+d^2-\frac{2E}{F}\right)k_s^2\log k_s\right]\\ &+\frac{\mathcal{N}}{\mathcal{M}-\mathcal{N}}\frac{d^2-\frac{E}{F}}{\sqrt{2d(1-d^2)}}\left[1-\frac{M_0}{\pi}\left(1+d^2-\frac{2E}{F}\right)k_s^2\log k_s\right]+O(k_s^2),\end{aligned} \tag{6.1.53}$$

$$\begin{aligned}\frac{K_1^\tau}{\tau_0} =& -\frac{\mathcal{M}}{\mathcal{N}-\mathcal{M}}\frac{1-\frac{E}{F}}{\sqrt{2(1-d^2)}}\left[1-\frac{L_0}{\pi}\left(1+d^2-\frac{2E}{F}\right)k_s^2\log k_s\right]\\ &-\frac{\mathcal{N}}{\mathcal{M}-\mathcal{N}}\frac{1-\frac{E}{F}}{\sqrt{2(1-d^2)}}\left[1-\frac{M_0}{\pi}\left(1+d^2-\frac{2E}{F}\right)k_s^2\log k_s\right]+O(k_s^2),\end{aligned} \tag{6.1.54}$$

$$\begin{aligned}\frac{K_d^{\mathcal{H}}}{\tau_0} =& \frac{1}{\mathcal{N}-\mathcal{M}}\frac{d^2-\frac{E}{F}}{\sqrt{2d(1-d^2)}}\left[1-\frac{L_0}{\pi}\left(1+d^2-\frac{2E}{F}\right)k_s^2\log k_s\right]\\ &+\frac{1}{\mathcal{M}-\mathcal{N}}\frac{d^2-\frac{E}{F}}{\sqrt{2d(1-d^2)}}\left[1-\frac{M_0}{\pi}\left(1+d^2-\frac{2E}{F}\right)k_s^2\log k_s\right]+O(k_s^2)\end{aligned} \tag{6.1.55}$$

and

$$\begin{aligned}\frac{K_1^{\mathcal{H}}}{\tau_0} =& -\frac{1}{\mathcal{N}-\mathcal{M}}\frac{1-\frac{E}{F}}{\sqrt{2(1-d^2)}}\left[1-\frac{L_0}{\pi}\left(1+d^2-\frac{2E}{F}\right)k_s^2\log k_s\right]\\ &-\frac{1}{\mathcal{M}-\mathcal{N}}\frac{1-\frac{E}{F}}{\sqrt{2(1-d^2)}}\left[1-\frac{M_0}{\pi}\left(1+d^2-\frac{2E}{F}\right)k_s^2\log k_s\right]+O(k_s^2).\end{aligned} \tag{6.1.56}$$

2. In the absence of phason fields that means $R_3 = 0,\ K_2 = 0,\ d_{15} = 0$ and in this case PQCs transformed into conventional Piezoelectric materials (PEM). In this case $\mathcal{R} = 0,\ \mathcal{K} = 0$ and the normalized DSIFs of phonon field are acquired as

$$\begin{aligned}\frac{K_d^{\tau}}{\tau_0} =& -(1-\chi_1)\frac{d^2-\frac{E}{F}}{\sqrt{2d(1-d^2)}}\left[1-\frac{L_0}{\pi}\left(1+d^2-\frac{2E}{F}\right)k_s^2\log k_s\right]\\ &+\frac{e_{15}}{\epsilon_{11}}\frac{\mathcal{D}_0(1-\mathcal{D}_r)}{\tau_0}\frac{d^2-\frac{E}{F}}{\sqrt{2d(1-d^2)}}+O(k_s^2)\end{aligned} \tag{6.1.57}$$

and

$$\begin{aligned}\frac{K_1^{\tau}}{\tau_0} =& (1-\chi_1)\frac{1-\frac{E}{F}}{\sqrt{2(1-d^2)}}\left[1-\frac{L_0}{\pi}\left(1+d^2-\frac{2E}{F}\right)k_s^2\log k_s\right]\\ &-\frac{e_{15}}{\epsilon_{11}}\frac{\mathcal{D}_0(1-\mathcal{D}_r)}{\tau_0}\frac{1-\frac{E}{F}}{\sqrt{2(1-d^2)}}+O(k_s^2).\end{aligned} \tag{6.1.58}$$

3. Following Sarkar et al. (1994) when $d \to 0$, we obtain the normalized DSIF of phonon field and crack opening displacement respectively for a single crack

$$\begin{aligned}\frac{K_1^{\tau}}{\tau_0} =& -\frac{(1-\chi_1)\mathcal{M}}{\mathcal{N}-\mathcal{M}}\frac{1}{\sqrt{2}}\left[1-\frac{L_0}{\pi}k_s^2\log k_s\right]-\frac{(1-\chi_2)\mathcal{N}}{\mathcal{M}-\mathcal{N}}\frac{1}{\sqrt{2}}\left[1-\frac{M_0}{\pi}k_s^2\log k_s\right]\\ &-\frac{e_{15}}{\epsilon_{11}}\frac{\mathcal{D}_0(1-\mathcal{D}_r)}{\tau_0}\frac{1}{\sqrt{2}}+O(k_s^2)\end{aligned} \tag{6.1.59}$$

and

$$\begin{aligned}\Delta u_z(x,0) = &-\frac{2a}{\pi}\frac{(1-\chi_1)}{(\mathcal{N}-\mathcal{M})\mathcal{R}(a+\mathcal{K})}\left[1-\frac{L_0}{\pi}k_s^2\log k_s\right]E(\sin^{-1}\sqrt{1-x^2},1)\\&+\frac{2\mathcal{R}}{\pi}\frac{(1-\chi_2)}{(\mathcal{M}-\mathcal{N})(a\mathcal{K}-\mathcal{R}^2)}\left[1-\frac{M_0}{\pi}k_s^2\log k_s\right]E(\sin^{-1}\sqrt{1-x^2},1)\\&+O(k_s^2),\quad |x|\leq 1\end{aligned} \tag{6.1.60}$$

6.1.7 Numerical results and discussion

The DSIFs of phonon and phason fields, COD and Electric displacement are depicted graphically to elucidate the effect of crack length and crack face boundary conditions. The following material constants are used (Zhou and Li, 2019a):

$$C_{44}=70.19\ GPa,\ e_{15}=5.8\ Cm^{-2},\ K_2=24\ GPa,\ R_3=0.2\ GPa,\ d_{15}=-0.168\ Cm^{-2},$$
$$\epsilon_{11}=56.4\times10^{-10}\ C^2/(Nm^2),\ \mathcal{D}_0=2\times10^{-3}\ Cm^{-2},\ \tau_0=2\times10^4\ Nm^{-2}.$$

The wave number (k) is determined as $k=\frac{k_s}{\sqrt{\mu_0}}$, where $\mu_0=C_{44}-R_3\left(\frac{R_3\epsilon_{11}+e_{15}d_{15}}{K_2\epsilon_{11}+d_{15}^2}\right)+e_{15}\left(\frac{e_{15}k_2-R_3d_{15}}{K_2\epsilon_{11}+d_{15}^2}\right)$. Therefore, wave number (k) and k_s are directly proportional, and since μ_0 can be determined by material constants, the curves depicting DSIFs versus wave number are likely to exhibit similarities with the curves showing DSIFs versus k_s. Here, the unit of k_s is $kg^{\frac{1}{2}}m^{-\frac{3}{2}}s^{-1}$.

In Figure 6.2 the normalized DSIF $\left(\frac{K_d^\tau}{\tau_0}\right)$ of phonon field at the inner crack tip is plotted against k_s for impermeable $(\mathcal{D}_r=0)$ and semi-permeable $(\mathcal{D}_r=0.5)$ crack face boundary conditions and different crack lengths. The observation reveals that as k_s increases, normalized DSIF diminishes and approaches zero. This pattern corresponds to the behavior depicted in the DSIF versus wave number graph by Yang and Li (2014) and Ma et al. (2023). $\frac{K_d^\tau}{\tau_0}$ is higher for small values of d i.e. for greater crack lengths normalized DSIF is higher. This observation aligns with the findings of Sarkar et al. (1994). The decreasing rate of normalized DSIF for semi-permeable crack face boundary condition is slower than impermeable crack face boundary condition.

Figure 6.3 represents the normalized DSIF $\left(\frac{K_1^\tau}{\tau_0}\right)$ of phonon field at the outer crack tip versus k_s for various crack lengths and crack face boundary conditions. The nature of the graph is similar to Figure 6.2. It is notable that the effect of crack length is less significant in case of normalized DSIF in outer crack tip than normalized DSIF in inner crack tip.

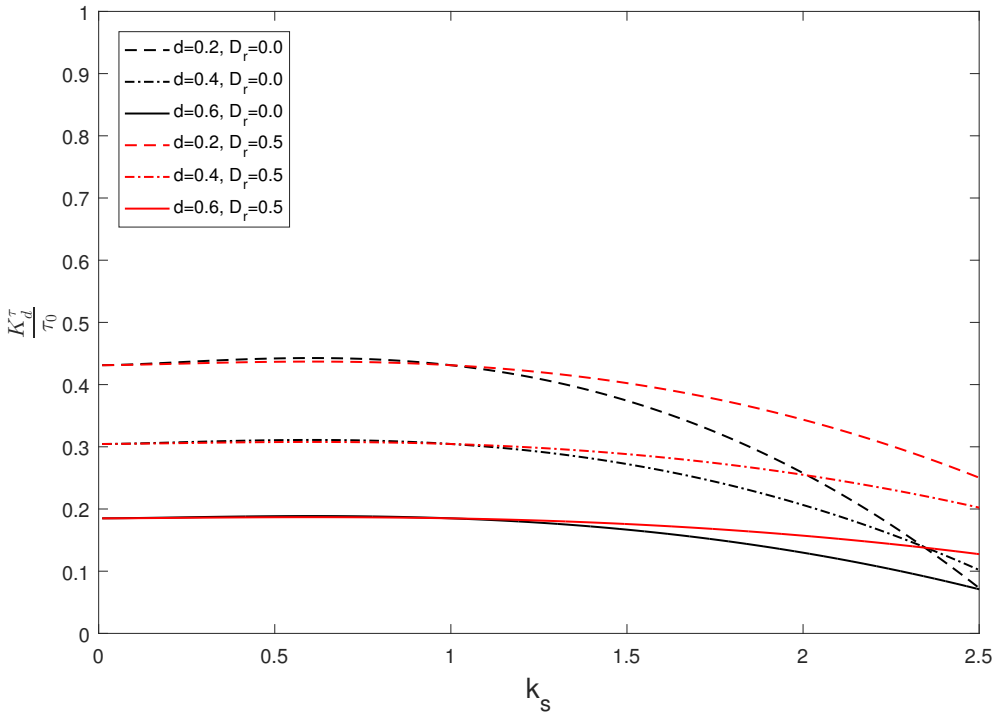

FIGURE 6.2: $\frac{K_d^\tau}{\tau_0}$ versus k_s $kg^{\frac{1}{2}}m^{-\frac{3}{2}}s^{-1}$ at inner crack tip

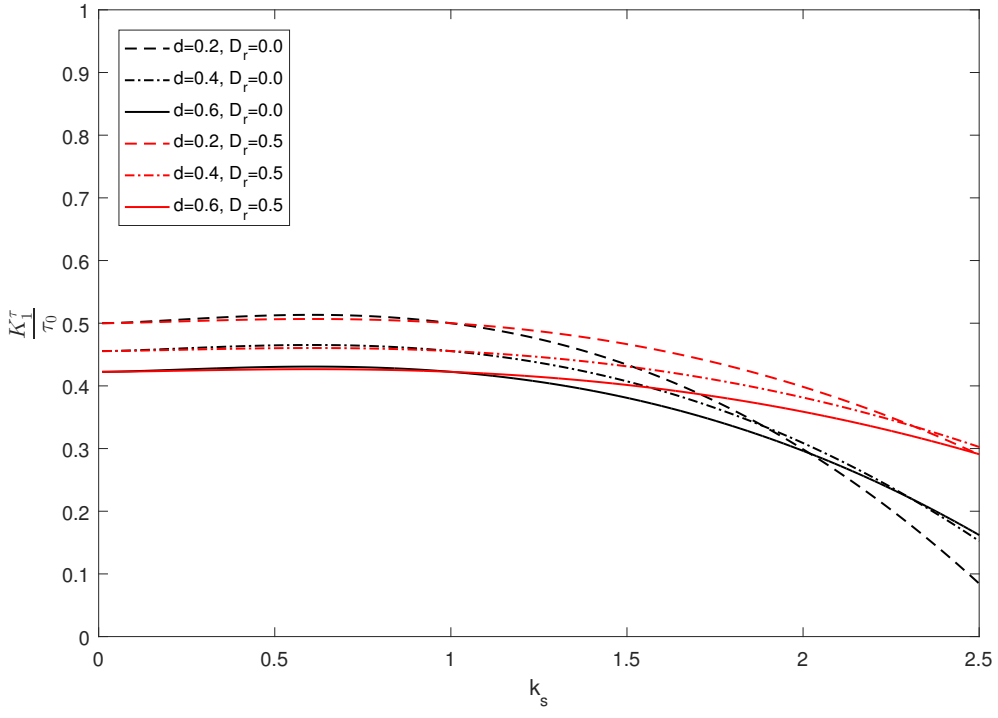

FIGURE 6.3: $\frac{K_1^\tau}{\tau_0}$ versus k_s $kg^{\frac{1}{2}}m^{-\frac{3}{2}}s^{-1}$ at outer crack tip

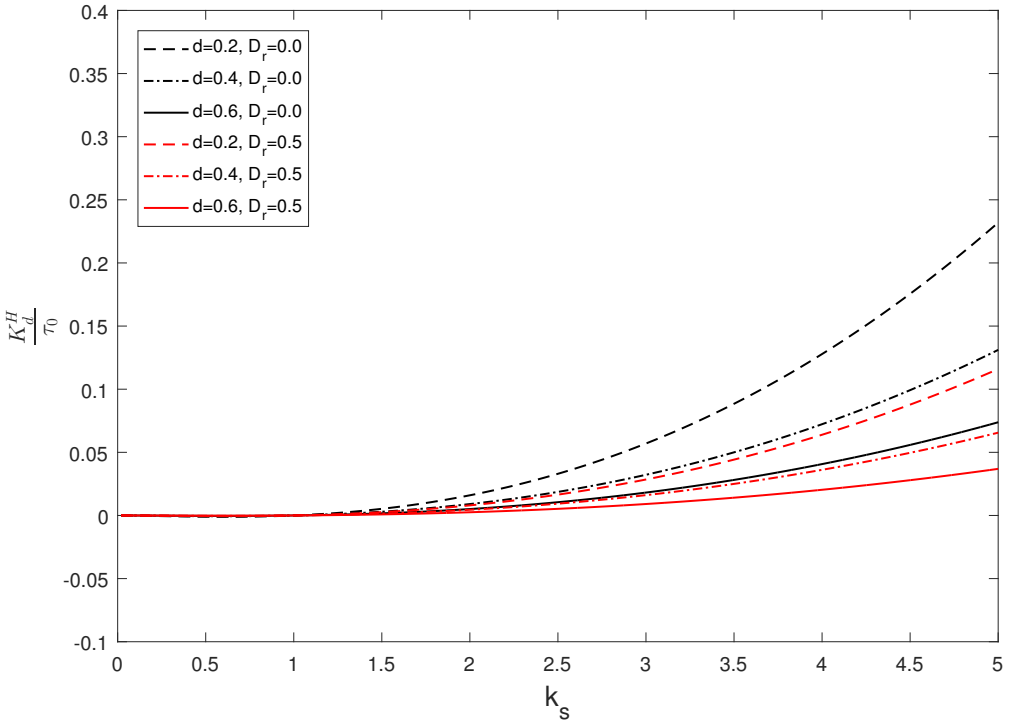

FIGURE 6.4: $\frac{K_d^H}{\tau_0}$ versus k_s $kg^{\frac{1}{2}}m^{-\frac{3}{2}}s^{-1}$ at inner crack tip

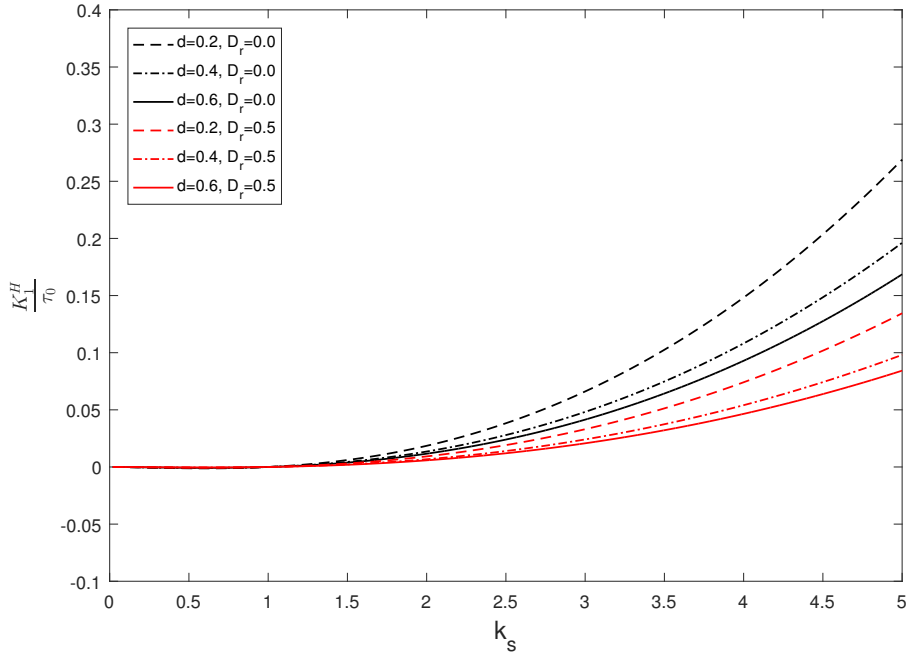

FIGURE 6.5: $\frac{K_1^H}{\tau_0}$ versus k_s $kg^{\frac{1}{2}}m^{-\frac{3}{2}}s^{-1}$ at outer crack tip

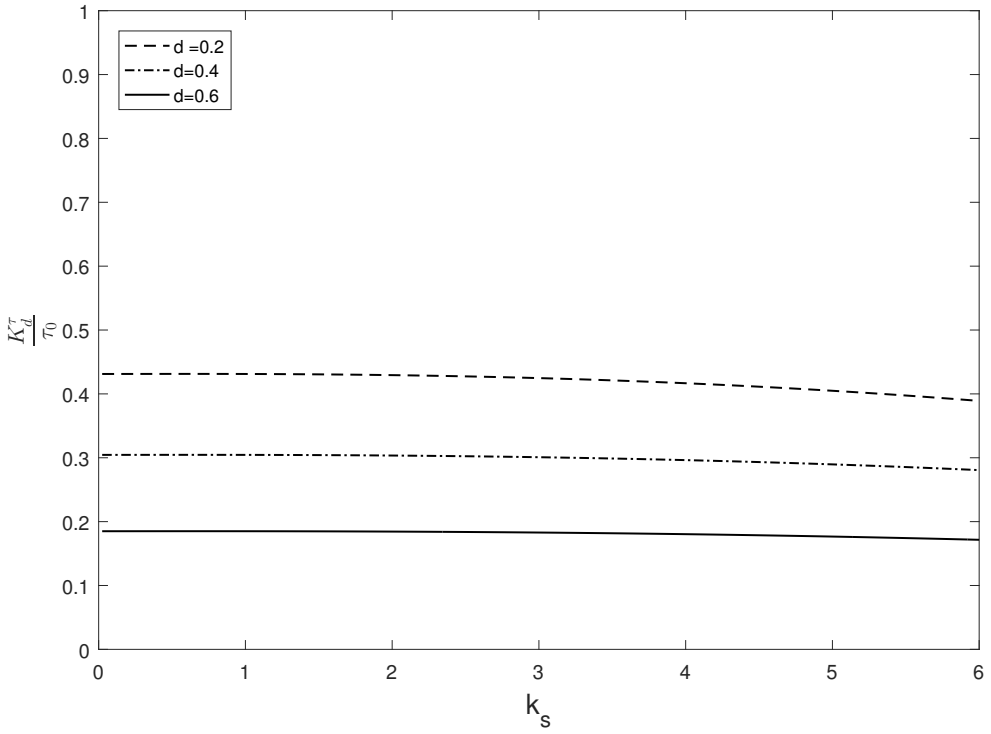

FIGURE 6.6: $\frac{K_d^\tau}{\tau_0}$ versus k_s $kg^{\frac{1}{2}}m^{-\frac{3}{2}}s^{-1}$ at inner crack tip

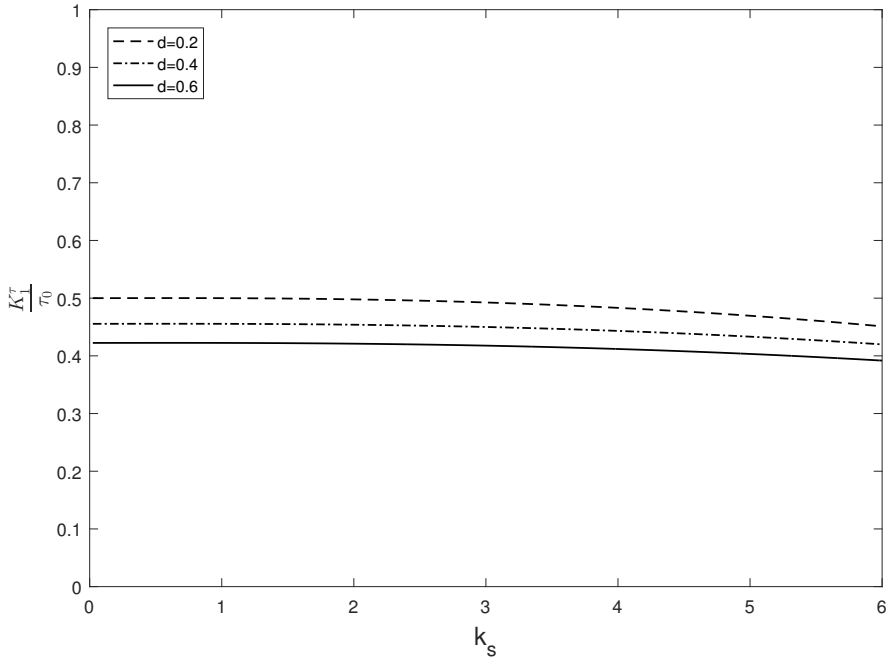

FIGURE 6.7: $\frac{K_1^\tau}{\tau_0}$ versus k_s $kg^{\frac{1}{2}}m^{-\frac{3}{2}}s^{-1}$ at outer crack tip

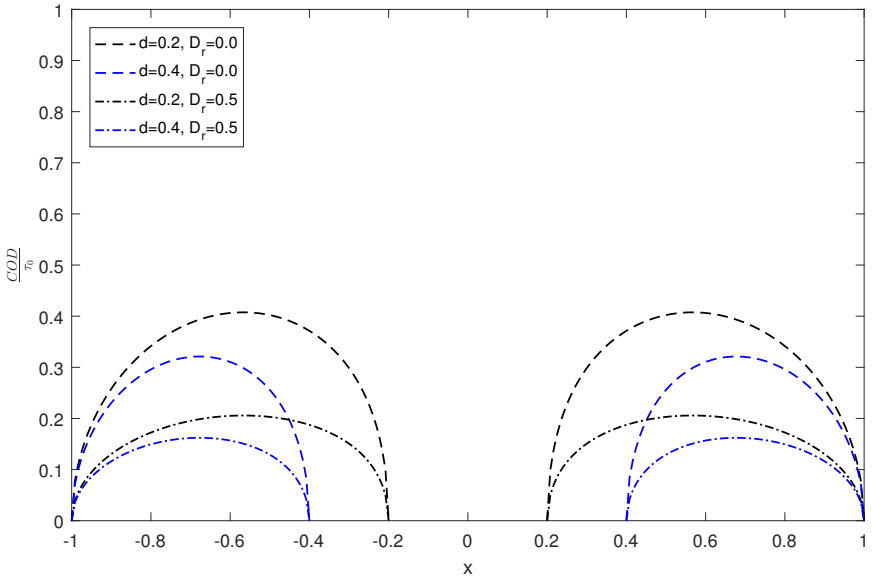

FIGURE 6.8: COD versus crack position

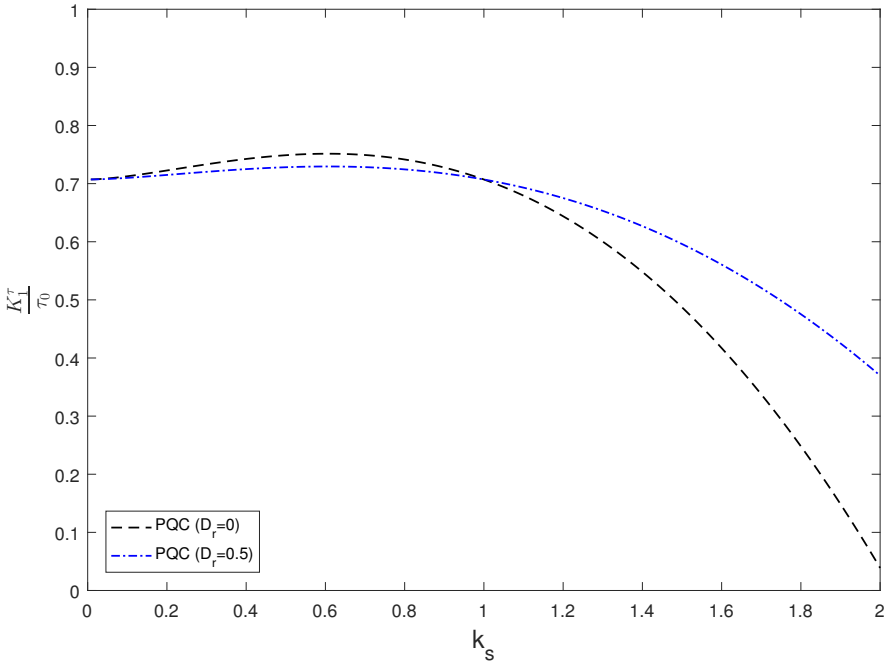

FIGURE 6.9: $\frac{K_1^\tau}{\tau_0}$ versus k_s $kg^{\frac{1}{2}}m^{-\frac{3}{2}}s^{-1}$ for single crack

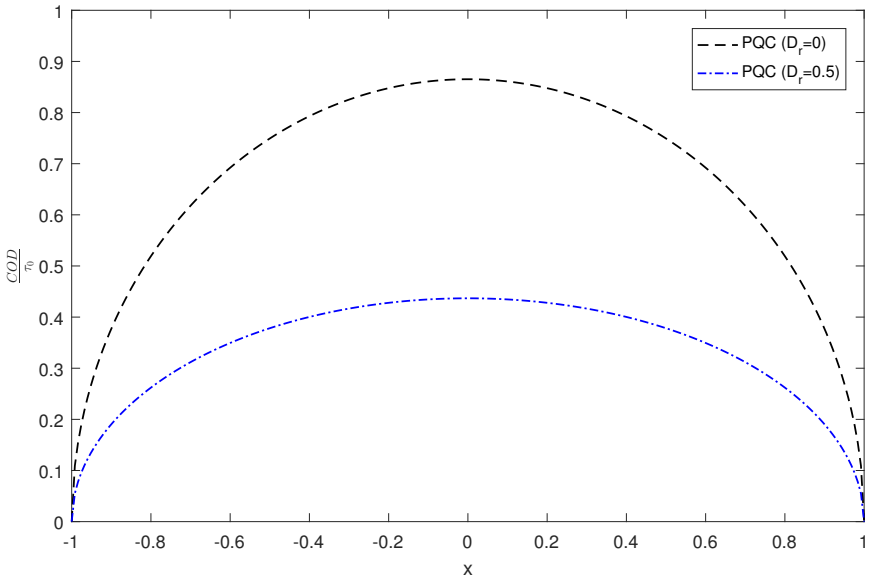

FIGURE 6.10: COD versus crack position for single crack

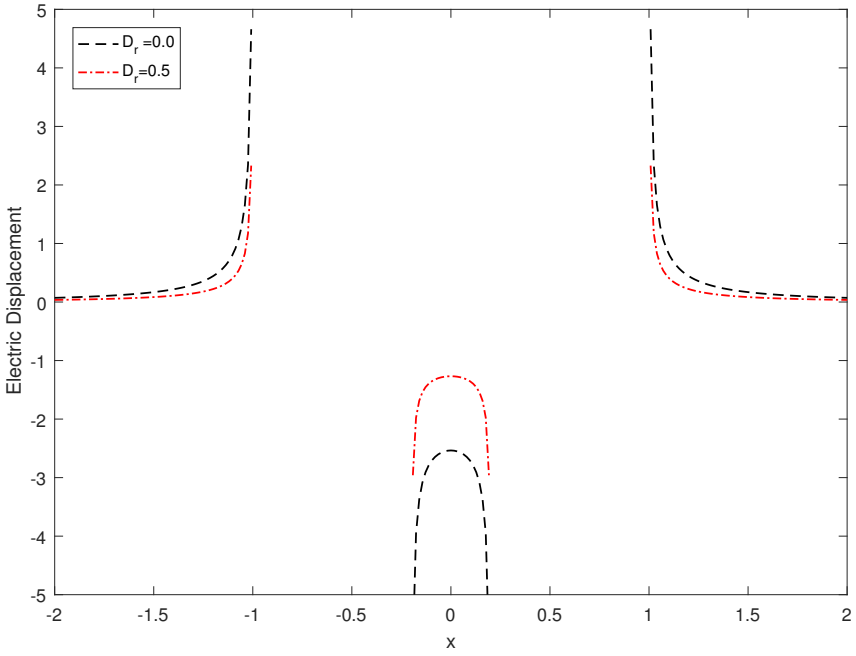

FIGURE 6.11: Electric Displacement versus x

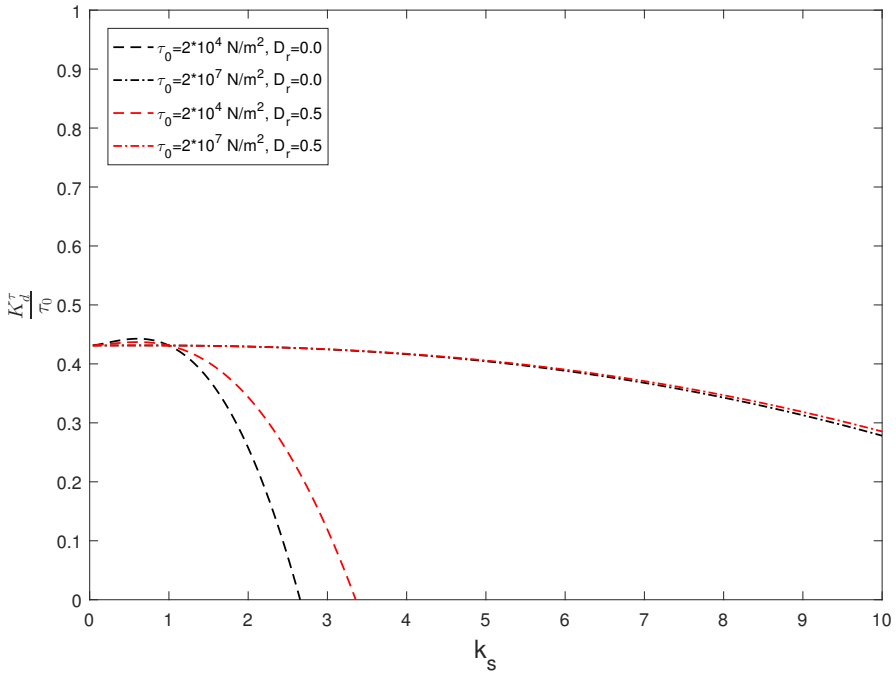

FIGURE 6.12: $\frac{K_d^\tau}{\tau_0}$ versus k_s $kg^{\frac{1}{2}}m^{-\frac{3}{2}}s^{-1}$ at inner crack tip

The value of the normalized DSIF $\frac{K_1^\tau}{\tau_0}$ (Figure 6.3) of phonon field with k_s at the outer tip of the crack is found to be higher than that of $\frac{K_d^\tau}{\tau_0}$.

In Figure 6.4 and 6.5, the normalized DSIFs of phason field are plotted with k_s at $x = d$ and $x = 1$ respectively. It is clear from both the figures that $\frac{K_d^\mathcal{H}}{\tau_0}$ and $\frac{K_1^\mathcal{H}}{\tau_0}$ are increasing in nature with the increasing values of k_s. Hence, the normalized DSIFs of the phason field at both crack tips show an inclination to rise as the wave number increases. In practical engineering scenarios, controlling the wave number could potentially mitigate crack tip propagation. There is no significant effect in normalized DSIFs of crack length and electric crack condition parameter (ECCP) for small frequency as the graphs coincide. Furthermore, when $k_s > 2$, the normalized DSIFs of the phason field at positions $x = d$ and $x = 1$, in the context of electrically impermeable cracks, exhibit greater values compared to those of semi-permeable cracks. This implies that an electrically impermeable crack tends to expand more readily than one that is filled with air. This impact of the ECCP on the normalized DSIFs of the phason field was similarly identified by Yang et al. (2023b)

Figure 6.6 and 6.7 are the plots of normalized DSIFs of phonon field for QCs at inner and outer crack tip respectively. It is obvious from both figures that normalized DSIFs decrease very slowly with the increase of the values of k_s. Comparing with the figures 6.2

and 6.3, it is found that the stress singularity of phonon field at the crack tips has a slow decreasing rate in the absence of piezoelectricity. So a significant effect of piezoelectric and dielectric coefficients on the normalized DSIFs are shown by figures 6.2, 6.3, 6.6 and 6.7.

The COD has been plotted for various crack lengths and two ECCPs in Figure 6.8 and for single crack in Figure 6.10. In each case COD rises consistently from zero, achives maximum at the center of the crack and then falls off to zero. It is observed that with the increase of d the values of COD decrease i.e. as the crack length decreases the values of COD decrease as well. Consequently, larger cracks experience more facile expansion, resulting in material damage. This finding agrees with the conclusions drawn by Sarkar et al. (1994). COD for impermeable crack face boundary condition is higher than semi-permeable crack face boundary condition. This outcome can be substantiated through the research conducted by Bhargava and Verma (2016). The COD graph is symmetric with respect to the mid position of the crack.

In Figure 6.9, the normalized DSIF of phonon field for single crack is depicted by means of graphs for PQCs. For small values of k_s the normalized DSIF is high but it decreases gradually and tends to zero when k_s increases. For $\mathcal{D}_r = 0.5$, the $\frac{K_I^\tau}{\tau_0}$ diminishes slowly than the graph for $\mathcal{D}_r = 0$.

Figure 6.11 is the graph of electric displacement versus x, outside the crack line. Electric displacement is maximum just outside the crack tip and it becomes lower with the increasing values of x and vanishes far away from the crack. Moreover, electric displacement is higher for $\mathcal{D}_r = 0$ than $\mathcal{D}_r = 0.5$.

Figure 6.12 illustrates the normalized Dynamic Stress Intensity Factor (DSIF) of the phonon field at the inner crack tip as a function of k_s, considering various loading conditions and different crack face boundary conditions. Notably, when higher values of τ_0 are considered, the decrease in the normalized DSIF is gradual, and there's minimal distinction between impermeable and semi-permeable cracks. However, when smaller τ_0 values are examined, the normalized DSIF experiences a steep reduction with increasing k_s. Increased load amplitudes correspond to greater crack expansion propensity, contributing to material degradation. As a result, adjusting the load amplitude to enhance material strength can mitigate the dynamic stress concentration around the crack tip. Additionally, the influence of crack face boundary conditions on the normalized DSIF is prominent, when $\tau_0 = 2 \times 10^4\ N/m^2$.

6.1.8 Conclusions

The interaction of anti-plane shear wave with two collinear cracks in a 1D hexagonal PQCs is studied. By employing Fourier transform, the MBVP is simplified to three pairs of dual integral equations, which are approximately solved by finite Hilbert transform technique. Numerical results for normalized DSIFs of phonon and phason field, COD and electric displacement are shown graphically. The following important points are calculated from this study:

- For given electrical loads, the value of fracture parameters i.e. DSIFs, COD and electric displacement for semi-permeable crack are always smaller than electrically impermeable crack, which implies that the electrically impermeable crack enlarges more smoothly than the semi-permeable crack. So, in engineering practice, the electrically semi-permeable crack can offer more feasible results.
- In the absence of electric field, the decreasing rate of normalized DSIFs of phonon field is very low, which means the effect of piezoelectric and dielectric parameters are very crucial in case of stress singularity. Theoretically it is observed that in practice application QCs material is more susceptible than PQCs where defects exists in the structure.
- The value of DSIFs of phonon field and COD is higher for small values of d i.e. for large crack the stress singularity at the crack tip and distance between two crack faces are higher. So, arrest of crack growth is not so easy for large crack, which is physically persistent for this theoretical analysis.

The proposed model may provide an idea to choose smart materials for engineering design and health monitoring of the structure. Also this theoretical study is useful to solve a wide range of multiple crack problems in piezoelectric quasicrystals.

Bibliography

Abd-Alla, A.-e.-N. N. and Abo-Dahab, S. (2008). The influence of the viscosity and the magnetic field on reflection and transmission of waves at interface between magneto-viscoelastic materials. *Meccanica*, 43:437–448.

Abdel-Hamid, B. (1999). Modelling non-fourier heat conduction with periodic thermal oscillation using the finite integral transform. *Applied Mathematical Modelling*, 23(12):899–914.

Abo-Dahab, S. and Singh, B. (2009). Influences of magnetic field on wave propagation in generalized thermoelastic solid with diffusion. *Archives of Mechanics*, 61(2):121–136.

Abouelregal, A. (2020a). On green and naghdi thermoelasticity model without energy dissipation with higher order time differential and phase-lags. *Journal of Applied and Computational Mechanics*, 6(3):445–456.

Abouelregal, A. E. (2019). Two-temperature thermoelastic model without energy dissipation including higher order time-derivatives and two phase-lags. *Materials Research Express*, 6(11):116535.

Abouelregal, A. E. (2020b). Generalized mathematical novel model of thermoelastic diffusion with four phase lags and higher-order time derivative. *The European Physical Journal Plus*, 135(2):263.

Abouelregal, A. E. and Abo-Dahab, S. (2018). A two-dimensional problem of a mode-i crack in a rotating fibre-reinforced isotropic thermoelastic medium under dual-phase-lag model. *Sādhanā*, 43:1–11.

Abramowitz, M. and Stegun, I. A. (1968). *Handbook of mathematical functions with formulas, graphs, and mathematical tables*, volume 55. US Government printing office.

Achenbach, J. (2012). *Wave propagation in elastic solids*. Elsevier.

Achenbach, J. and Brind, R. (1981). Scattering of surface waves by a sub-surface crack. *Journal of Sound and Vibration*, 76(1):43–56.

Ahmed, S. and Abo-Dahab, S. (2010). Propagation of love waves in an orthotropic granular layer under initial stress overlying a semi-infinite granular medium. *Journal of Vibration and Control*, 16(12):1845–1858.

Aki, K. and Richards, P. G. (2002). *Quantitative seismology*. University Science Books.

Ala, S., Gurijala, R., and Perati, M. R. (2020). Shear wave propagation in magneto poroelastic medium sandwiched between self-reinforced poroelastic medium and poroelastic half space. *Engineering Computations*, 37(9):3345–3359.

Alterman, Z. and Karal Jr, F. (1968). Propagation of elastic waves in layered media by finite difference methods. *Bulletin of the Seismological Society of America*, 58(1):367–398.

Angel, Y. (1986). Scattering of love waves by a surface-breaking crack. *Journal of Applied Mechanics*, 53(3):587–592.

Baksi, A., Das, S., and Bera, R. (2003). Impact response of a cracked orthotropic medium-revisited. *International Journal of Engineering Science*, 41(17):2063–2079.

Belfield, A., Rogers, T., and Spencer, A. (1983). Stress in elastic plates reinforced by fibres lying in concentric circles. *Journal of the Mechanics and Physics of Solids*, 31(1):25–54.

Bendersky, L. (1985). Quasicrystal with one-dimensional translational symmetry and a tenfold rotation axis. *Physical Review Letters*, 55(14):1461–1463.

Bhargava, R. and Verma, P. R. (2016). A study of crack-face boundary conditions for piezoelectric strip cut along two equal collinear cracks. *Advances in Applied Mathematics and Mechanics*, 8(4):573–587.

Bin, G., Shouwen, Y., Xiqiao, F., and Yiu-Wing, M. (2002). Scattering of love waves by an interface crack between a piezoelectric layer and an elastic substrate. *Acta Mechanica Solida Sinica*, 15(2).

Biot, M. A. (1940). The influence of initial stress on elastic waves. *Journal of Applied Physics*, 11(8):522–530.

Biot, M. A. (1956). Thermoelasticity and irreversible thermodynamics. *Journal of Applied Physics*, 27(3):240–253.

Brekhovskikh, L. (2012). *Waves in layered media*, volume 16. Elsevier.

Brock, L. and Hanson, M. (2006). Transient analysis of a suddenly-opening crack in a coupled thermoelastic solid with thermal relaxation. *Journal of Mechanics of Materials and Structures*, 1(7):1257–1268.

Bullen, K. E., Bullen, K. E., Bullen, K. A., and Bolt, B. A. (1985). *An introduction to the theory of seismology*. Cambridge university press.

Cao, X., Jin, F., Jeon, I., and Lu, T. J. (2009). Propagation of love waves in a functionally graded piezoelectric material (fgpm) layered composite system. *International Journal of Solids and Structures*, 46(22-23):4123–4132.

Cattaneo, C. (1958). A form of heat-conduction equations which eliminates the paradox of instantaneous propagation. *Comptes rendus*, 247:431–433.

Cauchy, A.-L. (1823). *Résumé of the lessons given at the Royal Polytechnic School on calculus infinitésimal*, volume 1. Royal Printing.

Chao, C. and Chang, R. (1993). Steady-state heat conduction problem of the interface crack between dissimilar anisotropic media. *International Journal of Heat and Mass Transfer*, 36(8):2021–2026.

Chao, C. and Kuo, L. (1993). Thermal problem of curvilinear cracks in bonded dissimilar materials with a point heat source. *International Journal of Heat and Mass Transfer*, 36(17):4085–4093.

Chapman, C. (2004). *Fundamentals of seismic wave propagation*. Cambridge university press.

Chattopadhyay, A. and Choudhury, S. (1990). Propagation, reflection and transmission of magnetoelastic shear waves in a self-reinforced medium. *International Journal of Engineering Science*, 28(6):485–495.

Chattopadhyay, A. and Choudhury, S. (1995). Magnetoelastic shear waves in an infinite self-reinforced plate. *International Journal for Numerical and Analytical Methods in Geomechanics*, 19(4):289–304.

Chattopadhyay, A., Gupta, S., and Singh, A. (2010). The dispersion of shear wave in multilayered magnetoelastic self-reinforced media. *International Journal of Solids and Structures*, 47(9):1317–1324.

Chattopadhyay, A., Gupta, S., Singh, A. K., Sahu, S. A., et al. (2011). Effect of point source, self-reinforcement and heterogeneity on the propagation of magnetoelastic shear wave. *Applied Mathematics*, 2(03):271.

Chattopadhyay, A. and Maugin, G. (1985). Diffraction of magnetoelastic shear waves by a rigid strip. *The Journal of the Acoustical Society of America*, 78(1):217–222.

Chattopadhyay, A. and Singh, A. K. (2012). Propagation of magnetoelastic shear waves in an irregular self-reinforced layer. *Journal of Engineering Mathematics*, 75:139–155.

Chattopadhyay, A. and Singh, A. K. (2014). Propagation of a crack due to magnetoelastic shear waves in a self-reinforced medium. *Journal of Vibration and Control*, 20(3):406–420.

Chattopadhyay, K., Lele, S., Thangaraj, N., and Ranganathan, S. (1987). Vacancy ordered phases and one-dimensional quasiperiodicity. *Acta Metallurgica*, 35(3):727–733.

Chen, E. (1978). Sudden appearance of a crack in a stretched finite strip. *Journal of Applied Mechanics*, 45(2):277–280.

Chen, K., Wu, Z., Jin, Y., Hu, J., Du, J., and Zhang, M. (2022). Love wave propagation in piezoelectric structures bonded with conductive polymer films. *Ultrasonics*, 118:106559.

Chen, T.-M. (2009). A hybrid green's function method for the hyperbolic heat conduction problems. *International Journal of Heat and Mass Transfer*, 52(19-20):4273–4278.

Cheng, J., Liu, B., Huang, X., and Li, Z. (2021). Anti-plane fracture analysis of 1d hexagonal piezoelectric quasicrystals with the effects of damage due to materials degradation. *Theoretical and Applied Fracture Mechanics*, 113:102939.

Choudhuri, S. R. (2007). On a thermoelastic three-phase-lag model. *Journal of Thermal Stresses*, 30(3):231–238.

Clebsch, A. (1863). On reflection from a spherical surface. *Journal of Pure and Applied Mathematics*, 1863(61):195–262.

Cooper Jr, H. F. (1967). Reflection and transmission of oblique plane waves at a plane interface between viscoelastic media. *The Journal of the Acoustical Society of America*, 42(5):1064–1069.

Das, A. and Ghosh, M. (1992). Two co-planar griffith cracks moving along the interface of two dissimilar elastic media. *Engineering Fracture Mechanics*, 41(1):59–69.

Davies, B. and Martin, B. (1979). Numerical inversion of the laplace transform: a survey and comparison of methods. *Journal of Computational Physics*, 33(1):1–32.

De, J. and Patra, B. (1989). Edge crack in orthotropic elastic half-plane. *Ind. J. Pure Appl. Math*, 20(9):923–930.

Dhabal, U., Panja, S., and Mandal, S. (2022). Shear wave interaction of two collinear finite cracks in an infinite magnetoelastic orthotropic media. *International Journal of Applied and Computational Mathematics*, 8(5):243.

Dhua, S., Singh, A. K., and Chattopadhyay, A. (2015). Propagation of torsional wave in a composite layer overlying an anisotropic heterogeneous half-space with initial stress. *Journal of Vibration and Control*, 21(10):1987–1998.

Dryden, J. R. and Zok, F. (2001). Thermal phase lag in a solid containing periodic planar cracks. *International Journal of Heat and Mass Transfer*, 44(21):4035–4046.

Du, J., Jin, X., Wang, J., and Xian, K. (2007). Love wave propagation in functionally graded piezoelectric material layer. *Ultrasonics*, 46(1):13–22.

Dunkin, J. and Eringen, A. (1963). On the propagation of waves in an electromagnetic elastic solid. *International Journal of Engineering Science*, 1(4):461–495.

Erdogan, F. (1995). *Fracture Mechanics: 25th Volume*, volume 1220. Astm International.

Erdogan, F. and Gupta, G. (1972). On the numerical solution of singular integral equations. *Quarterly of Applied Mathematics*, 29(4):525–534.

Erdogan, F., Gupta, G., and Cook, T. (1973). Numerical solution of singular integral equations. In *Methods of analysis and solutions of crack problems: Recent developments in fracture mechanics Theory and methods of solving crack problems*, pages 368–425. Springer.

Fan, T. (2011). *Mathematical theory of elasticity of quasicrystals and its applications*. Springer.

Fan, T.-y., Li, X.-f., and Sun, Y.-f. (1999). A moving screw dislocation in a one-dimensional hexagonal quasicrystal. *Chinese Physics B*, 8(4):288–295.

Fang, X.-Q., Ma, H.-W., and Zhu, C.-S. (2022). Non-local multi-fields coupling response of a piezoelectric semiconductor nanofiber under shear force. *Mechanics of Advanced Materials and Structures*, pages 1–8.

Farnell, G. W. and Adler, E. (2012). Elastic wave propagation in thin layers. *Physical Acoustics*, 9:35–127.

Feng, Y., Lu, G., and Withers, R. (1989). An incommensurate structure with cubic point group symmetry in rapidly solidified v-ni-si alloy. *Journal of Physics: Condensed Matter*, 1(23):3695–3700.

Fox, L. and Goodwin, E. (1953). The numerical solution of non-singular linear integral equations. *Philosophical Transactions of the Royal Society of London. Series A, Mathematical and Physical Sciences*, 245(902):501–534.

Fung, K. K., Yang, C., Zhou, Y., Zhao, J., Zhan, W., and Shen, B. (1986). Icosahedrally related decagonal quasicrystal in rapidly cooled al-14-at.%-fe alloy. *Physical Review Letters*, 56(19):2060–2063.

Gao, C.-F. and Noda, N. (2004). Thermal-induced interfacial cracking of magnetoelectroelastic materials. *International Journal of Engineering Science*, 42(13-14):1347–1360.

Gradshteyn, I. S. and Ryzhik, I. M. (2014). *Table of integrals, series, and products*. Academic press.

Graff, K. F. (2012). *Wave motion in elastic solids*. Courier Corporation.

Green, A. and Naghdi, P. (1992). On undamped heat waves in an elastic solid. *Journal of Thermal Stresses*, 15(2):253–264.

Green, A. and Naghdi, P. (1993). Thermoelasticity without energy dissipation. *Journal of Elasticity*, 31(3):189–208.

Green, A. E. and Lindsay, K. (1972). Thermoelasticity. *Journal of Elasticity*, 2(1):1–7.

Griffith, A. A. (1921). Vi. the phenomena of rupture and flow in solids. *Philosophical Transactions of the Royal Society of London. Series A, containing papers of a mathematical or physical character*, 221(582-593):163–198.

Gu, B., Yu, S.-W., and Feng, X.-Q. (2002a). Elastic wave scattering by an interface crack between a piezoelectric layer and an elastic substrate. *International Journal of Fracture*, 116:29–34.

Gu, B., Yu, S.-W., and Feng, X.-Q. (2002b). Transient response of an interface crack between dissimilar piezoelectric layers under mechanical impacts. *International Journal of Solids and Structures*, 39(7):1743–1756.

Guo, J., Zhang, Z., and Xing, Y. (2016). Antiplane analysis for an elliptical inclusion in 1d hexagonal piezoelectric quasicrystal composites. *Philosophical Magazine*, 96(4):349–369.

Guo, L.-C., Wu, L.-Z., and Zeng, T. (2005). The dynamic response of an edge crack in a functionally graded orthotropic strip. *Mechanics Research Communications*, 32(4):385–400.

Gupta, S. and Bhengra, N. (2017). Implementation of finite difference approximation on the sh-wave propagation in a multilayered magnetoelastic orthotropic composite medium. *Acta Mechanica*, 228:3421–3444.

Gupta, S., Majhi, D., Kundu, S., and Vishwakarma, S. (2013). Propagation of love waves in non-homogeneous substratum over initially stressed heterogeneous half-space. *Applied Mathematics and Mechanics*, 34:249–258.

Haskell, N. A. (1953). The dispersion of surface waves on multilayered media. *Bulletin of the Seismological Society of America*, 43(1):17–34.

Hu, C., Wang, R., and Ding, D.-H. (2000). Symmetry groups, physical property tensors, elasticity and dislocations in quasicrystals. *Reports on Progress in Physics*, 63(1):1.

Hu, K., Jin, H., Yang, Z., and Chen, X. (2019). Interface crack between dissimilar one-dimensional hexagonal quasicrystals with piezoelectric effect. *Acta Mechanica*, 230:2455–2474.

Hudson, J. A. (1980). *The excitation and propagation of elastic waves*. CUP Archive.

Inglis, C. E. (1913). Stresses in a plate due to the presence of cracks and sharp corners. *Trans Inst Naval Archit*, 55:219–241.

Irwin, G. R. (1957). Analysis of stresses and strains near the end of a crack traversing a plate. *Journal of Applied Mechanics*, 24(3):361–364.

Itou, S. (1978). Dynamic stress concentration around two coplanar griffith cracks in an infinite elastic medium. *Journal of Applied Mechanics*, 45:803–806.

Itou, S. (1980a). Diffraction of an antiplane shear wave by two coplanar griffith cracks in an infinite elastic medium. *International Journal of Solids and Structures*, 16(12):1147–1153.

Itou, S. (1980b). Transient analysis of stress waves around two coplanar griffith cracks under impact load. *Engineering Fracture Mechanics*, 13(2):349–356.

Jain, D. and Kanwal, R. (1972). Diffraction of elastic waves by two coplanar griffith cracks in an infinite elastic medium. *International Journal of Solids and Structures*, 8(7):961–975.

Kaliski, S. and Petykiewicz, J. (1959). Equation of motion coupled with the field of temperature in a magnetic field involving mechanical and electrical relaxation for anisotropic bodies. In *Proc. Vibr. Probl*, volume 4(1), pages 1–12.

Kalyani, V. (1990). Dispersion of love waves in an initially stressed multilayered crust. *Indian J. Pure Appl. Math*, 21(11):1029–1035.

Kalyani, V. K., Sinha, A., Pallavika, Chakraborty, S. K., and Mahanti, N. (2008). Finite difference modeling of seismic wave propagation in monoclinic media. *Acta Geophysica*, 56:1074–1089.

Kar, A., Chan, C., and Mazumder, J. (1992). Comparative studies on nonlinear hyperbolic and parabolic heat conduction for various boundary conditions: analytic and numerical solutions. *Journal of Heat Transfer*, pages 14–20.

Kassir, M. and Bandyopadhyay, K. (1983). Impact response of a cracked orthotropic medium. *Journal of Applied Mechanics*, 50(3):630–636.

Keer, L., Lin, W., and Achenbach, J. (1984). Resonance effects for a crack near a free surface. *Journal of Applied Mechanics*, 51(1):65–70.

Keer, L. and Luong, W. (1974). Diffraction of waves and stress intensity factors in a cracked layered composite. *The Journal of the Acoustical Society of America*, 56(6):1681–1686.

Kelly, K. R., Ward, R. W., Treitel, S., and Alford, R. M. (1976). Synthetic seismograms: a finite-difference approach. *Geophysics*, 41(1):2–27.

Knopoff, L. (1955). The interaction between elastic wave motions and a magnetic field in electrical conductors. *Journal of Geophysical Research*, 60(4):441–456.

Kolosov, G. (1909). On an application of complex function theory to a plane problem of the mathematical theory of elasticity. *Yuriev, Russia*.

Kolsky, H. (1963). *Stress waves in solids*, volume 1098. Courier Corporation.

Krenk, S. (1975). On the use of the interpolation polynomial for solutions of singular integral equations. *Quarterly of Applied Mathematics*, 32(4):479–484.

Kumar, S., Majhi, S., and Pal, P. (2015). Reflection and transmission of plane sh-waves in two semi-infinite anisotropic magnetoelastic media. *Meccanica*, 50:2431–2440.

Kumari, C., Kundu, S., and Kumhar, R. (2019). Dispersion characteristics of sh wave propagation in a viscous fiber-reinforced stratified media. In *AIP Conference Proceedings*, volume 2061(1). AIP Publishing.

Kundu, T. (1987). The transient response of two cracks at the interface of a layered half space. *International Journal of Engineering Science*, 25(11-12):1427–1439.

Kunji, C., Guomin, M., Duan, F., Ying, Y., Jiafang, D., Zhifeng, L., Hong, C., and Fritzsche, H. (1987). Quasiperiodic a-si: H/a-sinx: H multilayer structures. *Journal of Non-Crystalline Solids*, 97:341–344.

Kwon, S. (2004). On the dynamic propagation of an anti-plane shear crack in a functionally graded piezoelectric strip. *Acta Mechanica*, 167:73–89.

Kwon, S. M. (2003). Electrical nonlinear anti-plane shear crack in a functionally graded piezoelectric strip. *International Journal of Solids and Structures*, 40(21):5649–5667.

Kwon, S. M. and Lee, K. Y. (2003). An anti-plane propagating crack in a functionally graded piezoelectric strip bonded to a homogeneous piezoelectric strip. *Archive of Applied Mechanics*, 73:348–366.

Lamb, H. (1904). I. on the propagation of tremors over the surface of an elastic solid. *Philosophical Transactions of the Royal Society of London. Series A, Containing papers of a mathematical or physical character*, 203(359-371):1–42.

Levine, D. and Steinhardt, P. J. (1984). Quasicrystals: a new class of ordered structures. *Physical Review Letters*, 53(26):2477–2480.

Lewandowska, M. and Malinowski, L. (1998). Hyperbolic heat conduction in the semi-infinite body with the heat source which capacity linearly depends on temperature. *Heat and Mass Transfer*, 33(5):389–393.

Li, X., Wang, Z., and Huang, S. (2004). Love waves in functionally graded piezoelectric materials. *International Journal of Solids and Structures*, 41(26):7309–7328.

Loeber, J. and Sih, G. (1968). Diffraction of antiplane shear waves by a finite crack. *The Journal of the Acoustical Society of America*, 44(1):90–98.

Lord, H. W. and Shulman, Y. (1967). A generalized dynamical theory of thermoelasticity. *Journal of the Mechanics and Physics of Solids*, 15(5):299–309.

Lotfy, K. and El-Bary, A. (2024). A mode-i crack for a rotational fibre-reinforced thermoelastic medium with thermal relaxation time. *Waves in Random and Complex Media*, 34(1):252–273.

Love, A. E. H. (1911). *Some Problems of Geodynamics: Being an Essay to which the Adams Prize in the University of Cambridge was Adjudged in 1911*. University Press.

Love, A. E. H. (1927). *A treatise on the mathematical theory of elasticity*. University press.

Love, A. E. H. (2013). *A treatise on the mathematical theory of elasticity*. Cambridge university press.

Lowengrub, M. and Srivastava, K. (1968). On two coplanar griffith cracks in an infinite elastic medium. *International Journal of Engineering Science*, 6(6):359–362.

Ma, Y., Zhou, Y., Yang, J., Zhao, X., and Ding, S. (2023). Interface crack behaviors disturbed by love waves in a 1d hexagonal quasicrystal coating–substrate structure. *Zeitschrift für Angewandte Mathematik und Physik*, 74(2):61.

Majhi, S., Pal, P., and Kumar, S. (2017). Reflection and transmission of plane sh-waves in an initially stressed inhomogeneous anisotropic magnetoelastic medium. *Journal of Seismology*, 21:155–163.

Mal, A. (1970a). Interaction of elastic waves with a penny-shaped crack. *International Journal of Engineering Science*, 8(5):381–388.

Mal, A. (1972). A note on the low frequency diffraction of elastic waves by a griffith crack. *International Journal of Engineering Science*, 10(7):609–612.

Mal, A. K. (1970b). Interaction of elastic waves with a griffith crack. *International Journal of Engineering Science*, 8(9):763–776.

Mandal, P. and Mandal, S. (2017). Interface crack at orthotropic media. *International Journal of Applied and Computational Mathematics*, 3:3253–3262.

Mandal, S. and Ghosh, M. (1994). Interaction of elastic waves with a periodic array of coplanar griffith cracks in an orthotropic elastic medium. *International Journal of Engineering Science*, 32(1):167–178.

Maugin, G. A. (1981). Wave motion in magnetizable deformable solids. *International Journal of Engineering Science*, 19(3):321–388.

Maxwell, J. C. (1873). *A treatise on electricity and magnetism*, volume 1. Oxford: Clarendon Press.

Miklowitz, J. (2012). *The theory of elastic waves and waveguides*. Elsevier.

Mishra, P. K. and Das, S. (2018). Two interfacial collinear griffith cracks in thermo-elastic composite media. *Thermal Science*, 22(1B):423–433.

Mitchell, A. R. and Mitchell, A. R. (1969). *Computational methods in partial differential equations*, volume 3. John Wiley & Sons.

Naciri, T., Navi, P., and Granacher, O. (1989). On the harmonic waves propagation in multilayered viscoelastic media. In *Modern Practice in Stress and Vibration Analysis*, pages 145–151. Elsevier.

Narita, F. and Shindo, Y. (1998). Scattering of love waves by a surface-breaking crack in piezoelectric layered media. *JSME International Journal Series A Solid Mechanics and Material Engineering*, 41(1):40–48.

Narita, F. and Shindo, Y. (1999a). The interface crack problem for bonded piezoelectric and orthotropic layers under antiplane shear loading. *International Journal of Fracture*, 98:87–102.

Narita, F. and Shindo, Y. (1999b). Scattering of antiplane shear waves by a finite crack in piezoelectric laminates. *Acta Mechanica*, 134(1-2):27–43.

Naskar, S. and Mandal, S. (2018). P-wave diffraction by a crack under impact load. *International Journal of Applied and Computational Mathematics*, 4:1–9.

Nayfeh, A., Taylor, T., and Chimenti, D. (1988). Theoretical wave propagation in multilayered orthotropic media. *Wave propagation in Structural Composites*, 90:17–27.

Neerhoff, F. L. (1979). Diffraction of love waves by a stress-free crack of finite width in the plane interface of a layered composite. *Applied Scientific Research*, 35:265–315.

Niraula, O. P. and Wang, B. (2006). Thermal stress analysis in magneto-electro-thermo-elasticity with a penny-shaped crack under uniform heat flow. *Journal of Thermal Stresses*, 29(5):423–437.

Noble, B. (1963). The solution of bessel function dual integral equations by a multiplying-factor method. In *Mathematical Proceedings of the Cambridge Philosophical Society*, volume 59(2), pages 351–362. Cambridge University Press.

Novotnỳ, O. and Vaněk, J. (1973). On some modifications of thomson-haskell matrices for love waves. *Studia Geophysica et Geodaetica*, 17(2):186–188.

Othman, M. and Abed-Elaziz, E. (2017). Effect of rotation and gravitational on a micropolar magneto-thermoelastic medium with dual-phase-lag model. *Microsyst. Tech*, 23(10):4979–4987.

Othman, M. I. and Atwa, S. Y. (2013). 2-d problem of a mode-i crack for a generalized thermoelasticity under green-naghdi theory. *Meccanica*, 48:1543–1551.

Othman, M. I., Hasona, W., and Abd-Elaziz, E. M. (2014a). Effect of rotation on micropolar generalized thermoelasticity with two temperatures using a dual-phase lag model. *Canadian Journal of Physics*, 92(2):149–158.

Othman, M. I., Hasona, W., and Abd-Elaziz, E. M. (2014b). The effect of rotation on the problem of fiber-reinforced under generalized magnetothermoelasticity subject to thermal loading due to laser pulse: a comparison of different theories. *Canadian Journal of Physics*, 92(9):1002–1015.

Othman, M. I., Hasona, W., and Abd-Elaziz, E. M. (2015). Effect of rotation and initial stress on generalized micropolar thermoelastic medium with three-phase-lag. *Journal of Computational and Theoretical Nanoscience*, 12(9):2030–2040.

Othman, M. I. and Lotfy, K. (2011). Effect of rotation on plane waves in generalized thermo-microstretch elastic solid with one relaxation time. *Multidiscipline Modeling in Materials and Structures*, 7(1):43–62.

Othman, M. I. and Lotfy, K. (2015). The influence of gravity on 2-d problem of two temperature generalized thermoelastic medium with thermal relaxation. *Journal of Computational and Theoretical Nanoscience*, 12(9):2587–2600.

Othman, M. I. and Singh, B. (2007). The effect of rotation on generalized micropolar thermoelasticity for a half-space under five theories. *International Journal of Solids and Structures*, 44(9):2748–2762.

Ozisik, M. and Tzou, D. (1994). On the wave theory in heat conduction. *Journal of Heat Transfer*, 116(3):526–535.

Panja, S. K. and Mandal, S. (2022). Propagation of love wave in multilayered viscoelastic orthotropic medium with initial stress. *Waves in Random and Complex Media*, 32(2):1000–1017.

Panja, S. K. and Mandal, S. C. (2021). Interaction of a finite crack with shear waves in an infinite magnetoelastic medium. *Applied and Computational Mechanics*, 15(1):45–56.

Payton, R. (1983). *Elastic wave propagation in transversely isotropic media*, volume 4. Springer Science & Business Media.

Pekeris, C. (1955). The seismic surface pulse. *Proceedings of the National Academy of Sciences of the United States of America*, 41(7):469.

Pilant, W. L. (2012). *Elastic waves in the earth*, volume 11. Elsevier.

Poisson, S.-D. (1828). *Memory on the balance and movement of éelastic bodies*. F. Didot.

Pujol, J. (2003). *Elastic wave propagation and generation in seismology*, volume 227. Cambridge University Press Cambridge.

Rama Mohana Rao, K., Hemagiri Rao, P., and Chaitanya, B. (2007). Piezoelectricity in quasicrystals: a group-theoretical study. *Pramana*, 68:481–487.

Rayleigh, L. (1887). Xvii. on the maintenance of vibrations by forces of double frequency, and on the propagation of waves through a medium endowed with a periodic structure. *The London, Edinburgh, and Dublin Philosophical Magazine and Journal of Science*, 24(147):145–159.

Rice, J. (1967). Stresses in an infinite strip containing a semi-infinite crack. *Trans. ASME, Ser. E, J. Appl. Mech.*, 34:248–250.

Rice, R. G. and Do, D. D. (2012). *Applied mathematics and modeling for chemical engineers*. John Wiley & Sons.

Richards, P. G. and Aki, K. (1980). *Quantitative seismology: theory and methods*, volume 859. Freeman San Francisco, CA.

Rizk, A. E.-F. A. and Radwan, S. F. (1992). Transient thermal stress problem for a cracked semi-infinite medium. *Journal of Thermal Stresses*, 15(4):451–468.

Romeo, M. (2003). Interfacial viscoelastic sh waves. *International Journal of Solids and Structures*, 40(9):2057–2068.

Royer, D. and Dieulesaint, E. (1999). *Elastic waves in solids I: Free and guided propagation*. Springer Science & Business Media.

Sadab, M. and Kundu, S. (2024). Analysis of love-type waves in functionally graded composite structure with interfacial imperfections. *International Journal of Geomechanics*, 24(8):04024170.

Said, S. M., Abd-Elaziz, E. M., and Othman, M. I. (2022). The effect of initial stress and rotation on a nonlocal fiber-reinforced thermoelastic medium with a fractional derivative heat transfer. *ZAMM-Journal of Applied Mathematics and Mechanics/Zeitschrift für Angewandte Mathematik und Mechanik*, 102(1):e202100110.

Salah, I. B., Wali, Y., and Ghozlen, M. H. B. (2011). Love waves in functionally graded piezoelectric materials by stiffness matrix method. *Ultrasonics*, 51(3):310–316.

Sarkar, J., Mandal, S., and Ghosh, M. (1993). Diffraction of sh-waves by a griffith crack in nonhomogeneous elastic strip. *Arch. Mech*, 45(3):285–294.

Sarkar, J., Mandal, S., and Ghosh, M. (1994). Interaction of elastic waves with two coplanar griffith cracks in an orthotropic medium. *Engineering Fracture Mechanics*, 49(3):411–423.

Sarkar, J., Mandal, S., and Ghosh, M. (1995). Diffraction of elastic waves by three coplanar griffith cracks in an orthotropic medium. *International Journal of Engineering Science*, 33(2):163–177.

Sarkar, N. and Atwa, S. Y. (2019). Two-temperature problem of a fiber-reinforced thermoelastic medium with a mode-i crack under green–naghdi theory. *Microsystem Technologies*, 25:1357–1367.

Shechtman, D., Blech, I., Gratias, D., and Cahn, J. W. (1984). Metallic phase with long-range orientational order and no translational symmetry. *Physical Review Letters*, 53(20):1951–1953.

Shindo, Y. (1977). The linear magnetoelastic problem for a soft ferromagnetic elastic solid with a finite crack. *Journal of Applied Mechanics*, 44(1):47–50.

Shindo, Y. (1985). Impact response of a cracked soft ferromagnetic medium. *Acta Mechanica*, 57(1):99–112.

Shindo, Y., Nozaki, H., and Higaki, H. (1986). Impact response of a finite crack in an orthotropic strip. *Acta Mechanica*, 62(1):87–104.

Shodja, H., Ghafarollahi, A., and Enzevaee, C. (2017). Surface/interface effect on the scattering of love waves by a nano-size surface-breaking crack within an ultra-thin layer bonded to an elastic half-space. *International Journal of Solids and Structures*, 108:63–73.

Sih, G. and Chen, E. (1980). Normal and shear impact of layered composite with a crack: dynamic stress intensification. *Journal of Applied Mechanics*, 47(2):351–358.

Singh, A. K., Mistri, K. C., and Das, A. (2017). Propagation of sh-wave in a corrugated viscous sandy layer sandwiched between two elastic half-spaces. *Waves in Random and Complex Media*, 27(2):213–240.

Slawinski, M. A. (2003). *Seismic waves and rays in elastic media*. Elsevier.

Srivastava, K., Gupta, O., and Palaiya, R. (1978). Interaction of elastic waves in two bonded dissimilar elastic half-planes having griffith crack at interface—i. *International Journal of Fracture*, 14:145–154.

Srivastava, K., Gupta, O., and Palaiya, R. (1981). Interaction of elastic waves with a griffith crack situated in an infinitely long strip. *ZAMM-Journal of Applied Mathematics and Mechanics/Zeitschrift für Angewandte Mathematik und Mechanik*, 61(11):583–587.

Srivastava, K. and Lowengrub, M. (1970). Xx.—finite hilbert transform technique for triple integral equations with trigonometric kernels. *Proceedings of the Royal Society of Edinburgh Section A: Mathematics*, 68(4):309–321.

Srivastava, K., Palaiya, R., and Karaulia, D. (1980). Interaction of antiplane shear waves by a griffith crack at the interface of two bonded dissimilar elastic half-spaces. *International Journal of Fracture*, 16(4):349–358.

Srivastava, K., Palaiya, R., and Karaulia, D. (1983). Interaction of shear waves with a griffith crack situated in an infinitely long elastic strip. *International Journal of Fracture*, 21(1):39–48.

Stehfest, H. (1970). Algorithm 368: Numerical inversion of laplace transforms [d5]. *Communications of the ACM*, 13(1):47–49.

Sun, J.-L., Zhou, Z.-G., and Wang, B. (2005). Dynamic behavior of a crack in a functionally graded piezoelectric strip bonded to two dissimilar half piezoelectric material planes. *Acta Mechanica*, 176(1-2):45–60.

Terauchi, H., Noda, Y., Kamigaki, K., Matsunaka, S., Nakayama, M., Kato, H., Sano, N., and Yamada, Y. (1988). X-ray diffraction patterns of configurational fibonacci lattices. *Journal of the Physical Society of Japan*, 57(7):2416–2424.

Thomson, W. T. et al. (1950). Transmission of elastic waves through a stratified solid medium. *Journal of Applied Physics*, 21(2):89.

Tian-Hu, H. and Zi-Yuan, S. (1994). A new electric boundary condition of electric fracture mechanics and its applications. *Engineering Fracture Mechanics*, 47(6):793–802.

Tupholme, G. (2017). One-dimensional piezoelectric quasicrystals with an embedded moving, non-uniformly loaded shear crack. *Acta Mechanica*, 228(2):547–560.

Tzou, D. Y. (1995a). Experimental support for the lagging behavior in heat propagation. *Journal of Thermophysics and Heat Transfer*, 9(4):686–693.

Tzou, D. Y. (1995b). A unified field approach for heat conduction from macro-to micro-scales. *Journal of Heat Transfer*, 117(1):8–16.

Urban, K., Mayer, J., Rapp, M., Wilkens, M., Csanady, A., and Fidler, J. (1986). Studies on aperiodic crystals in al-mn and al-v alloys by means of transmission electron microscopy. *Le Journal de Physique Colloques*, 47(C3):C3–465.

Verma, P. (1986). Magnetoelastic shear waves in self-reinforced bodies. *International Journal of Engineering Science*, 24(7):1067–1073.

Verma, P. and Rana, O. (1983). Rotation of a circular cylindrical tube reinforced by fibres lying along helices. *Mechanics of Materials*, 2(4):353–359.

Verma, P., Rana, O., and Verma, M. (1988). Magnetoelastic transverse surface waves in self-reinforced elastic bodies. *Indian Journal of Pure and Applied Mathematics*, 19(7):713–716.

Verma, S. and Jain, D. (1990). Diffraction of obliquely incident p waves by two parallel and coplanar griffith cracks. *Journal of Applied Physics*, 67(11):6787–6793.

Vernotte, P. (1958). The paradoxes of the continuous theory of the heat equation. *Reports*, 246:3154–3155.

Wang, B. and Han, J. (2012a). A crack in a finite medium under transient non-fourier heat conduction. *International Journal of Heat and Mass Transfer*, 55(17-18):4631–4637.

Wang, B. and Han, J. (2012b). Fracture mechanics associated with non-classical heat conduction in thermoelastic media. *Science China Physics, Mechanics and Astronomy*, 55(3):493–504.

Wang, B. and Li, J. E. (2013). Hyperbolic heat conduction and associated transient thermal fracture for a piezoelectric material layer. *International Journal of Solids and Structures*, 50(9):1415–1424.

Wang, B. and Mai, Y. (2002). A cracked piezoelectric material strip under transient thermal loading. *J. Appl. Mech.*, 69(4):539–546.

Wang, B. and Noda, N. (2004). Exact thermoelectroelasticity solution for a penny-shaped crack in piezoelectric materials. *Journal of Thermal Stresses*, 27(3):241–251.

Wang, B., Sun, Y., and Zhu, Y. (2011). Fracture of a finite piezoelectric layer with a penny-shaped crack. *International Journal of Fracture*, 172(1):19–39.

Wang, N., Chen, H., and Kuo, K. (1987). Two-dimensional quasicrystal with eightfold rotational symmetry. *Physical Review Letters*, 59(9):1010–1013.

Wang, R., Yang, W., Hu, C., and Ding, D.-h. (1997). Point and space groups and elastic behaviours of one-dimensional quasicrystals. *Journal of Physics: Condensed Matter*, 9(11):2411–2422.

Wang, X. (2006). The general solution of one-dimensional hexagonal quasicrystal. *Mechanics Research Communications*, 33(4):576–580.

Wang, X. and Pan, E. (2008). Analytical solutions for some defect problems in 1d hexagonal and 2d octagonal quasicrystals. *Pramana*, 70:911–933.

Weibull, W. (1939a). The phenomenon of rupture in solids. *IVA Handlingar*, 153.

Weibull, W. (1939b). A statistical theory of strength of materials. *IVB-Handl.*

Wells, A. (1961). Unstable crack propagation in metals: cleavage and fast fracture. In *Proceedings of the crack propagation symposium*, volume 1(84).

Wu, B., Zhu, J.-g., Peng, D., Jones, R., Gao, S.-h., and Lu, Y.-y. (2017). Thermoelastic analysis for two collinear cracks in an orthotropic solid disturbed by antisymmetrical linear heat flow. *Mathematical Problems in Engineering*, 2017.

Yang, H. and Bogy, D. (1985). Elastic wave scattering from an interface crack in a layered half space. *Journal of Applied Mechanics*, 52(1):42–50.

Yang, J. and Li, X. (2014). Scattering of the sh wave by a crack magneto-electro-elastic material substrate bonded to piezoelectric material. *Theoretical and Applied Fracture Mechanics*, 74:109–115.

Yang, J. and Li, X. (2015). The scattering of the sh wave on a limited permeable crack in a functionally graded piezoelectric substrate bonded to a homogeneous piezoelectric strip. *Acta Mechanica*, 226:3205–3219.

Yang, J., Wang, X., Ding, S.-H., and Li, X. (2023a). Scattering of sh wave by a crack in a functionally graded one dimensional hexagonal piezoelectric quasicrystals. *ZAMM-Journal of Applied Mathematics and Mechanics/Zeitschrift für Angewandte Mathematik und Mechanik*, 103(2):e202200071.

Yang, J., Xu, Y., Ding, S., and Li, X. (2023b). Dynamic fracture of a partially permeable crack in a functionally graded one-dimensional hexagonal piezoelectric quasicrystal under a time-harmonic elastic sh-wave. *Mathematics and Mechanics of Solids*, page 10812865221138838.

Yang, J., Zhou, Y.-T., Ma, H.-L., Ding, S.-H., and Li, X. (2017). The fracture behavior of two asymmetrical limited permeable cracks emanating from an elliptical hole in one-dimensional hexagonal quasicrystals with piezoelectric effect. *International Journal of Solids and Structures*, 108:175–185.

Yang, W. (1996). Some new stable one-dimensional quasicrystals in an al65cu20fe10mn5 alloy. *Philosophical Magazine Letters*, 74(5):357–366.

Ye, H., Wang, D., and Kuo, K. (1985). Fivefold symmetry in real and reciprocal spaces. *Ultramicroscopy*, 16(2):273–277.

Zakian, V. (1970). Optimisation of numerical inversion of laplace transforms. *Electronics Letters*, 6(21):677–679.

Zenkour, A. M. (2018). Refined two-temperature multi-phase-lags theory for thermo-mechanical response of microbeams using the modified couple stress analysis. *Acta Mechanica*, 229:3671–3692.

Zhang, Z., Ye, H., and Kuo, K. (1985). A new icosahedral phase with m35 symmetry. *Philosophical Magazine A*, 52(6):L49–L52.

Zhou, Y.-B. and Li, X.-F. (2018). Two collinear mode-iii cracks in one-dimensional hexagonal piezoelectric quasicrystal strip. *Engineering Fracture Mechanics*, 189:133–147.

Zhou, Y.-B. and Li, X.-F. (2019a). Fracture analysis of an infinite 1d hexagonal piezoelectric quasicrystal plate with a penny-shaped dielectric crack. *European Journal of Mechanics-A/Solids*, 76:224–234.

Zhou, Y.-B. and Li, X.-F. (2019b). A yoffe-type moving crack in one-dimensional hexagonal piezoelectric quasicrystals. *Applied Mathematical Modelling*, 65:148–163.

Zhou, Y.-B., Liu, G.-t., and Li, L.-h. (2021). Effect of t-stress on the fracture in an infinite one-dimensional hexagonal piezoelectric quasicrystal with a griffith crack. *European Journal of Mechanics-A/Solids*, 86:104184.

Zhou, Z.-G., Li, H.-C., and Wang, B. (2001). Investigation of the scattering of anti-plane shear waves by two collinear cracks in a piezoelectric material using a new method. *Acta Mechanica*, 147:87–97.

Zhou, Z.-G. and Wang, B. (2005). Investigation of the interaction of two collinear cracks in anisotropic elasticity materials by means of the nonlocal theory. *International Journal of Engineering Science*, 43(13-14):1107–1120.

Zhu, C.-S., Fang, X.-Q., Liu, J.-X., and Li, H.-Y. (2017). Surface energy effect on nonlinear free vibration behavior of orthotropic piezoelectric cylindrical nano-shells. *European Journal of Mechanics-A/Solids*, 66:423–432.

List of Publication and communicated papers

List of Published Papers

- Panja, S. K., & Mandal, S. C. (2021). Interaction of a finite crack with shear waves in an infinite magnetoelastic medium. Applied and Computational Mechanics. 15(1), p. 45-56. https://doi.org/10.24132/acm.2021.623
- Panja, S. K., & Mandal, S. C. (2021). Interaction of magnetoelastic shear waves with a Griffith crack in an infinite strip. Journal of Engineering Mathematics, 126(1), 2. https://doi.org/10.1007/s10665-020-10085-0
- Panja, S. K., & Mandal, S. C. (2021). Impact response of a finite crack in the presence of magnetic field. Engineering Fracture Mechanics, 253, 107851. https://doi.org/10.1016/j.engfracmech.2021.107851
- Panja, S. K., Lahiri, A., & Mandal, S. C. (2023). A thermoelastic model with higher order time derivatives for a crack in a rotating solid. International Journal for Computational Methods in Engineering Science and Mechanics, 24(2), 107-118. https://doi.org/10.1080/15502287.2022.2066033
- Panja, S. K., & Mandal, S. C. (2023). Two collinear cracks in a transversely isotropic medium under the hyperbolic heat conduction law. Journal of Mechanics of Materials and Structures, 18(3), 375-389. https://doi.org/10.2140/jomms.2023.18.375
- Panja, S. K., & Mandal, S. C. (2022). Propagation of Love wave in multilayered viscoelastic orthotropic medium with initial stress. Waves in Random and Complex Media, 32(2), 1000-1017. https://doi.org/10.1080/17455030.2020.1810359

- Panja, S. K., & Mandal, S. C. (2024). Interaction of anti-plane shear waves with two collinear cracks in 1D hexagonal piezoelectric quasicrystals. ZAMM-Journal of Applied Mathematics and Mechanics/Zeitschrift für Angewandte Mathematik und Mechanik, 104(2), e202300393. https://doi.org/10.1002/zamm.202300393

List of communicated paper

- Panja, S. K., Alam, S., & Mandal, S.C. Interaction of Love wave with an interface crack. (Continuum Mechanics and Thermodynamics)